CRANFIELD INSTITUTE OF TECHNOLOGY

SCHOOL OF MECHANICAL ENGINEERING

DEPARTMENT OF FLUID ENGINEERING AND INSTRUMENTATION

Ph.D. THESIS

ACADEMIC YEAR 1989/90

G.SULTAN

THEORETICAL AND EXPERIMENTAL STUDIES OF THE CORIOLIS MASS FLOWMETER

SUPERVISOR: DR. J. HEMP

MARCH 1990

ABSTRACT

The Coriolis mass flowmeter is modelled using the theory of vibrating beams. Tube deformations for the fundamental mode and the next two modes of natural (out-of-plane) vibration are worked out for many tube geometries. An improved model taking into account the effects of elastic boundary conditions and added masses of the electromagnetic drive and detectors is also discussed. A method for predicting the optimum detection positions is suggested in relation to signal-to-noise ratio. In addition, an argument for prediction of the effects of a dilute suspension of small bubbles or particles in the fluid is presented. Finally, experimental studies are conducted in order to demonstrate the validity of the theoretical models.

TO

THE BEST AND LARGEST FAMILY IN THE WORLD

FATHER ABDUL-RAHMAN SULTAN

MOTHER SULTANA SULTAN

BROTHERS:

YOUSIF

ADNAN

ADEL

MUTH'HER

BURHAN

IHSAAN

KASEM

SISTERS:

SAHERA

MAHERA

NAJEHA

MAY

AND THEIR WIVES, HUSBANDS AND CHILDREN.

ACKNOWLEDGEMENTS

The author conveys his gratitude to Dr. J.HEMP for his professional supervision and never ending interest and patience throughout the work.

Sincere appreciation is sent to the Government of the Republic of IRAQ, the Ministry of Higher Education and Scientific Research for their financial support and interest.

Thanks are also due to Professor W.S.HEMP for helping in the early stages of the work, to Professor M.L.SANDERSON for electronic advice, to Professor R.C.BAKER for general support, to Mr. H.K.VERSTEEG, Dr. J.R.HERITAGE and Mr. G.ODDIE for many useful discussions, to Mr. R.DUNN and Mr. D. MacLEOD for technical assistance and last but not least to Micro Motion Inc. for the loan of their instrument.

CONTENTS

LIST OF FIGURES

LIST OF TABLES

NOTATION

A	TUBE INTERIOR AREA (Section 1.4) and AMPLITUDE OF VIBRATION (Section 4.2).
A_{ij}	CONSTANTS.
a	RADIUS OF CIRCULAR TUBE (Section 2.1.1) and CONSTANT (Section 6.3).
a_A	CENTRIPETAL ACCELERATION.
a_b	ACCELERATION OF PARTICLE.
a_C	CORIOLIS ACCELERATION (Section 1.4) and ACCELERATION OF THE SPHERICAL CONTAINER (Section 6.3).
a_1, a_2	RADIUS OF CIRCULAR SECTIONS OF GENERAL TUBE GEOMETRY.
B_0, B_1	CONSTANTS.
b	WIDTH OF THE BRACE BAR (Section 3.1.4) and THE LENGTH OF STRAIGHT TUBE (Section 3.3).
b_e	WIDTH OF THE END SUPPORT.
$b_1, b_2, \ldots$	LENGTHS OF STRAIGHT SECTIONS OF GENERAL TUBE GEOMETRY.
c	THE ARM OF CORIOLIS MOMENT (section 1.4) and CONSTANT (Section 6.3).
d	DIAMETER OF BRACE BAR HOLE.
d_e	DIAMETER OF END SUPPORT HOLE.
d_o	O.D. OF THE TUBE.
E	TUBE YOUNG'S MODULUS.
E_b	BRACE BAR YOUNG'S MODULUS.
F	LOAD (for tension, bending and torsion section 3.1.4).
F_C	CORIOLIS FORCE.
F_I	INERTIA FORCE.
F_r	REACTION FORCE.
f	TUBE FREQUENCY.

G	TUBE SHEAR MODULUS.
G_b	BRACE BAR SHEAR MODULUS.
h	DISTANCE BETWEEN THE CENTRE LINES OF THE HOLES OF BRACE BAR.
h_e	HIGHT OF END SUPPORT.
I, I_x	SECOND MOMENT OF AREA OF THE TUBE.
I_z	MOMENT OF INERTIA OF THE U-TUBE.
J	POLAR MOMENT OF AREA.
K	STIFFNESS CONSTANT (Section 1.4) and =GJ/EI in section 2.3.4
K_1	TRANSLATIONAL STIFFNESS COEFFICIENT.
K_2	ROTATIONAL STIFFNESS COEFFICIENT.
K_3	TORSIONAL STIFFNESS COEFFICIENT.
$L_1, L_2, \ldots$	NON-DIMENSIONAL LENGTHS OF GENERAL TUBE GEOMETRY.
ℓ	LENGTH OF THE STRAIGHT SECTION OF THE U-TUBE.
M	BENDING MOMENT (OUT-OF-PLANE).
M'	BENDING MOMENT (IN-PLANE).
M_{c1}, M_{c2}, M_{c3}	MASSES OF ELECTROMAGNETIC DRIVE AND DETECTORS.
M_{act}	ACTUAL MASS.
M_{eff}	EFFECTIVE MASS.
M_f	FLUID MASS PER UNIT LENGTH.
M_t	TUBE MASS PER UNIT LENGTH.
$\dot{m}$	MASS FLOWRATE.
N	AMPLITUDE OF SUPERIMPOSED RANDOM NOISE.
P	TANGENTIAL FORCE.
P_b	PRESSURE OF A BUBBLE.
P_l	PRESSURE OF LIQUID.
R	RADIUS OF CURVATURE OF THE TUBE.
R_b	RADIUS OF CURVATURE OF THE BRACE BAR (section 3.1.4) and RADIUS OF A PARTICLE (Section 6.3).
R_l	RADIUS OF THE SPHERICAL CONTAINER.

r	MEAN RADIUS OF TUBE (section 2.1.1) and SPHERICAL CO-ORDINATE (section 6.3).
S	SHEAR FORCE (IN-PLANE).
S'	SHEAR FORCE (OUT-OF-PLANE).
s	TUBE LENGTH CO-ORDINATE.
T	TORQUE
t	TIME OR TUBE THICKNESS.
t_b	BRACE BAR THICKNESS.
t_e	END SUPPORT THICKNESS.
Δt	TIME DELAY OR TIME DIFFERENCE.
U	FLUID MEAN VELOCITY.
u	FLUID VELOCITY (Section 1.4) and IN-PLANE DISPLACEMENT COMPONENT (Section 2.1.1)
$\bar{u}$	NON-DIMENSIONAL FLUID VELOCITY.
V_b	VIBRATIONAL VELOCITY OF A PARTICLE.
V_l	VIBRATIONAL VELOCITY OF A LIQUID.
V_c	VIBRATIONAL VELOCITY OF SPHERICAL CONTAINER.
v	TUBE VELOCITY (section 1.4) and OUT-OF-PLANE DISPLACEMENT COMPONENT (Section 2.1.1).
$\bar{v}_{act}(\bar{s})$	DISPLACEMENT MODE SHAPE.
$\dot{W}$	THE RATE OF WORK.
w	TANGENTIAL DISPLACEMENT COMPONENT.
y,$\dot{y}$	DISPLACEMENT AND VELOCITY OF THE U-TUBE.

GREEK

α	VOID FRACTION.
$\alpha_1,\alpha_2,...$	ROOTS OF THE COMPLEX POLYNOMIAL EQUATION (2.33).
β	MASS RATIO.
Γ	TWIST ANGLE (Section 3.1.4).

$\gamma_1,\gamma_2,\gamma_3$	NON-DIMENSIONAL ADDED MASSES.
δ	DISPLACEMENT (Section 3.1.4)
ζ	SLOPE (section 3.1.4)
$\eta(\bar{s})$	DISPLACEMENT MODE SHAPE FUNCTION.
ϵ	STRAIN
θ	TWIST ANGLE (Section 1.4) and POLAR CO-ORDINATE (sections 2.1.1 and 6.3)
$\lambda_1,\lambda_2,...$	ROOTS OF THE COMPLEX POLYNOMIAL EQUATION (2.29)
ξ	TORSIONAL DISPLACEMENT.
ρ_f	FLUID DENSITY.
ρ_t	TUBE MATERIAL DENSITY.
σ	POISSON RATIO.
σ_y	NODAL STRESS.
τ	SHEAR STRESS.
Φ	LOCAL TWIST ANGLE (Section 2.1.1) and PHASE OF A SIGNAL (Section 4.2).
ϕ	ROTATIONAL DISPLACEMENT (TWIST).
$\phi_{act}(\bar{s})$	TWIST MODE SHAPE.
$\Delta\phi$	PHASE DIFFERENCE.
$\psi(\bar{s})$	TWIST MODE SHAPE FUNCTION.
Ω	ANGULAR VELOCITY.
ω	ANGULAR FREQUENCY.

CHAPTER ONE

INTRODUCTION

CHAPTER ONE

INTRODUCTION

1.1 GENERAL

Mass flow measuring techniques have been the focus of attention in many aspects of modern technology since the 1950's and several surveys of mass flow meters such as those by Siev [1],Flanagan and Colman [2], Orlando and Jennings [3] and Brain [4] have been published. The increase in demand for accurate mass flow measurement devices was stimulated by the development of modern production systems.

Most previous work on flow rate measurement concentrated on volume flow rate as opposed to mass flow rate which now appears more significant. In many industrial processes, particularly the fuel and chemical industries both mass flow and its integral are needed in order to determine mass and energy balances in fuel distribution systems and process plants.

The major advantage of determining mass flow rate of a fluid rather than the volume rate is that the former is completely independent of variations in fluid properties. Hence mass flow information is generally of greater value than volumetric flow.

Two general approaches are employed to measure mass flow [5]. The first, known as Indirect or Inferential mass flow measurement, involves simultaneous measurements of both volume flow rate and density of fluid , followed by calculation of the mass flow rate. The other, more basic approach, is to design a meter whose output is a direct function of mass flow. Such a meter is known as a "Direct or True mass flow meter". While the indirect methods are often satisfactory and in wide use, the direct methods may have advantages with respect to accuracy, simplicity, cost, weight, space, etc., in certain applications. Mass flow can also be determined by weighing methods. This is certainly acceptable for batch type processes but is

not really practical for continuous processes.

Direct mass flow meters are "additive" flow meters (energy being conveyed to the fluid stream). Generally they sense force or its equivalent (torque, pressure, etc.,)to effect a measure of mass flow rate. In this thesis, investigation is restricted to the Coriolis-Type Mass Flow Meter, which falls into the "Direct Mass Flow Meter" category.

In the Coriolis mass flow meter an angular movement is imparted to a tube conveying fluid . This angular movement can be either a steady rotation or a harmonic vibration. This additional motion communicated to the flowing fluid causes particles of the fluid to undergo a Coriolis acceleration. As a result forces proportional to the product of fluid density and velocity act through the fluid medium and generate pressure on the conduit walls producing a measurable effect. In the present work we are concerned only with meters that employ harmonic vibration of a tube.

1.2 HISTORICAL REVIEW OF THE CORIOLIS MASS FLOWMETER

As early as 1835 Professor Gustave De Coriolis (1792-1843) successfully quantified the natural phenomenon which causes objects moving freely over the surface of the earth to appear to curve [6]. Nowadays this is called the Coriolis effect; an effect which provides the basis for the Coriolis-type flow meter.

Through observation of the numerous patents of Coriolis flow meters it becomes apparent that since the early 1950's until now there has been steady development and interest in this area, as can be seen in Figure 1.1.

The earliest publication on Coriolis flow metering was by Li and Lee [7] in 1953, which reports a mass flow meter commonly called a "Li" meter which incorporates a Y-shaped tube and utilizes pure rotation as excitation. The fluid flows through a double tube system which revolves at a constant angular velocity as shown in Figure 1.2. The

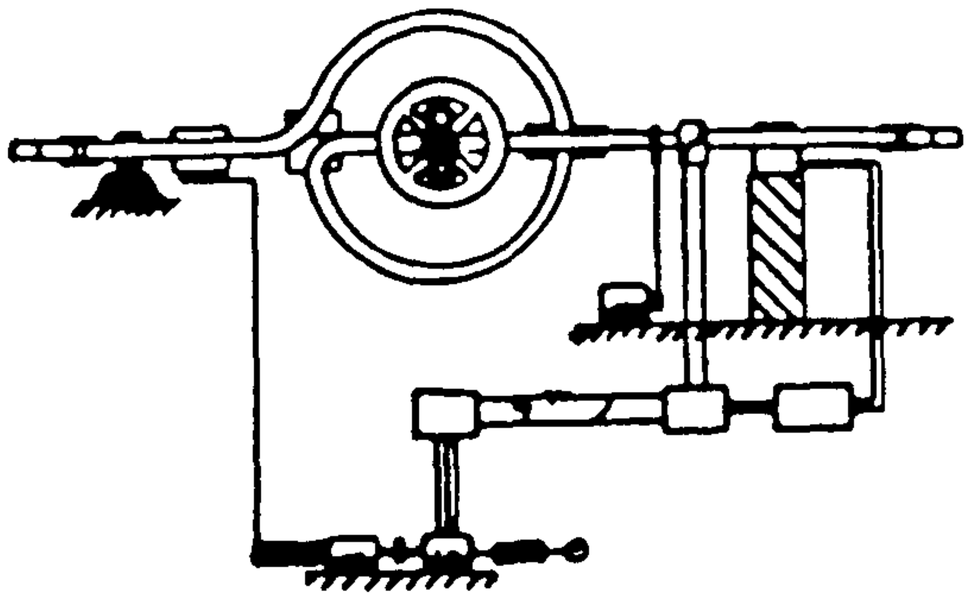

PEARSON 1953 [8]

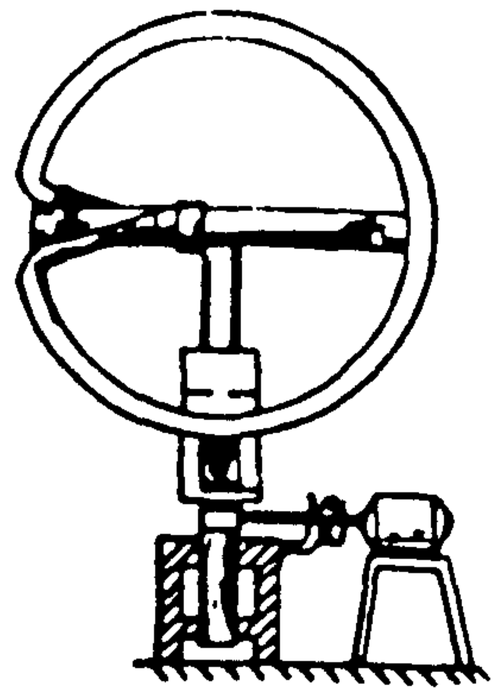

ROTH 1958 [9]

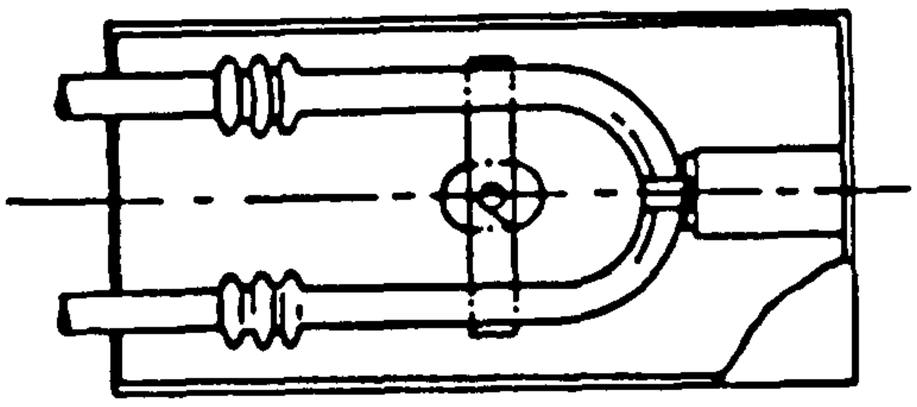

ROTH 1962 [10]

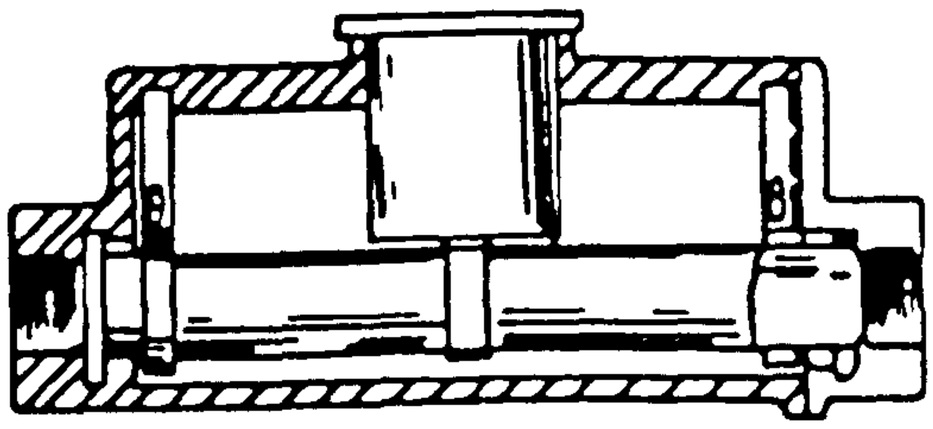

SIPIN 1967 [11]

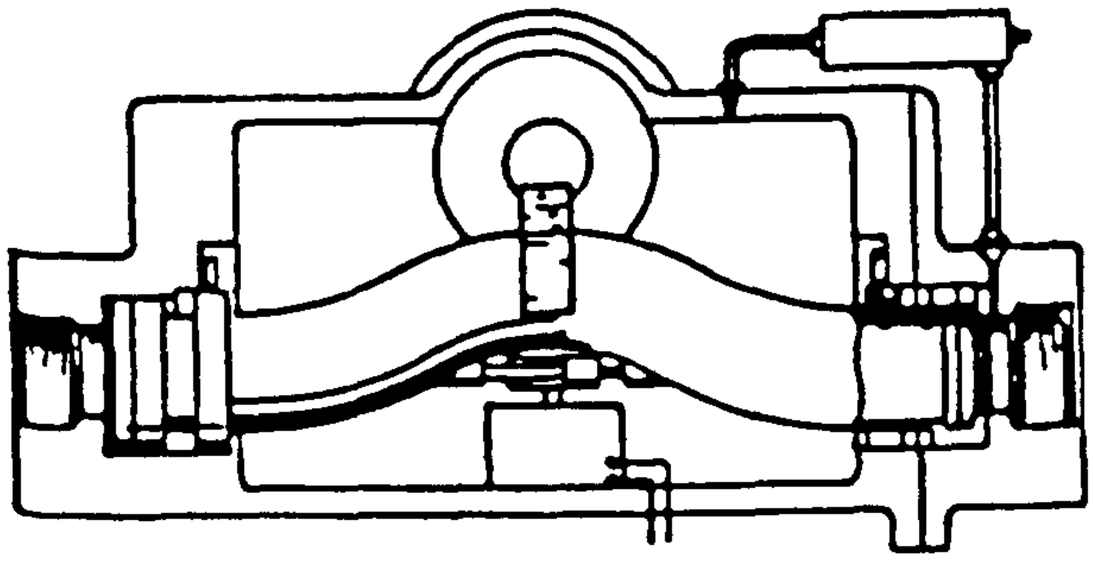

SIPIN 1967 [12]

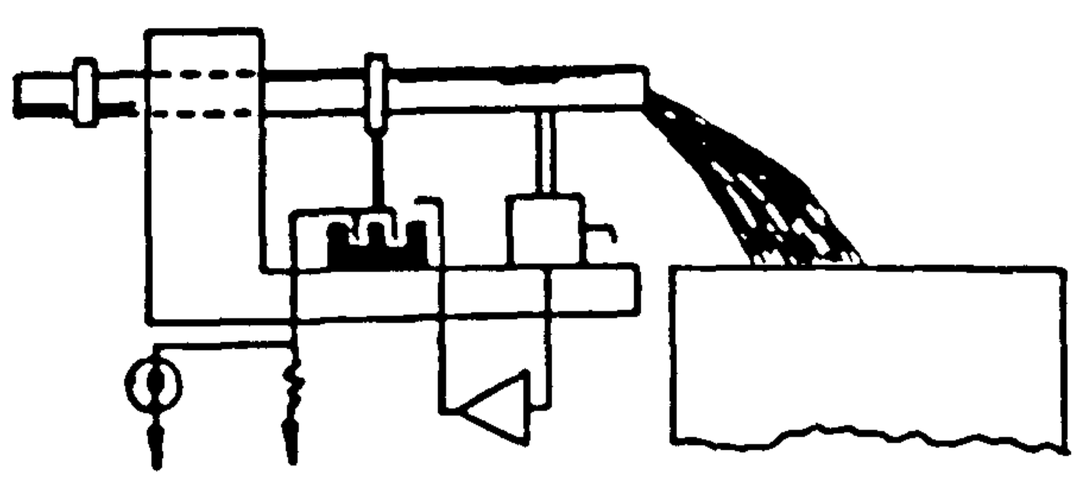

WILEY et al 1963 [13]

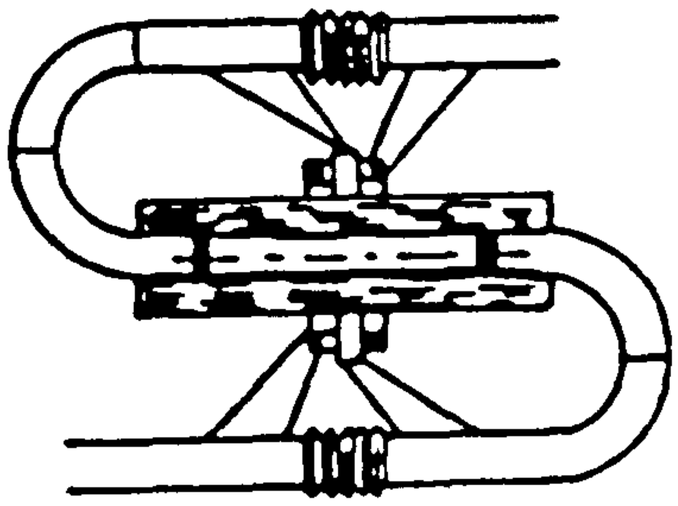

PAVLIN et al 1975 [14]

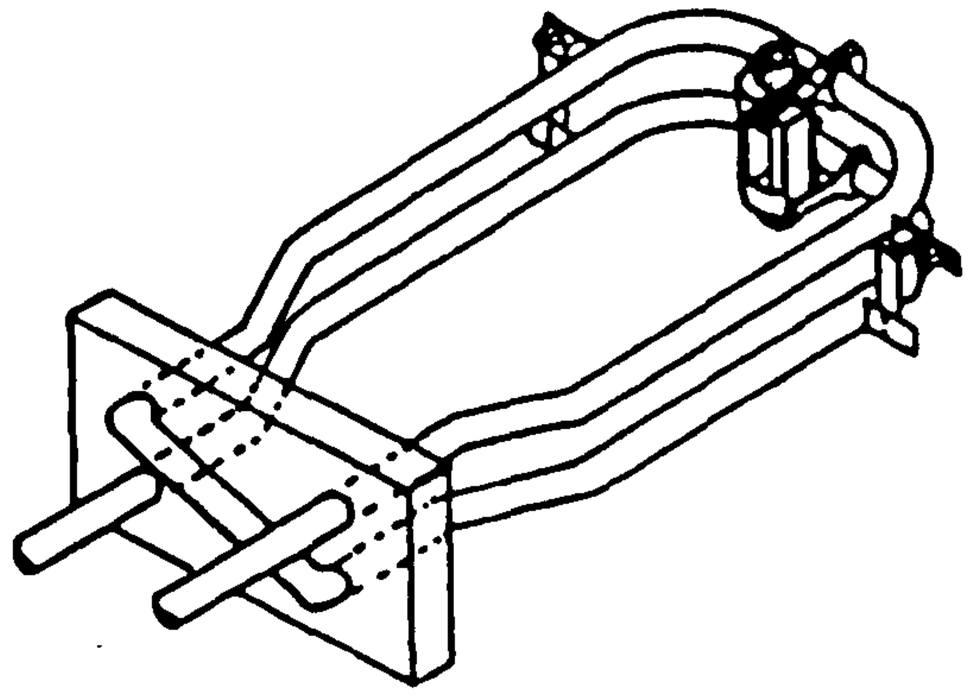

COX et al 1982 [15]

Figure 1.1 CORIOLIS-TYPE MASS FLOWMETERS 1950s TO 1980s

tube system consists of two parts joined by flexible connections. Under the action of Coriolis acceleration a moment develops , whose magnitude is proportional to the flow of the fluid. The use of rotating mass, in this manner ,is nowadays considered undesirable because it requires sealed rotating bearings and may be troublesome with chemically active fluids or fluids at high pressures. These problems appear to have been eliminated by vibrating the tube system.

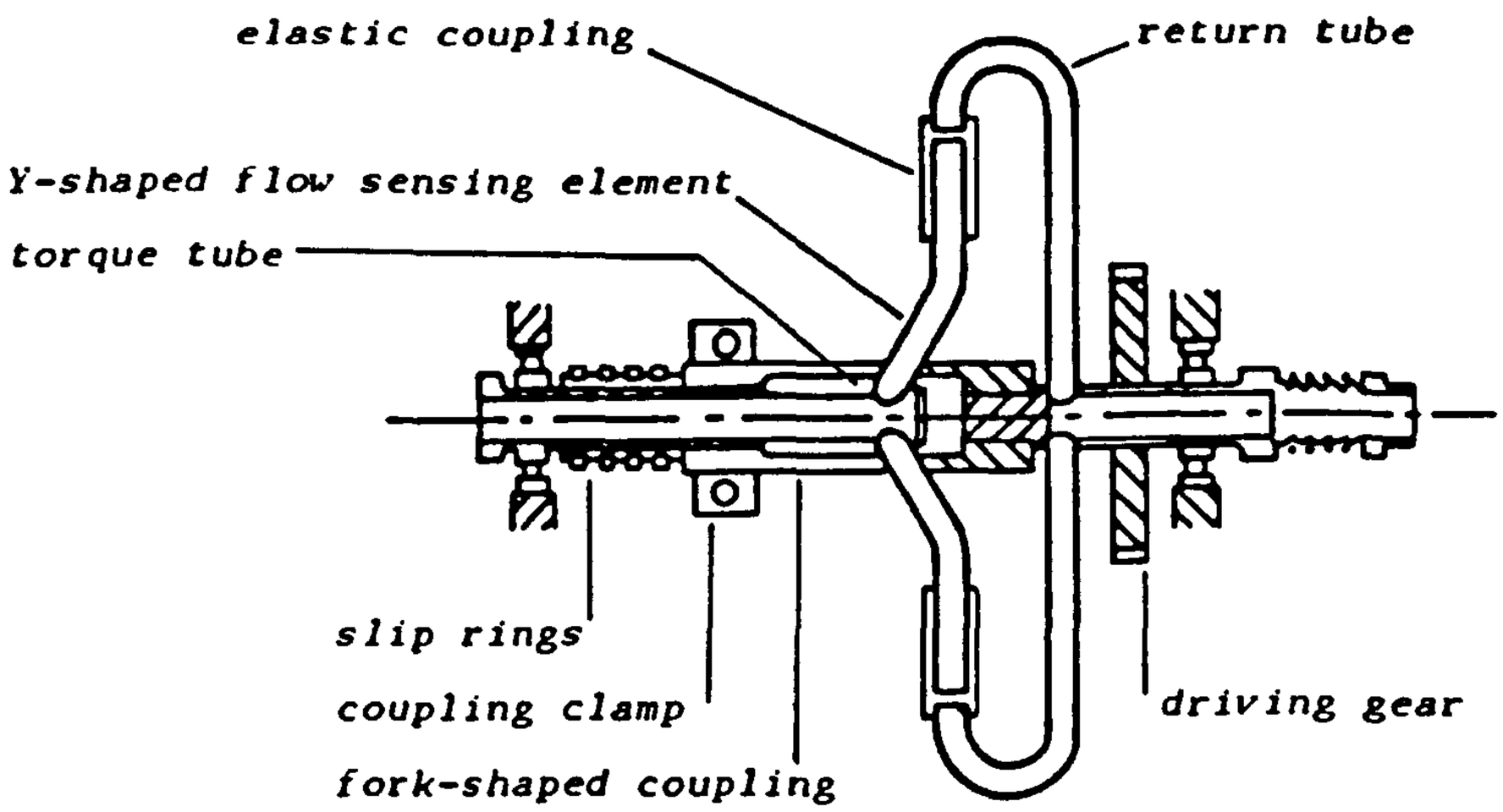

Figure 1.2 Y-TUBE ROTATORY CORIOLIS MASS FLOWMETER

Then, the moment has the same frequency as the the vibration and is proportional to mass flow. The major problem faced by the early flow meters was that the constant Coriolis force, being so minute, was overshadowed by other forces (eg. friction) and consequently inaccurately measured.

Despite such developments only two meters had become commercially available by 1986, MICROMOTION Inc. manufactured and extensively marketed their meter, to be followed shortly by the meter of EXAC Corp.. In 1986 six similar instruments were manufactured by BOPP & REUTHER GmbH., SMITH Inc., NEPTUNE Ltd., ENDRESS & HAUSER Ltd., DANFOSS Ltd. and KROHN Ltd. (fig. 1.3). Each of the above

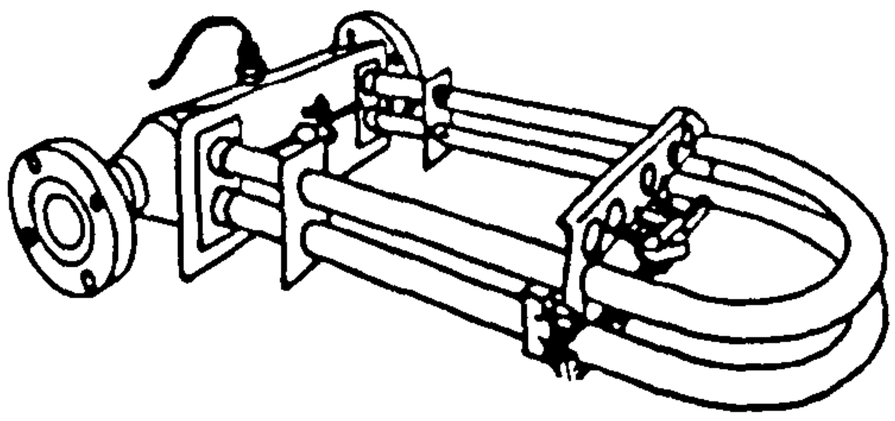

(a) Micro Motion Flowmeter
(by Micro Motion Inc.)

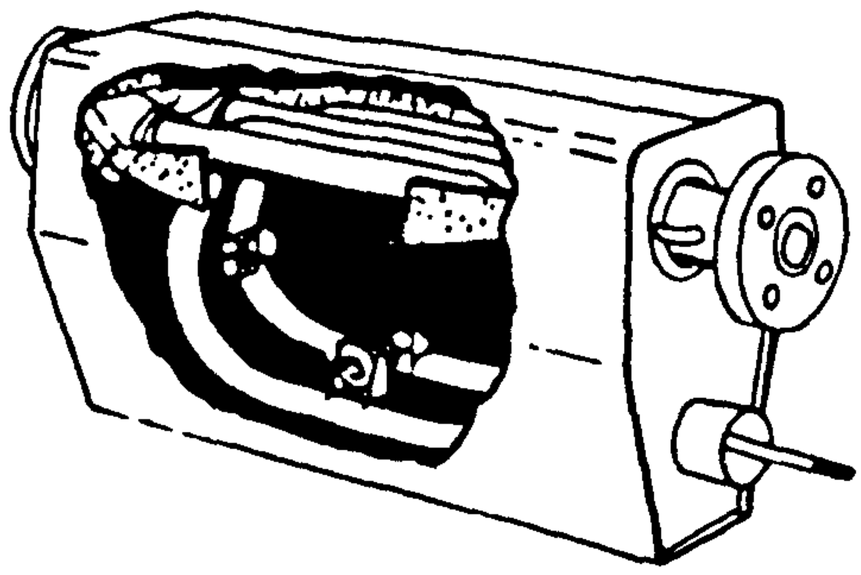

(b) Exac Flowmeter
(by Exac Corp.)

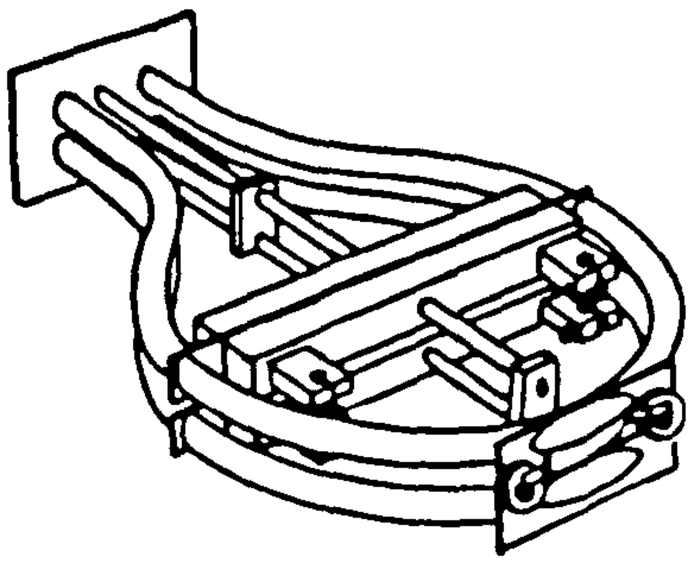

(c) RHM Flowmeter
(by Bopp & Reuther GmbH.)

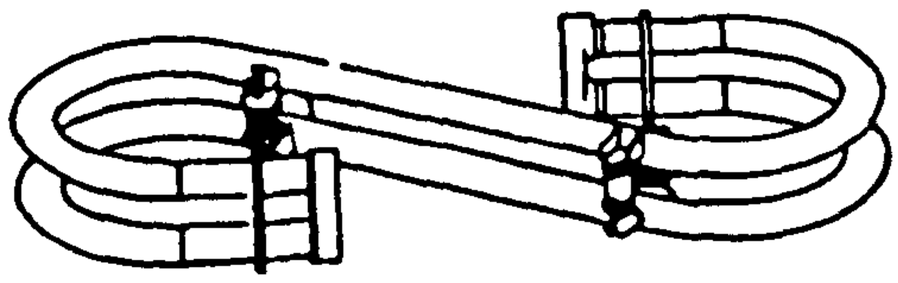

(d) S-Flowmeter
(by Smith M Inc.)

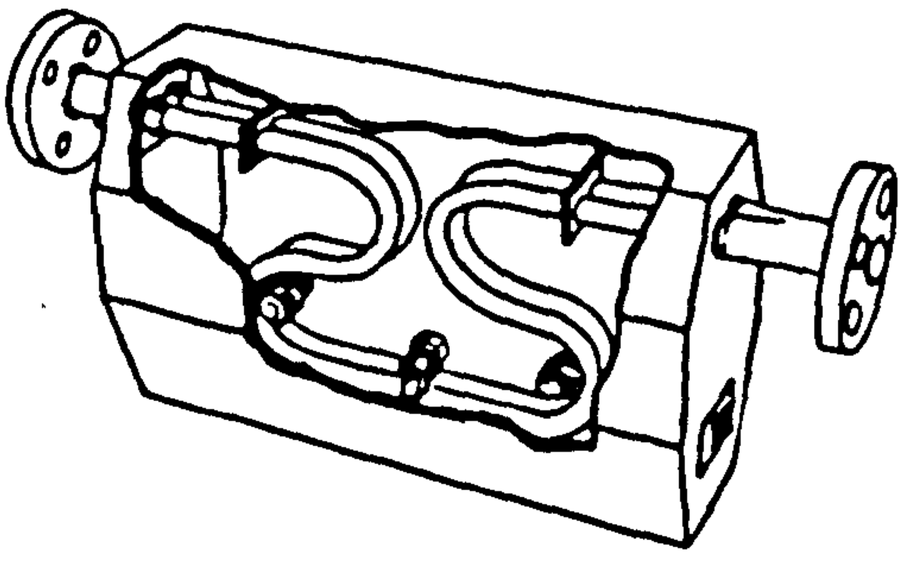

(e) ṁ-Flowmeter
(by Neptune M Ltd.)

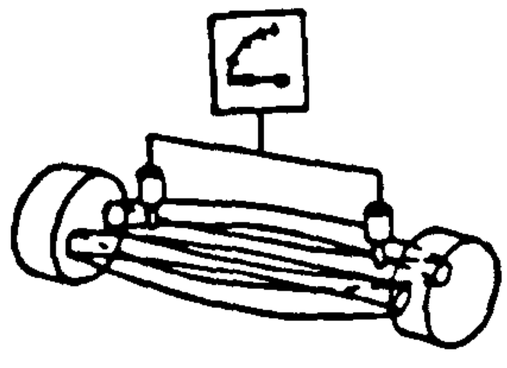

(f) M-Point Flowmeter
(by Endress & Hauser Ltd.)

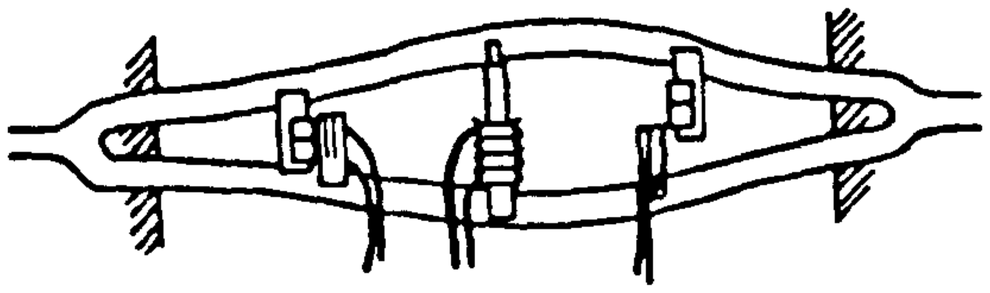

(g) Massflo Flowmeter
(by Danfoss FM Ltd.)

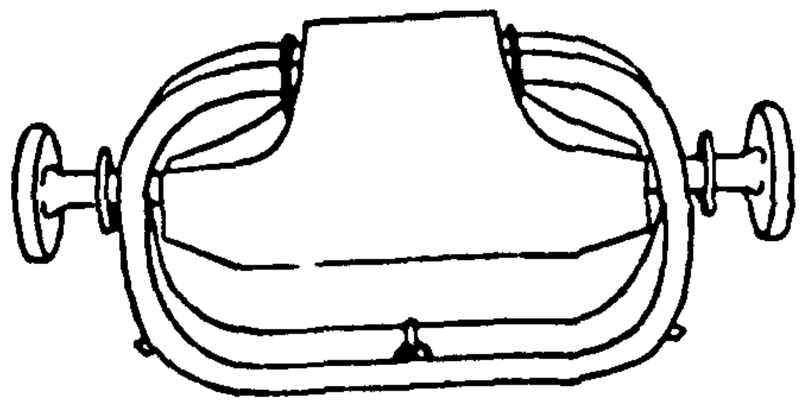

(h) Corimass flowmeter
(by Kröhne M&C Ltd.)

Figure 1.3 COMMERCIAL CORIOLIS MASS FLOWMETERS

manufacturers claims superb performance of their meter in vast applications, including two phase flows.

A brief discussion will now be given of the historical progression of the Coriolis mass flow meter manufactured by Micromotion Inc.(a similar progression took place in other manfacturers of commercial flow meters). The first flow meter presented by Micromotion Inc. was built using optical sensors to measure the twist angle of a single u-tube as shown in fig. 1.4a .

Various modifications gave rise to a new flow meter where a counterbalance tube, filled with a stationary fluid, was used to minimize fluid density effects and reduce external vibration effects (fig. 1.4b). This design increased the possibility of the tubes cracking since the two tubes oscillated out of phase thus increasing the stress concentration around the clamped ends [16]. Introduction of brace bars linking the two tubes together decreased such stresses.

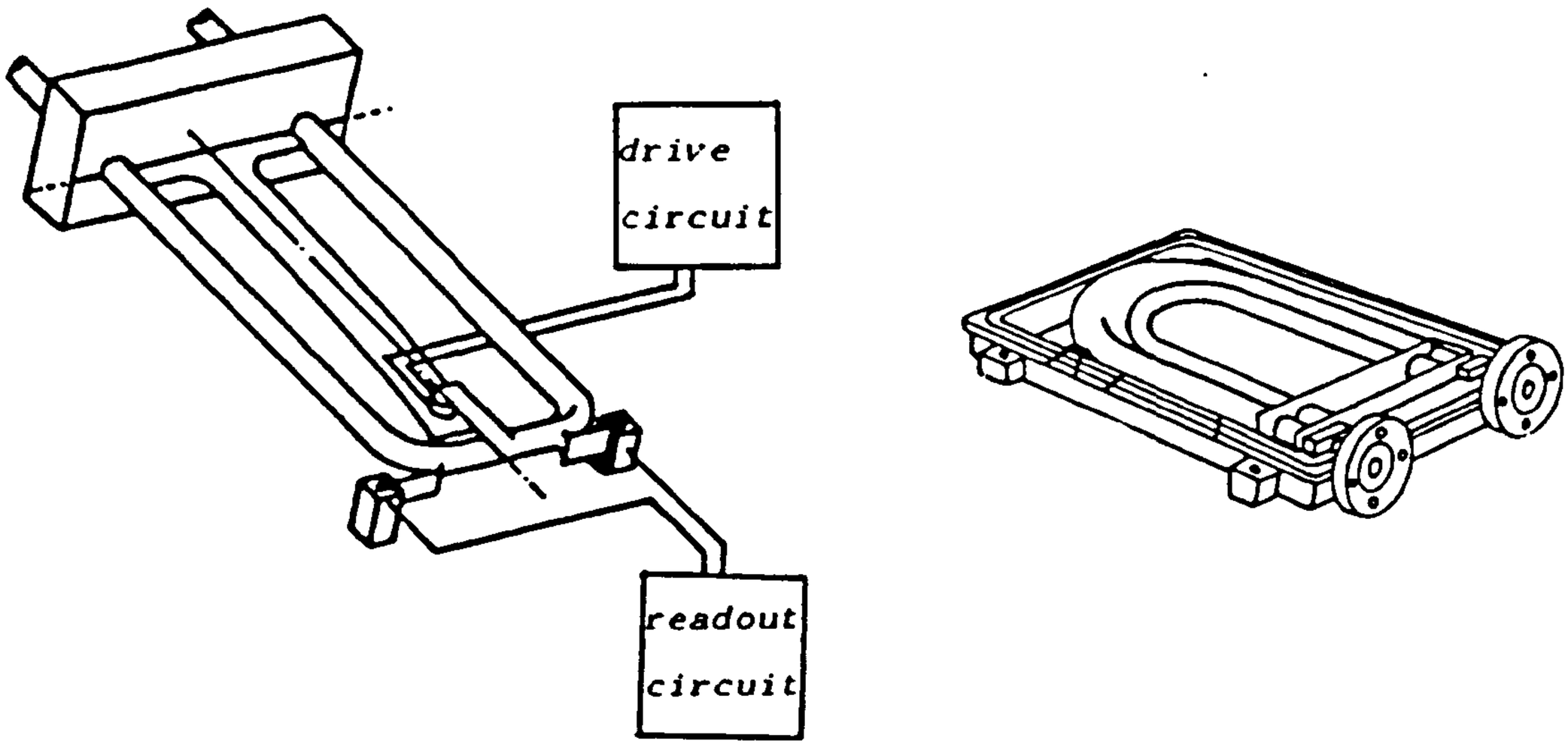

Figure 1.4 EARLY COMMERCIAL CORIOLIS MASS FLOWMETER (BY MICRO MOTION INC.)

In 1982 an improved flow meter was designed replacing optical sensors,

which were causing zero drift problems, with magnetic sensors and also improving fabrication techniques. Mid 1983 brought the most current production of flow meter in which the main design alteration involved replacement of the counterbalance tube for a second flow tube, thus reducing the temperature effects fig. 1.3a .

Indeed, development continues indefinitely in an attempt to gain greater accuracy and efficiency in Coriolis mass flow measurement. Thus, very recently Casctta et al [17] reported a prototype Coriolis mass flowmeter based on elastic suspension. The flowmeter prototype is composed of dual u-tubes rigidly fixed to plexiglas plates as shown in fig. 1.5 . The system being suspended by elastic elements attached to the rigid bases, resulting in no deformation in the tubes and consequently providing independent measurement of mass flow rate from elastic properties of the tubes.

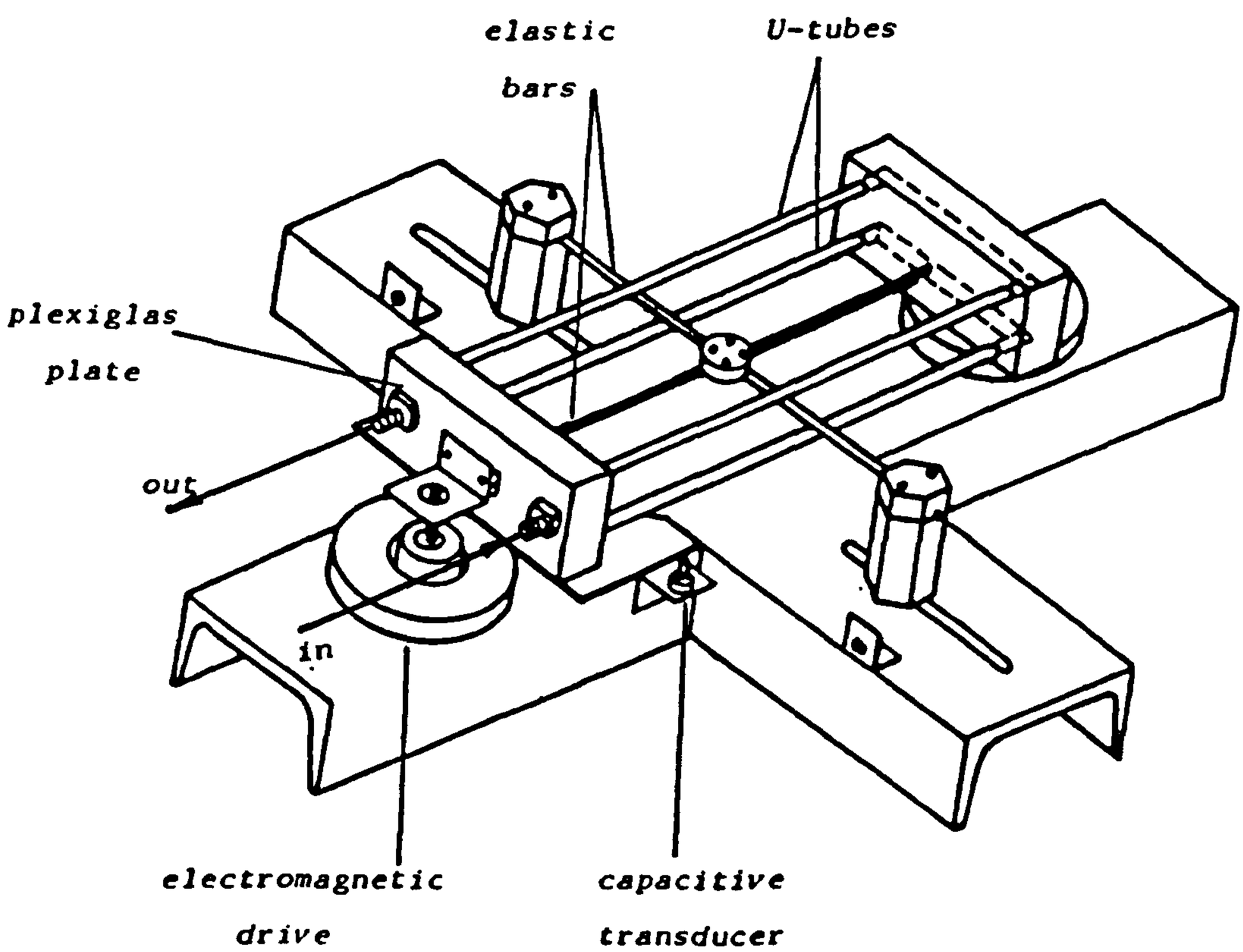

Figure 1.5 PROTOTYPE CORIOLIS MASS FLOWMETER BASED ON ELASTIC SUSPENSION (BY CASCTTA et al [17])

1.3 THE ELEMENTS OF A CORIOLIS MASS FLOWMETER

The chief difference between the various meters is geometric as shown in Figure 1.3. Meters generally incorporate :

A- The Primary Element

This consists of :

(i) A tube (or dual tubes) conveying fluid lying in one plane and clamped at its ends.

(ii) An electromagnetic drive.

(iii) Two electromagnetic detectors.

(iv) A feedback circuit for maintaining vibration at the fundamental frequency or higher harmonic.

B- The Secondary Element

This is some electronic means for measuring the phase difference (due to flow) between signals received from the detectors.

1.4 BASIC THEORY

Figure 1.6a shows a straight and uniform cyiindrical section of a tube, which is rotating with an angular velocity Ω about a z-axis. Inside the tube, fluid is moving substantially parallel to the axis of the tube with mean velocity u, and experiencing a change in angular momentum and centrifugal acceleration.

To understand the physical meaning of Coriolis acceleration, consider the absolute velocity of an element of fluid mass at time t and at time t+Δt (Figure 1.6b). At time t the velocity may be resolved into its components u and v, and at time t+Δt into u'and v'. Drawing these components from same origin as shown in Figure 1.6c, note that the change in velocity during the time Δt can be represented by the

sum of three vectors RR',TT" and T"T' which result in the appropriate inertia terms required for dynamic equilibrium in such a system.

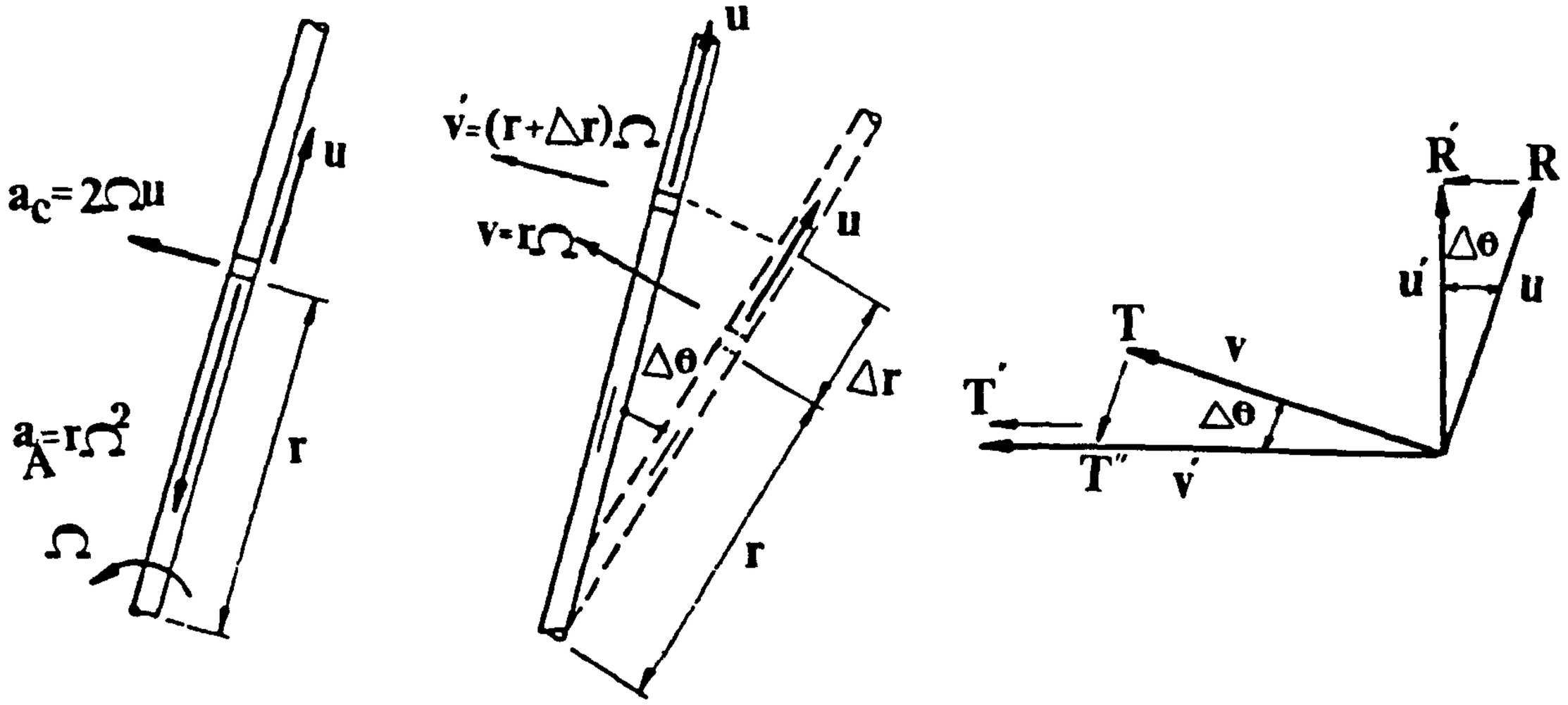

(a) (b) (c)

Figure 1.6 CORIOLIS AND CENTRIPETAL ACCELERATIONS IN ROTATING TUBE CONVEYING FLUID

Vector TT" presents the change in direction of v , resulting in centripetal acceleration as follows

$$\lim_{\Delta t \to 0} \frac{TT''}{\Delta t} = \lim_{\Delta t \to 0} v \frac{\Delta\theta}{\Delta t} = r\Omega^2 \qquad (1.1)$$

Vector RR' measures the change in direction of u due to rotation and vector T"T' presents the change in magnitude of v due to u. Coriolis acceleration can be presented as a combined effect of the relative velocity u and rotation Ω and can be written as

$$\lim_{\Delta t\to 0}\left[\frac{RR'+T''T'}{\Delta t}\right] = \lim_{\Delta t\to 0}\left[\, u\,\frac{\Delta\theta}{\Delta t} + \Omega\,\frac{\Delta r}{\Delta t}\,\right] = 2\Omega u \qquad (1.2)$$

Coriolis acceleration can also be generated by vibrating the tube, resulting in an oscillatory acceleration with the same frequency as the main vibration.

More specifically, consider a flowmeter of U-tube configuration as shown in Figure 1.7a (other configurations can be treated similarly). Here, the electromagnetic driver causes the tube to perform an approximate oscillatory rotation about the x-axis with angular velocity Ω where

$$\Omega = \Omega_o \cos \omega t \qquad (1.3)$$

Fluid flows in opposite directions in the straight limbs of the U-tube so the effect of Coriolis acceleration is to cause an oscillatory twisting of the tube about the z-axis. In this system, any particle of mass m and velocity $\underline{u}$ experiences a Coriolis force $2m\underline{u}\times\underline{\Omega}$ [18]. This gives rise to forces $\pm Fc$ on straight parts of the U-tube (Figure 1.6b) where

$$F_C = 2\rho\, \Omega_o \cos(\omega t)\, u\ell A \qquad (1.4)$$

A is the tube interior area. These forces are the result of pressure gradients in the y-direction in the fluid.

The forces $\pm Fc$ cause a twisting of the tube about the z-axis. If θ is the angle of the twist (Figure 1.7b) then the equation of motion of the twisting [19] can be written as

$$F_C\, d = K\theta + I\ddot{\theta} \qquad (1.5)$$

This secondary motion is exceedingly small compared with the main vibration about the x-axis. The solution of (1.5) is

$$\dot{\theta} = \theta_o \cos \omega t \qquad (1.6)$$

Where

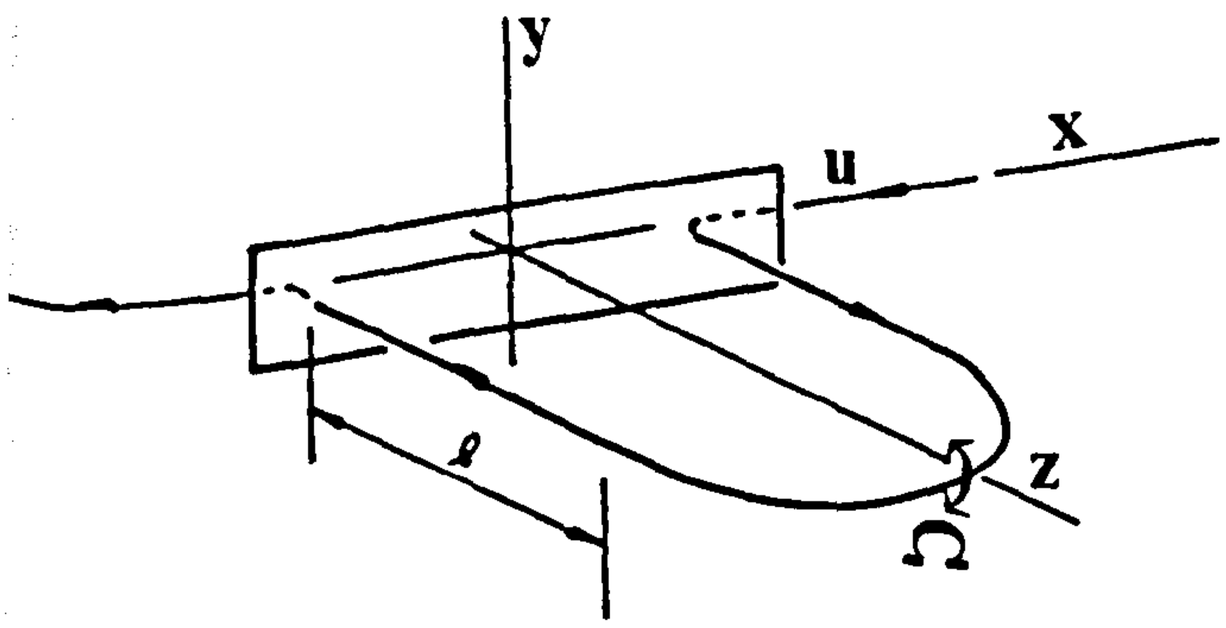

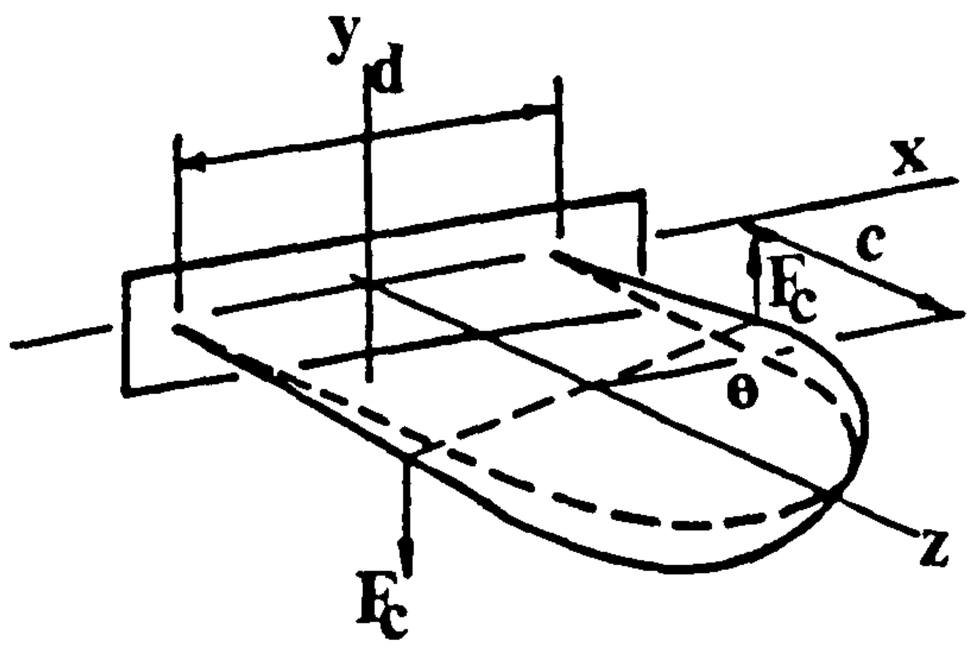

(a) U-Tube Configuration

(b) Twisting of the U-tube

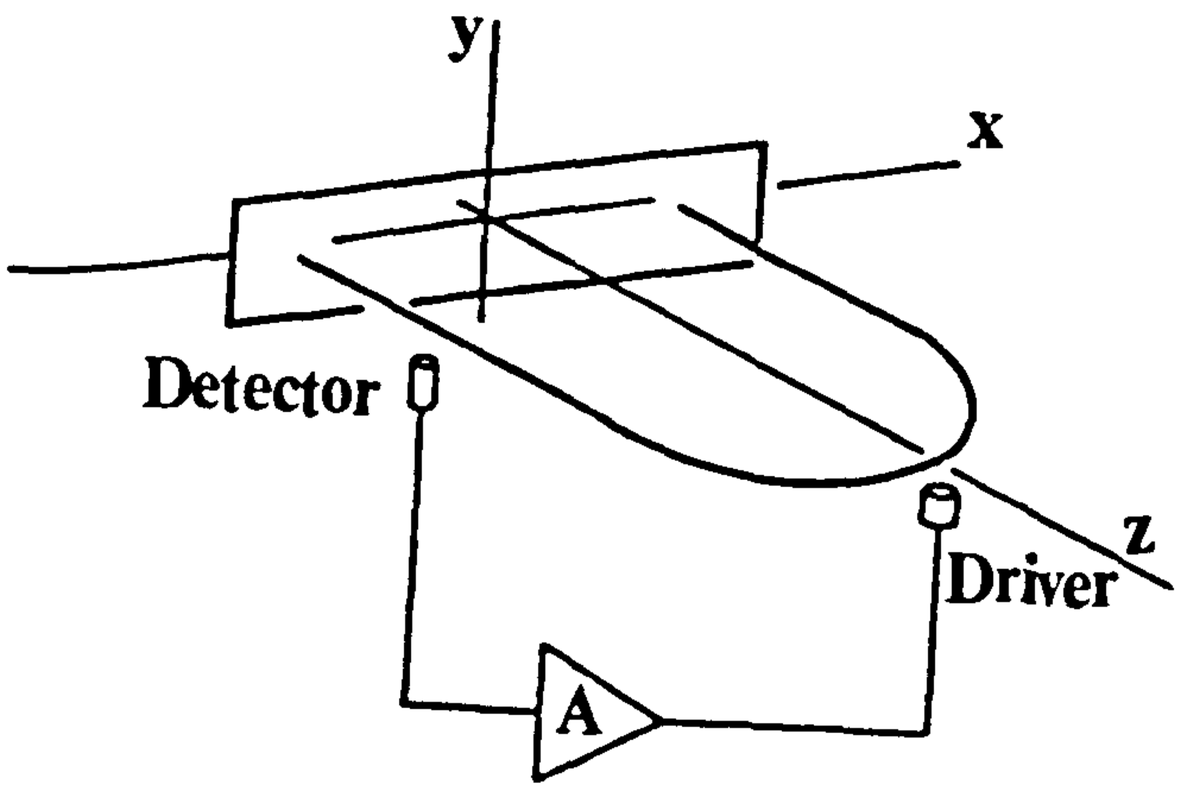

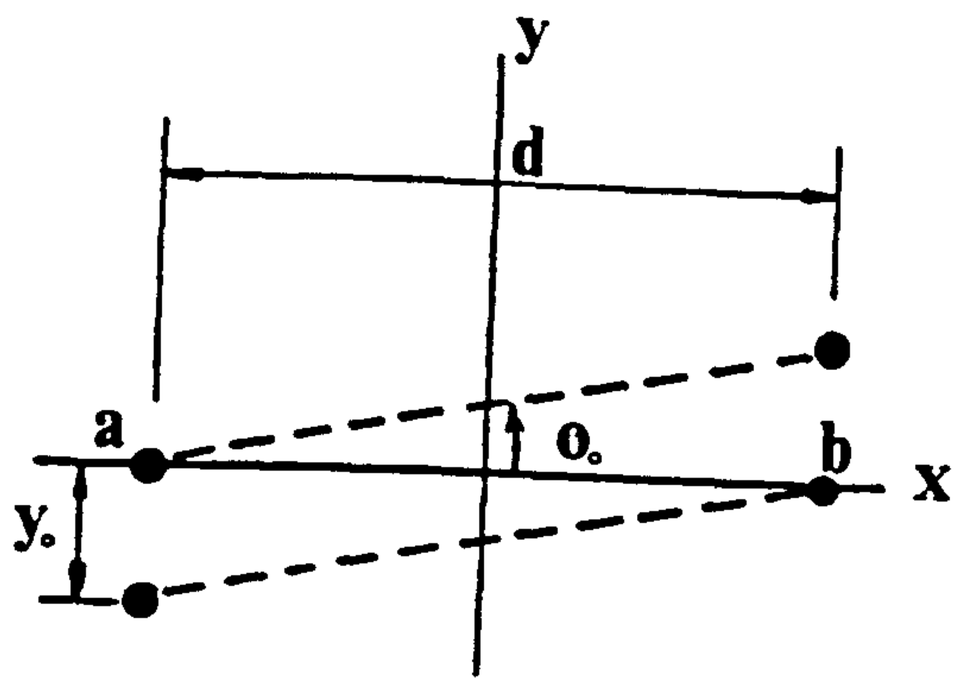

(c) Resonance Excitation

(d) Time Interval Between a and b

Figure 1.7 VIBRATING U-TUBE CORIOLIS MASS FLOWMETER

$$\theta o = \frac{2\rho\Omega_o u \ell A d}{K - I\omega^2} \tag{1.7}$$

The frequency of free twisting vibration is [19]

$$\omega_{nt} = \sqrt{K/I} \tag{1.8}$$

By substituting (1.8) in (1.7) mass flow rate $\dot{m}=\rho uA$ can be related to θ_o by

$$\dot{m} = \frac{K\{1 - (\omega/\omega_{nt})^2\}}{2\Omega_o \ell d}\theta_o \tag{1.9}$$

Equation (1.9) illustrates how the mass flow rate of the fluid can be calculated from a measurement of amplitude Θ_o of twisting.

It is essential to select carefully the drive frequency with respect to the natural frequency of twist mode. This is to ensure adequate signal to noise ratio and the accurate metering of fluids of different density without changing calibration.

According to (1.9), for constant mass flow rate Θ_o can be expressed as

$$\Theta_o = \frac{2\Omega_o \ell d}{K\,\{1 - (\omega/\omega_{nt})^2\}}\ \dot{m} \qquad (1.10)$$

Consequently the Θ_o increases as the two frequencies converge. However, Θ_o can also be increased by increasing the length of the moment arm d and/or decreasing stiffness of the tube. According to equation (1.10) and fig. 1.8 at low driving frequencies, $(\omega/\omega_{nt}) \ll 1$, Θ_o varies linearly with Ω_o and $\dot{m}$ regardless of density [9].

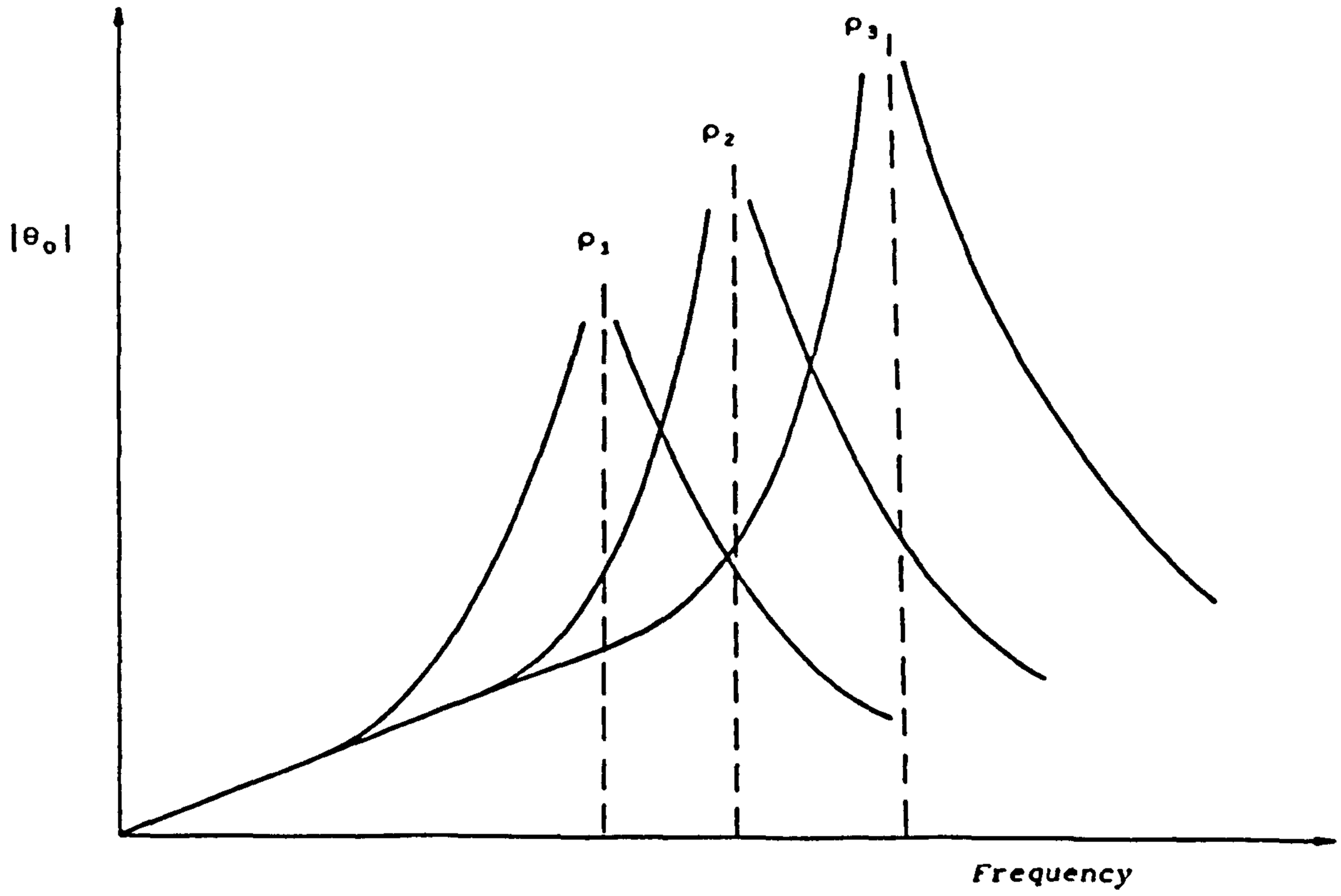

Figure 1.8 DRIVE FREQUENCY VERSUS TWISTING ANGLE FOR DIFFERENT FLUID DENSITIES (from[9])

When the driving frequency approaches the twisting natural frequency, $(\omega/\omega_{nt}) \approx 1$, then a very large increase in twist angle θ_o is obtained. Once the driving frequency becomes much greater than twisting frequency then θ_o reduces inversely with square of frequency. Note that I, and therefore by (1.8), ω_{nt} depends on fluid density. Thus, if the device is driven at a fixed frequency ω (not $\ll \omega_{nt}$) and fixed amplitude Ω_o the sensitivity is depent on fluid density.

Problems associated with fluids of varying density may be eliminated by vibrating the tube at its natural (fundamental) frequency ω_n (for example by using a feedback circuit as shown in Figure 1.7c). The fundamental frequency is less than the twisting natural frequency (1st harmonic) and the ratio (ω_n/ω_{nt}) is now constant for fluids of different density.

Equation (1.10) provides the basic relation between mass flow rate and twist. The mass flow is only proportional to the twisting amplitude θ_o if the angular velocity amplitude Ω_o of the main vibration is a constant. More usefully it is possible to base the flow measurement on the time difference Δt between signals measured at two points (for example a and b (Figure 1.7b)) using optical or electromagnetic detectors.

The y coordinate of point a or b (without flow) is $y = y_o \sin \omega t$ and at t=0 the velocity is $(\dot{y}_o = \omega y_o)$. Under flow conditions a small twist θ_o is present causing a small difference Δt between the times that a and b cross the xz plane as shown in Figure 1.7d. Obviously

$$\Delta t = \frac{\theta_o \, d}{\omega \, y_o} \qquad (1.11)$$

provided $\theta_o d \ll y_o$ and using (1.10), (1.11) and the relation

$$\dot{y}_o = \omega \, y_o \approx - \, \Omega_o \, c \qquad (1.13)$$

the relation between mass flow rate and time difference can be obtained as

$$\dot{m} = \frac{c\,K\,\{\,1 - (\omega/\omega_{nt})^2\}}{2\,\ell\,d^2}\,\Delta t \qquad (1.14)$$

The mass flow rate is therefore independent of the amplitude of main vibration and depends only on geometry, stiffness K and the frequencies ω and ω_{nt} (see appendix A for calculation of stiffness constant (K) and natural frequencies (ω_n and ω_{nt})).

1.5 LITERATURE REVIEW

1.5.1 CORIOLIS MASS FLOWMETER

The general concepts of Coriolis flowmeters can be found in Katys's book [20] which provides the most complete publication on Coriolis flowmeters, giving a review and suggesting basic theories for different Coriolis flowmeters.

Palche [21] reported on an early single tube Coriolis flowmeter, manufactured by Micromotion Inc., giving the basic relation between mass flow rate and phase difference. Gast and Furness [22] reviewed different oscillatory mass flowmeters and the progress made in their development.

Tullis and Smith [23] produced experimental data on three different sizes of coriolis flowmeter (Micromotion Inc.) in steady and unsteady water flow, limited data on steady air flow and two-phase air-water flow tests. They concluded that the meters have an exceptionally wide range and accuracy for water tests. For air measurements they suggested design modification, including length and wall thickness of the tube, in order to obtain similar accuracies for water flow. In two-phase flow they showed that the smaller meters were more suitable. However they stated that the ability of the meter, in larger sizes, to measure two-phase flows remains an unanswered question. Camponovo and Gerlich [24] summarized their experiences using the early single tube

Coriolis flowmeter (Micromotion Inc.) in a semi-batch process. They identified the effect of temperature and humidity on zero drift.

Altfillisch et al [25,26,27] attempted to improve the performance of an early rotatory Coriolis-gyroscopic flowmeter in the measurement of two-phase (gas-liquid) mixtures. Since the heavy particles of the fluid move under centrifugal force outwardly while the lighter particles move inwardly (toward the rotating axis) separation occurs. Altfillisch et al employed three different geometrical alterations to eliminate accumulation of light particles of fluid in the flowmeter. Druzhkova [28] studied theoretically the damping effect of gas-liquid mixtures on a cantilever Coriolis flowmeter. He introduced a non-dimensional parameter representing the damping coefficient which depends on relative vibrational velocities, density and viscosity ratios and other physical characteristics of the components. Druzhkova et al [29] designed a cantilever Coriolis flowmeter for measuring two-phase flows. They developed an expression for the coefficient of attenuation and the natural frequency of oscillation. The result of laboratory testing of the flowmeter showed that an error of 10% existed in the approximate theory. Tucker and Hayes [30,31] extensively studied the performance of a so called vibrating pendulum two-phase flowmeter designed by Rivkia et al [32]. They summarized an analytical technique to assess the error in oil flow rate prediction for any given oil well fluid mixture condition. Grumski and Bajura [33] have experimentally studied the effect of two-phase (gas-liquid) mixtures on two Coriolis flowmeters (Micromotion Inc.). A series of air-water and air-glycol tests were conducted involving different flow conditions and various mounting and piping configurations. They showed the toleration and failure of the flowmeters with respect to void fraction.

Baucum [34] investigated the feasibility of Coriolis flowmeters for measuring multi-phase flow of pulverized coal/gas mixtures. The flowmeter accurately measured dense phase coal flows on a continuous basis. In less dense flows, the flowmeter behaved eratically. Indeed the work by Mathur and Klinzig [35] and Kleizen and Van Brakel [36] elicited the same results. Domnick et al [37] presented a method to measure simultaneously the individual mass and volume flow rates of

particulate two-phase (solid-liquid) mixtures using Coriolis and magnetic flowmeters in series. They stated that the Coriolis flowmeter is able to measure the total mass flow rate provided the solid particles follow the oscillation.

Very recently a number of problems were investigated by several authors such as Wagner [38] who outlined the effects of tube design and application characteristics on Coriolis flowmeters. He highlighted many effects including tube geometry, stress corrosion cracking, viscosity, pressure drop, two-phase flows, external vibration and zero offset. Hemp [39] developed an analytical expression for a weight vector to analyse velocity profile effects in Coriolis flowmeters. He also indicated how the reciprocity principle can be applied to remove zero drift due to changes in the physical state of the meter. Hemp and Sultan [40] reviewed some recent developments in the theory of the Coriolis flowmeter including; the use of beam theory for computing the frequency and sensitivity of the meter, the concept of reciprocal operation for eliminating zero drift, a basis for the analysis of velocity profile effects, and finally a simple theory for prediction of the effect of a suspension of small bubbles or particles. Keita [41] modelled the straight tube Coriolis flowmeter using the finite element method (Discrete Mass Model) and introduced a damping factor and non-symmetrical elastic end conditions in order to simulate the effect of zero drift.

Krakar [42] discussed the performance of the Coriolis flowmeter used as a density meter, giving a mathematical theory and details of measurement of a variety of dependent variables using microprocessor technology. Birker [43] demonstrated the basic theory and performance of a straight tube Coriolis flowmeter (manufactured by Danfoss Ltd.) pointing out the dependence of modulus of elasticity of the tube material on temperature. Kiehl and Gartner [44] studied the interaction problem between two Coriolis flowmeters (manufactured by Krohnë Ltd.) in one line. They stated that this interaction tends to reduce measurement accuracy and repeatability. They provided installation guidelines to overcome the problem. Finally, an extensive experimental investigation was undertaken by Frankvoort and Nederlof [45] on a straight tube Coriolis flowmeter (manufactured by

Endress and Hauser Ltd). The work discussed the problems that can arise with zero drift, effects of density, viscosity, temperature, pressure of the fluid, external vibration and installation. The results showed some influence of the temperature and the static pressure, a very small effect of viscosity and density, more effect of mechanical conditions of the installation and a very large effect of zero drift.

1.5.2 FLOW INDUCED VIBRATION

Until recently there has been no detailed modelling of the Coriolis mass flowmeter (at least not in the public domain). There is however considerable literature on the dynamics of tubes conveying fluids, mostly in connection with the study of flow induced vibrations [46,47]. The mathematics of flow induced vibrations has much in common with that of the change in external vibrations due to flow - the subject of interest in the present thesis.

The dynamics of tubes conveying fluid has been studied extensively by several authors since the 1950's. The principal aims of those studies were to investigate the effects of the fluid velocity, pressure, density, tube geometries, and boundary conditions on the natural frequency and the stability of the pipe systems.

It appears that the description of the vibration of tubes conveying fluid was first attempted by Ashley and Haviland [48]. Their model analysed the bending vibration of a simply supported pipe behaving as a beam. Housner [49] derived the equations of motion for both free and forced vibration from Hamilton's principle and provided an analytical solution. Long [50] studied theoretically and experimentally the free transverse vibrations for a single span tube containing a flowing fluid. The experimental results agreed reasonably well with his power series approximate solution. Benjamin [51] used the Lagrangian approach to analyse systems of articulated pipes conveying fluid for different boundary conditions. He pointed

out the fluid-pipe energy balance and showed that pipe systems are conservative for fixed conditions and non-conservative for free end conditions. Gregory and Paidoussis [52] analysed the case of tubular cantilevers conveying fluid. They used a numerical product solution to obtain the complex frequency of the system. Stein and Tobriner [53] considered the effects of foundation modulus and internal pressure on the dynamic stability, frequency response and wave propagation characteristics of undamped systems. Hill and Swanson [54] investigated the effects of lumped masses on the stability of tubes conveying fluid.

Unny et al [55] studied the hydroelastic instability of a uniformly curved pipe containing a flowing fluid. The equation of in-plane motion was derived using Hamilton's principle. Chen [56] derived the equation of in-plane motion from the equilibrium of a tube/fluid element and defined the natural frequency and the boundary separating stable and unstable regions. Chen [57] used Hamilton's principle to derive both in-plane and out-of-plane equations of motion. Hill and Davis [58] analysed the effect of inertia forces on the vibration and stability of curved, clamped, fluid conveying tubes by the finite-element technique. Numerical results were presented for circular arc S, L and Spiral configurations. The longitudinal torsional and transverse equations of motion were formulated by Doll and Mote [59] for curved and twisted cylinders transporting fluid, the finite element method was used in this analysis. Kohli and Nakra [60] reported a simplified finite element analysis in which straight beam elements were used to determine the natural frequencies of vibration of straight and curved tubes conveying fluid. Chen and Fan [61] presented finite element procedure for the stability analysis of elastically supported pipes conveying fluid, considering the effects of lumped masses, fluid pressure and friction.

Hara [62] analysed theoretically the effect of two-phase (gas-liquid) flows in inducing vibrations in piping systems. He concluded that the mechanism of excitation is parametric due to a periodic change of the mass of the system. Hiramatsu et al [63] studied theoretically and experimentlly two-phase (gas-liquid) flow induced vibration. The theoretical analysis used the transfer matrix method for vibration

responses of the system excited by the forces of a travelling liquid piston and the momentum change of two-phase flow. Experiments were carried out with a horizontally supported U-pipe conveying an air-water two-phase flow. The comparison between theory and experiments showed positive quantitative agreement

1.6 THE PRESENT WORK

1.6.1 Objectives

The objectives of this work can be summarized as follows

(i) To give details of a method of modelling the Coriolis mass flowmeter using beam theory.

(ii) To predict the optimum measuring distances between the detectors.

(iii) To predict the effect of a dilute suspension of small bubbles or particles in the liquid on Coriolis mass flowmeters.

(iv) To conduct an experimental study to check the validity of the theoretical models.

1.6.2 Layout Of This Thesis

Chapter One describes the Coriolis mass flowmeter giving the basic theory. A review of the previous work, which is of a particular relevance to this thesis, has been made.

Chapter Two contains details of a method of modelling Coriolis mass flowmeter using beam theory. The general tube geometry is approximated by means of a series of straight and circular tubes.

In ***Chapter Three*** an improved model of Coriolis mass flowmeter is considered. The effect of brace bars and added masses (of the drive and detectors) are taken into account.

In ***Chapter Four*** a method is suggested for predicting the optimum positions of the detectors for phase difference measurement.

In ***Chapter Five*** single-phase flow experiments were conducted on two flowmeters (i) U-shape commercial Coriolis mass flowmeter and (ii) straight tube experimental Coriolis flowmeter.

In ***Chapter Six*** a method is given for predicting the effect of a dilute suspension of small bubbles or particles in the liquid on a Coriolis mass flowmeter. An attempt is also made to determine experimentally the feasibility of using a Coriolis mass flowmeter for measuring the total mass flow of bubbly (water-nitrogen) flows.

In ***Chapter Seven*** frequency and time delay predictions for both commercial and experimental flowmeters were compared with experimental results. The predicted values of optimum measuring positions and the effect of gas bubbles were also compared with corresponding experimental data.

Chapter Eight contains the conclusions of the thesis and some suggestions for further work.

CHAPTER TWO

THEORETICAL ANALYSIS

CHAPTER TWO

THEORETICAL ANALYSIS

In this chapter details of a method of modelling the Coriolis mass flowmeter are given. The method assumes the tube is made of straight and circular lengths joined together. A general tube geometry is then approximated by means of a series of straight and circular tubes; rigidly connected to each other at their ends. The solution of the basic equations governing displacement and twist is reduced to a problem of solving a set of algebraic linear equations and a computer program is written to solve these equations and the transcendental characteristic equation for the frequency.

2.1 VIBRATION OF CIRCULAR TUBES

An account of the theory of linear vibrations of circular rods (ie thin rings or portions of thin rings) of circular cross-section is given in section 293 of Love [64]. Ojalvo [65] analysed the three-dimensional linear motion of an elastic ring of rectangular cross-section using Hamilton's principle. The following sections provide a simplified derivation of the equations of motion of circular tubes.

2.1.1 Displacements, Rotations, Forces and Couples

In its normal unstrained state let the tube lie so its centre line is in the xy plane (Figure 2.1a) forming there a circular arc with centre of curvature at the origin and radius a. Let the cross-section be as shown in Figure 2.1b, r being the mean radius of the tube and t the tube wall thickness (assumed small compared with r). The area A of

the tube material section, the second moment I of area about a diameter and the polar moment J of area are given by

$$A = 2\pi rt \ , \ I = \pi r^3 t \ , \ J = 2\pi r^3 t \qquad (2.1)$$

where $t \ll r$.

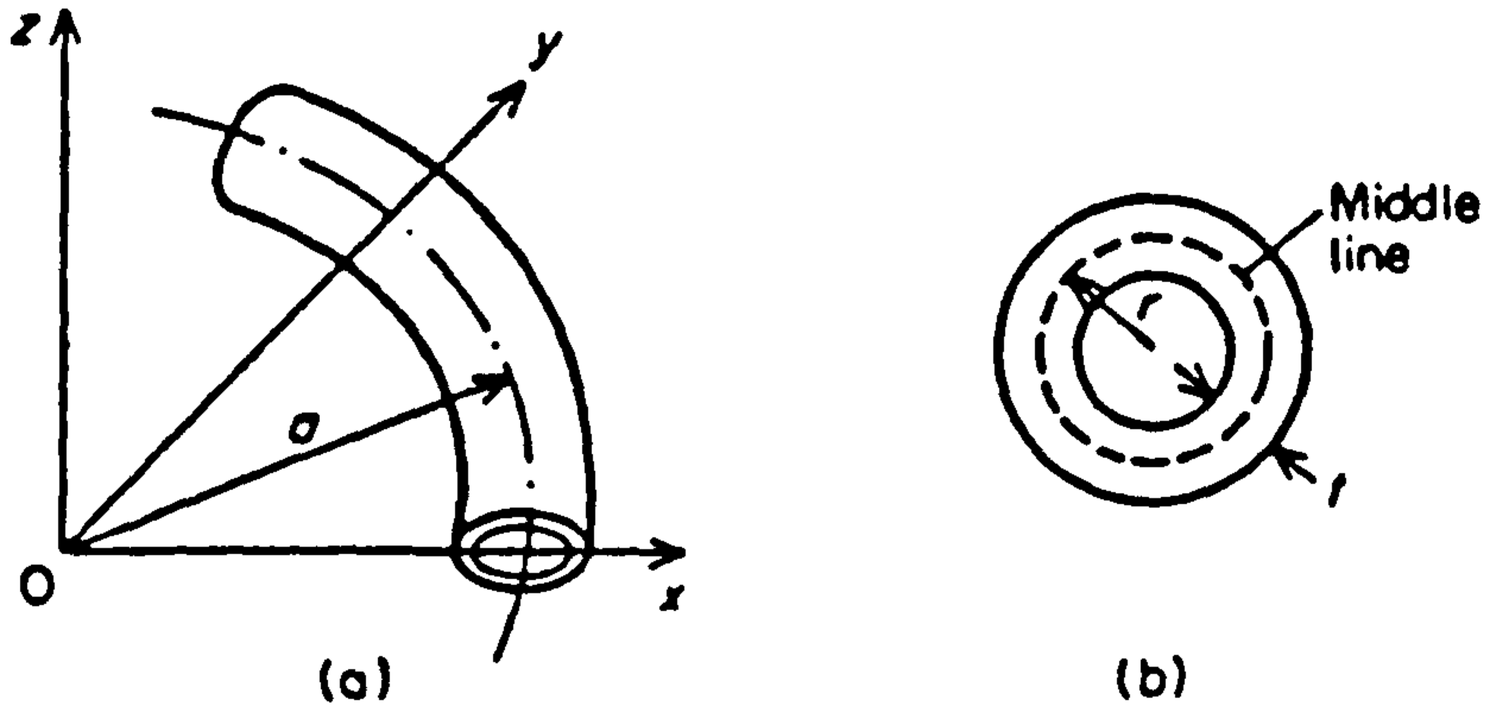

Figure 2.1 CIRCULAR TUBE, CO-ORDINATES AND DIMENSIONS

Let the components of displacement be u, v, w in the directions shown in Figure 2.2a . The vector components of rotation of a section are as shown in Figure 2.2b . Rotations in the bi-normal (z) direction and in the principle direction are directly related to u, v, w or their derivatives with respect to the arc length s as indicated in Figure 2.2b . The rotation ϕ in the tangential direction is not directly related to the displacements. The longitudinal strain of the centre line, ie $\partial w/\partial s - u/a$, is , in accordance with beam theory, assumed to be zero.

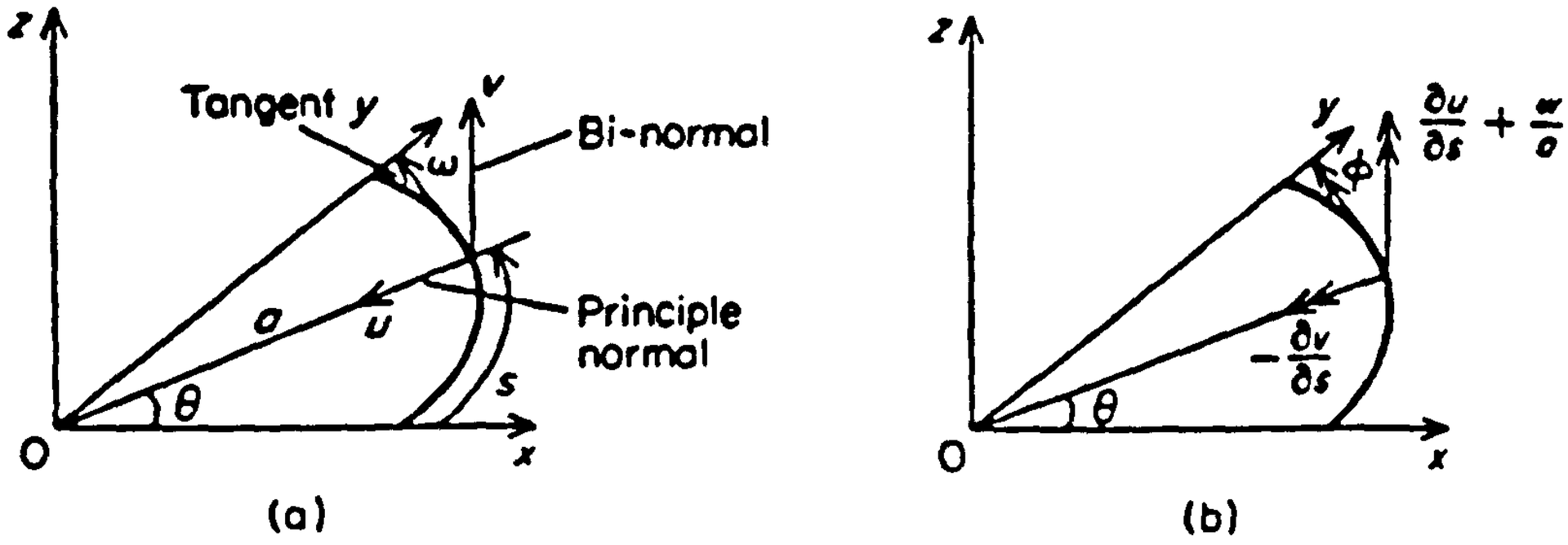

Figure 2.2 NOTATION FOR DISPLACEMENTS AND ROTATIONS

The notation for internal forces and couples is as shown in Figure 2.3 . The couples M, M' and T are related to the amount of local bending and twisting.

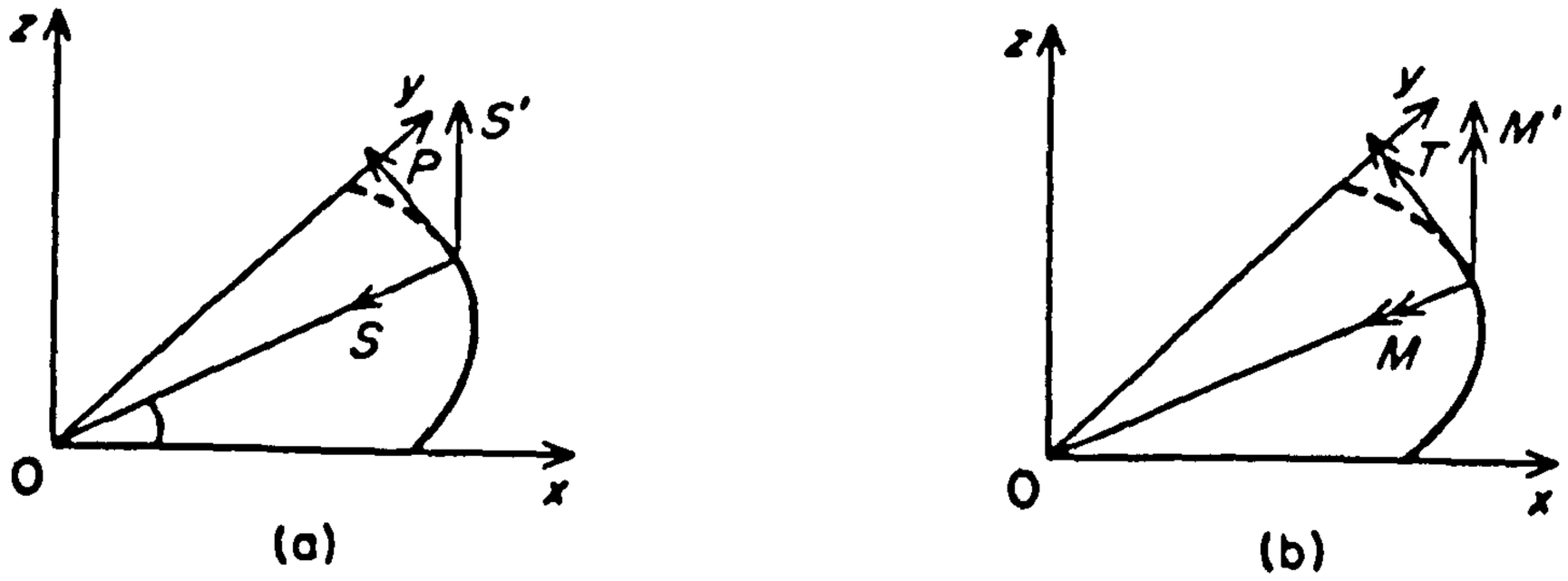

Figure 2.3 (a)INTERNAL FORCES (b)COUPLES ACTING ON THE SOLID LINE PART OF THE TUBE

Force equilibrium on an element of tube shown in Figure 2.4a results in

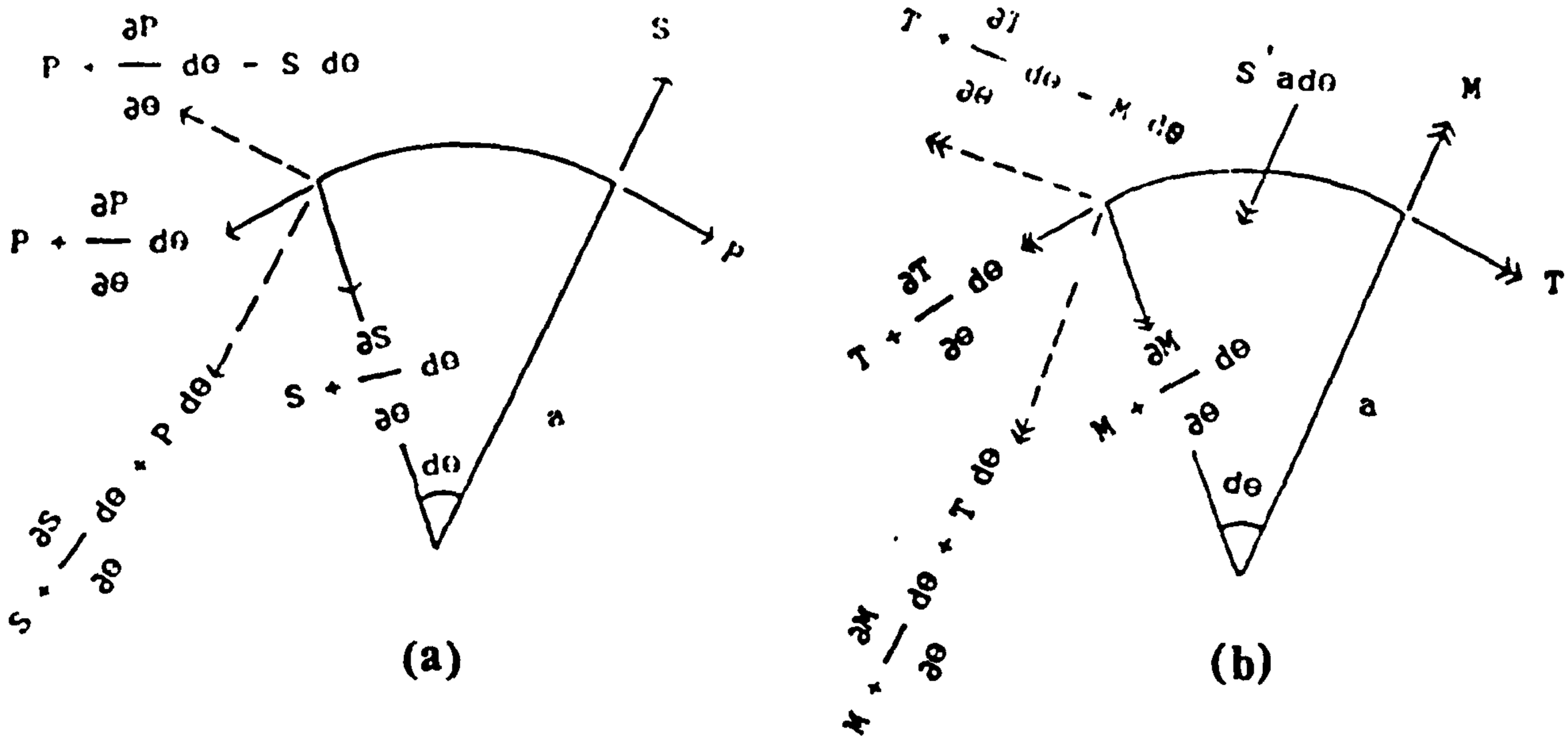

Figure 2.4 (a)FORCE EQUILIBRIUM (b)MOMENT EQULIBRIUM

$$\left.\begin{aligned} \frac{\partial S}{\partial \theta} + P &= (\rho A a)\,\frac{\partial^2 u}{\partial t^2} \\ \frac{\partial P}{\partial \theta} - S &= (\rho A a)\,\frac{\partial^2 w}{\partial t^2} \\ \frac{\partial S'}{\partial \theta} &= (\rho A a)\,\frac{\partial^2 v}{\partial t^2} \end{aligned}\right\} \qquad (2.2)$$

Moment equilibrium (Figure 2.4b) requires that

$$\left.\begin{aligned} \frac{\partial M}{\partial \theta} + T - S'a &= (\rho I a)\,\frac{\partial^2}{\partial t^2}\left(-\frac{\partial v}{a\partial \theta}\right) \\ \frac{\partial T}{\partial \theta} - M &= (\rho J a)\,\frac{\partial^2 \phi}{\partial t^2} \\ \frac{\partial M'}{\partial \theta} + Sa &= (\rho I a)\,\frac{\partial^2}{\partial t^2}\left(\frac{\partial u}{a\partial \theta} + \frac{w}{a}\right) \end{aligned}\right\} \qquad (2.3)$$

whilst moment-displacement and/or twist relations require calculating the rate of change of curvature and twist. Figure 2.5 shows absolute rotations of the tube element. The rate of change of the curvature and twist required is the relative rotation of the ends divided by $ad\theta$. The change in curvature in the normal plane and the in-plane and the twist are respectively

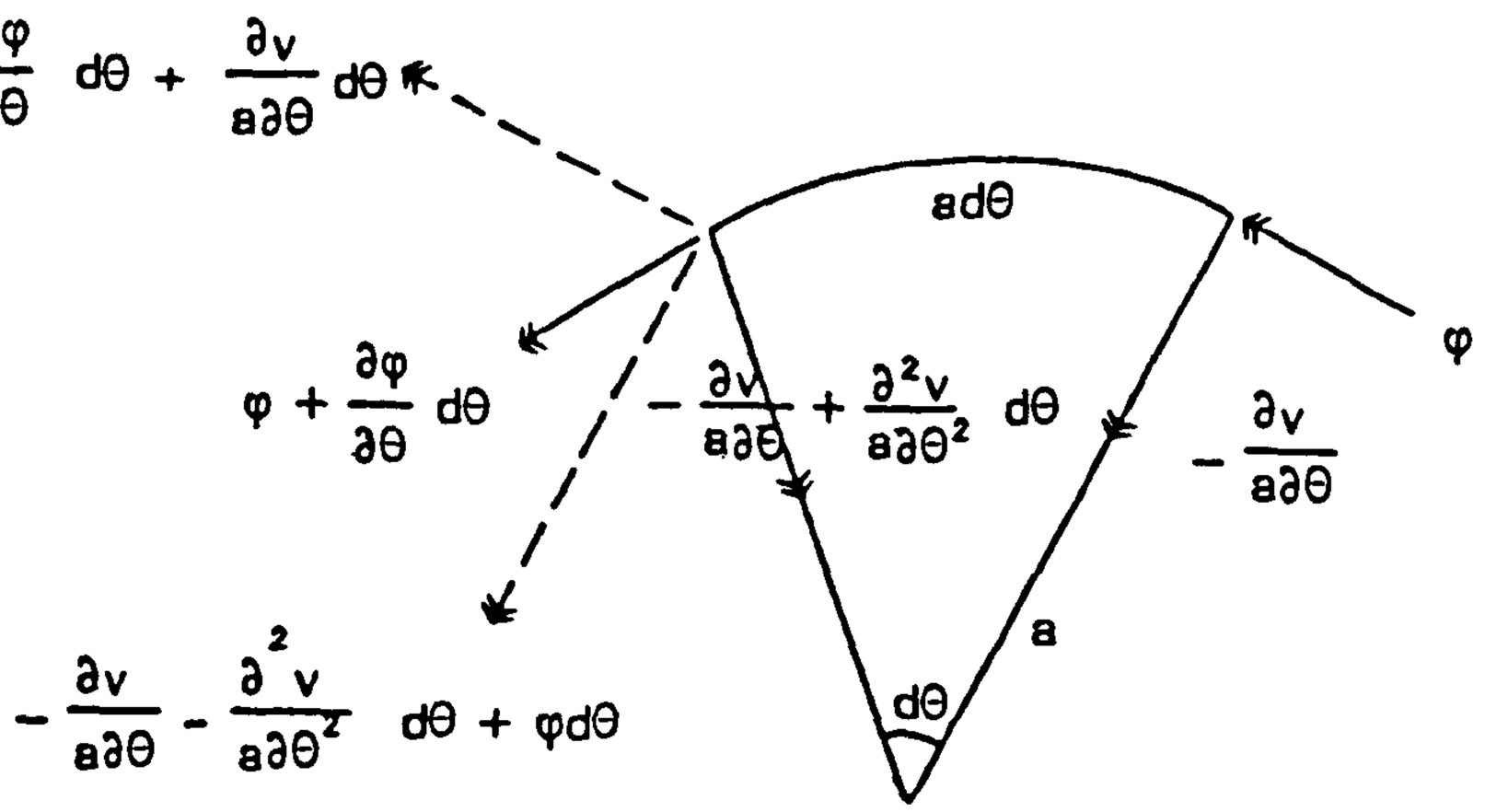

Figure 2.5 THE RATE OF CHANGE IN ROTATION

$$\left.\begin{aligned} &-\frac{\partial^2 v}{a^2 \partial\theta^2}+\frac{\Phi}{a}\\ &\frac{\partial^2 u}{a^2 \partial\theta^2}+\frac{\partial w}{a^2 \partial\theta}\\ \text{and}\\ &\frac{\partial \Phi}{a\partial\theta}+\frac{\partial v}{a^2\partial\theta} \end{aligned}\right\} \qquad (2.4)$$

The couples M, M' and T are related to these by simple theory of bending and torsion [66] neglecting the shear deformation

$$\frac{M}{I}=\frac{E}{R} \quad \text{and} \quad \frac{T}{J}=G\Phi \qquad (2.5)$$

which give

$$\left.\begin{aligned} M &= EI\left(-\frac{\partial^2 v}{\partial s^2}+\frac{\Phi}{a}\right)\\ M' &= EI\left(\frac{\partial^2 u}{\partial s^2}+\frac{1}{a}\frac{\partial w}{\partial s}\right)\\ T &= GJ\left(\frac{\partial \Phi}{\partial s}+\frac{1}{a}\frac{\partial v}{\partial s}\right) \end{aligned}\right\} \qquad (2.6)$$

Where E is Young's modulus, G is shear modulus, R is radius of curvature and Φ is local twist angle per unit length.

2.1.2 Equations of Motion

Since r<a is assumed and since interest lies only in the lower frequencies of vibration it is possible to neglect the rotational inertia of any element of length of the tube. Under these conditions

equations (2.3) become

$$\left.\begin{aligned} &\frac{\partial M}{\partial s} + \frac{1}{a} T - S' = 0 \\ &\frac{\partial M'}{\partial s} + S = 0 \\ &\frac{\partial T}{\partial s} - \frac{1}{a} M = 0 \end{aligned}\right\} \qquad (2.7)$$

Substituting for M, M' and T in (2.7) gives the equations of motion of the circular tube in terms of u, v, w and ϕ as follows

$$\left.\begin{aligned} &\frac{\partial^2}{\partial s^2}\left(\frac{\partial^2}{\partial s^2} + \frac{1}{a^2}\right)\left(\frac{\partial u}{\partial s} + \frac{w}{a}\right) = \frac{\rho A}{EI}\frac{\partial^2}{\partial t^2}\left(\frac{w}{a} - \frac{\partial u}{\partial s}\right) \\ &\frac{u}{a} = \frac{\partial w}{\partial s} \end{aligned}\right\} \qquad (2.8)$$

and

$$\left.\begin{aligned} &\frac{\partial^2}{\partial s^2}\left(\frac{GJ}{EI}\frac{v}{a^2} - \frac{\partial^2 v}{\partial s^2}\right) + \frac{1}{a}\left(1 + \frac{GJ}{EI}\right)\frac{\partial^2 \phi}{\partial s^2} = \frac{\rho A}{EI}\frac{\partial^2 v}{\partial t^2} \\ &\frac{1}{a}\left(1 + \frac{GJ}{EI}\right)\frac{\partial^2 v}{\partial s^2} + \left(\frac{GJ}{EI}\frac{\partial^2}{\partial s^2} - \frac{1}{a^2}\right)\phi = 0 \end{aligned}\right\} \qquad (2.9)$$

The equations of motion and relations for a straight tube follow from the equations of the circular tube by simply letting $a \to \infty$.

2.2 *BOUNDARY CONDITIONS*

Let s represent the distance measured along the length of a tube whether straight or circular and let the same convention for directions of displacements, forces and couples in relation to the

direction of increasing s (Figures 2.2 and 2.3) apply for straight and circular tubes.

At a fixed end the boundary conditions are thus always

$$u = w = \frac{\partial u}{\partial s} + \frac{w}{a} = 0 \qquad (2.10)$$

and

$$v = \phi = -\frac{\partial v}{\partial s} = 0 \qquad (2.11)$$

At a junction between two tubes (both in one and the same plane) the following apply

$$u,\ w,\ \frac{\partial u}{\partial s} + \frac{w}{a},\ P,\ S \text{ and } M' \text{ are continuous} \qquad (2.12)$$

and

$$v,\ \phi,\ -\frac{\partial v}{\partial s},\ S',\ M \text{ and } T \text{ are continuous} \qquad (2.13)$$

Note that the differential equations of motion and boundary conditions separate into 'in-plane' and 'out-of-plane' cases. This allows independent mathematical treatment of these two types of vibration. In the present work interest is in the out-of-plane vibrations goverened by equations (2.9), the first and last of (2.7) and equations (2.11) and (2.13).

2.3 MODELLING OF THE FLOWMETER

In this section the extra inertia terms, needed to account for the presence of flowing fluid in the tube, will be derived. The general case of a tube geometry (made up of three straight lengths and two circular lengths) is then treated. Thus various shapes of meters

(Figure 1.3) can be modelled.

2.3.1 *Inertia Terms Due to the Fluid*

When the tube is filled with fluid the mass M_f of fluid per unit length of tube adds to the mass M_t ($=\rho A$) of the tube itself. If the fluid is at rest the term ρA in equation (2.9) (and of course in the other equations of motion) must be replaced by M_t+M_f. This is because the local acceleration of fluid is identical to that of the tube.
Suppose the fluid flows with mean velocity U (=total volume flowrate divided by cross-sectional area of tube interior) in the direction of increasing s as shown in Figure 2.6 .

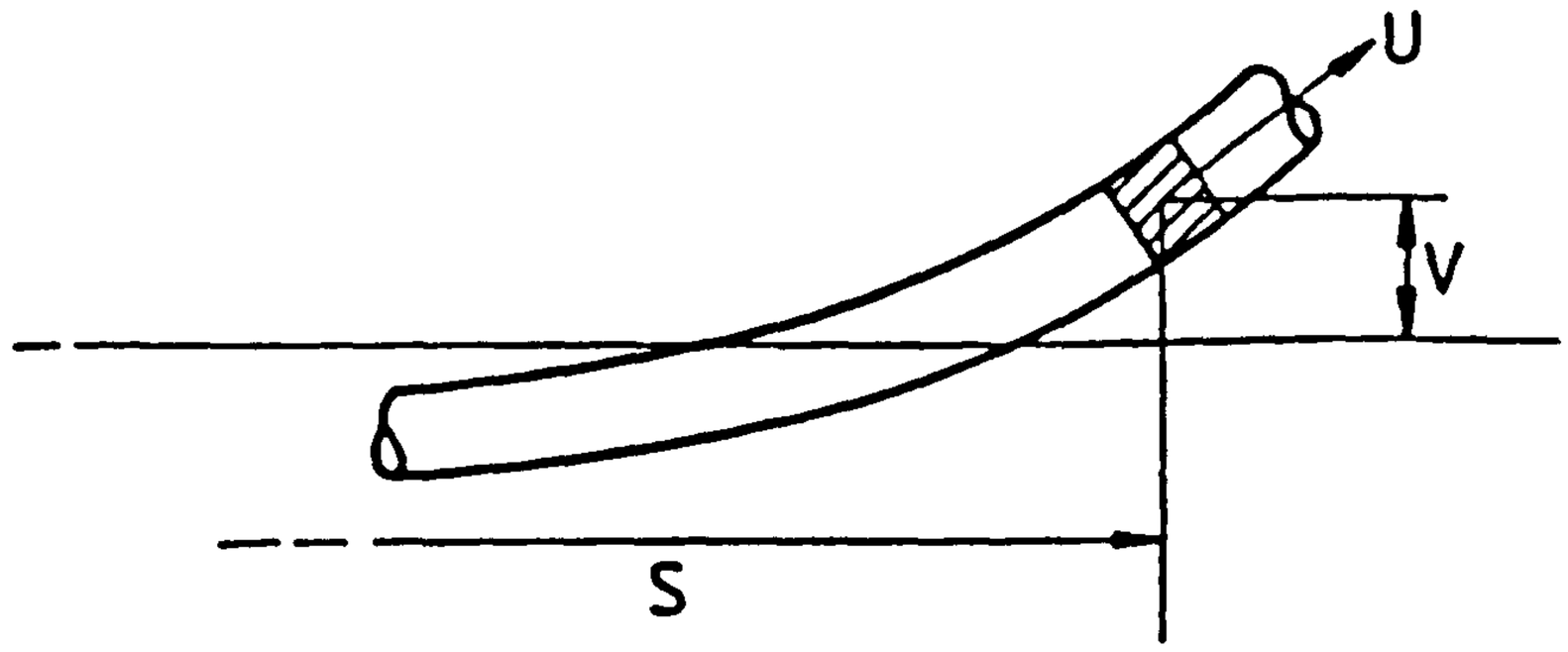

Figure 2.6 VIBRATION OF A TUBE CONTAINING FLOWING FLUID

Let us assume effects of flow are adequately modelled by considering a flat velocity profile of speed U relative to the tube. The total velocity of a fluid element in the bi-normal direction is dv/dt, where v is the displacement as in Figure 2.2a and d/dt is the time derivative with respect to the motion. Now

$$\frac{dv}{dt} = \frac{\partial v}{\partial s}\frac{\partial s}{\partial t} + \frac{\partial v}{\partial t} = \frac{\partial v}{\partial s}U + \frac{\partial v}{\partial t} \qquad (2.14)$$

This is a function of s and t. The acceleration of a element in the bi-normal direction is therefore

$$\frac{d^2v}{dt^2} = \frac{\partial^2 v}{\partial s^2} U^2 + 2 \frac{\partial^2 v}{\partial s \partial t} U + \frac{\partial^2 v}{\partial t^2} + \frac{\partial U}{\partial t} \frac{\partial v}{\partial s} \qquad (2.15)$$

Assuming steady-state flow the last term can be omitted from the above equation. The total inertia term for out-of-plane vibration is thus

$$M_t \frac{\partial^2 v}{\partial t^2} + M_f \left(U^2 \frac{\partial^2 v}{\partial s^2} + 2U \frac{\partial^2 v}{\partial s \partial t} + \frac{\partial^2 v}{\partial t^2} \right) \qquad (2.16)$$

This must replace the factor $\rho A \, \partial^2 v/\partial t^2$ on the R.H.S of the first of equation (2.9).

The three terms in the brackets of (2.16) are, in order, associated with centripetal, Coriolis and ordinary inertia forces. The second term involves a first derivative with respect to time and might therefore be regarded as causing a damping or amplifying effect. However the total work done by this 'force' around the whole length of the tube is zero as can be seen as follows. The rate of work is

$$\dot{W} = M_f \, 2U \int \frac{\partial^2 v}{\partial s \partial t} \frac{\partial v}{\partial t} \, ds \qquad (2.17)$$

where the integral is conducted along the whole length of the tube between its clamped ends.

Since

$$\frac{\partial v}{\partial s \partial t} \frac{\partial v}{\partial t} = \frac{1}{2} \frac{\partial}{\partial s} \left(\frac{\partial v}{\partial t} \right)^2$$

and since v is continuous at junctions and zero at the clamped ends it can be seen that $\dot{W}=0$. It is assumed that the presence of fluid causes no rotational inertia. This is in keeping with neglect of rotational inertia of the tube itself.

Account might be taken of fluid pressure, at least in as far as this

gives rise to stresses in the tube, which contribute to the force on elements of the tube during the motion. In this thesis, effects due to fluid pressure are neglected as they are usually small in practice.

2.3.2 *Validity of Flat Velocity Profile Assumption*

The assumption that the flat velocity profile is adequate for modelling the effect of flow is open to question. Flat profiles (of ordinary fluids) are actually present only in straight tubes at very high Reynolds numbers. Upstream fittings (such as bends and valves), lower Reynolds numbers and the curved form of the flowmeter tubes themselves can all cause deviation from a flat profile.

It is expected, however, that in flowmeters made of tubes whose diameter is small compared with their lengths and their radii of curvature (and this corresponds to the beam theory approach here adopted) velocity profile effects are small. This follows from the fact that the velocity components can change only slowly with distance along the tube and can be regarded as independent of axial distance over short lengths of the tube. The inertia term due to fluid in an element of length of tube arises from the acceleration of the centre of gravity of the fluid element. Since the velocity field in the element can be regarded as independent of axial distance, this centre of gravity moves along the tube axis with the mean speed U as can be easily shown. Hence the above derivation of (2.16) holds true for any velocity distribution likely to be present in the relatively narrow tubes. This includes swirling flow distributions and/or flows with axial flow component profiles of any shape, as long as these change only gradually along the length of the tube.

At first glance a swirling flow appears to change the magnitude of Coriolis forces. In fact, swirling flow generates a secondary gyroscopic effect in the plane perpendicular to the plane of main motion as shown in Figure 2.7a . This will not contribute to the Coriolis forces generated in the direction of main motion, assuming perfect isolation between in and out-of-plane motions of the tube. For axial non-uniform flow component profiles (Figure 2.7b) a possible

effect seems to be a twisting motion, which contributes (through viscosity) to the main out-of-plane motion in curved tube flowmeters due to the nature of the coupled bending-twisting motion of such systems.

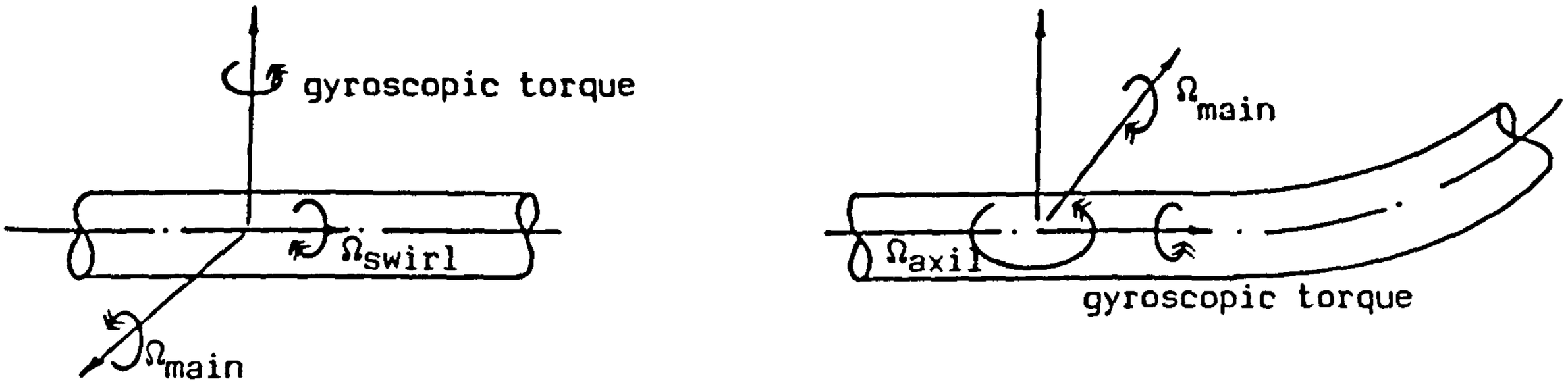

Figure 2.7 (a)SWIRLING FLOW (b)NON-UNIFORM AXIAL FLOW

In reality, velocity profile can slightly affect the calibration factors of Coriolis mass flowmeters. The only published mention of this effect is a brief note by Katys [20]. He reports that an experimental study shows effects of secondary flow (or relative motion of individual particles) to be present in a Coriolis flowmeter of T-tube configuration. Katys concludes that these effects are largest in short tube meters and are negligible for tube length to diameter ratios greater than or equal to 10.

2.3.3 Equations for the General Tube Geometry

For the general tube geometry (S-tube configuration) dimensions are defined as in Figure 2.8 , taking the origin for s at one of the fixed ends.

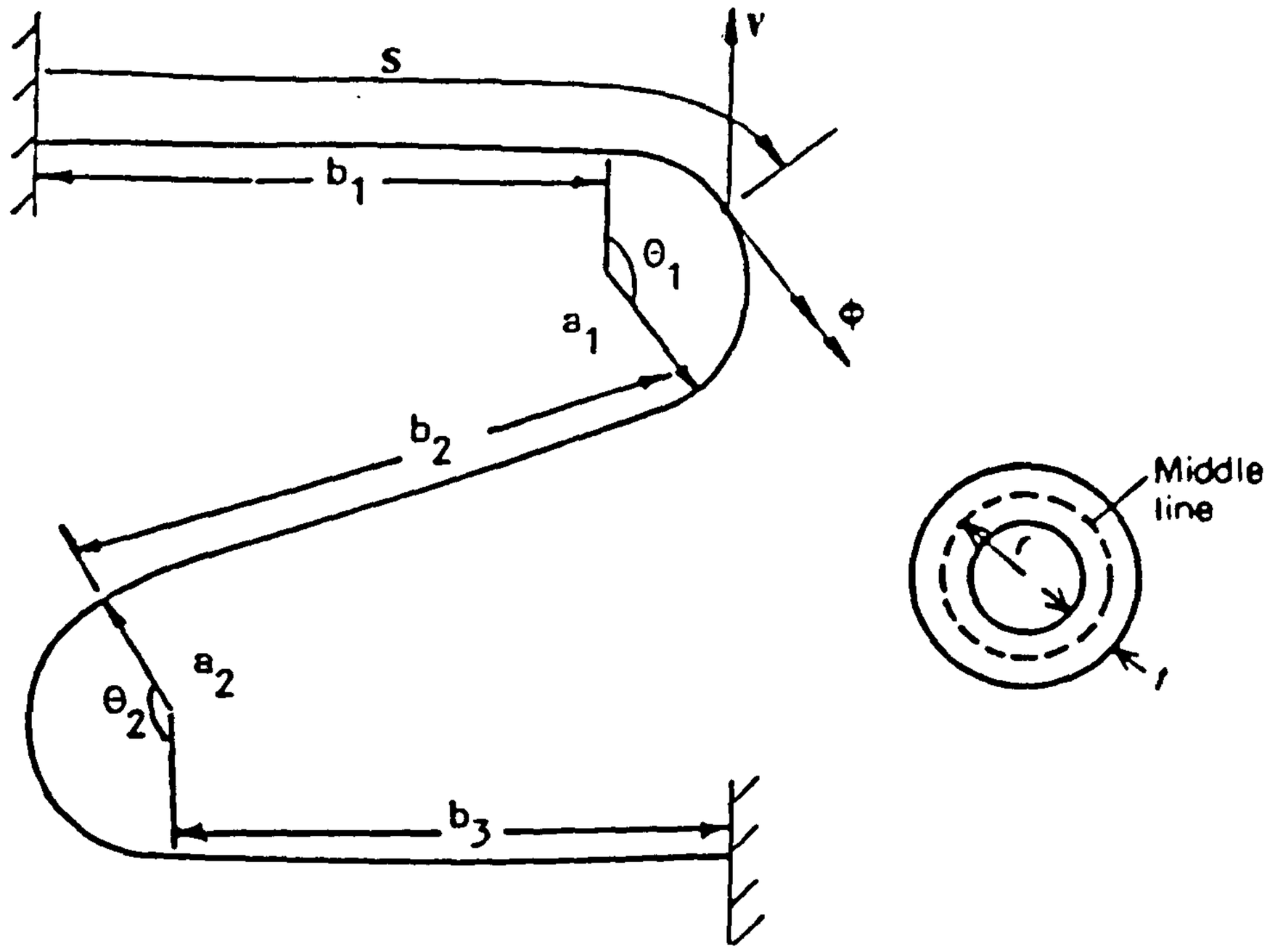

Figure 2.8 MODEL OF THE CORIOLIS MASS FLOWMETER

For the straight lengths of tube the differential equations are (2.9) with $a \to \infty$ and with the full inertia terms (2.16). These are

$$\left.\begin{aligned} &\frac{\partial^4 v^*}{\partial s^4} + 2\frac{M_f}{EI}U\frac{\partial^2 v^*}{\partial s \partial t} + \frac{M_f}{EI}U^2\frac{\partial^2 v^*}{\partial s^2} + \frac{M_f + M_t}{EI}\frac{\partial^2 v^*}{\partial t^2} = 0 \\ &\frac{\partial^2 o^*}{\partial s^2} = 0 \end{aligned}\right\} \quad (2.18)$$

Here the asterisk denotes quantities pertaining only to straight lengths. For curved lengths the differential equations are the full equations (2.9) with full inertia terms (2.16), ie

$$\left.\begin{aligned}
&\frac{\partial^4 v}{\partial s^4} - \frac{GJ}{EIa}\frac{\partial^2 v}{\partial s^2} - \frac{1+\frac{GJ}{EI}}{a}\frac{\partial^2 \phi}{\partial s^2} + 2\frac{M_f}{EI}U\frac{\partial^2 v}{\partial s \partial t} + \frac{M_f}{EI}U^2\frac{\partial^2 v}{\partial s^2} \\
&\qquad + \frac{M_f + M_t}{EI}\frac{\partial^2 v}{\partial t^2} = 0 \\
&\frac{\partial^2 \phi}{\partial s^2} - \frac{EI}{a^2 GJ}\phi + \frac{1}{a}\left(1+\frac{EI}{GJ}\right)\frac{\partial^2 v}{\partial s^2} = 0
\end{aligned}\right\} \quad (2.19)$$

Equations (2.19) are equivalent to equations derived by Chen [57] using Hamilton's principle.

The boundary conditions (2.11) and (2.13) give

$$v^* = \frac{\partial v^*}{\partial s} = \phi^* = 0 \qquad \text{at} \qquad s = 0 \text{ and } s = \sum_{i=1}^{3} b_i + \sum_{i=1}^{2} a_i\theta_i \quad (2.20)$$

and the relations

$$\left.\begin{aligned}
&v = v^*, \ \frac{\partial v}{\partial s} = \frac{\partial v^*}{\partial s}, \ \phi = \phi^* \\
&-\frac{\partial^2 v^*}{\partial s^2} = -\frac{\partial^2 v}{\partial s^2} + \frac{\phi}{a} \\
&\frac{\partial \phi^*}{\partial s} = \frac{\partial \phi}{\partial s} + \frac{1}{a}\frac{\partial v}{\partial s} \\
&-\frac{\partial^3 v^*}{\partial s^3} = -\frac{\partial^3 v}{\partial s^3} + \frac{GJ}{EIa^2}\frac{\partial v}{\partial s} + \frac{EI+GJ}{EIa}\frac{\partial \phi}{\partial s}
\end{aligned}\right\} \quad (2.21)$$

Note in the above equations a can be either for first or second circular tube.

At $s = b_1$, $b_1 + a_1\theta_1$, $\sum_{i=1}^{2} b_i + a_1\theta_1$ and $\sum_{i=1}^{2} b_i + a_i\theta_i$.

The last three relations of (2.21) are derived from the continuity of S', M and T using the first and last of relations (2.6) and the first

of (2.7).

Equations (2.18)-(2.21) are the complete set of equations in v and ϕ for free vibrations of the general tube geometry (S-tube) with flow. Other quantities (eg M, T and S') relating to out-of-plane motions can be expressed directly in terms of v and ϕ and their derivatives and are therefore given once v and ϕ are calculated.

2.3.4 *Non-Dimensional Solution of the Equations*

Periodic sinusoidal solutions with angular frequency ω (a positive constant) are sought. Let non-dimensional quantites $\tilde{v}$, $\tilde{s}$,... be related to actual quantities v, s,... as follows:

$$\tilde{v} = \frac{v}{a_1}, \qquad \tilde{s} = \frac{s}{a_1}, \qquad \tilde{t} = t\, a_1^{-2}\left[\frac{M_f + M_t}{EI}\right]^{-\frac{1}{2}},$$

$$\tilde{U} = U\, a_1\left[\frac{M_f}{EI}\right]^{\frac{1}{2}}, \qquad \tilde{\omega} = \omega\, a_1^2\left[\frac{M_f + M_t}{EI}\right]^{\frac{1}{2}}$$

Also let

$$\beta = M_f / (M_f + M_t), \qquad K = GJ / EI \qquad (2.23)$$

(Note for the tube cross-section in Figure 2.8 , $J/I = 2$ and $K = (1+\sigma)^{-1}$ where σ is the Poisson ratio.) It is now necessary to determine the functions $v(\tilde{s},\tilde{t})$ and $\phi(\tilde{s},\tilde{t})$, which are of the forms

$$\left.\begin{aligned} v &= n(\tilde{s})\, e^{i\tilde{\omega}\tilde{t}} \\ \phi &= \psi(\tilde{s})\, e^{i\tilde{\omega}\tilde{t}} \end{aligned}\right\} \qquad (2.24)$$

respectively. Equations for n and ψ obtained from expressions (2.18) and (2.19) are

$$\left.\begin{aligned} &(D^4 + \bar{U}^2D^2 + 2\,\bar{U}\beta^{1/4}\,i\bar{\omega}D - \bar{\omega}^2)\,\eta^* = 0 \\ &D^2\psi^* = 0 \end{aligned}\right\} \qquad (2.25)$$

and

$$\left.\begin{aligned} &(D^4 + (\bar{U}^2-K)D^2 + 2\bar{U}\beta^{1/4}i\bar{\omega}D - \bar{\omega}^2)\,\eta + (1+K)D^2\,\psi = 0 \\ &(1+1/K)D^2\,\eta + (D^2-1/K)\,\psi = 0 \end{aligned}\right\} \qquad (2.26)$$

where $D=d/d\bar{s}$ and the asterisk denotes quantities pertaining to straight lengths of tube.

Equations (2.26) are mixed equations in η and ψ. To separate them one can multiply the first by $(1+1/K)D^2$ and the second by $D^4+(\bar{U}^2+K)D^2+2\bar{U}\beta^{1/4}i\bar{\omega}D-\bar{\omega}^2$ and subtract. This gives

$$\begin{aligned} &(\,D^6 + (2+\bar{U}^2)\,D^4 + 2\bar{U}\beta^{1/4}i\bar{\omega}\,D^3 + (1-\bar{\omega}^2-\bar{U}^2/K)\,D^2 \\ &\qquad - (2\bar{U}\beta^{1/4}i\bar{\omega}/K)\,D + \bar{\omega}^2/K\,)\,\psi = 0 \end{aligned} \qquad (2.27)$$

The solution of equation (2.27) can be found in the form

$$\psi(\bar{s}) = \sum_{i=1}^{6} A_{ij}\, e^{\lambda_i \bar{s}} \qquad (2.28)$$

where A_{ij} and λ_i are constants and j integer denotes the segments number of the tube (equal to 2 or 4 for the curved parts of the tube). Substituting expression (2.28) in equation (2.27) gives the algebraic equation

$$\begin{aligned} &\lambda^6 + (2+\bar{U}^2)\lambda^4 + 2\bar{U}\beta^{1/4}i\bar{\omega}\lambda^3 + (1-\bar{\omega}^2-\bar{U}^2/K)\lambda^2 - (2\bar{U}\beta^{1/4}i\bar{\omega}/K)\lambda \\ &\qquad + \bar{\omega}^2/K = 0 \end{aligned} \qquad (2.29)$$

whose six roots are the required constants λ_i.

n for the curved lengths can be related to ψ as follows. Integration of the second of equations (2.26) gives

$$n = (1+K)^{-1}\left[\int\int \psi\, d\tilde{s}\, d\tilde{s} + E_1\tilde{s} + E_o - K\psi\right] \qquad (2.30)$$

where E_1 and E_o constants. Substituting expression (2.28) in equation (2.30) gives

$$n(\tilde{s}) = (1+K)^{-1}\left[\sum_{i=1}^{6} A_{ij}\,(\lambda_i^{-2} - K)\, e^{\lambda_i\tilde{s}} + E_1\tilde{s} + E_o\right] \qquad (2.31)$$

where E_1 and E_o must be zero in order that expression (2.28) and (2.31) satisfy the original equations (2.26)

For straight parts of the tube one has the more direct solution

$$n^*(\tilde{s}) = \sum_{i=1}^{4} A_{ij}\, e^{\alpha_i\tilde{s}} \qquad (2.32)$$

where the α_i are the roots of

$$\alpha^4 + \tilde{U}^2\alpha^2 + 2\tilde{U}\beta^{1/2} i\tilde{\omega}\alpha - \tilde{\omega}^2 = 0 \qquad (2.33)$$

Also

$$\psi^*(\tilde{s}) = B_{1j}\,\tilde{s} + B_{oj} \qquad (2.34)$$

where j=1,3 or 5 for straight lengths of the tube.

Thirty relations between the thirty constants A_{ij}, B_{1j} and B_{oj} can be found from the boundary conditions (2.20) and (2.21), these relations are summarized in appendix **B**, and they can be written in matrix form as

$$[Y]\{X\} = \{0\} \tag{2.35}$$

where Y is a 30×30 matrix whose elements are known functions of L_j ($L_j=b_i/a_1$ or $a_i\pi/a_1$), α_i, λ_i and K and where X is column vector whose 30 elements are the A_{ij}, B_{ij} and B_{oj}.

Equation (2.35) has non-zero solutions only when the determinant of Y vanishes:

$$|Y| = 0 \tag{2.36}$$

For given L_j and K this is an equation in the roots α_i and λ_i of equations (2.33) and (2.29). Equation (2.33) and (2.29) for the roots contain $\tilde{\omega}$. Therefore, only for certain values of $\tilde{\omega}$ will equation (2.36) be satisfied. The main interest is in the lower few positive real values of $\tilde{\omega}$ that satisfy equation (2.36). These correspond to the fundamental and second natural modes of vibration in which flowmeters normally operate. Solutions of equation (2.36) should not involve any complex values of $\tilde{\omega}$ which correspond to unstable vibrations. These unstable vibrations occur only at flow velocities far large than those encountered in flowmeter applications, wherein the flow only slightly alters the frequency and character of the vibrations. Once the suitable $\tilde{\omega}$ is found one can return to equation (2.35) to find the values of A_{ij}, B_{ij} and B_{oj} to within a common constant arbitrary factor. This latter operation is carried out by putting one of the elements of X (which is not zero (like B_{o1}) equal to unity, dropping one of the equations (2.35) and solving the remainder as a set of 29 linear equations in 29 unknowns.

2.3.5 Numerical Method

To obtain numerical values for A_{ij}, B_{ij} and B_{oj} use can be made of NAG (Numerical Algorithms Group) Library routines [67] as follows.

The complex polynomial equations (2.33) and (2.29) for the α_i and λ_i

can be solved using routine CO2ADF. This finds all the roots of a complex polynomial, using the method of Grant and Hitchins. The output of this routine gives the four complex values of α_i and the six complex values of λ_i for any supplied real positive value of $\tilde{\omega}$. Calculated α_i and λ_i can then be used in the evaluation of |Y| which is done using routine FO3ADF. This calculates the determinant of a complex matrix using the factorisation method of Crout. The modulus of |Y| is reduced to zero by adjustment of $\tilde{\omega}$ using minimising routine EO4ABF which searches for a minimum using a method based on quadratic interpolation. This process can be used to locate the fundamental frequency and also higher resonant frequencies by increasing the lower and upper bounds of the search for $\tilde{\omega}$. Figure 2.9 shows the flow chart of the computer programme used here.

When $\tilde{\omega}$ is found, the linear equations (appendix A) are solved by putting $A_{62} = 1$, dropping the corresponding equation and employing the simultaneous linear equation solvers FO3AHF and FO4AKF to obtain the remaining 29 constants. FO3AHF decomposes a complex matrix into triangular matrices by Crout's method and evaluates the determinant. FO4AKF calculates the approximate solution of a set of complex linear equations Ax = B with where A has been decomposed into trianguiar matrices using FO3AHF, see appendix C for the listing of the computer programme

2.3.6 Numerical Results

Having obtained values for the constants A_{jj}, B_{ij} and B_{oj}, mode shapes are calculated using equations (2.28), (2.31), (2.32) and (2.34). The actual (non-dimensional) displacement and twist are taken as the real parts of the right hand sides of (2.24) thus

$$\left.\begin{aligned} \bar{v}_{act} &= |n(\bar{s})| \cos(\tilde{\omega}\bar{t} + \angle\, n(\bar{s})) \\ \Phi_{act} &= |\Psi(\bar{s})| \cos(\tilde{\omega}\bar{t} + \angle\, \Psi(\bar{s})) \end{aligned}\right\} \qquad (2.37)$$

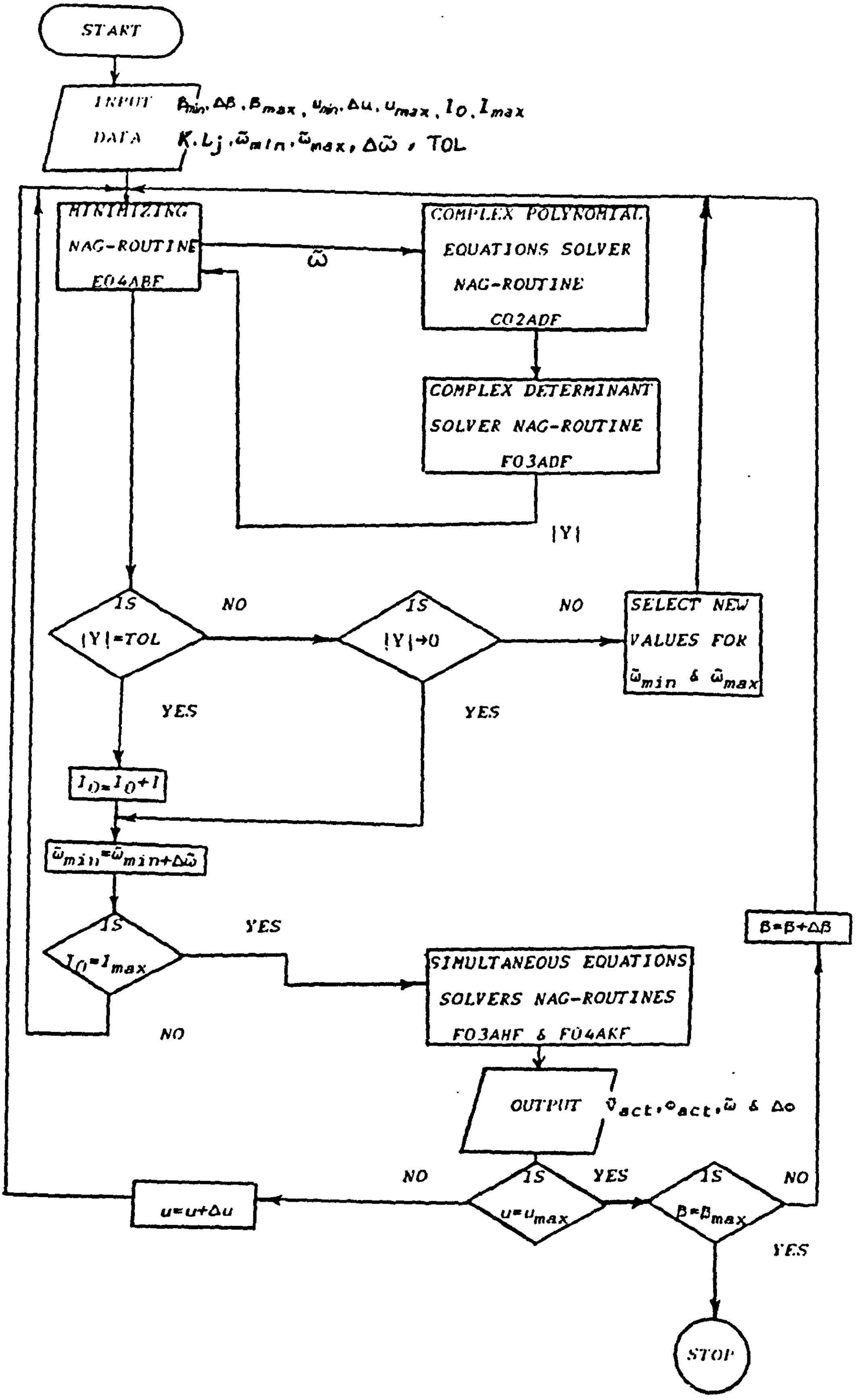

Figure 2.9 THE FLOWCHART OF THE COMPUTER PROGRAMME

Mode shapes at $\tilde{t} = 0$ for the fundamental and for the next two natural vibrations for the S-tube configuration with $\beta = 0$, $\tilde{u} = 0$, K=0.7692 (as for stainless steel) and $L_1 = L_3 = L_5 = 2$ and $L_2 = L_4 = \pi$ are as shown in Figure 2.10 . Fig 2.11 shows the mode shapes for U-tube configuration using the same values for β, $\tilde{u}$ and K with $L_1 = L_3 = 2$, $L_2 = \pi$ and $L_4 = L_5 = 0$. The twist mode shapes show a kink at the transitions from the straight tube sections to the circular tube. There is no reason for $\partial\phi/\partial s$ to be continuous here.

Figure 2.12 shows non-dimensional frequency ($\tilde{\omega}$) of U-tube versus $L_1 (=L_3)$ and $L_2 = \pi$ with and without flow.

The phase difference $\Delta\phi$ between displacement (or velocity) at the two points $\tilde{s}=\tilde{s}_1$ $\tilde{s}=\tilde{s}_2$ is, by (2.37),

$$\Delta\phi = \left| \tan^{-1} \frac{Im(n)}{Re(n)} \right|_{\tilde{s}_1} - \left| \tan^{-1} \frac{Im(n)}{Re(n)} \right|_{\tilde{s}_2} \qquad (2.38)$$

In Figure 2.13 calculated values of $\Delta\phi$ (in the fundamental mode) are plotted against non-dimensional flow velocity for various values of mass ratio β for U-tube configuration with K = 0.7692, $L_1 = L_3 = 3$, $L_2 = \pi$, $\tilde{s}_1 = L_1$ and $\tilde{s}_2 = L_1 + L_2$. Note the non-linear effect at larger velocities.

The effect of fluid velocity and density on the fundamental frequency of the U-tube is shown in Fig 2.14 for K=0.7692, $L_1 = L_3 = 3$ and $L_2 = \pi$ (for r=2.54 cm, t=1 mm, a_1=15 cm, E=208 GN/m^2 and ρ_f=1000 Kg/m^3; the non-dimensional velocity u=0.002U).

Finally, Figure 2.15 illustrates the effect of Θ_1 on non-dimensional frequency (indicating geometrical effect) for $L_1=L_3$, $L_4=L_5=L_6=0$ and $\beta=u=0$.

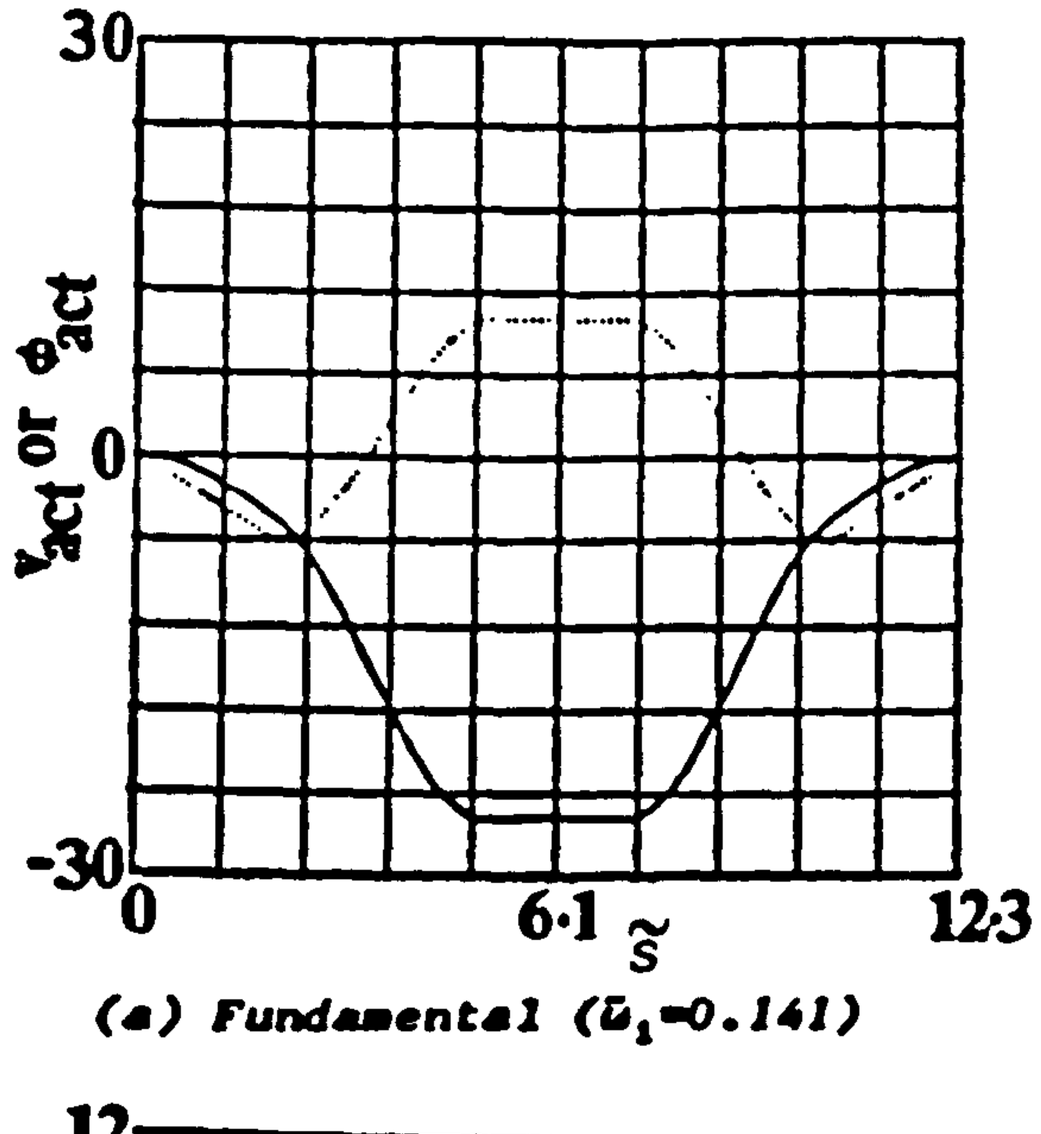

(a) Fundamental ($\tilde{\omega}_1$=0.141)

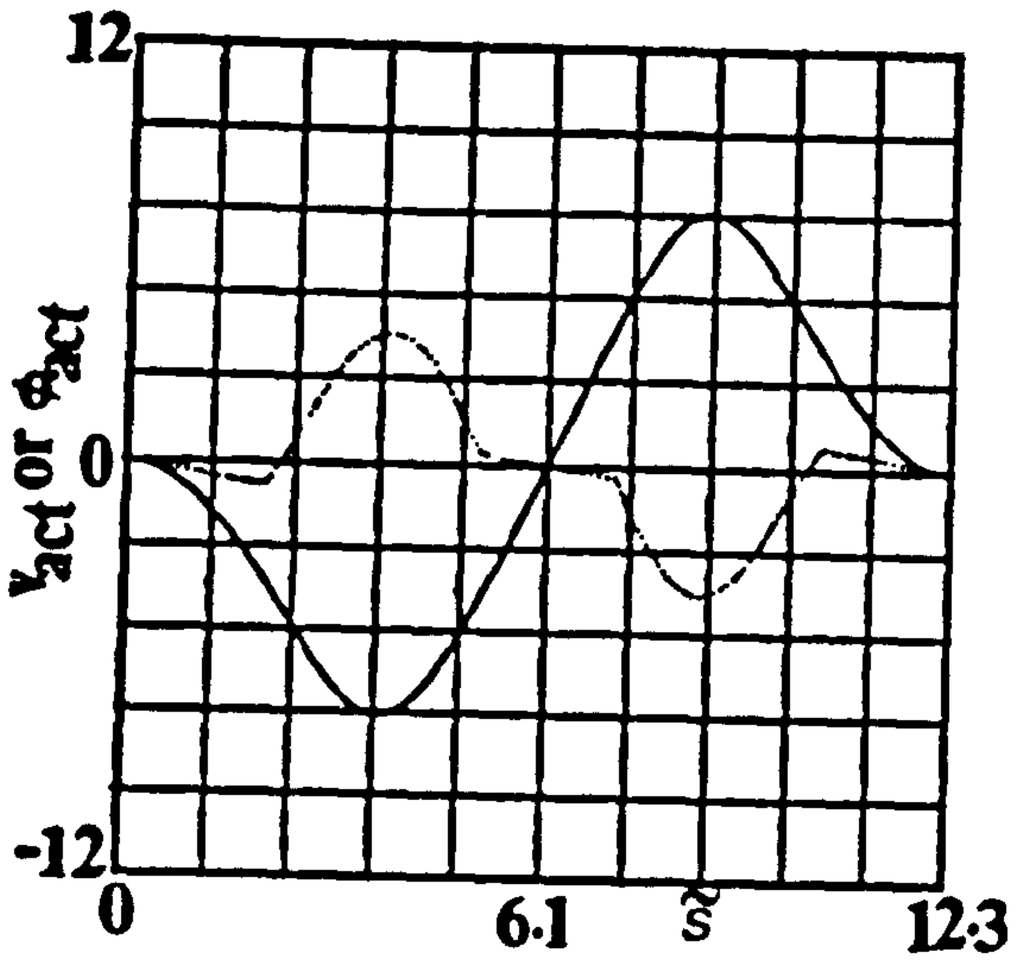

(b) Second Mode ($\tilde{\omega}_2$=0.204)

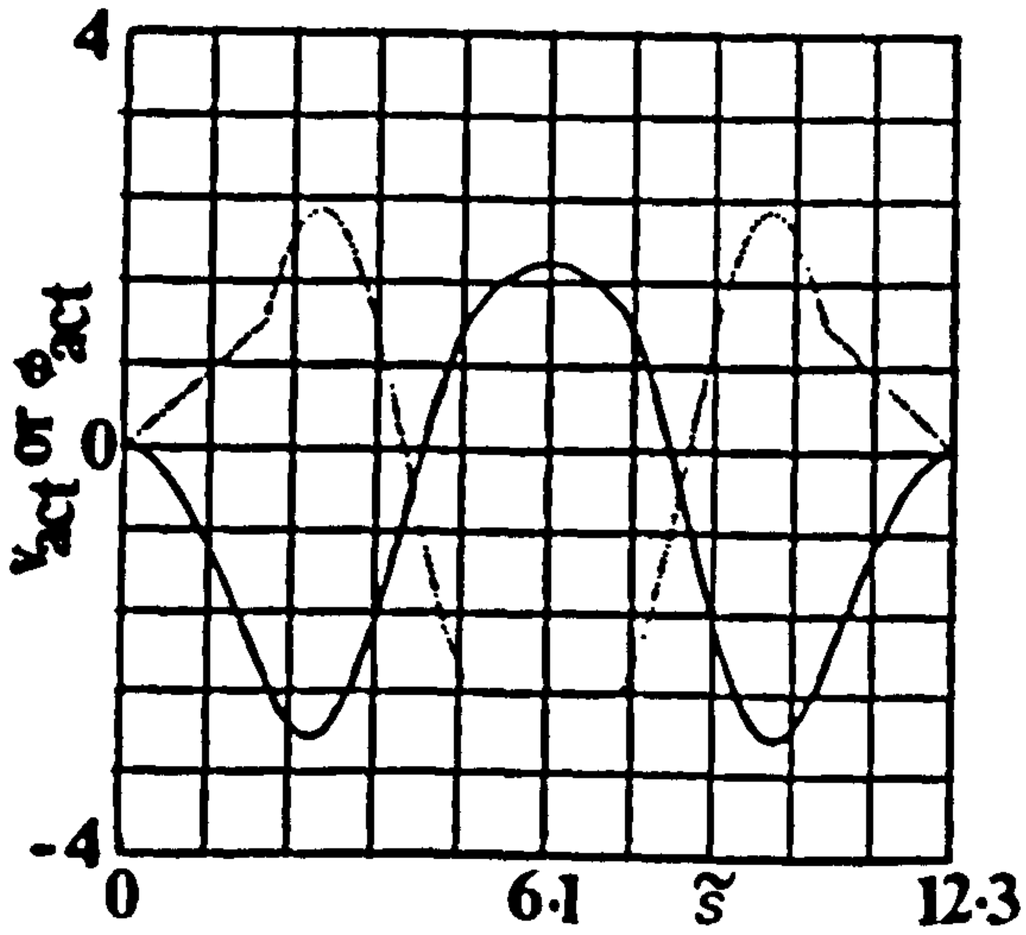

(c) Third Mode ($\tilde{\omega}_3$=0.407)

Figure 2.10 DISPLACEMENT AND TWIST MODE SHAPES FOR THE S-TUBE CONFIGURATION. —— Displacement , ... Twist

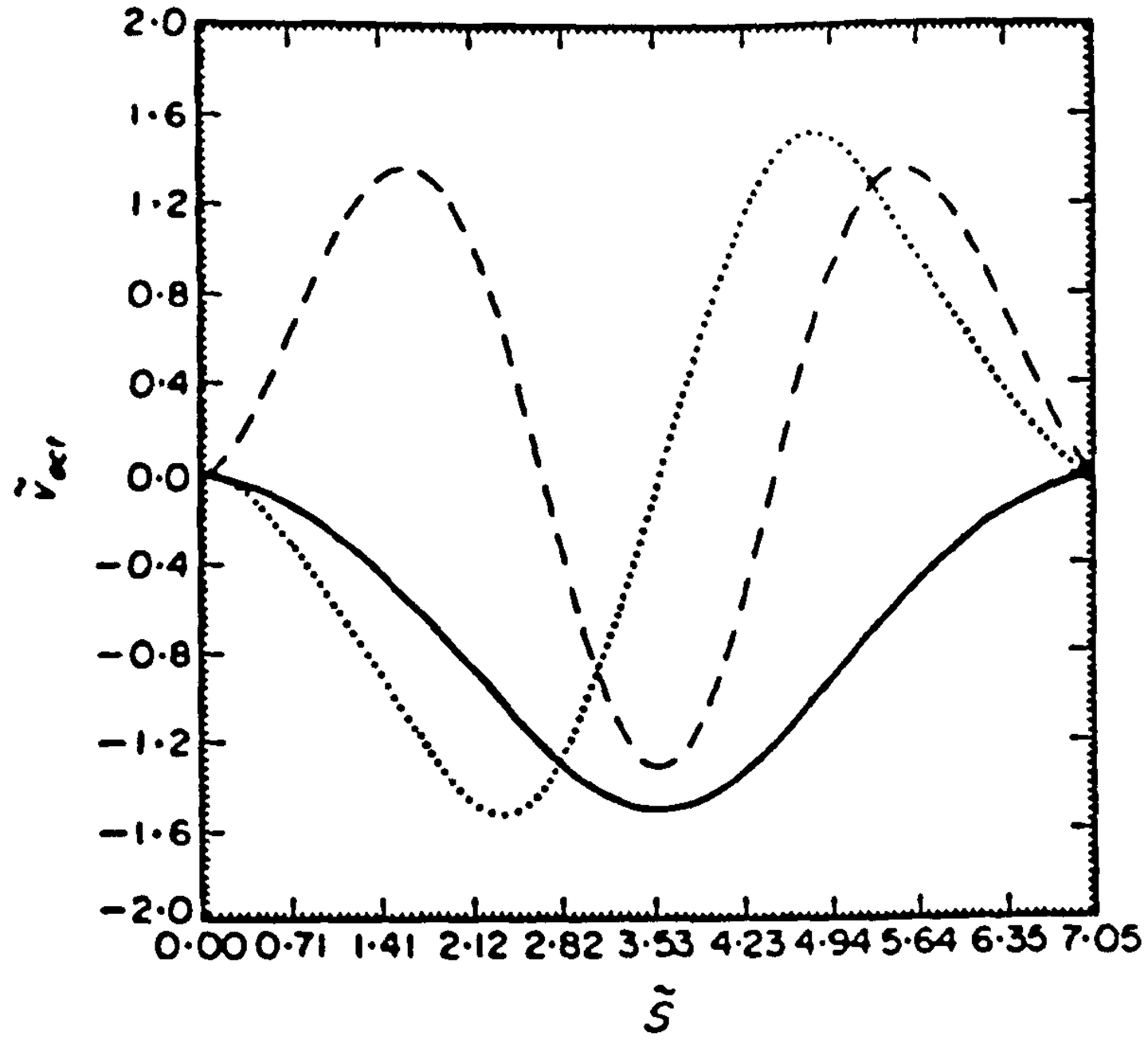

(a) Displacement Mode Shapes

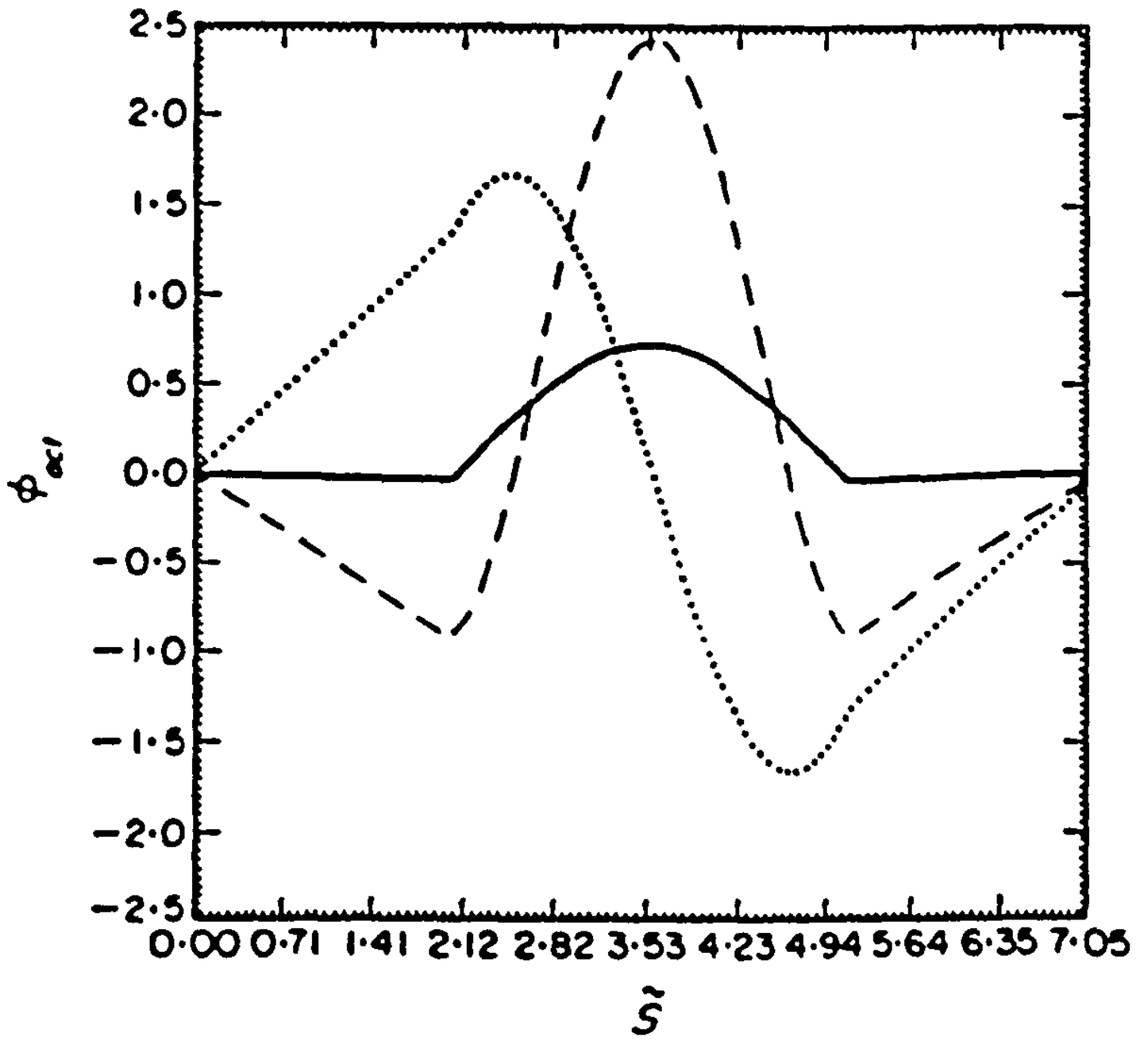

(b) Twist Mode Shapes

Figure 2.11 DISPLACEMENT AND TWIST MODE SHAPES FOR THE U-TUBE CONFIGURATION. ——, FUNDAMENTAL ($\tilde{\omega}_1$=0.299); ....., SECOND MODE ($\tilde{\omega}_2$=0.828); - - -, THIRD MODE ($\tilde{\omega}_3$=1.955).

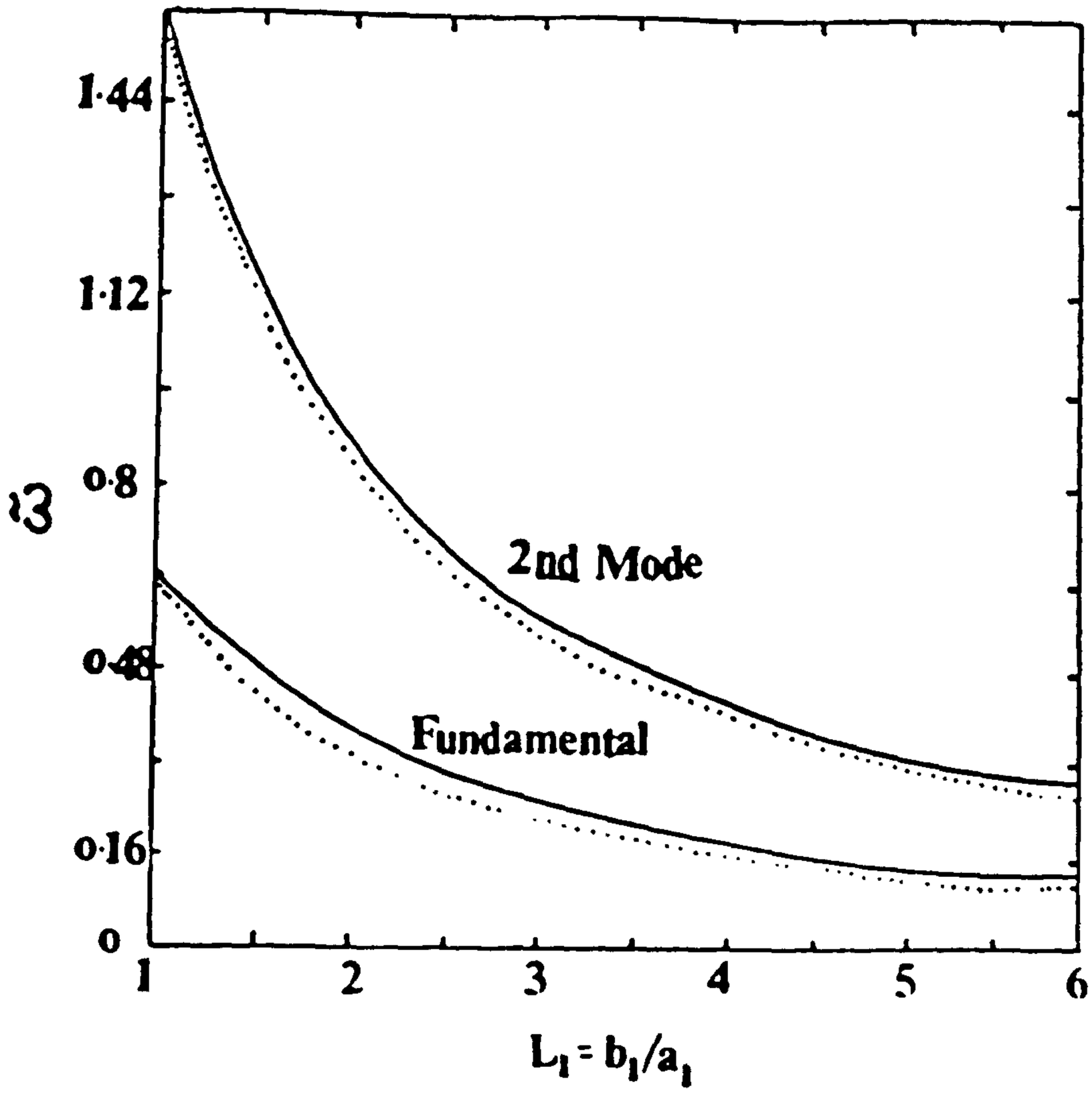

Figure 2.12 NON-DIMENSIONAL FREQUENCY VERSUS NON-DIMENSIONAL LENGTH $L_1(=L_2)$ OF U-TUBE. —— $\beta=u=0$, ····· $\beta=0.5$ and $u=0.2$

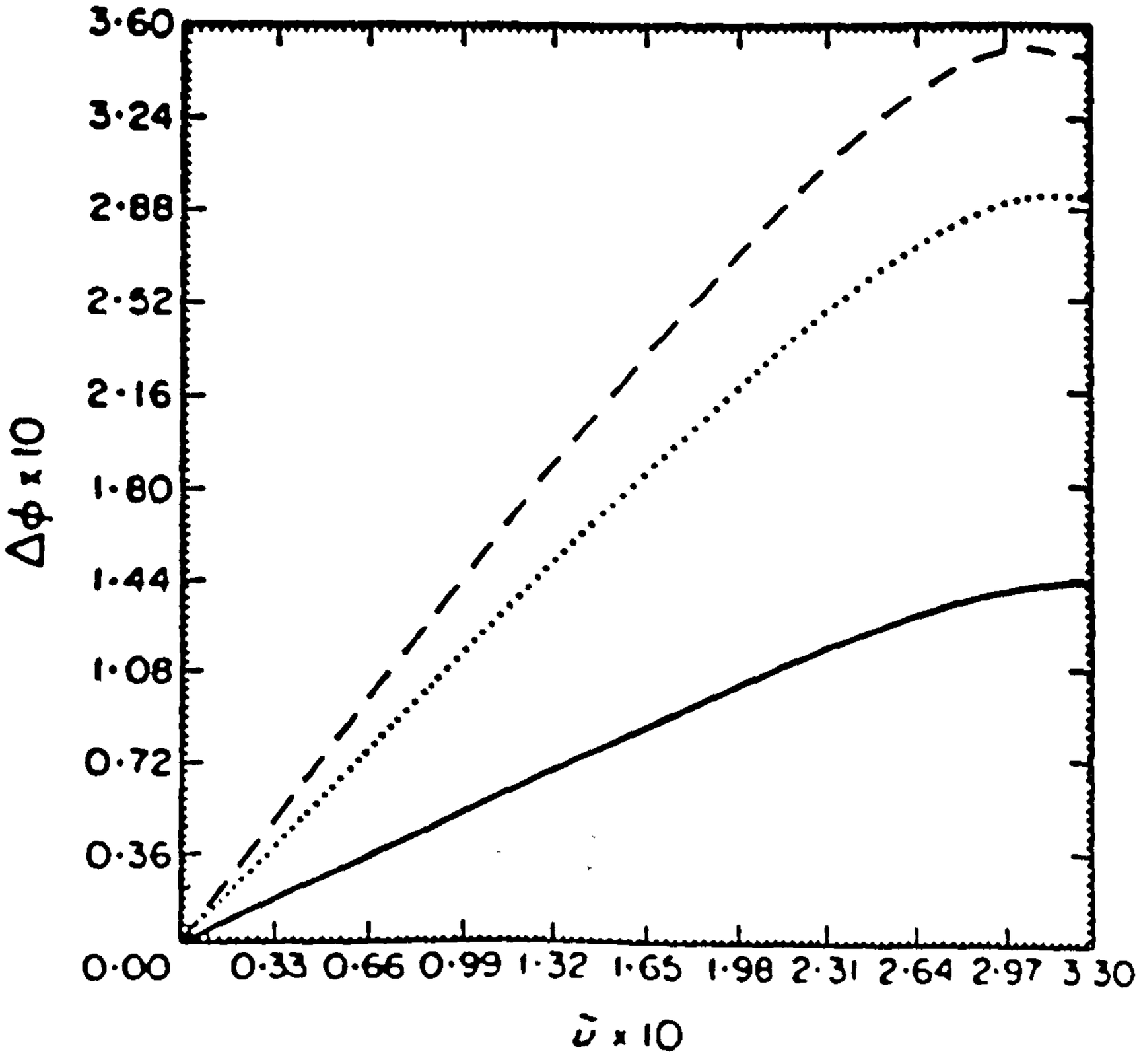

Figure 2.13 PHASE DIFFERENCE VERSUS NON-DIMENSIONAL FLUID VELOCITY FOR THREE MASS RATIOS. ——, $\beta=0.1$; ·····, $\beta=0.5$; – – –, $\beta=0.8$

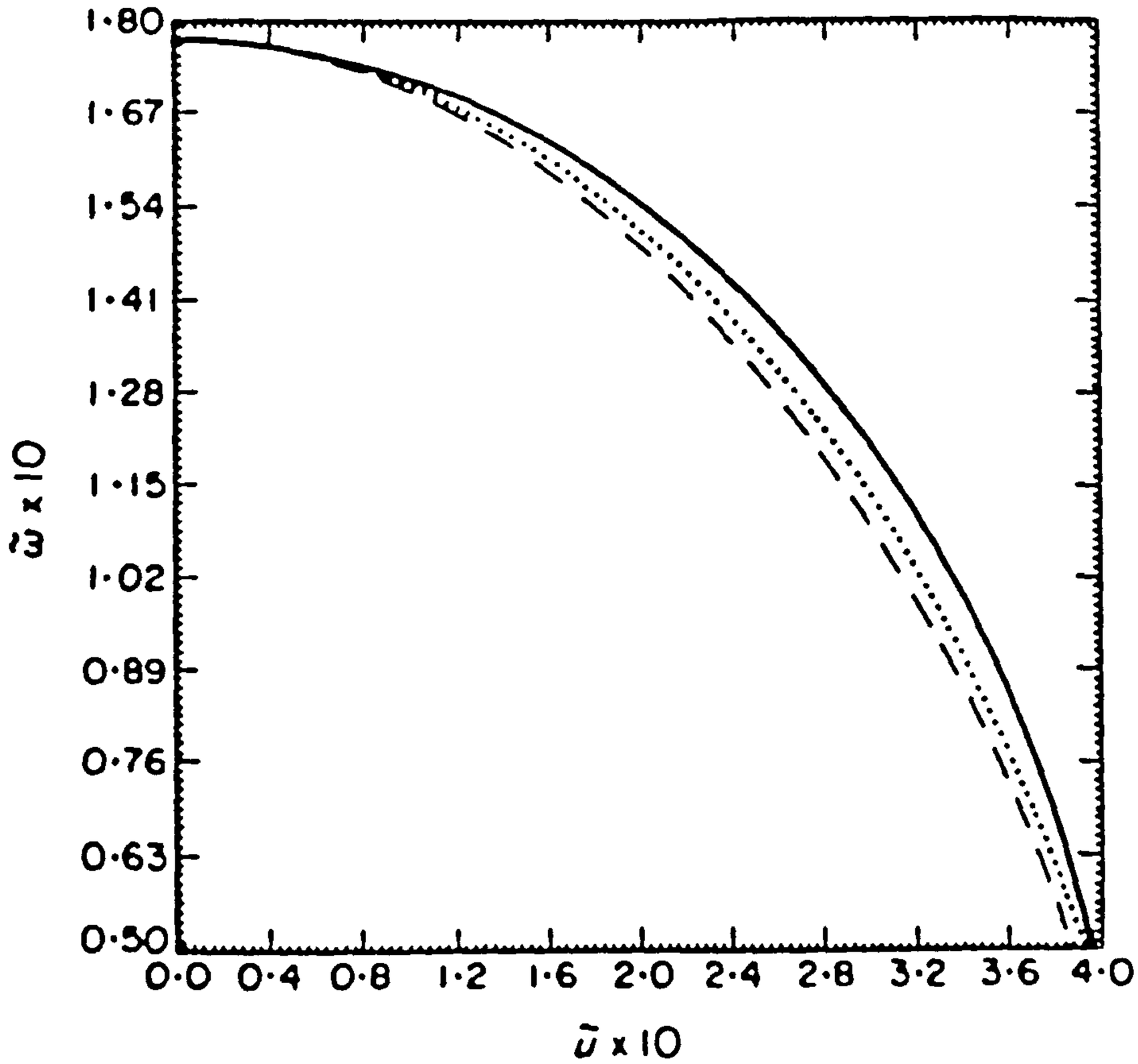

Figure 2.14 · AS FIGURE 2.13 , BUT FOR NON-DIMENSIONAL FREQUENCY

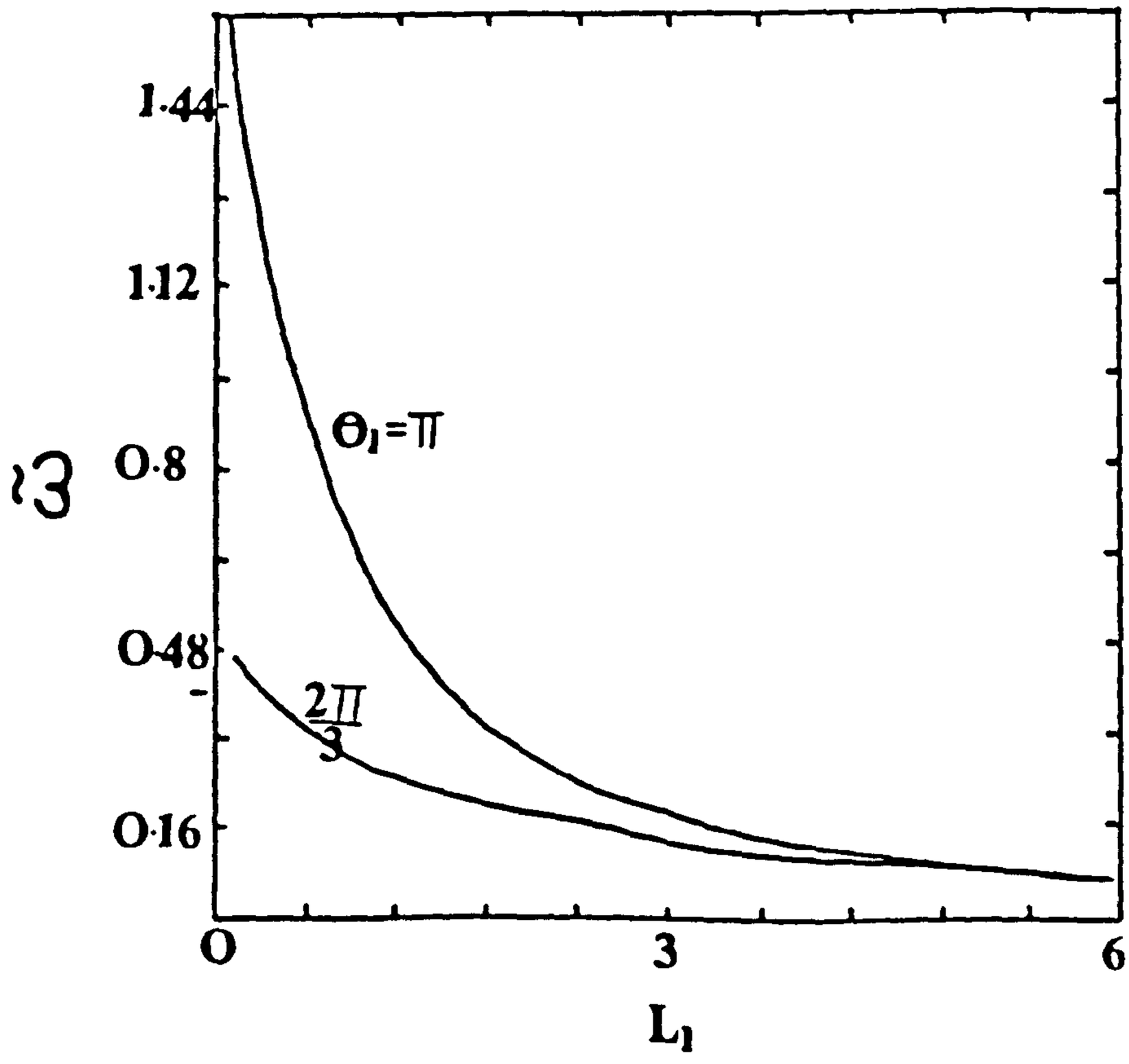

Figure 2.15 GEOMETRY EFFECT ON TUBE NON-DIMENSIONAL FREQUENCY

2.4 *THE EFFECT OF TUBE GEOMETRY AND DIMENSIONS ON TIME DELAY (Δt)*

This section is concerned with the comparison of different tube geometries and the effect of tube thickness and length on time delay (Δt).

2.4.1 *Comparison of Different Tube Geometries*

In order to compare between different tube geometries (straight and U-tube geometries are considered here) Δt (=Δo/ω) is calculated and the following parameters : overall length (O.L.), thickness (t), Young's and shear moduli (E and G), inner diameter (d_i) of the tubes, mass raio (β) and distance between measuring points (D) are set to be constant for all the geometries.

Under these conditions the comparison between straight and U-tube geometries works out as shown in Figure 2.16. Straight tube geometry seems to produce higher time delay for the same fluid velocity compared to U-tube geometry.

2.4.2 *The Effect of Tube Dimensions*

For two fluid velocities time delay (Δt) is plotted against tube thickness (for straight tube configuration) in Figure 2.17. It is seen that increasing tube thickness leads to an exponential decrease in time delay. Frequency variation according to tube thickness is indicated in Table 2.1.

Increase in the tube length leads to considerable increase in Δt as shown in Figure 2.18. Table 2.2 shows the variation in tube frequency with tube length.

COMPARISON

O.L= 1(m)
D = 0.5 (m)
E=202.75 (GN/m²)
t= 1 (mm)
r_i=13.35 (mm)
β= 0.44

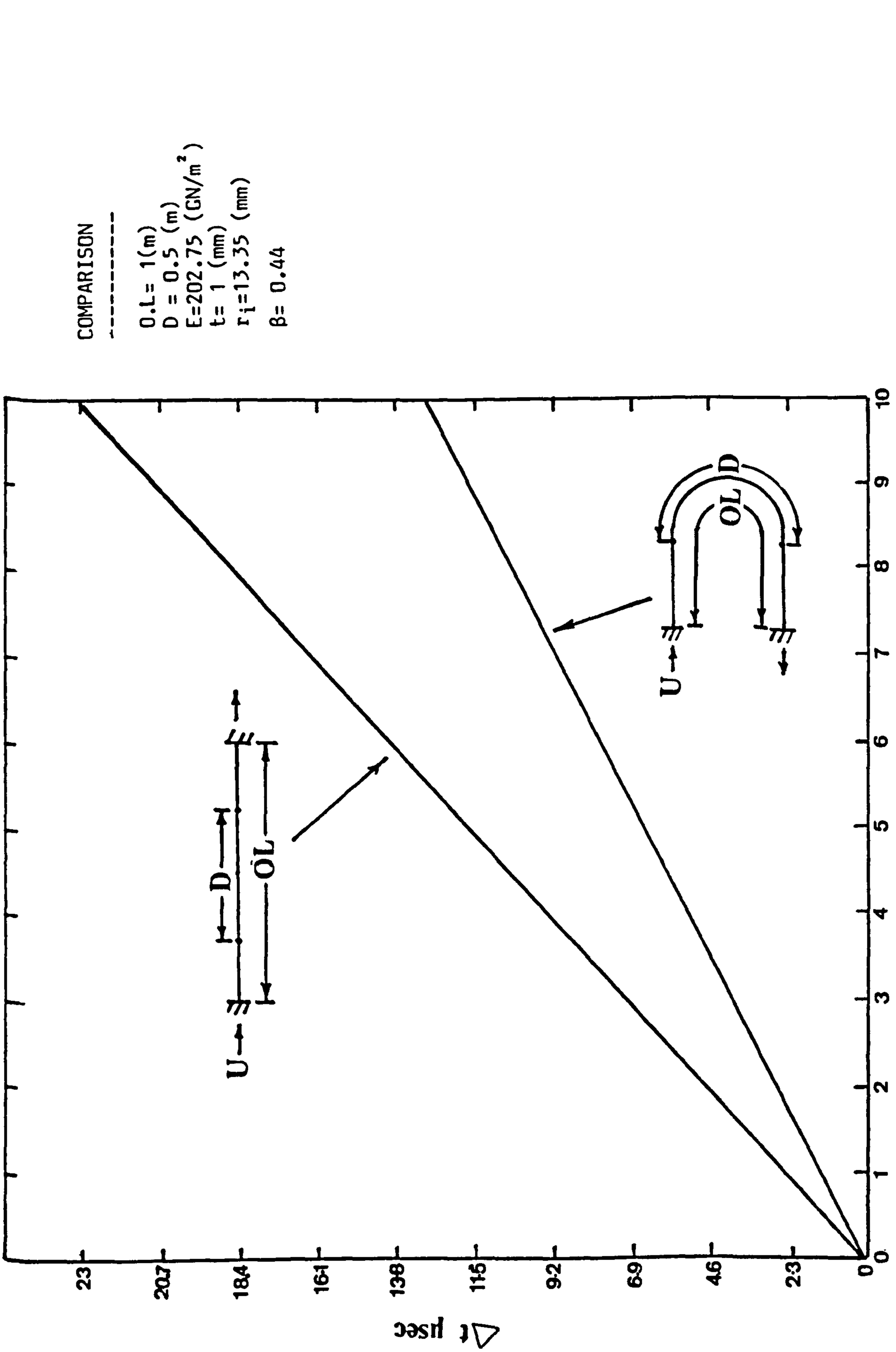

Figure 2.16 COMPARISON BETWEEN STRAIGHT AND U-TUBE GEOMETRIES.

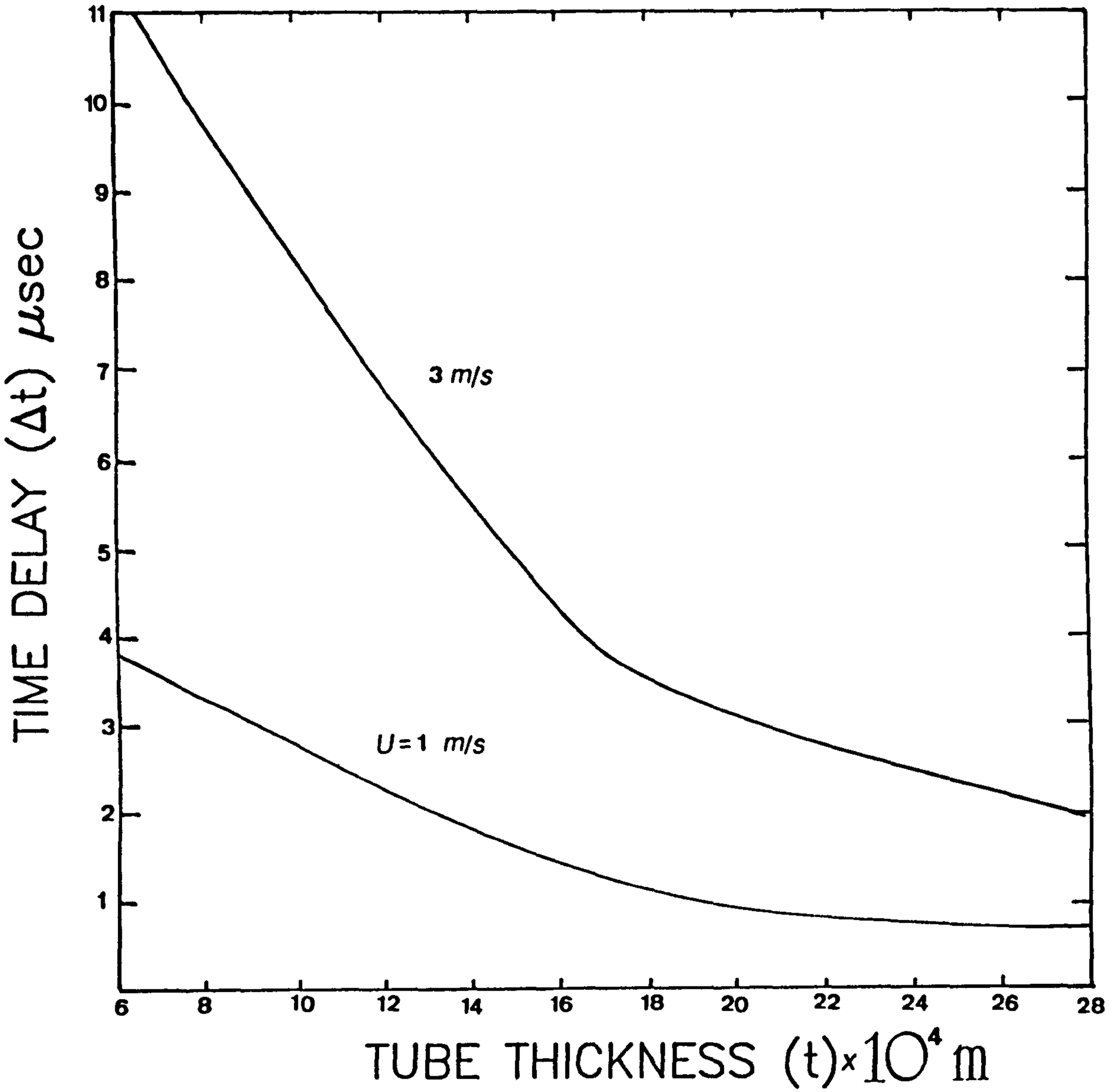

STRAIGHT TUBE CONFIGURATION

Tube Length (b)=1 (m)

E=202.75 (GN/m²)

D=0.5 (m) , ri=13.35 (mm)

$\rho_f = 998$ kg/m³

$\rho_t = 7918$

Figure 2.17 TIME DELAY VERSUS TUBE THICKNESS

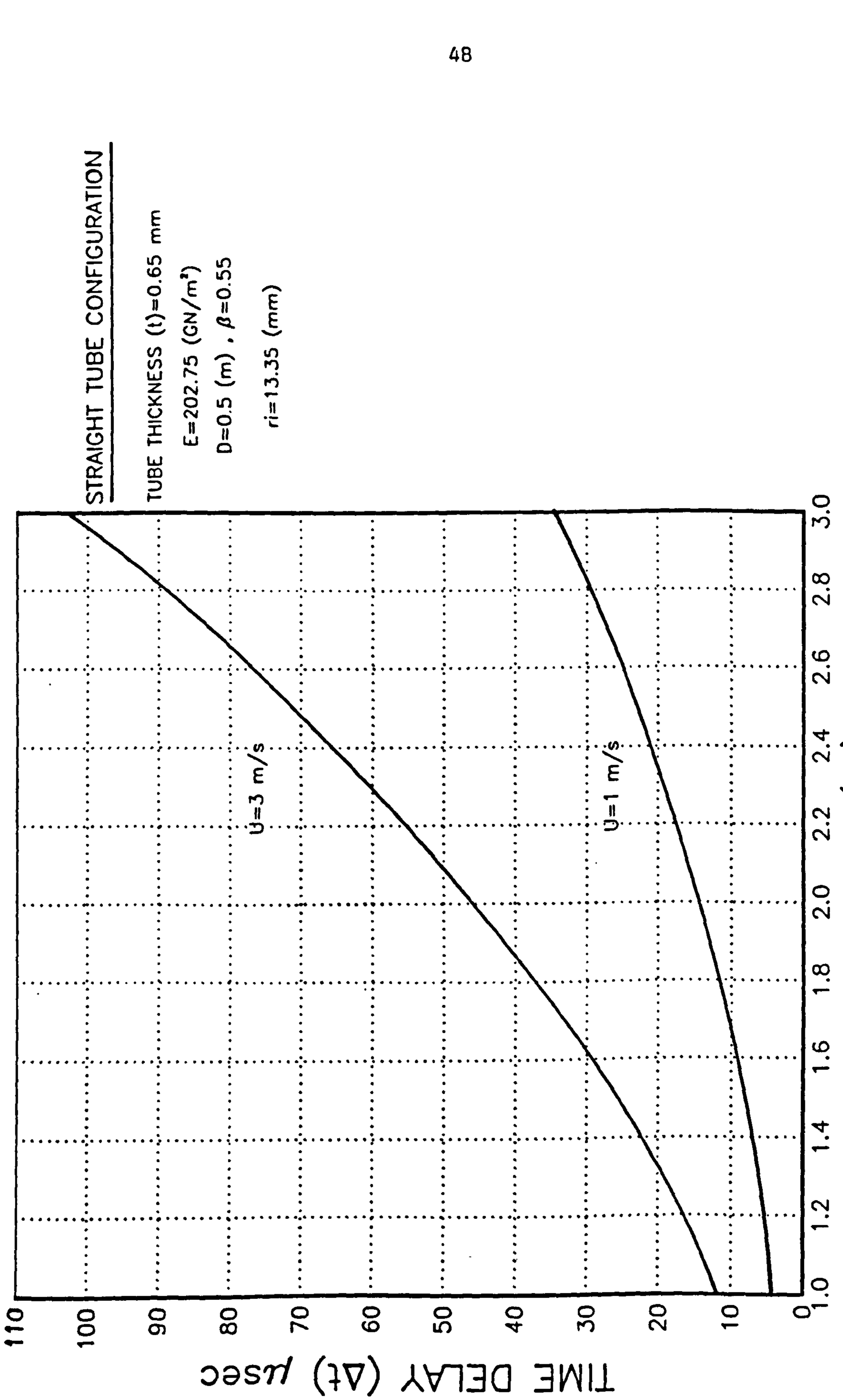

Figure 2.18 TIME DELAY VERSUS TUBE LENGTH

TUBE THICKNESS t (mm)	MASS RATIO β (/)	FREQUENCY f (Hz)
0.65	0.55	115.835
1.65	0.32	148.694
2.65	0.22	165.367

b=1 m, U=1 m/s , ρ_f=998.2, ρ_t=7918, E=202.75 GN/m^2 and r_i=13.35 mm.

Table 2.1 FREQUENCY VARIATION WITH TUBE THICKNESS.

TUBE LENGTH b (m)	FREQUENCY f (Hz)
1	115.834
2	28.958
3	12.869

t=0.65 m, U=1 m/s , β=0.55, E=202.75 GN/m^2.

Table 2.2 FREQUENCY VARIATION WITH TUBE LENGTH.

CHAPTER THREE

ELASTIC BOUNDARY CONDITIONS AND ADDED MASS EFFECTS

CHAPTER THREE

ELASTIC BOUNDARY CONDITIONS AND ADDED MASS EFFECTS

In this chapter an improved model of Coriolis flowmeter is considered, taking into account elastic intermediate and end conditions and effects of the masses of electromagnetic drive and detectors.

3.1 MODELLING OF THE INTERMEDIATE SUPPORTS

A typical arrangement of the tubes of Coriolis mass flowmeter is shown in Figure 3.1 indicating intermediate supports (so called BRACE BARS). The incorporation of brace bars within the Coriolis flowmeter is the result of mechanical design considerations [16] and aims to achieve greater stiffness (high Q factor) and reduce the stress concentrations at the clamp ends.

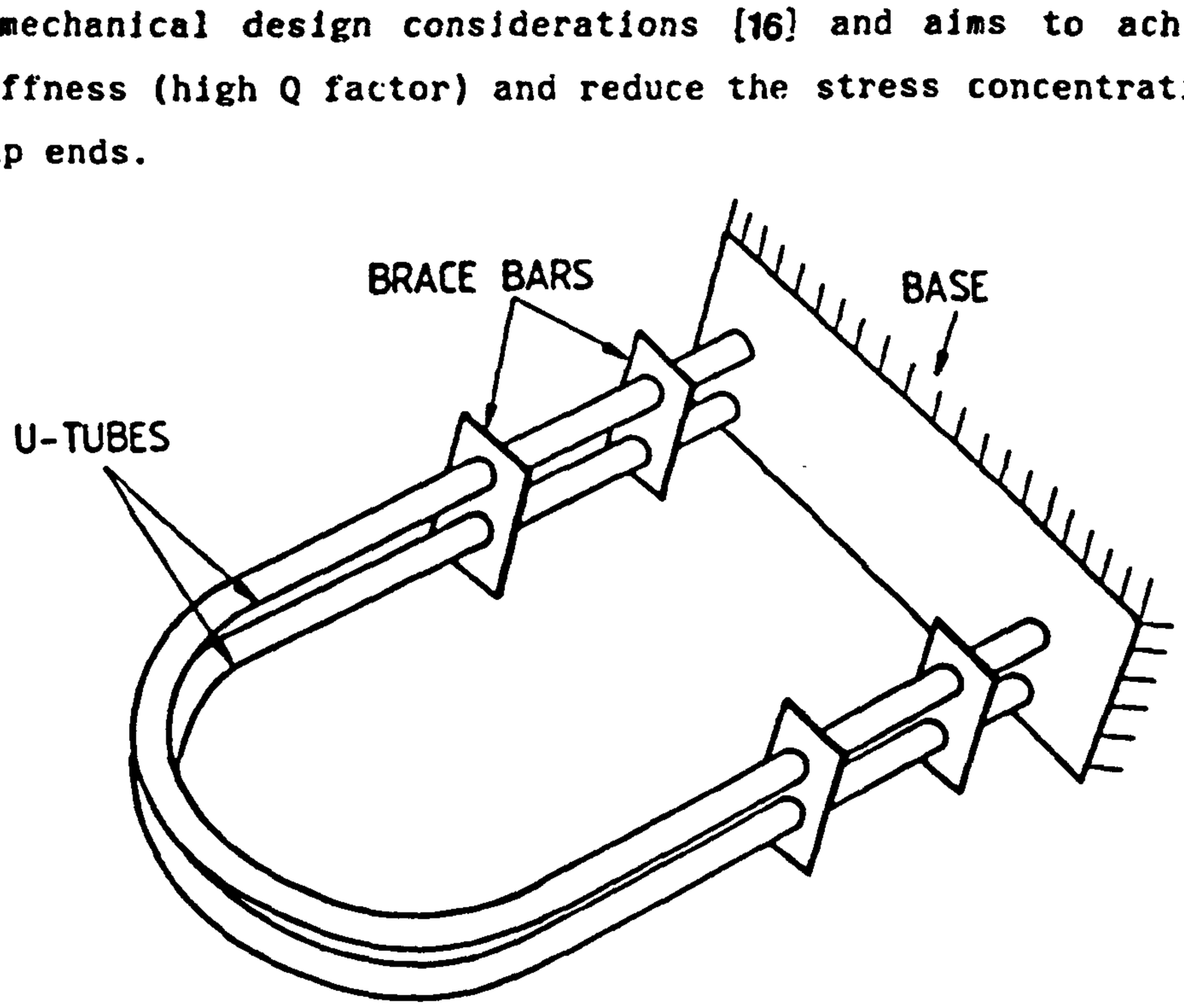

Figure 3.1 TUBE ARRANGEMENT OF CORIOLIS MASS FLOWMETER

3.1.1 Boundary Conditions

In the modelling of Coriolis flowmeter, the simple boundary conditions (clamped or pinned) do not precisely represent the true conditions because deflection, rotation and twist can take place in the brace bars due to their elastic nature [68].

Figure 3.2 shows an exaggerated example of a deformed state of brace bars caused by deflection of the tubes. Taking one tube, the brace bars can be modelled as three independent springs (translational, for tension and compression, rotational for bending and torsional for twisting).

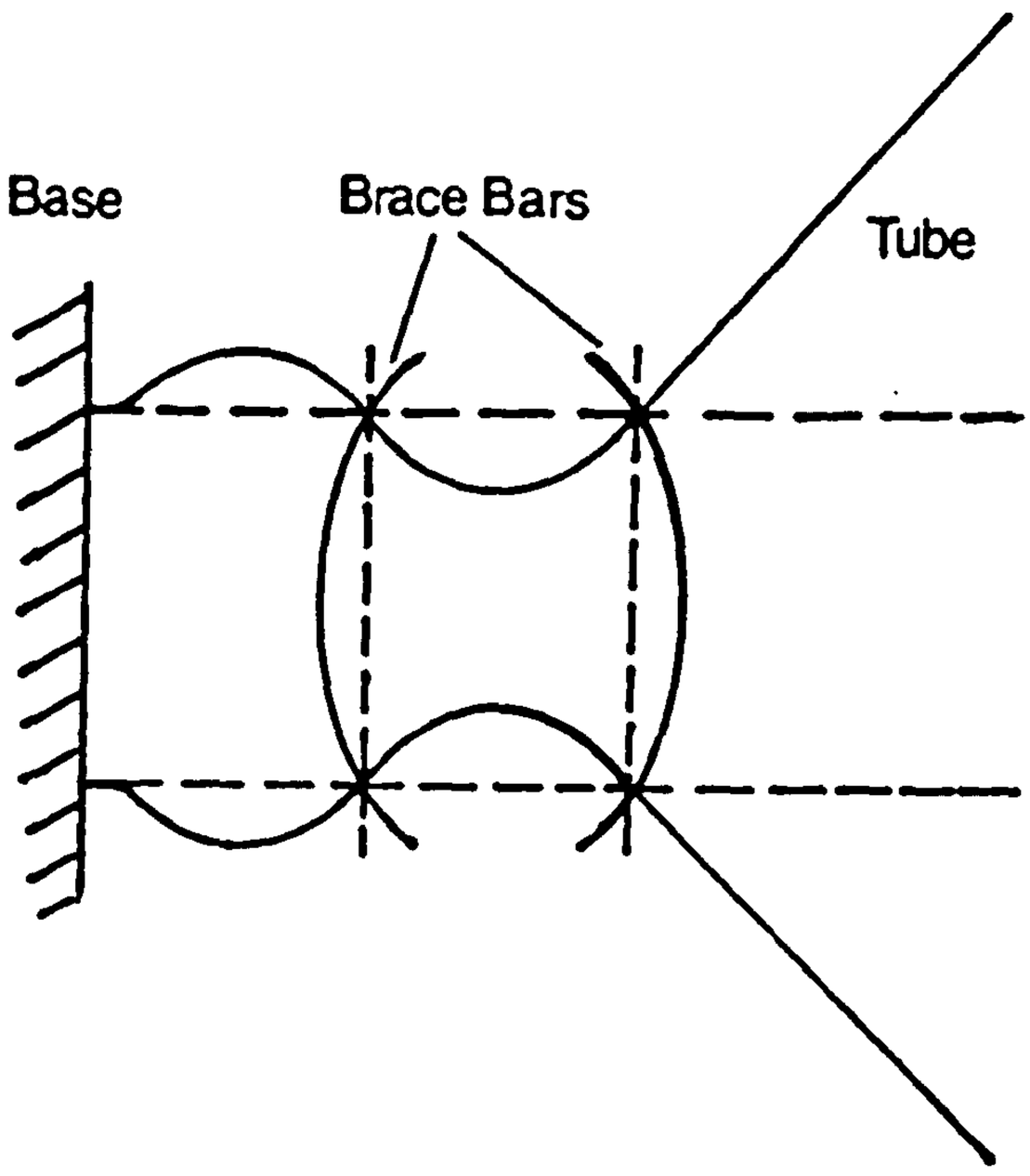

Figure 3.2 DEFORMATION OF BRACE BARS DUE TO DEFLECTION OF THE TUBES

Now consider a system as shown in Figure 3.3, in which three springs are attached at one point of a straight tube. Assuming both that the tube is undergoing bending and twisting and that the springs are massless, then continuity and boundary conditions at the attached point can be expressed as follows

(i) discontinuity of shear force, bending moment and torque

$$\left.\begin{aligned} S_2^{*\prime} - S_1^{*\prime} - K_1 v_1^* &= 0 \\ M_2^* - M_1^* + K_2 \,(\partial v_1^*/\partial s) &= 0 \\ T_2^* - T_1^* - K_3 \,\phi^* &= 0 \end{aligned}\right\} \qquad (3.1)$$

(ii) continuity of deflection, slope and twist

$$\left.\begin{aligned} v_1^* &= v_2^* \\ \partial v_1^*/\partial s &= \partial v_2^*/\partial s \\ \phi_1^* &= \phi_2^* \end{aligned}\right\} \qquad (3.2)$$

where * is used to denote quantities pertaining to straight tubes.

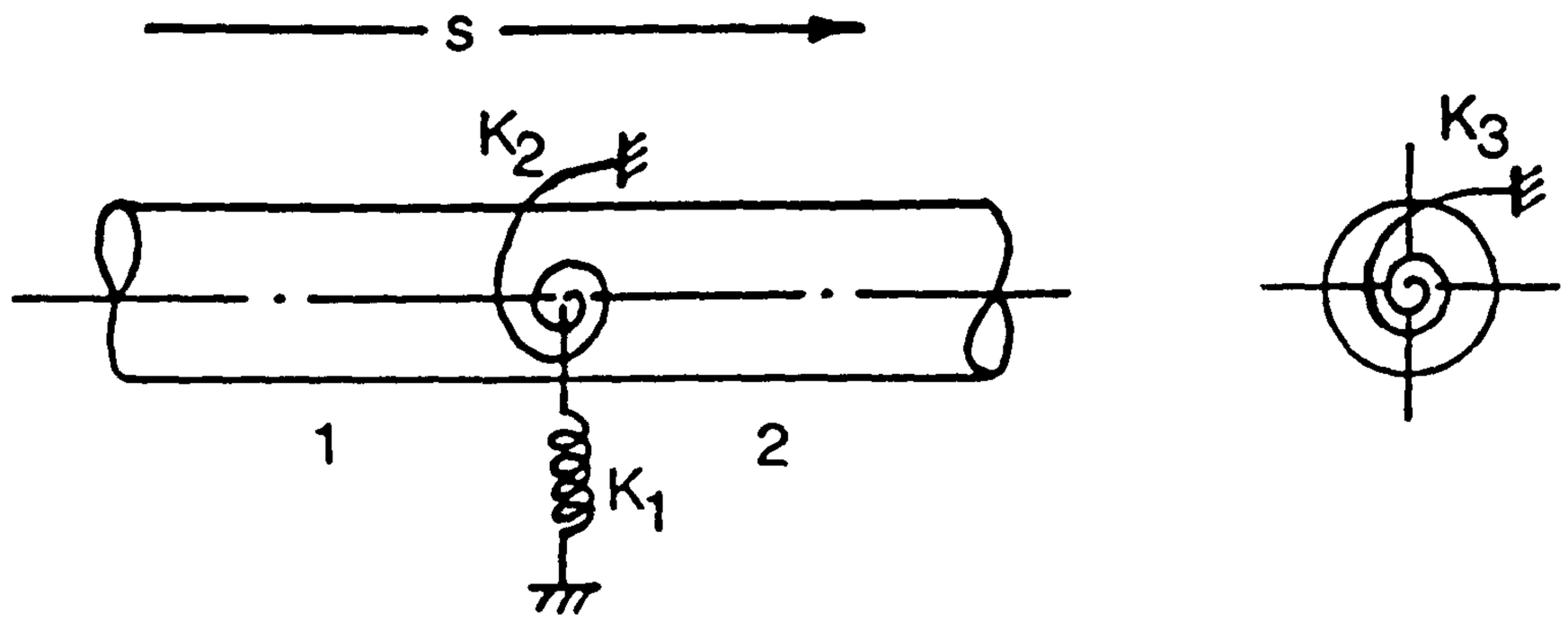

Figure 3.3 MODEL OF THE BRACE BAR

3.1.2 *Equations for U-Tube Configuration*

The above boundary conditions can be applied to the U-tube configuration in Figure 3.1 (other geometries can be treated in

similar fashion) as illustrated in Figure 3.4.

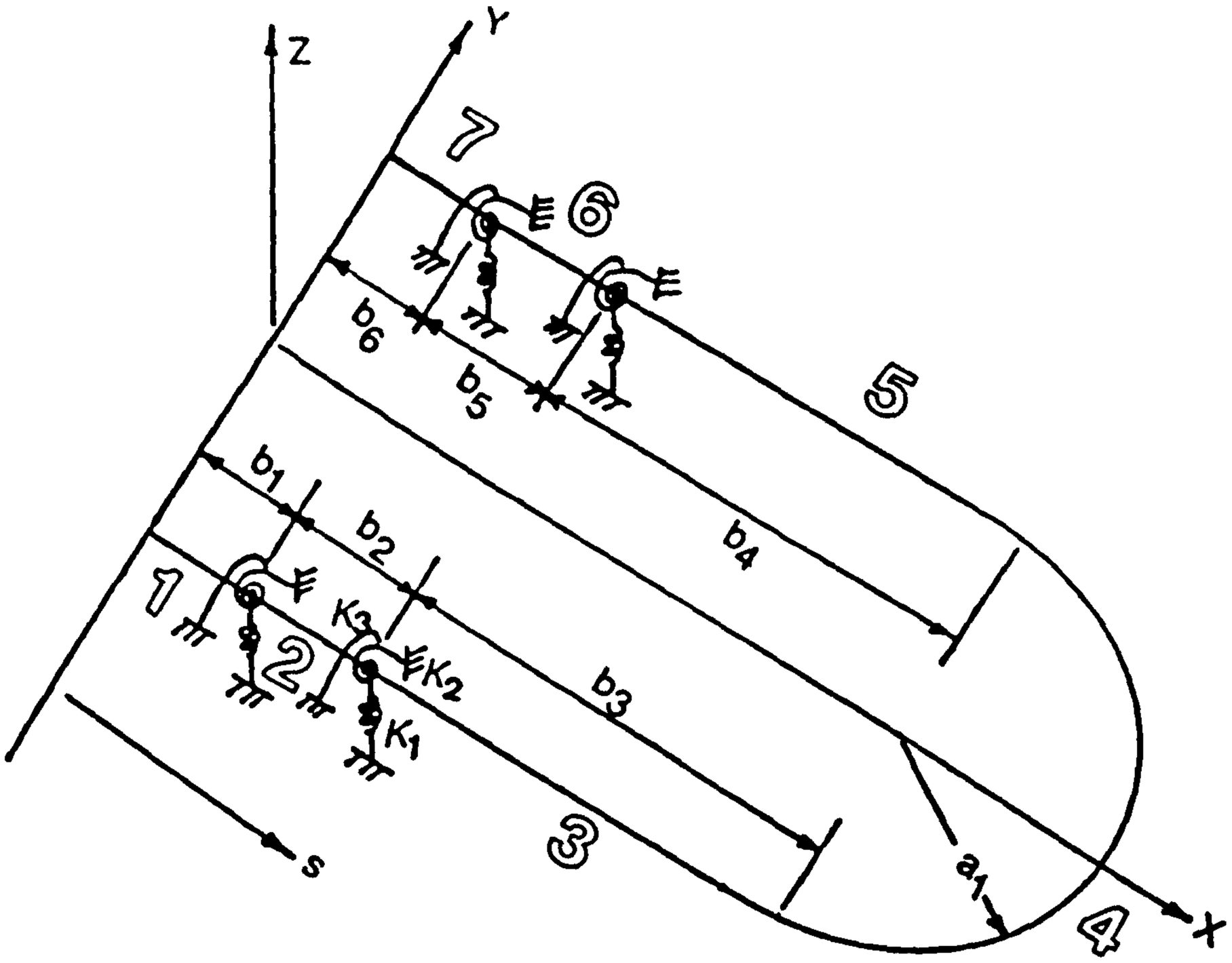

Figure 3.4 MODEL OF CORIOLIS MASS FLOWMETER INCORPORATING INTERMEDIATE SUPPORTS.

This incorporates six straight sections 1, 2, 3, 5, 6, 7 and a semi-circular tube 4. The positions of springs correspond to the brace bar locations and the ends of sections 1 and 7 on the y axis are clamped rigidly.

The boundary conditions (2.13), (2.19), (3.1) and (3.2) give

at $s = 0$ and $s = \sum_{i=1}^{6} b_i + a_1\pi$

$$v_1^* = v_7^* = \partial v_1^*/\partial s = \partial v_7^*/\partial s = \phi_1^* = \phi_7^* = 0 \qquad (3.3)$$

and the relations

$$\left.\begin{aligned} v_j^* &= v_4 \ , \ \partial v_j^*/\partial s = \partial v_4/\partial s \ , \ \phi_j^* = \phi_4 \ , \\ -\partial^2 v_j^*/\partial s^2 &= -\partial^2 v_4/\partial s^2 + \phi_4/a_1 \\ \partial \phi_j^*/\partial s &= \partial \phi_4/\partial s + a_1^{-1} \partial v_4/\partial s \\ -\partial^3 v_j^*/\partial s^3 &= -\partial^3 v_4/\partial s^3 + (GJ/EIa_1^2)\partial v_4/\partial s + ((EI+GJ)/EIa_1)\partial \phi_4/\partial s \end{aligned}\right\} \quad (3.4)$$

where j=3 or 5 at the junctions between straight and circular tube ($s = \sum_{i=1}^{3} b_i$ and $s = \sum_{i=1}^{3} b_i + a_1\pi$).

Finally at the spring attachments (for example $s=b_1$) the conditions are as follows

$$v_1^* = v_2^* \ , \ \partial v_1^*/\partial s = \partial v_2^*/\partial s \ , \ \phi_1^* = \phi_2^* \quad (3.5)$$

and

$$\left.\begin{aligned} \partial^3 v_1^*/\partial s^3 - (K_1/EI)v_1^* &= \partial^3 v_2^*/\partial s^3 \\ \partial^2 v_1^*/\partial s^2 + (K_2/EI)\partial v_1^*/\partial s &= \partial^2 v_2^*/\partial s^2 \\ \partial \phi_1^*/\partial s + (K_3/GJ)\phi_1^* &= \partial \phi_2^*/\partial s \end{aligned}\right\} \quad (3.6)$$

Expressions (3.5) and (3.6) can be applied to all other spring attachments by simply altering the straight tube numbers.

Now let non-dimensional quantities $\bar{K}_1$,$\bar{K}_2$ and $\bar{K}_3$ be related to actual quantities K_1, K_2 and K_3 as follows

$$\bar{K}_1 = (K_1/EI)a_1^3 \ , \ \bar{K}_2 = (K_2/EI)a_1 \ \text{ and } \ \bar{K}_3 = (K_3/GJ)a_1 \quad (3.7)$$

Using the same procedure as section 2.3.4 , fourty two relations between fourty two constants A_{ij}, B_{ij} and B_{0j} can be found from the boundary conditions (3.3), (3.4), (3.5) and (3.6), these relations are summarized in appendix **D**.

3.1.3 *Some Numerical Results*

The non-dimensional frequencies and mode shapes were calculated by the same numerical method as in section(2.3.5). Using the new boundary condition one obtains a [42x42] determinant (see appendix D) and a [41x41] reduced matrix for the U-tube configuration with four intermediate supports.

The effect of non-dimensional stiffness coefficient $\tilde{K}_1$ on the fundamental and second mode shapes is shown in Figure 3.5. Here $K=0.7692$, $\beta=u=0$ and $b_1/a_1=b_2/a=b_3/a_1=1$ (note that dashed circles indicate the spring positions) . They indicate the reduction in non-dimensional displacement with increasing $\tilde{K}_1$ at the attachment points. It is clearly seen that the effect of increasing $\tilde{K}_1$ is to increase the natural frequencies (see Figure 3.6 in which $K=0.7692$, $\beta=u=0$, $b_1/a_1=b_2/a_1=0.25$ and $b_3/a_1=1$).

Figure 3.7 shows the effect of the position of the second and third attachment points on the fundamental frequency for different $\tilde{K}_1$, where $\beta=u=0$, $K=0.7692$ and $b_1/a_1=0.1$.

In a similar fashion the influence of non-dimensional rotational and torsional stiffness coefficients ($\tilde{K}_2$ and $\tilde{K}_3$) is to increase the natural frequencies of the U-tube as shown in Figure 3.8 and 3.9) respectively (for $\beta=u=0$, $K=0.7692$, $b_1/a_1=b_2/a_1=0.25$ and $b_3/a_1=1$). Figure 3.10 shows the reduction in the slope with increasing $\tilde{K}_2$ (for fundamental and second mode) whilst Figure 3.11 shows the reduction in the twisting with increasing $\tilde{K}_3$ (for fundamental mode) , for $K=0.7692$, $\beta=u=0$ and $b_1/a_1=b_2/a_1=b_3/a_1=1$.

3.1.4 *Calculation of Stiffness Coefficients*

By way of an example the dimensions of a stainless steel brace bar of the commercial Micro Motion Coriolis flowmeter are adopted, as shown in Figure 3.12.

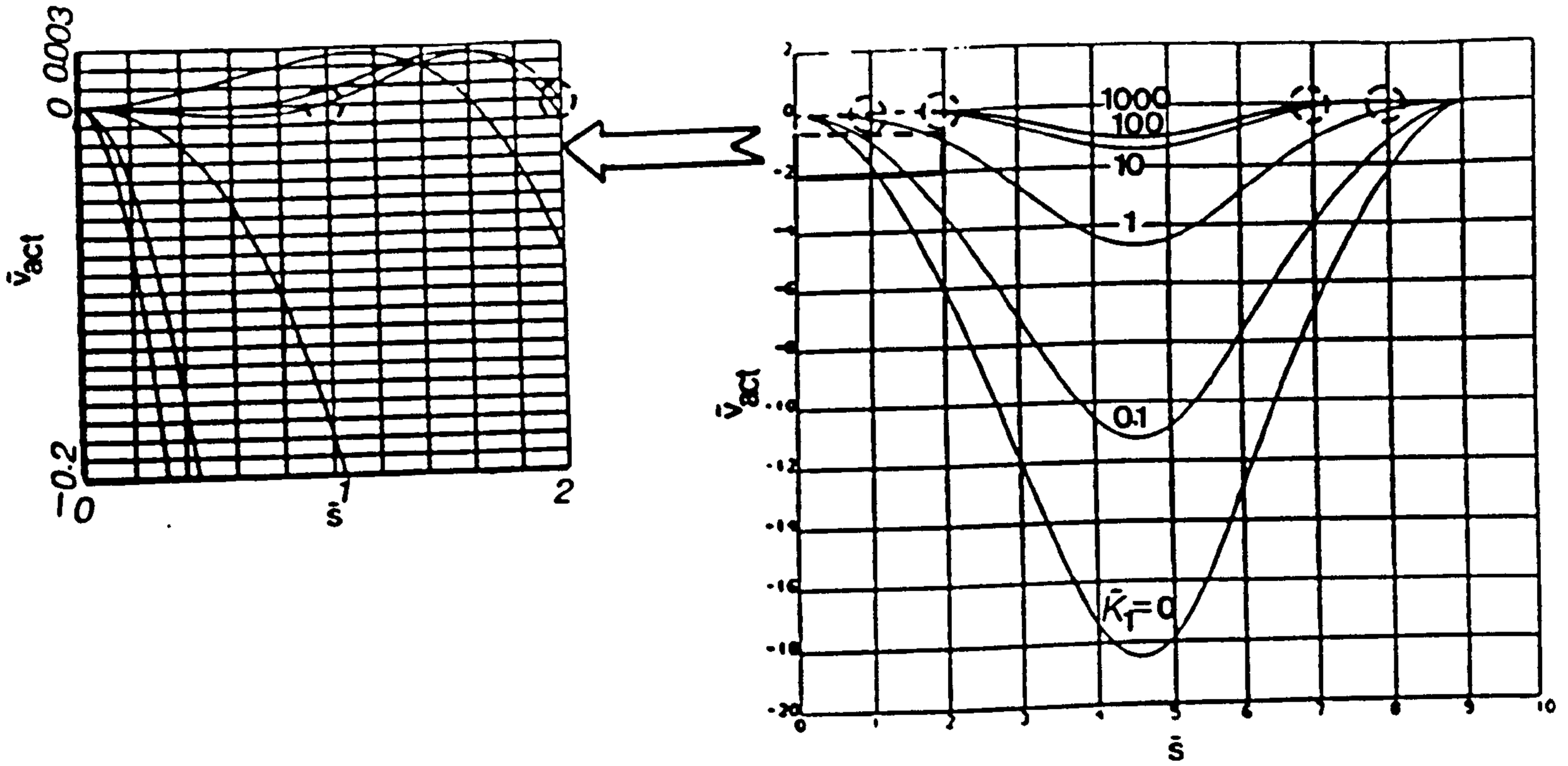

(a) Fundamental Mode

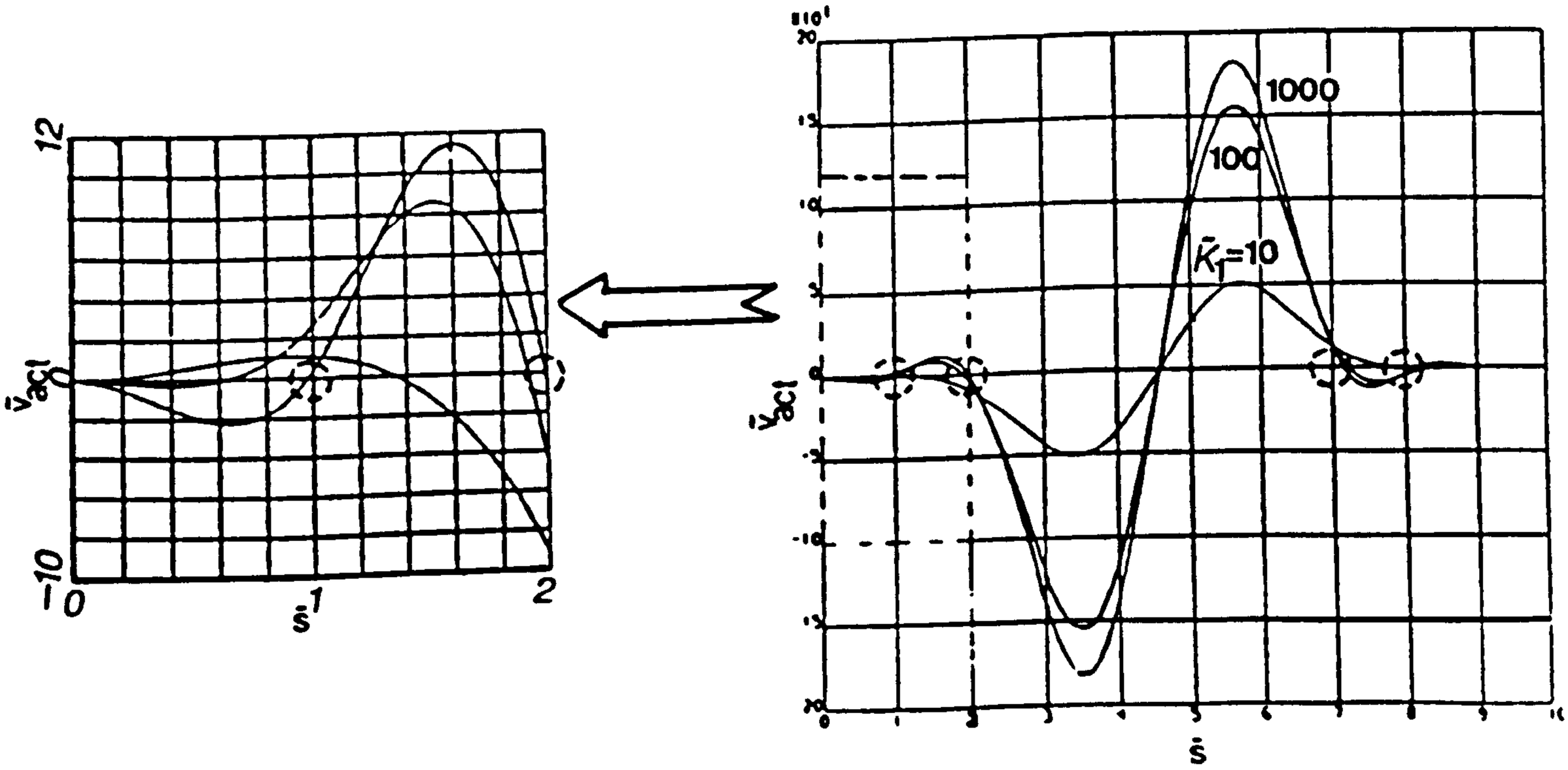

(b) Second Mode

Figure 3.5 THE EFFECT OF $\tilde{K}_1$ ON THE MODE SHAPES

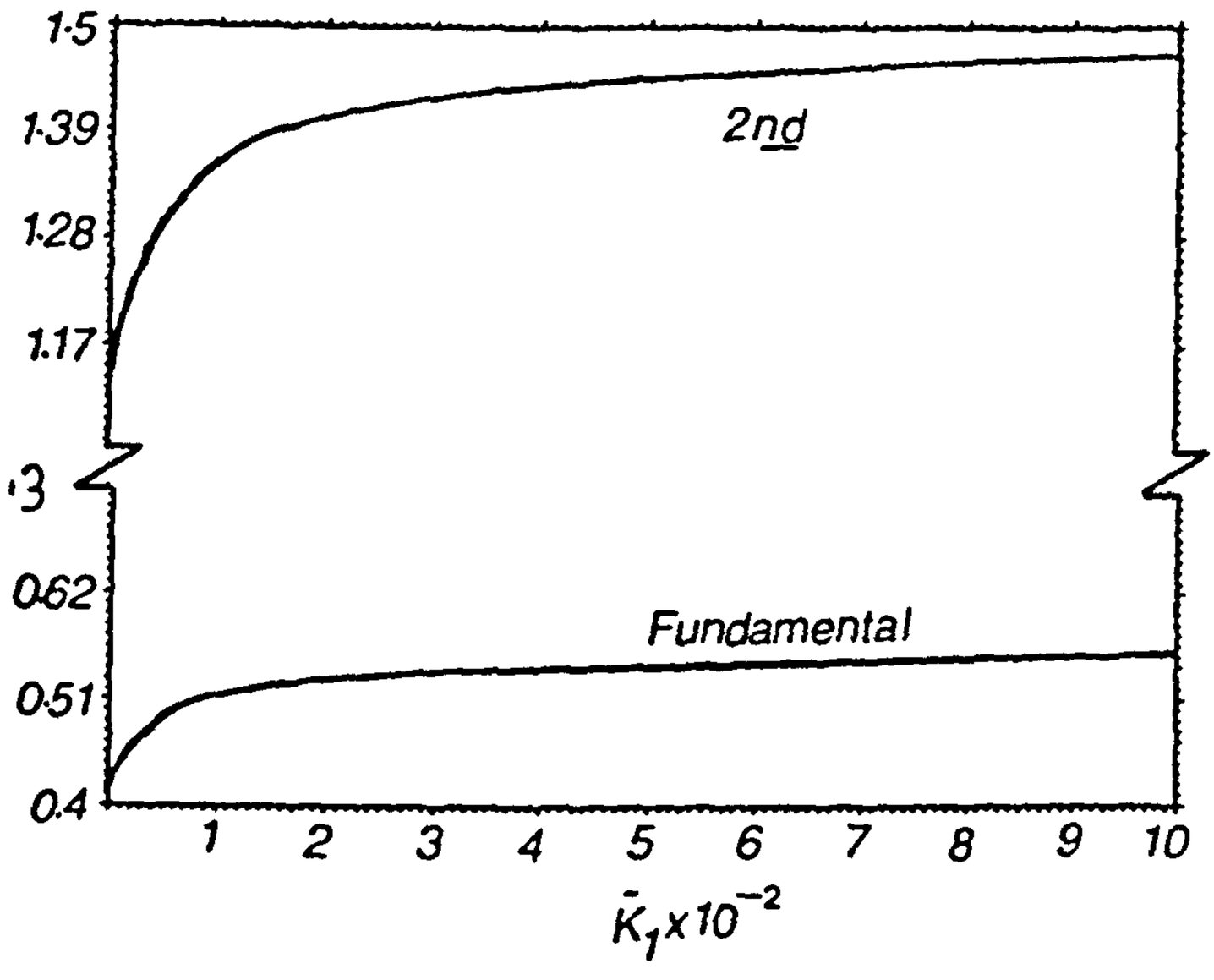

Figure 3.6 NON-DIMENSIONAL FREQUENCY VERSUS $\tilde{K}_1$

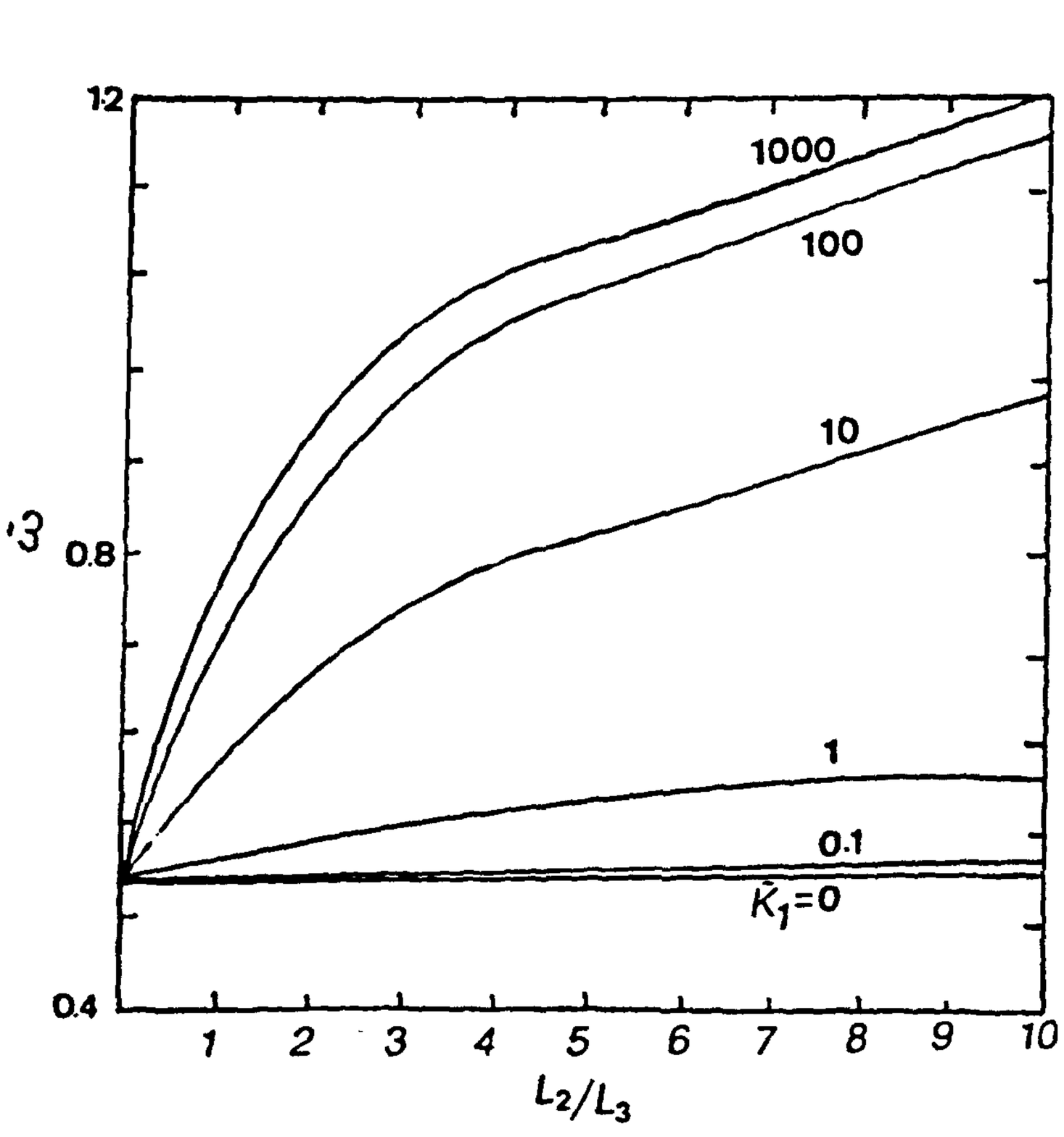

Figure 3.7 THE EFFECT OF TRANSLATIONAL SPRING POSITION ON NON-DIMENSIONAL FREQUENCY.

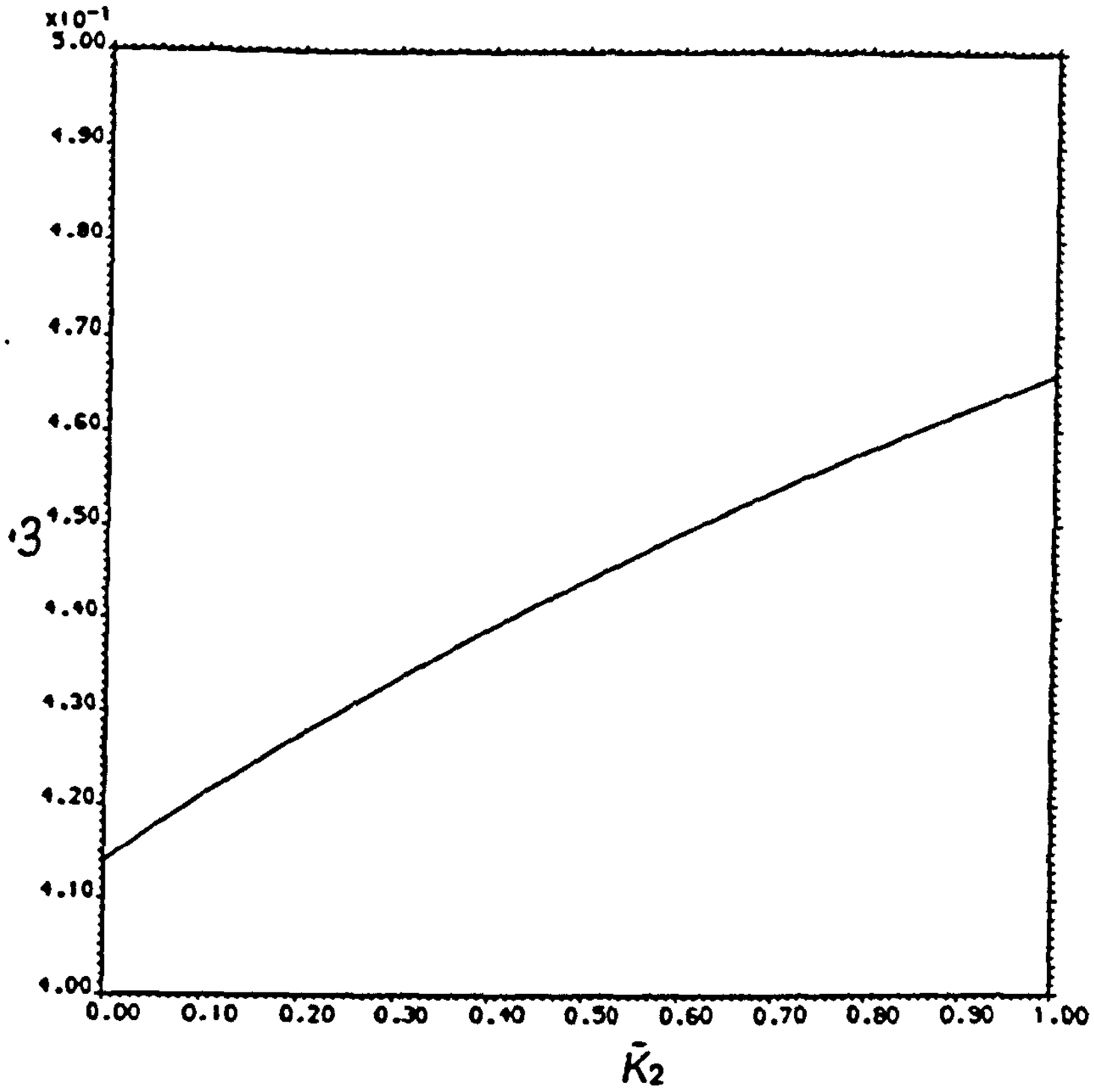

Figure 3.8 NON-DIMENSIONAL FREQUENCY VERSUS $\tilde{K}_2$

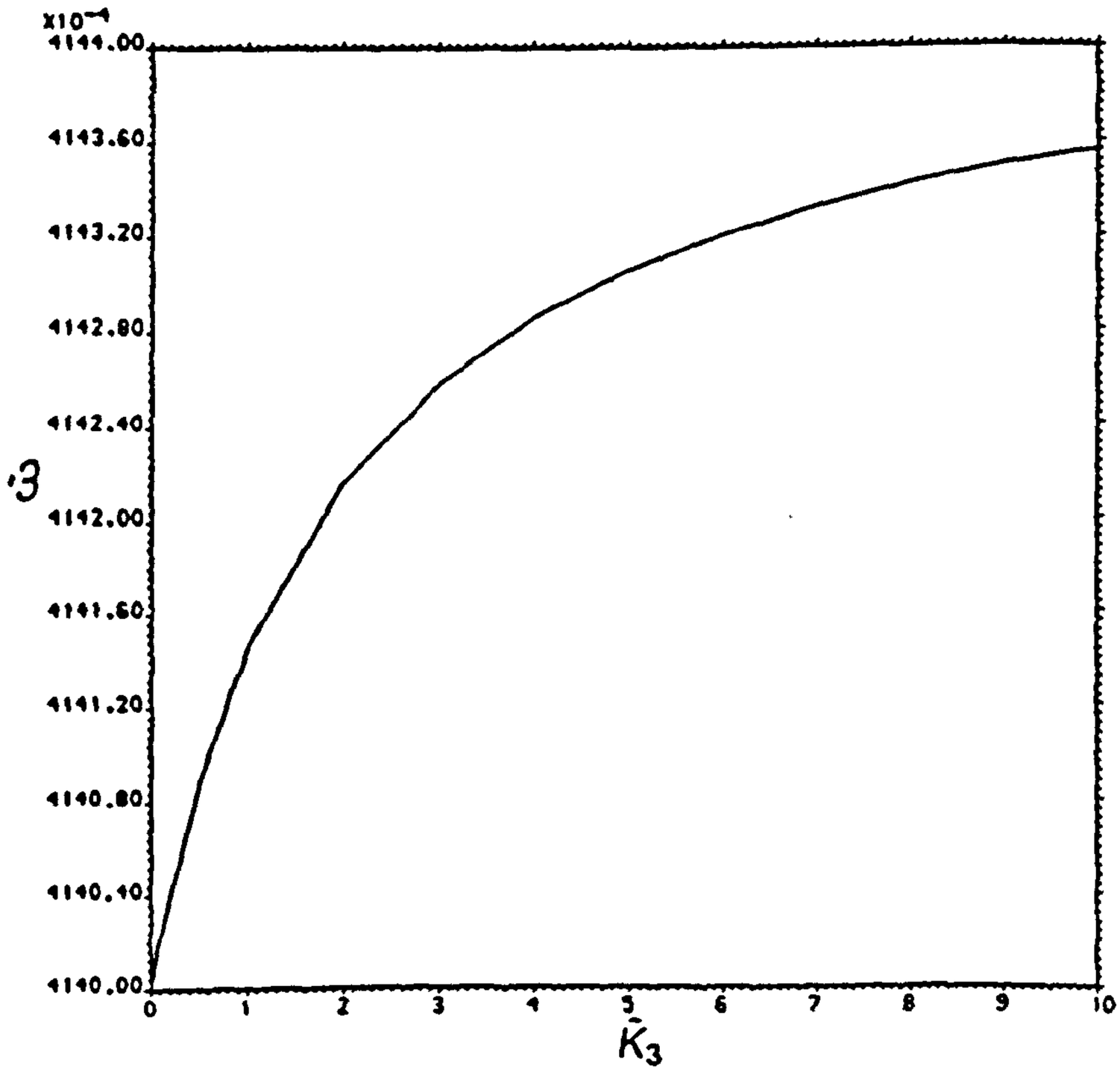

Figure 3.9 NON-DIMESIONAL FREQUENCY VERSUS $\tilde{K}_3$

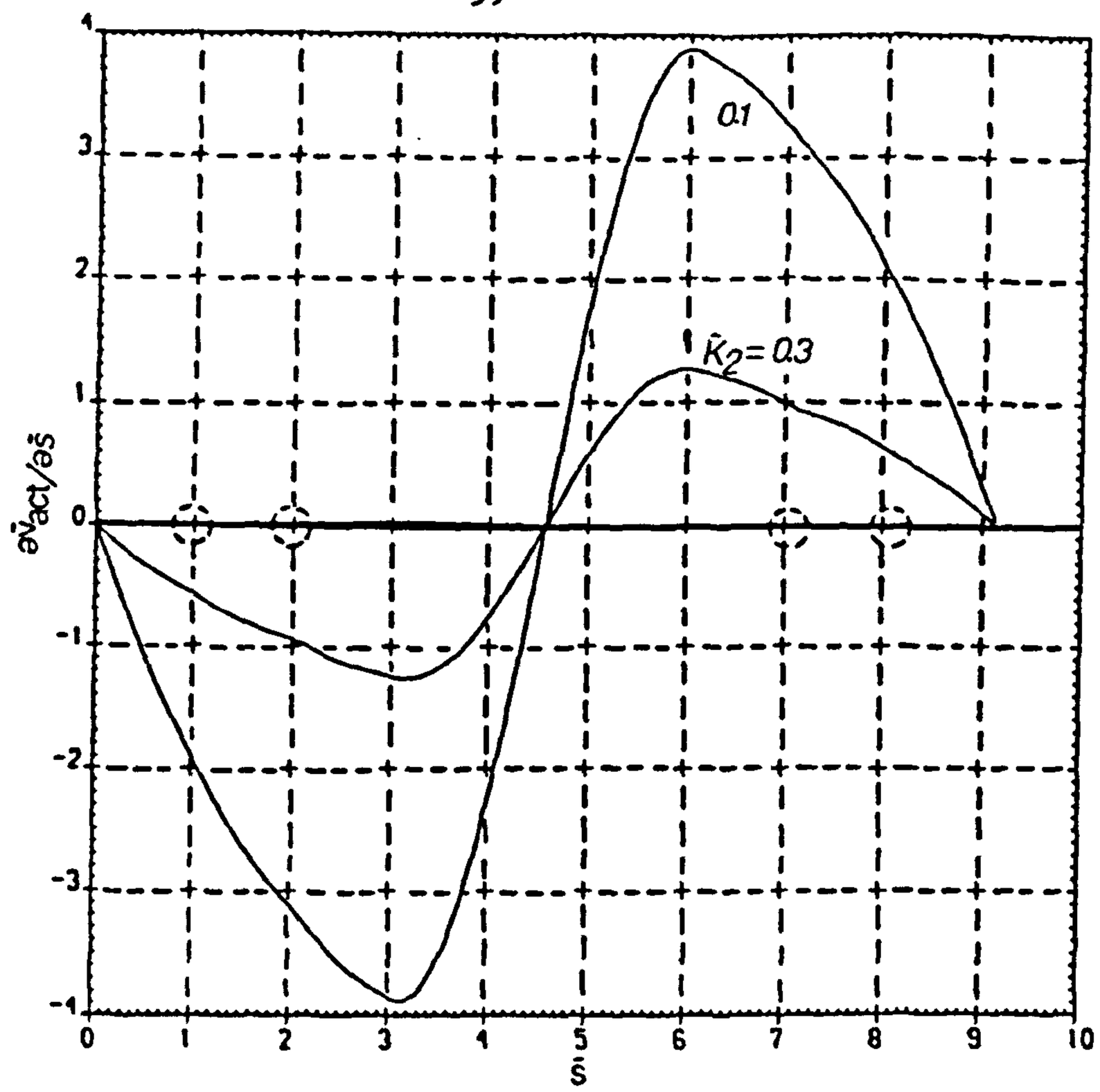

(a) Fundamental Mode

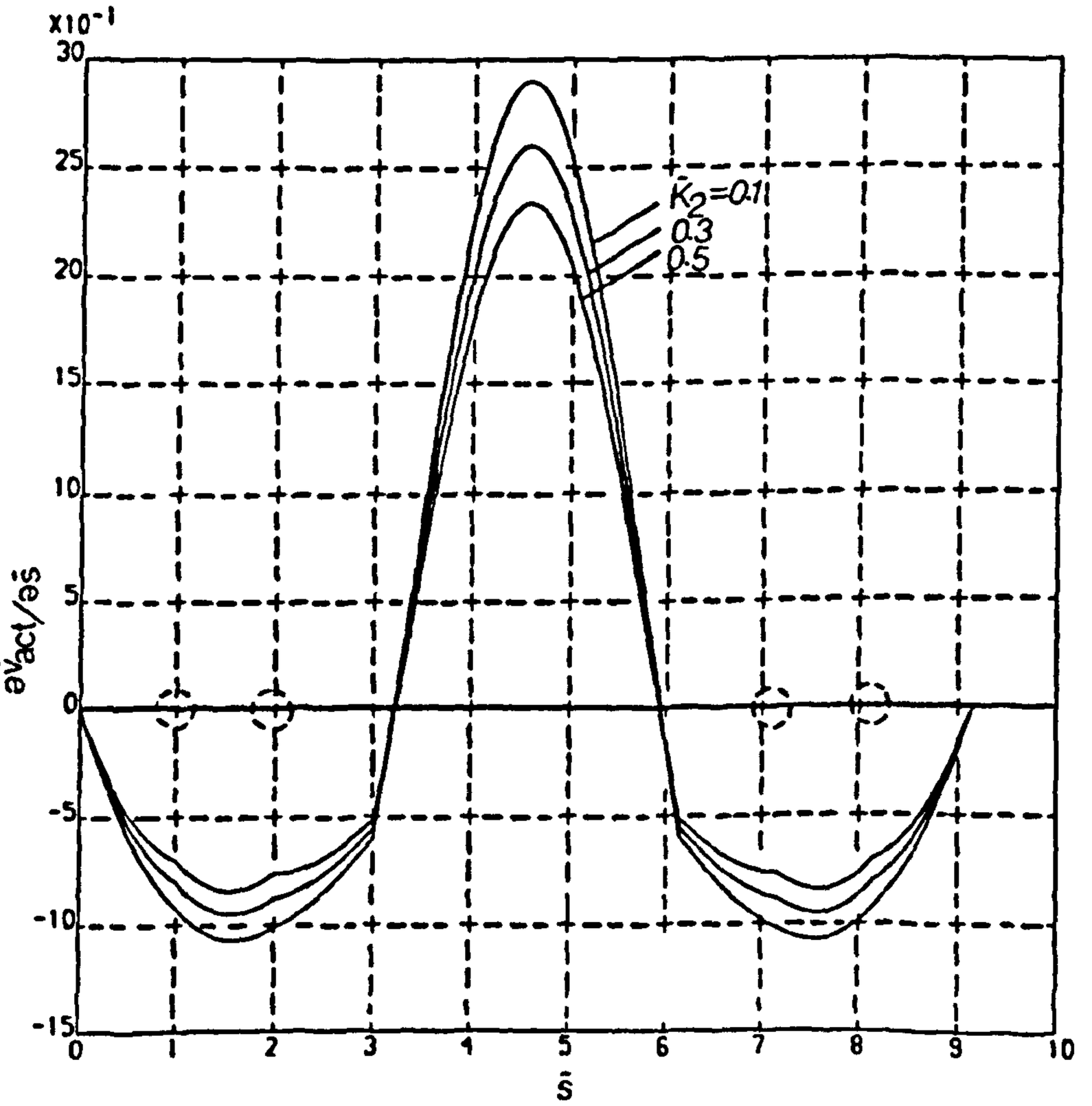

(b) Second Mode

Figure 3.10 THE EFFECT OF $\tilde{K}_2$ ON THE SLOPE

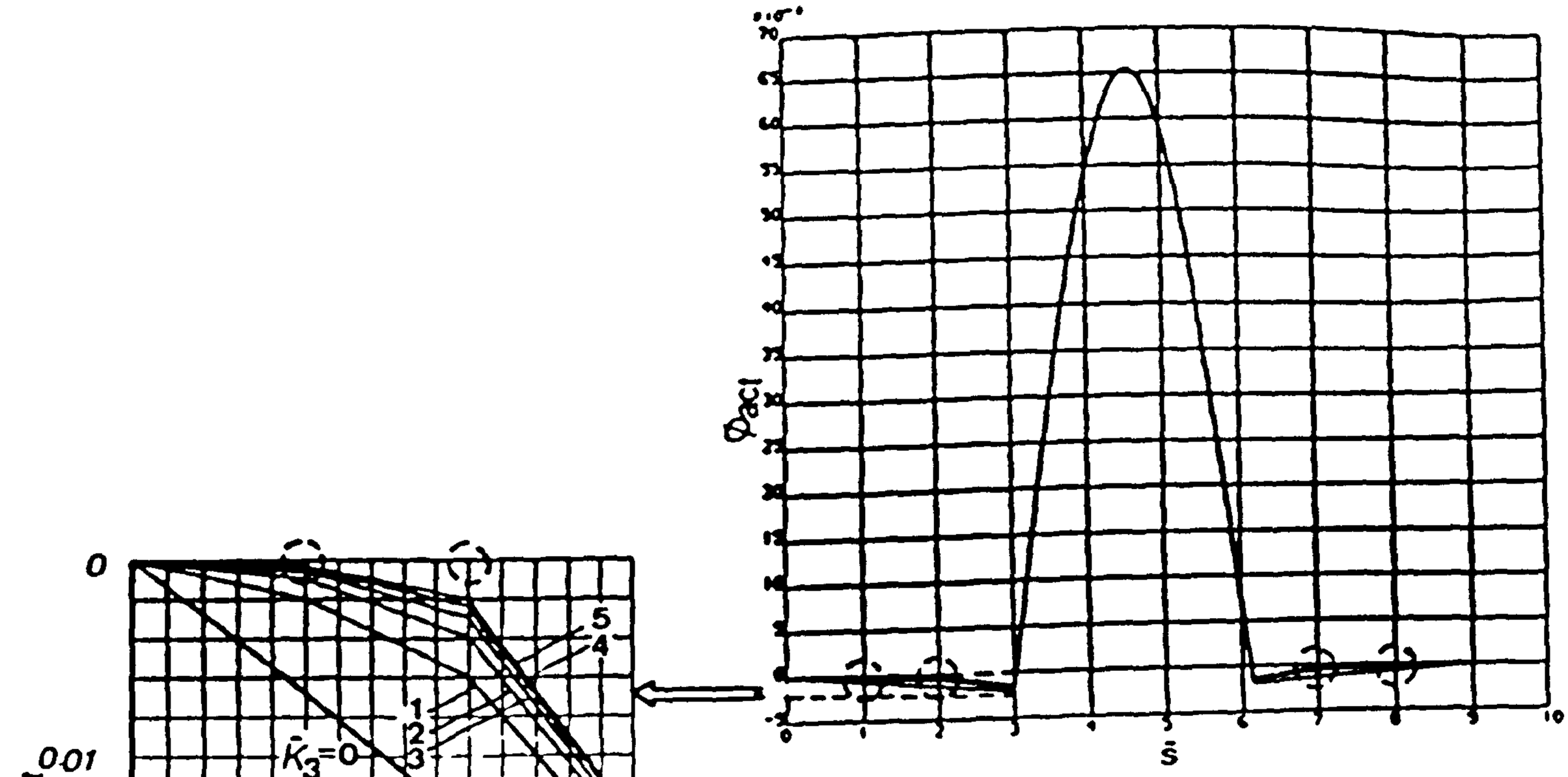

Figure 3.11 THE EFFECT OF $\bar{K}_3$ ON THE TWIST (*fundamental mode*)

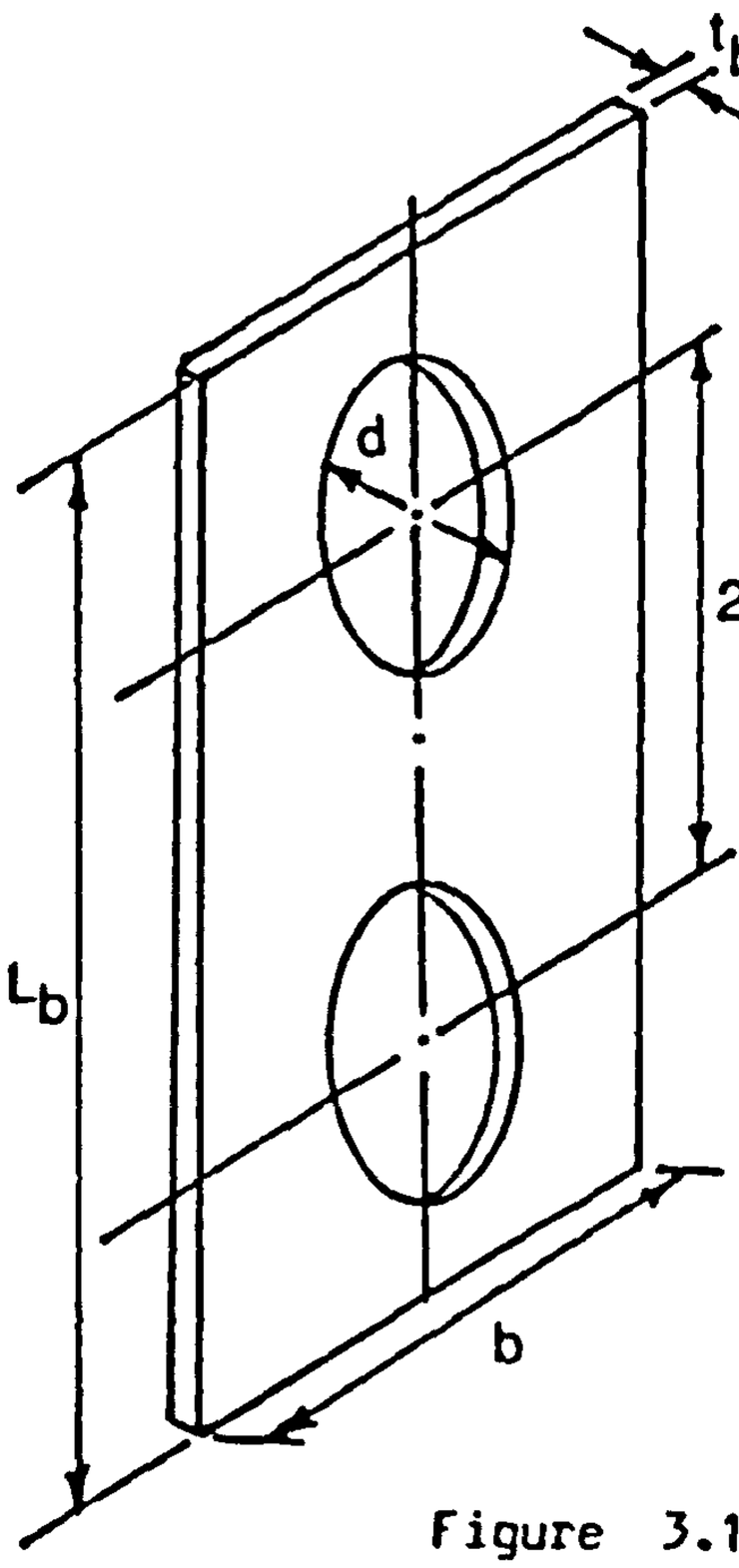

b= 76
h= 18
t_b= 4
d = 50·8
L_b= 139
(mm)

Figure 3.12 DIMENSIONS OF THE BRACE BAR

To calculate the three stiffness coefficients K_1, K_2 and K_3 of the brace bar, two methods are considered as follows

3.1.4.1 Simple Analytical Method

(i) Translational Stiffness Coefficient K_1

Take half of the brace (Figure 3.13a) and assume that the tube applies a load F at the centre of the shaded area. From the simple force-strain relation [66] we have

$$K_1 = F/\delta \tag{3.8}$$

and the stress-strain relation gives

$$\sigma_b = E_b \epsilon = F/t_b\, d \tag{3.9}$$

where σ_b and ϵ are the stress and strain respectively due to tension and E_b is Young's modulus of the brace. Since

$$\epsilon = \delta/h \tag{3.10}$$

then from equations (3.8), (3.9) and (3.10)

$$K_1 = E_b \frac{t_b\, d}{h} \tag{3.11}$$

Now, using the dimensions displayed in Figure 3.12 and E_b=208 GN/m^2 equation 3.11 gives

$$K_1 = 2.41517 \qquad [GN/m]$$

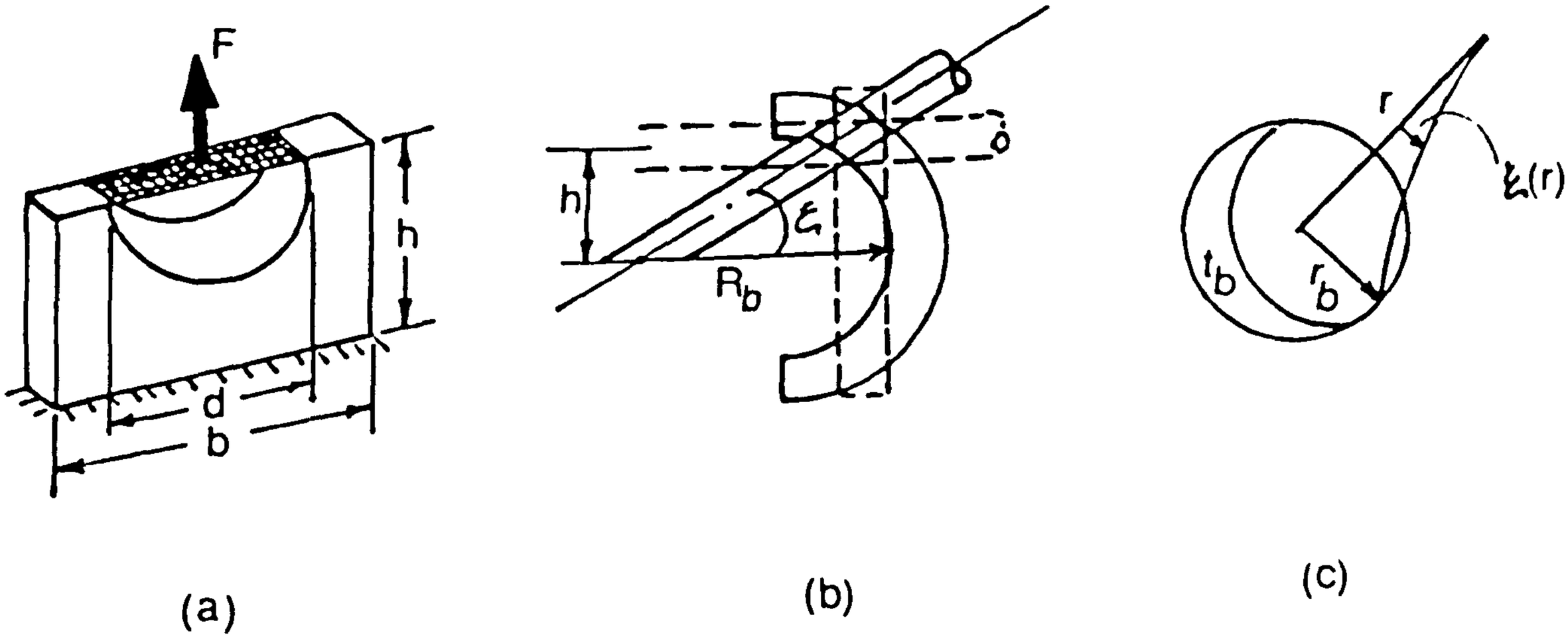

Figure 3.13 BRACE BAR UNDER (a) Tension, (b) Bending, (c) Torsion

(ii) Rotational Stiffness Coefficient K_z

Assume that the brace bends into a circle with a large radius of curvature R_b, as shown in Figure 3.13b.

Moment-slope relation [66] is

$$K_z = M/c \tag{3.12}$$

where c is the slope, and simple bending theory states

$$M_b = \frac{E_b\ I_b}{R_b} \tag{3.13}$$

substituting equation (3.13) in (3.12) gives

$$K_z = \frac{E_b\ I_b}{R_b\ c} \tag{3.14}$$

for small ϵ ; $R_b = h/\epsilon$ and substituting for R and $I_b = \frac{b\ t_b^3}{12}$ gives

$$K_2 = \frac{E_b\ b\ t_b^3}{12h} \qquad (3.15)$$

for the same dimensions as in Figure 3.12 and E_b=208 GN/m² equation (3.15) gives

$$K_2 = 4817.6762 \quad [N.m]$$

(iii) Torsional Stiffness Coefficient K_3

Assume that the torsional displacement (ξ) is some function of r as shown in Figure 3.13c.

Torque-twist relation states [66]

$$K_3 = T/\Gamma \qquad (3.16)$$

where Γ is twist angle. According to Figure 3.13c (for small Γ) $\Gamma=\xi/r$. On the other hand

$$\tau = G_b\ d\xi/dr \qquad (3.17)$$

and

$$T = -\tau(2\pi\ t_b\ r)\ r \qquad (3.18)$$

where τ, T and G_b are shear stress, torque and shear modulus respectively. Substituting (3.17) in (3.18) gives

$$T = -2\pi\ t_b\ G_b\ r^2\ d\xi/dr \qquad (3.19)$$

integrating with respect to r from r_b to ∞ gives

integrating with respect to r from r_b to ∞ gives

$$[\varepsilon]_{r_b} = \frac{T}{2\pi\, G_b\, t_b\, r_b} = r\, r_b \qquad (3.20)$$

substituting (3.20) in (3.16) gives

$$K_3 = 2\pi\, G_b\, t_b\, r_b^2 \qquad (3.21)$$

using dimensions as in Figure 3.12 and G_b=80 GN/m² equation (3.21) gives

$$K_3 = 1297.171 \quad [KN.m]$$

3.1.4.2 Standard Numerical Method

By adopting I-DEAS "Integrated Design Engineering Analysis Software" [69,70] and PAFEC "Programme for Automatic Finite Element Calculation" [71], the numerical values for K_1, K_2 and K_3 can be obtained. Figure 3.14 illustrates the main flow chart of this method.

The dimensions and geometry of Figure 3.12 are entered and regenerated by I-DEAS-GEOMOD modeller. The finite element mesh phase is then obtained by the I-DEAS-SUPERTAB modeller. The geometry and mesh information is then transferred to PAFEC via IDSPAF interface, resulting in a universal output file. The material properties, restraints and prescription of the loads are then entered.

Following the execution of PAFEC version 6.1, the resulting output file is transferred back to I-DEAS-SUPERTAB (using IDSPAF interface mode) in order to post-process the results and thus obtain the stress distributions and deformed geometry.

This procedure is repeated for three different load cases;compression, bending and torsion.

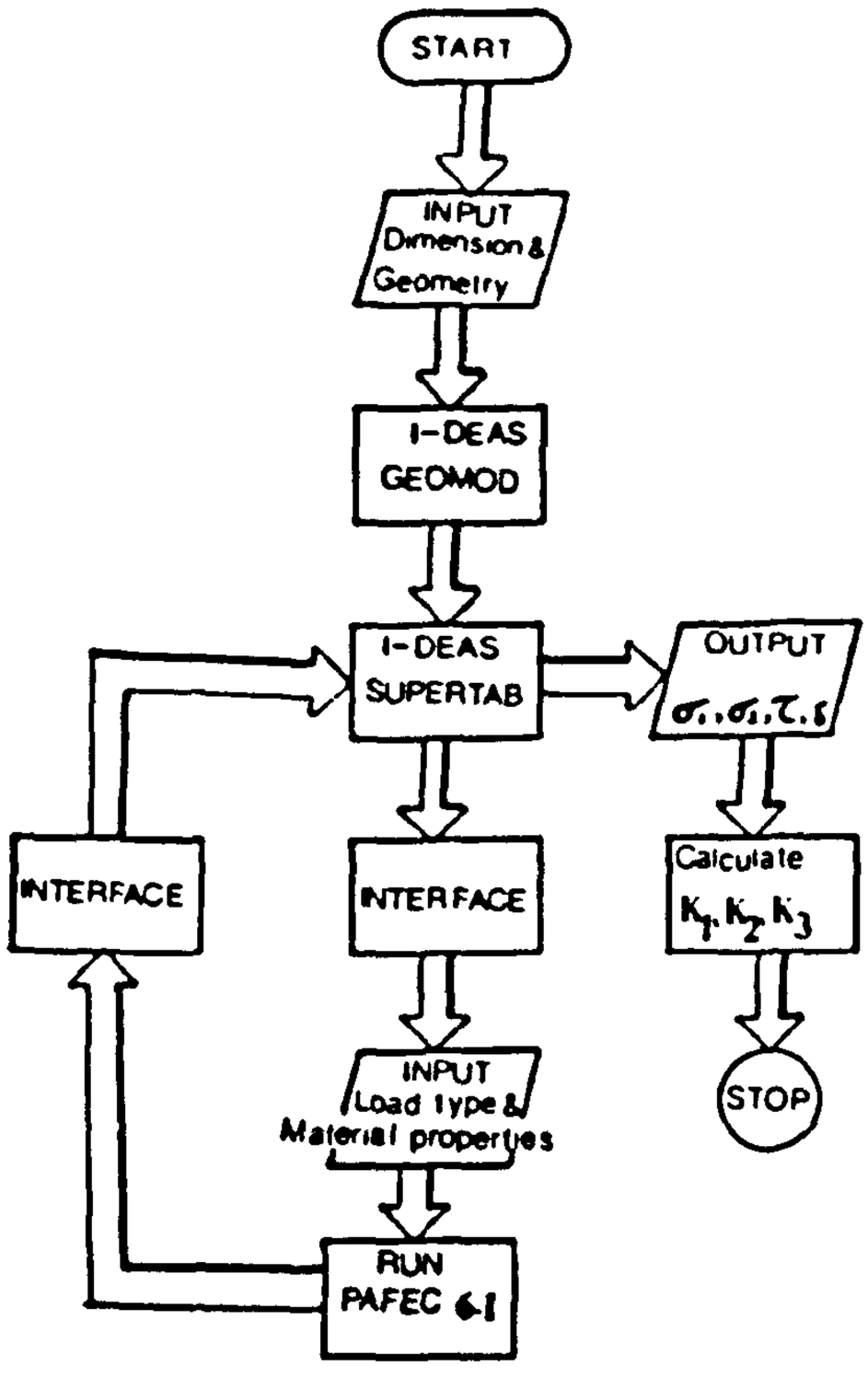

Figure 3.14 THE FLOW CHART OF THE NUMERICAL METHOD

(i) Compression

Utilizing symmetry, one quarter of Figure 3.12 is restrained at one end whilst a 0.1 mm displacement (simulating for compression load) is applied on the nodes around the hole, as shown in Figure 3.15a. The stress distributions and deformed geometry are as illustrated in Figures 3.15 and 3.16.

The reaction force (F_r) is given by integrating the nodal stress (σ_y) at the restrained end. Using Simpson's rule (Figure 3.17) gives

$$F_r = \int_0^{b/2} \sigma_y \, t \, dx = \frac{t\Delta x}{3} [\sigma y_0 + 4\sigma y_1 + 2\sigma y_2 + 4\sigma y_3 + \ldots + 2\sigma y_{n-2} + 4\sigma y_{n-1} + \sigma y_n] \qquad (3.21)$$

with $\Delta x = 1.9 \times 10^{-3}$ (m) , equation 3.21 gives

$$F_r = 218.3632 \quad \text{(KN)}$$

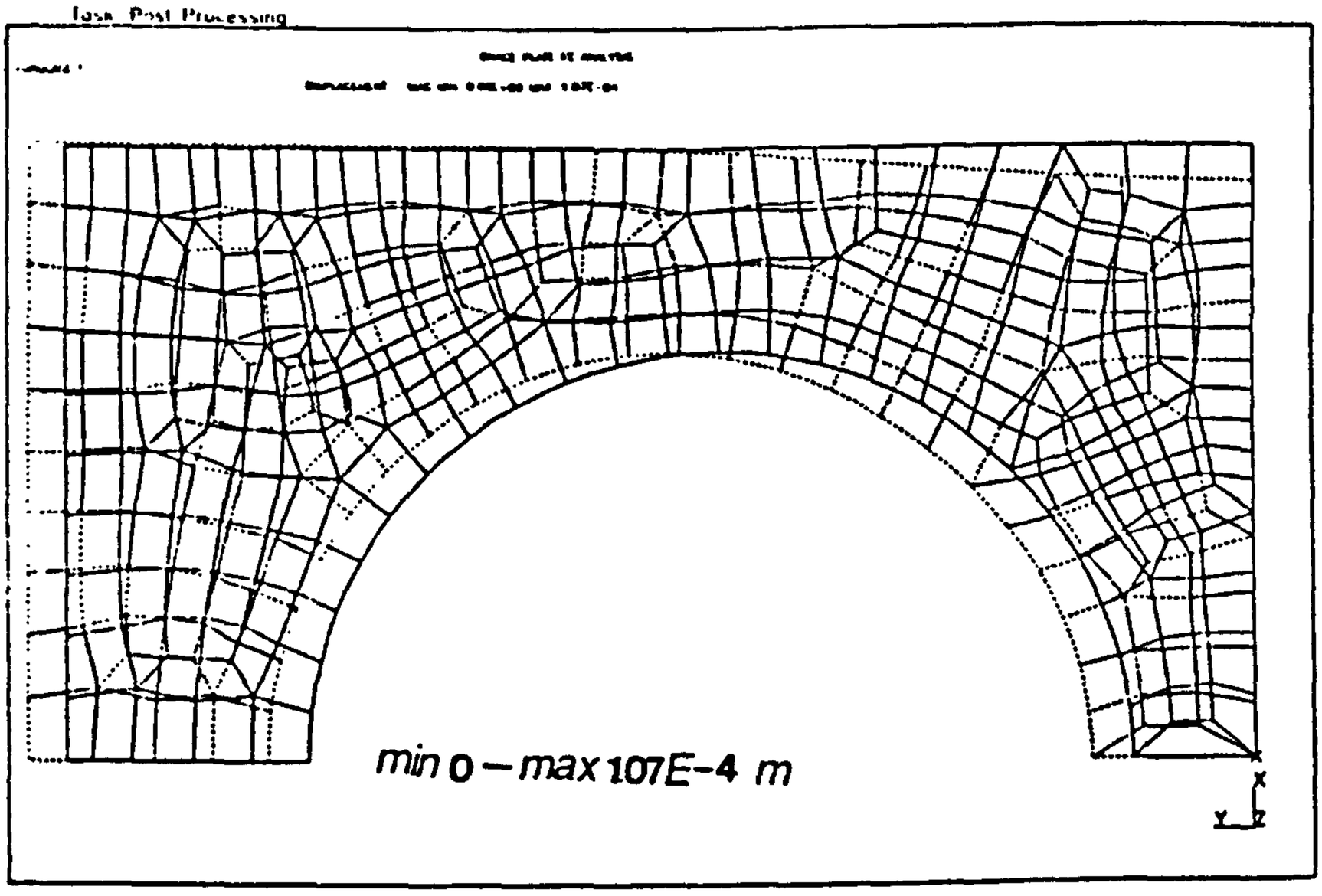

(a) Deformed Geometry

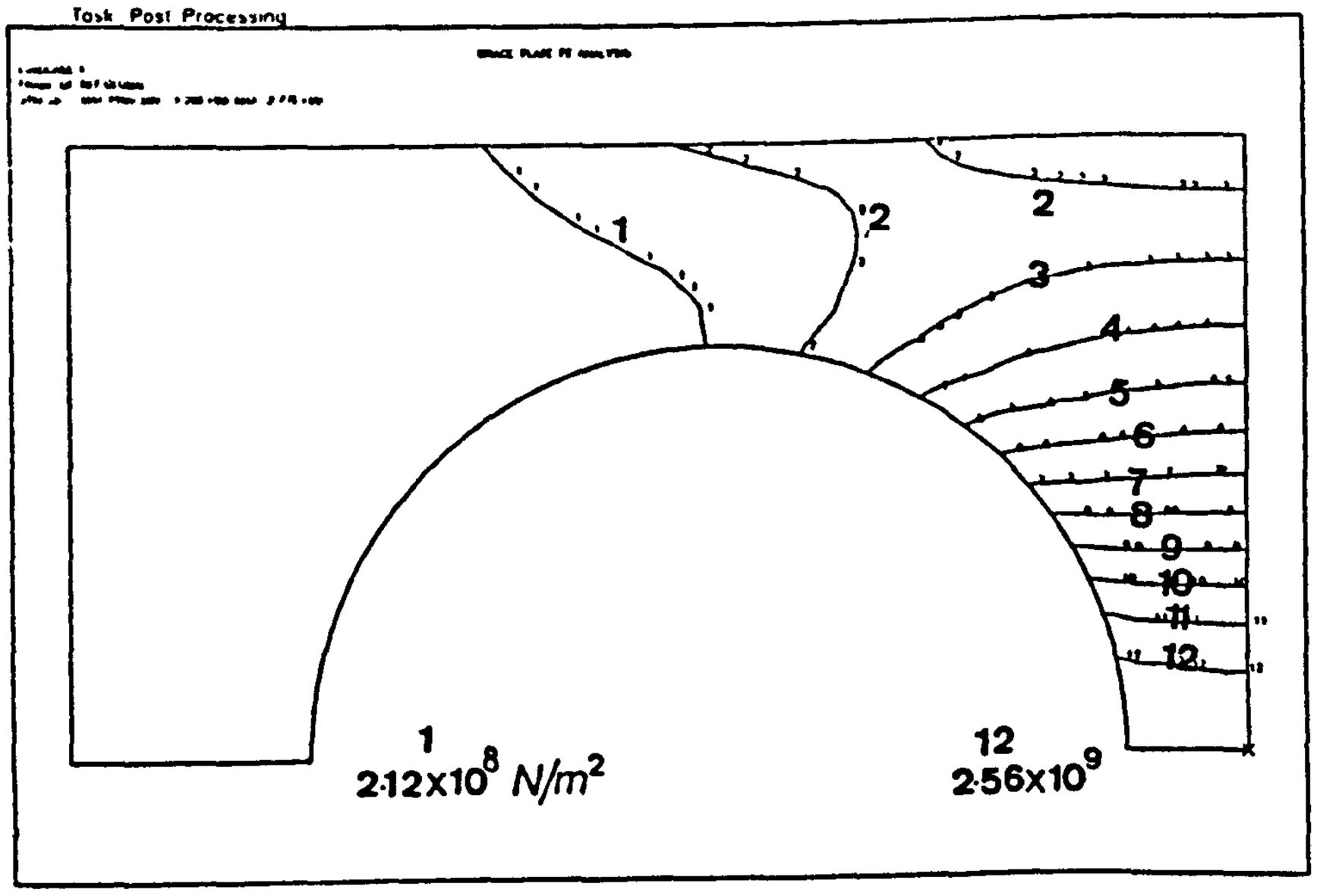

(b) Maximum principal stress

Figure 3.15 BRACE BAR UNDER COMPRESSION

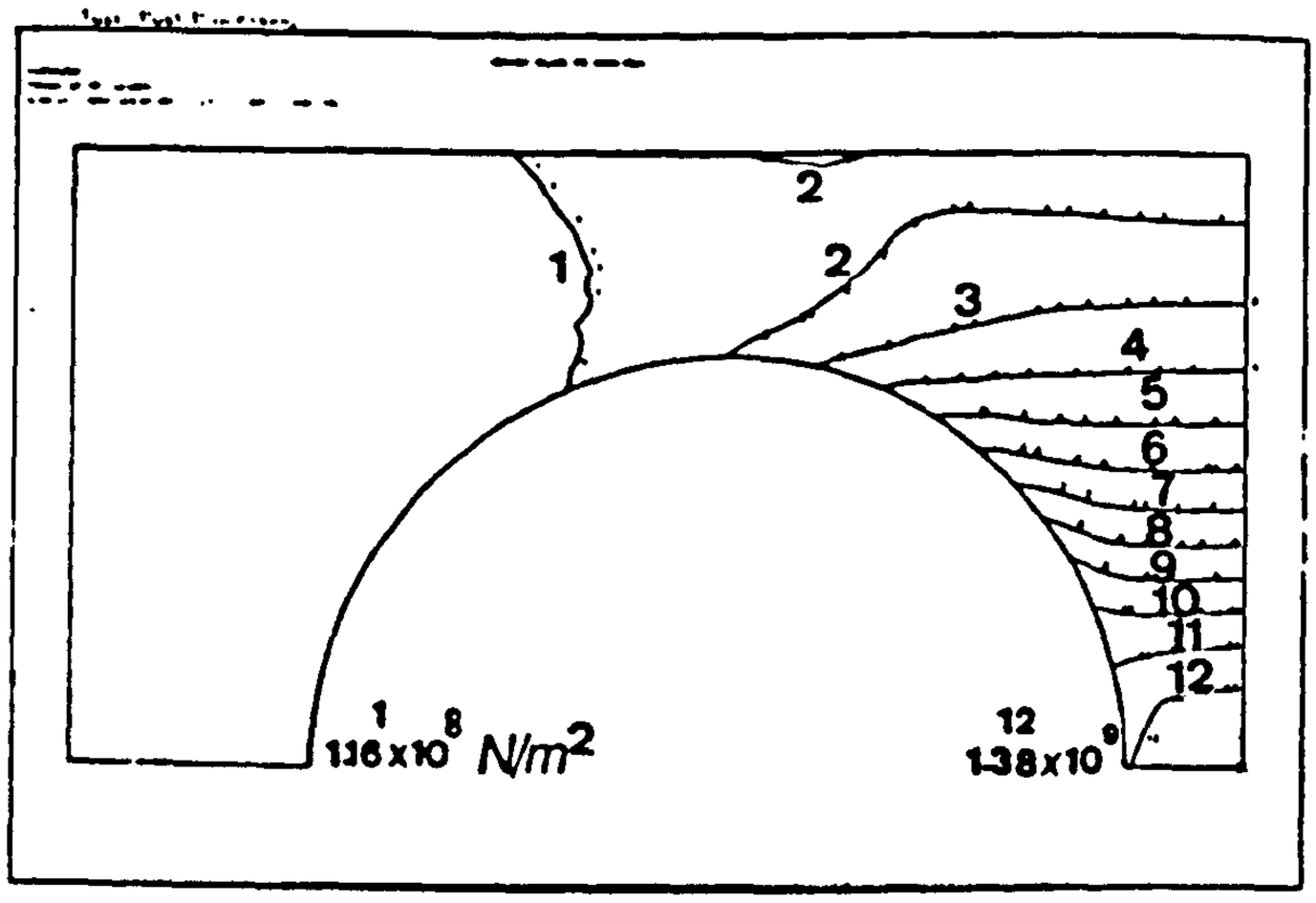

(a) maximum shear stress

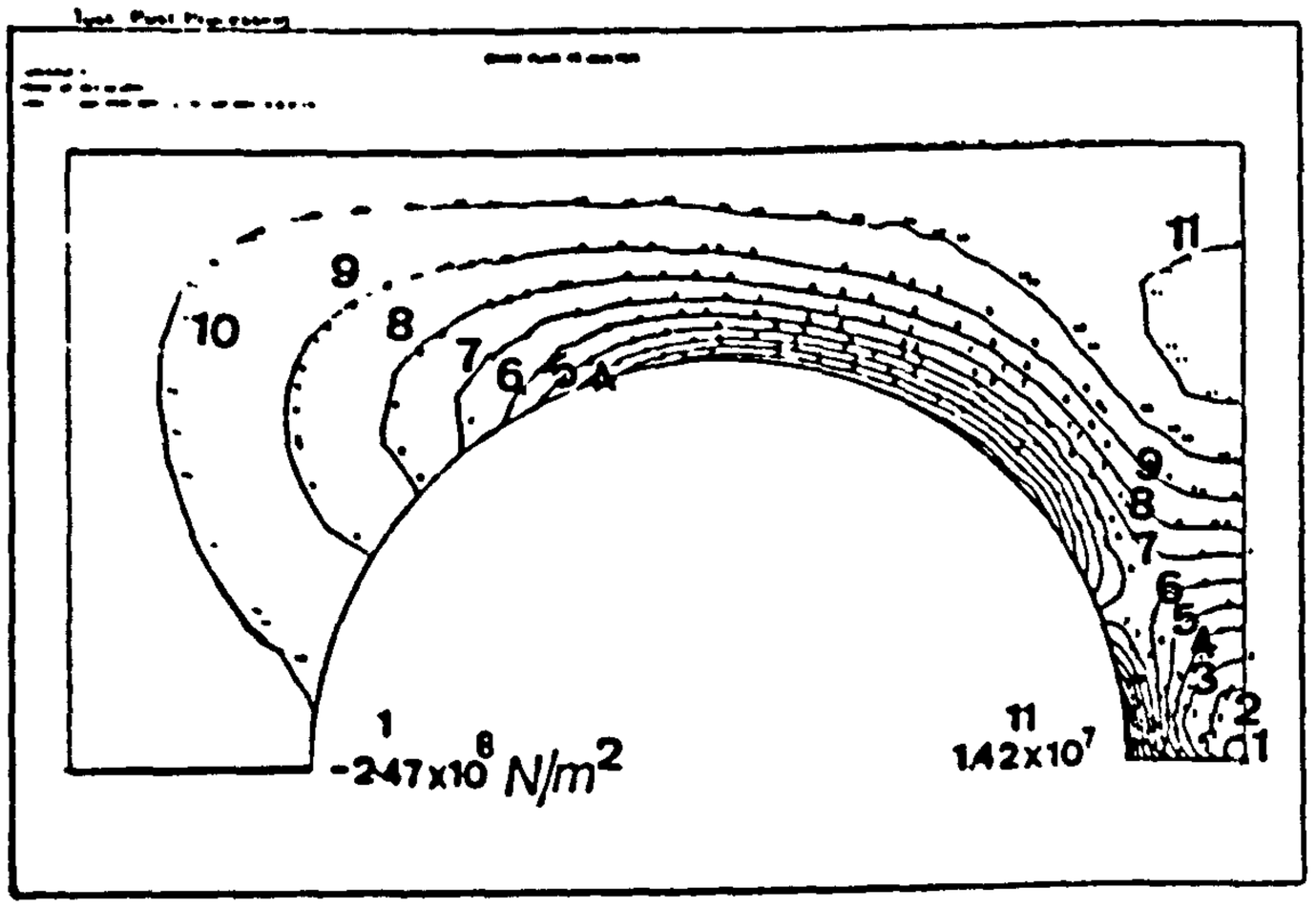

(b) mimimum principal stress

Figure 3.16 BRACE BAR UNDER COMPRESSION

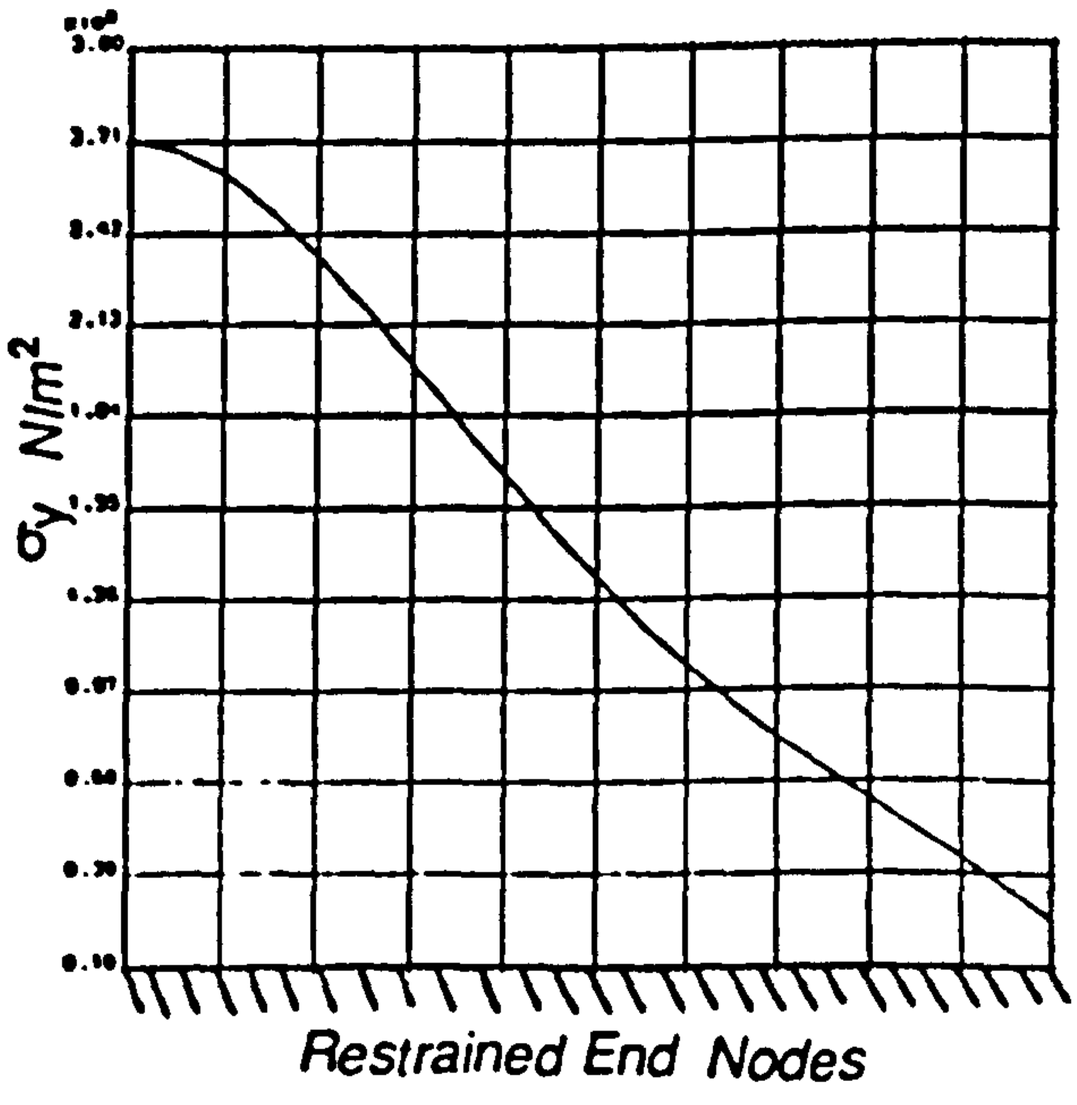

Figure 3.17 STRESS DISTRIBUTION ON THE RESTRAINED END

therefore

$$K_1 = 2.183632 \quad (GN/m)$$

(ii) Bending

To model bending, two forces equal in magnitude(50 N) and opposite in direction are applied vertically at two nodes on the hole as demonstrated in Figure 3.18a. Deformed geometry, stress distribution (see Figures 3.18 and 3.19) and the nodal slope (inclination of plane) at the centre are obtained using the previous procedure. K_2 can then be simply calculated as follows

$$K_2 = \frac{Fd}{slope} = 1273.8215 \quad (N.m)$$

where $d = 50.8$ (mm) and $slope = 1.994 \times 10^{-3}$ (rad)

(iii) Torsion

To represent torsion, two in-plane forces (equal in magnitude (50 N) and opposite in direction) are applied at two diametrically opposite nodes 1 and 2 on the hole as shown in Figure 3.20a. Maximum shear stress distribution and deformation geometry are obtained as shown in Figure 3.20. Twist angle can be calculated as follows

$$\theta_t = \tan^{-1} \delta/d = 2.894 \times 10^{-5} \quad (rad)$$

where δ is the displacement at node 1 - displacement at node 2 = 1.47×10^{-6} m.

therefore

$$K_3 = \frac{Fd}{\theta_t} = 87.777 \quad [KN.m]$$

When compared with the analytical results, the numerical method shows

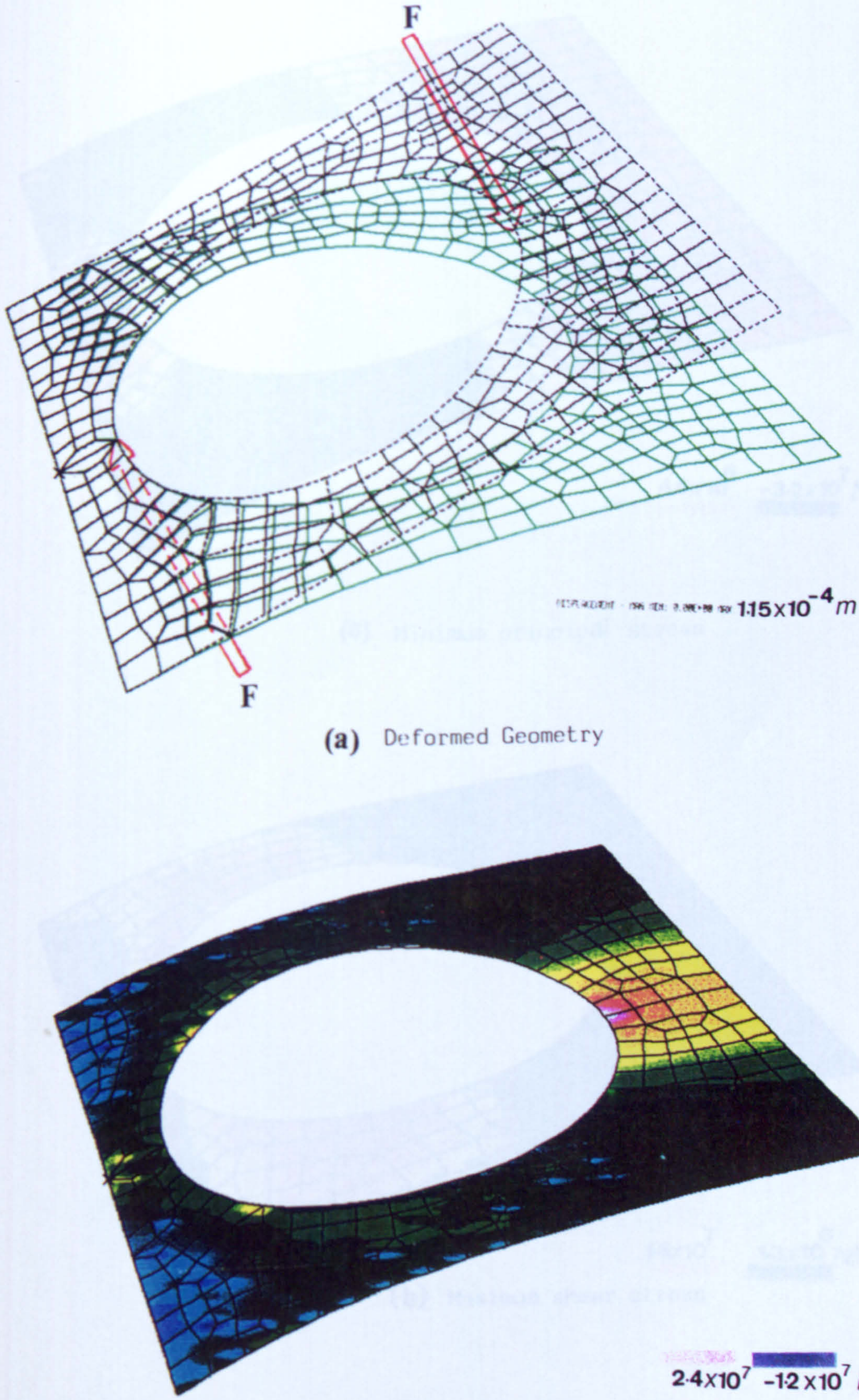

(a) Deformed Geometry

(b) Maximum principal stress

Figure 3.18 BRACE BAR UNDER BENDING

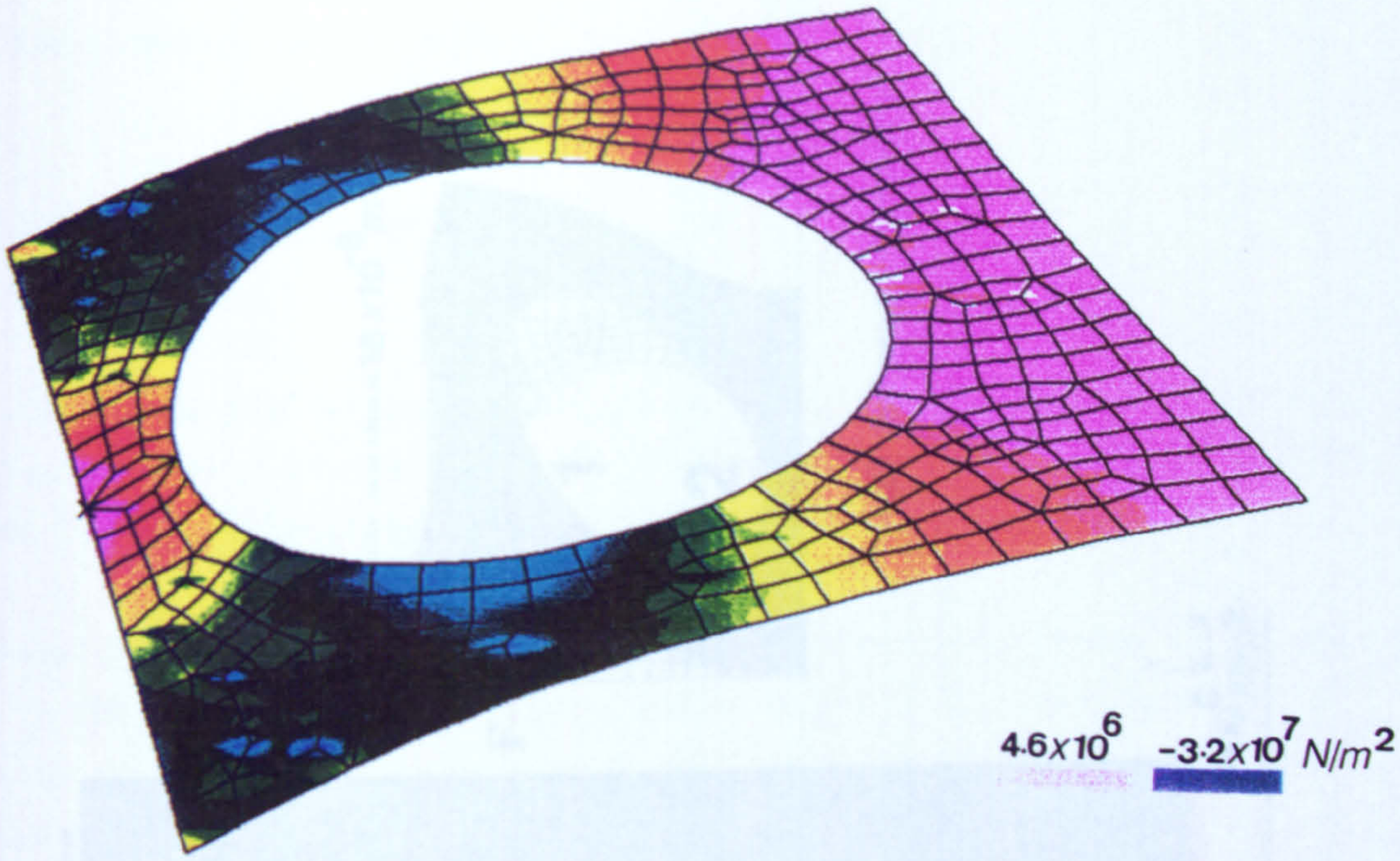

(a) Minimum principal stress

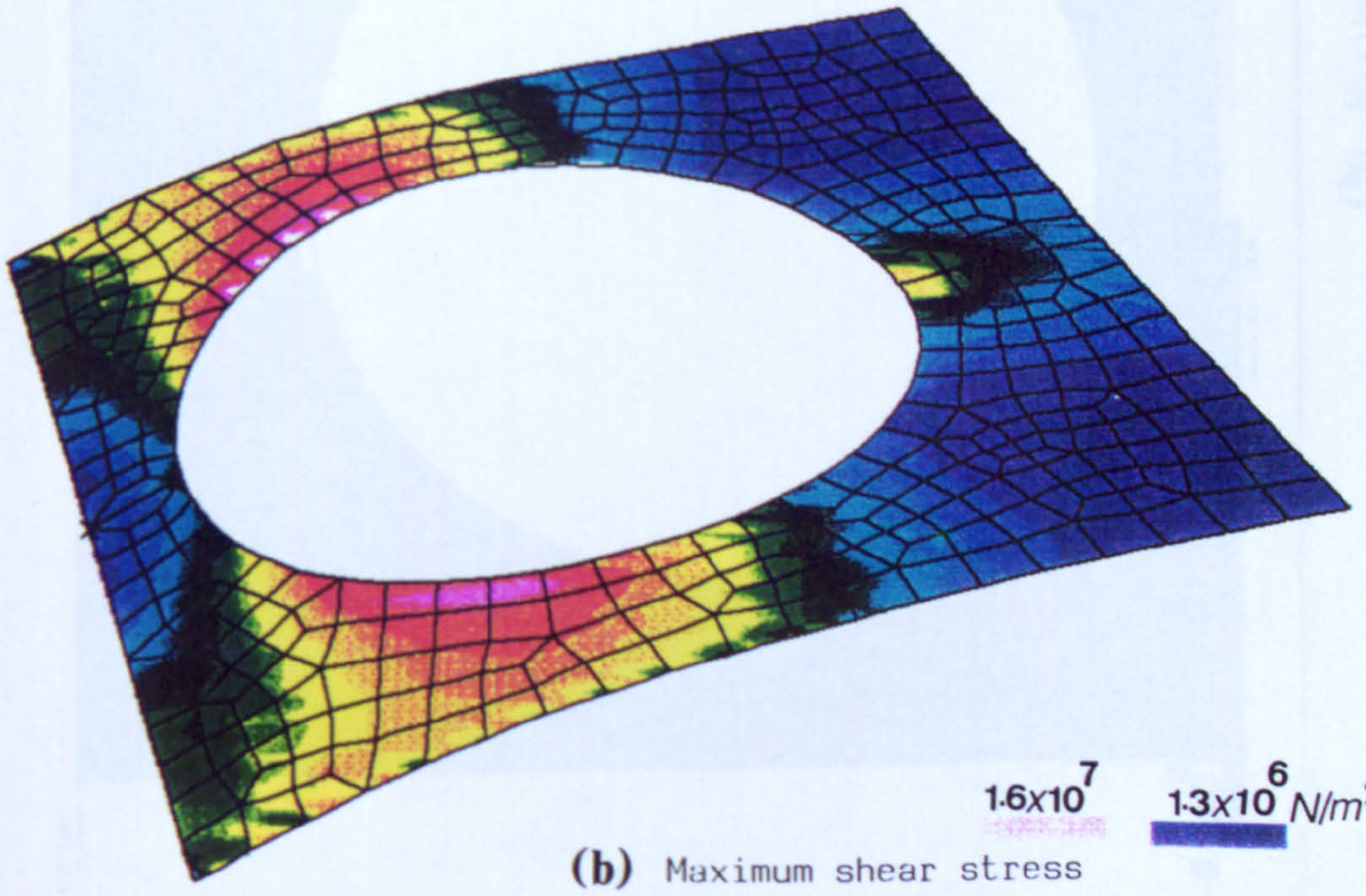

(b) Maximum shear stress

Figure 3.19 BRACE BAR UNDER BENDING

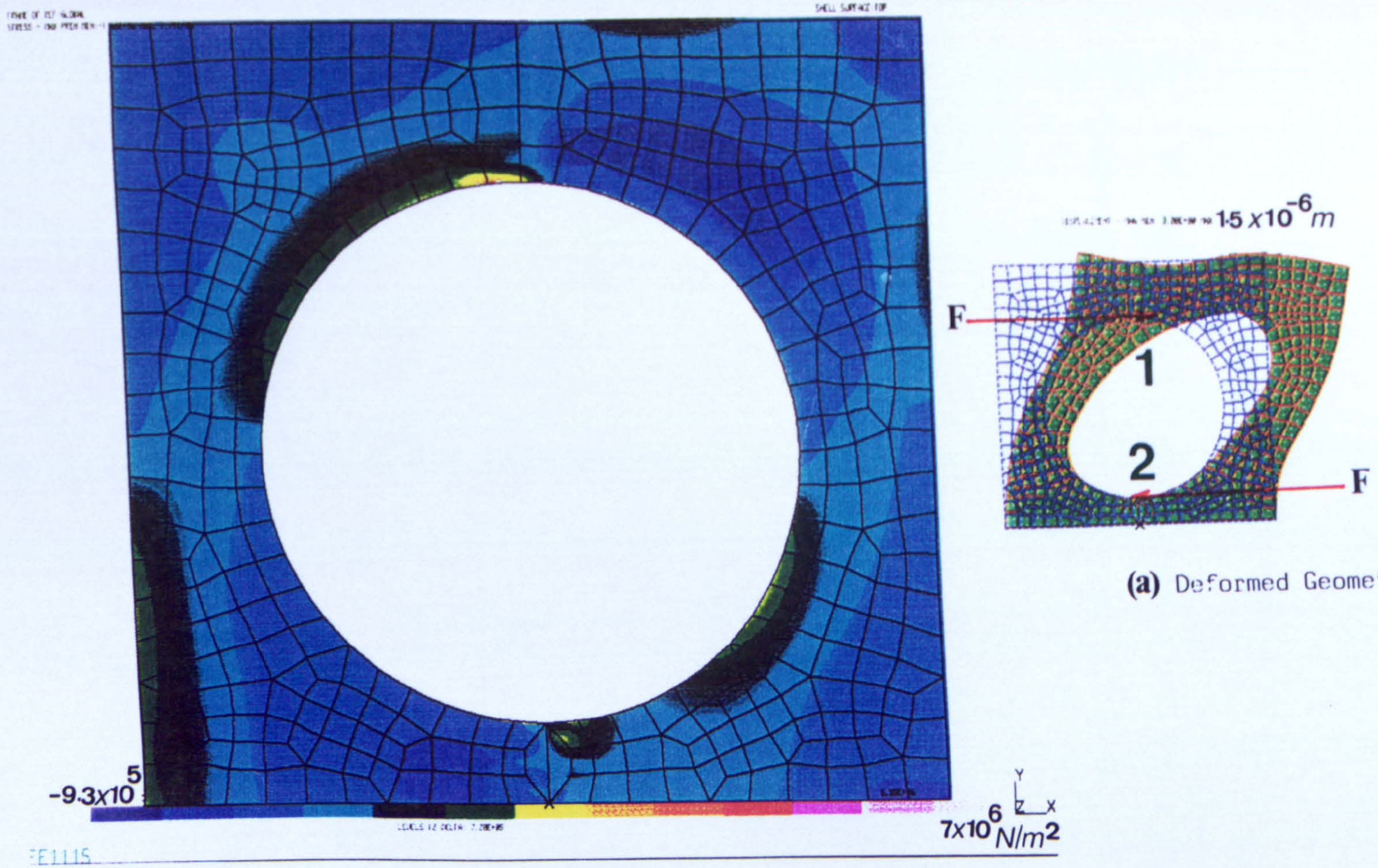

(b) Maximum shear stress

(a) Deformed Geometry

Figure 3.20 BRACE BAR UNDER A TORSION

considerable under estimation of K_3. This is because in the analytical method the brace bar is assumed infinitely large compared with the diameter of the hole.

3.2 ELASTIC END CONDITIONS

End conditions can be considered as an elastic foundation and it may be analysed as a thick brace bar. Hence tension and compression become the most significant effects to be accounted for [72].

To illustrate this, an arbitrary geometry is taken, as shown in Figure 3.21. The numerical method in section 3.1.4.2 is then applied in order to estimate the transitional stiffness coefficient. The load assumed here is a uniformly distributed force with an intensity of 40 N/m applied uniformly along a 45° arc of the circumference of the hole (modulus of elasticity E_e=280 GN/m² is used).

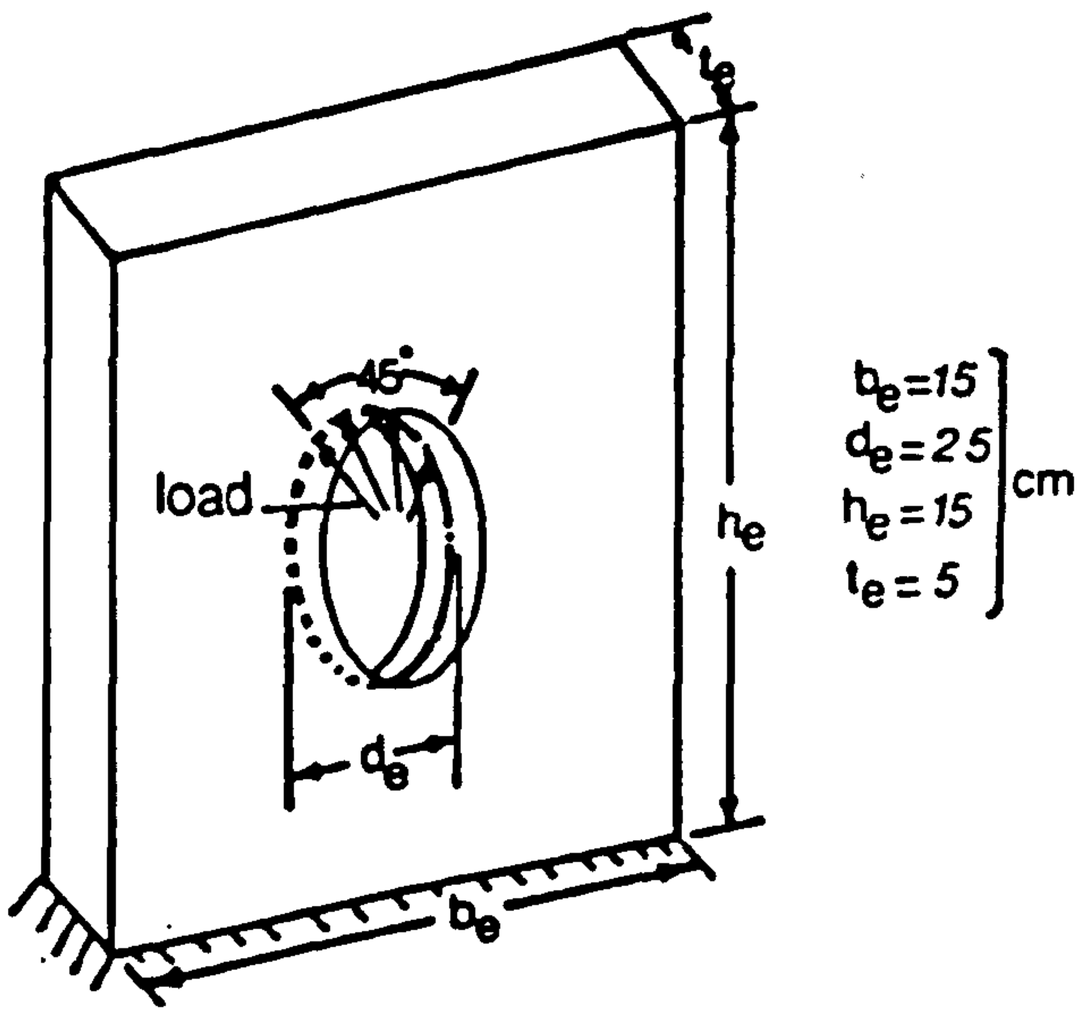

Figure 3.21 MODEL FOR END SUPPORT

Applying symmetry, one quarter of Figure 3.21 is analysed to obtain the deformed geometry and stress distributions shown in Figures 3.22 and 3.23. Translational stiffness coefficient K_{e1} is then calculated as follows

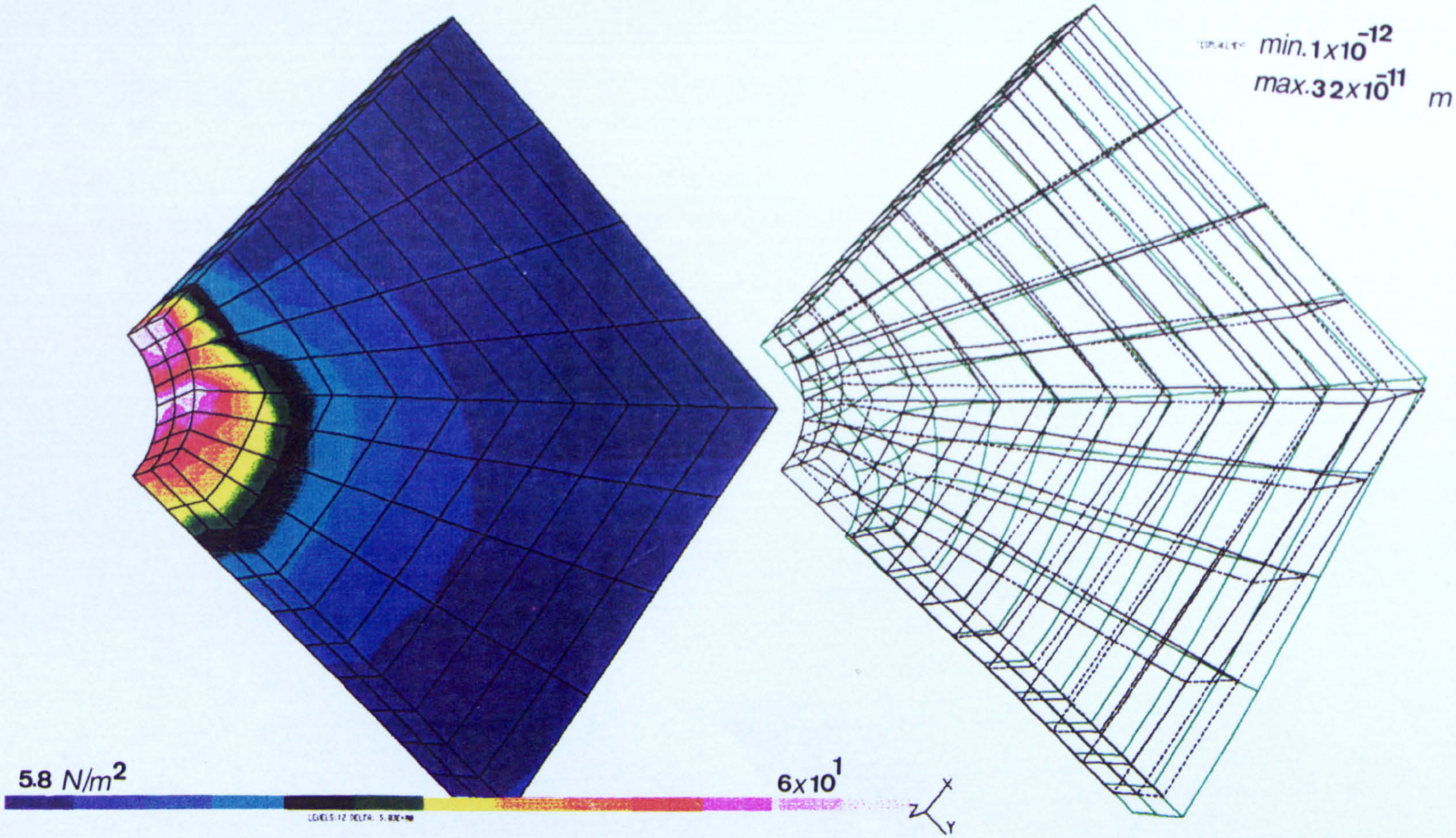

(b) Maximum principal stress

(a) Deformed Geometry

Figure 3.22 END SUPPORT UNDER COMPRESSION

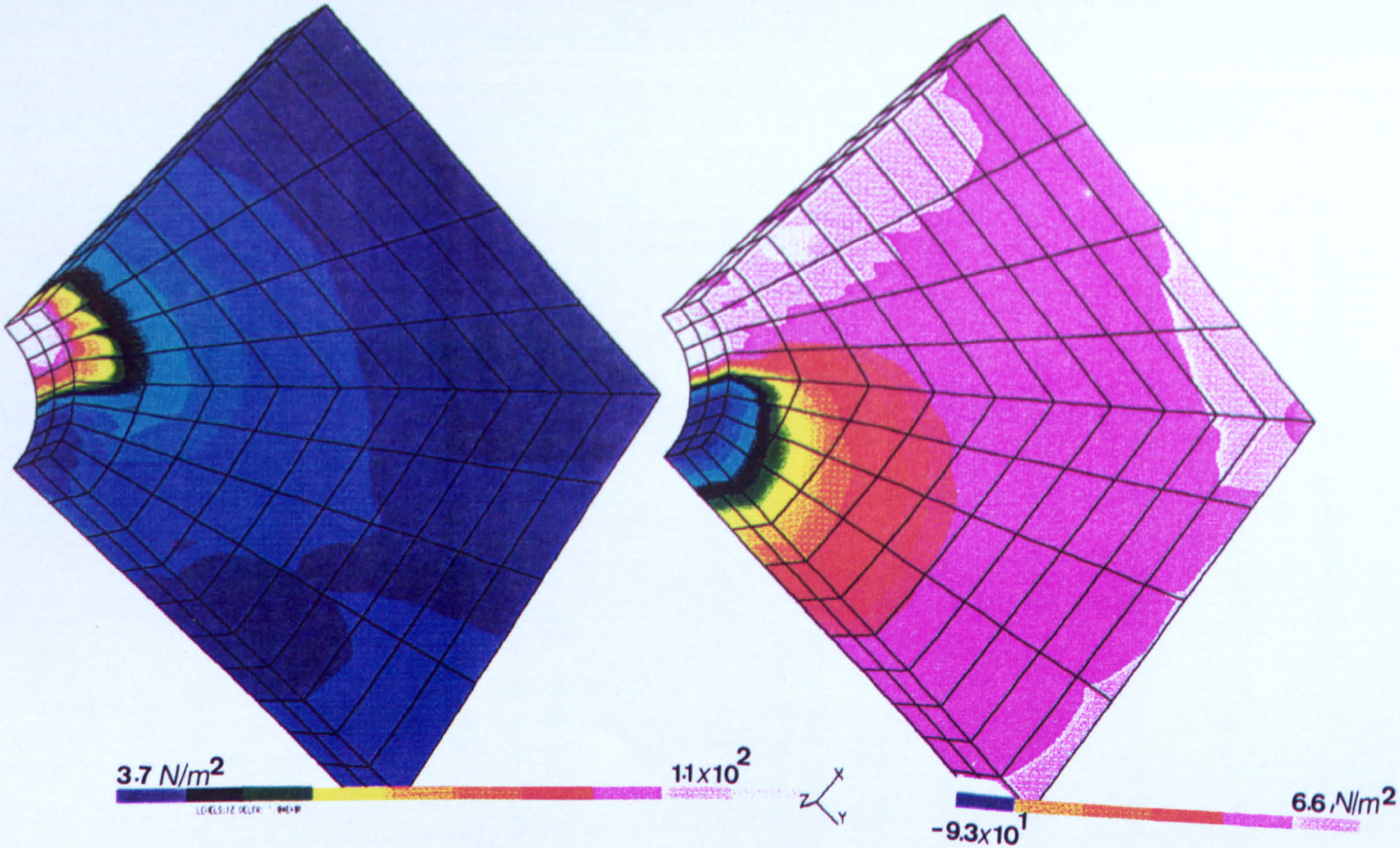

(b) Maximum shear stress

(a) Minimum principal stress

Figure 3.23 END SUPPORT UNDER COMPRESSION

$$K_{e1} = F/\delta = 49.8 \quad (GN/m)$$

where F = the resultant vertical force and $\delta = 3.2\text{x}10^{-11}$ (m) is the displacement at the point of the applied resultant force. It is clear from the above that small displacements can still take place in a thick support fixed rigidly at one end. Of course this example does not precisely represent the true end conditions in which deformation of the welded joints has to be taken into account.

3.3 ADDED MASS EFFECT

Generally, Coriolis flowmeters consist of an electromagnetic drive and two electromagnetic (or optical) sensors (section 1.3) whose masses are not negligible relative to the mass of the tube and must therefore be included in the model.

3.3.1 Boundary Conditions

It is obvious from general principles that the addition of a concentrated mass on the tube will slow down all modes of vibration. A concentrated mass at any point of the tube introduces a discontinuity into the shearing force [73].

Figure 3.24 shows a straight tube with a concentrated mass in the middle. Continuity and boundary conditions at the mass point are as follows

(i) discontinuity of shear force

$$S_2'^* - S_1'^* = M_C \frac{\partial^2 v_1^*}{\partial t^2} \qquad (3.22)$$

(ii) continuity of deflection, slope and moment

$$v_1^* = v_2^* \;,\; \frac{\partial v_1^*}{\partial s} = \frac{\partial v_2^*}{\partial s} \quad \text{and} \quad M_1^* = M_2^* \tag{3.23}$$

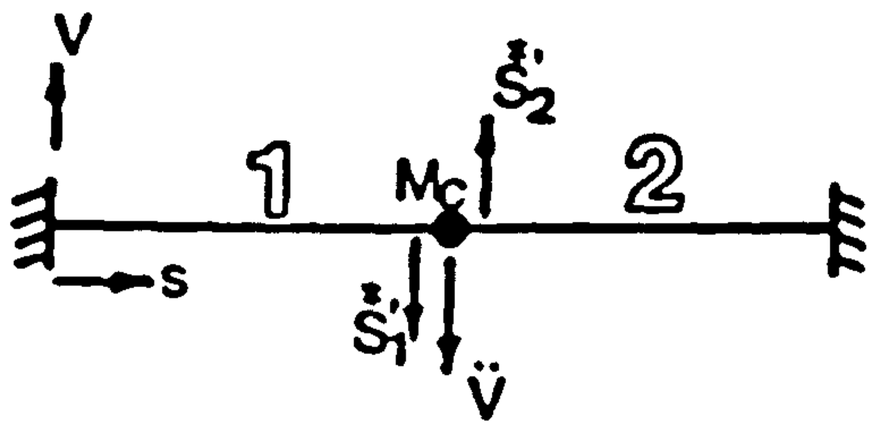

Figure 3.24 DISCONTINUITY OF SHEAR FORCE DUE TO THE ADDED MASS

3.3.2 Equations for Straight-Tube Configuration

The system under review is shown in Figure 3.25. It consists of a straight tube of length b, clamped at it's ends. Three concentrated masses (M_{C1}, M_{C2} and M_{C3}) are located at distances b_1, b_1+b_2 and $b_1+b_2+b_3$ from one fixed end.

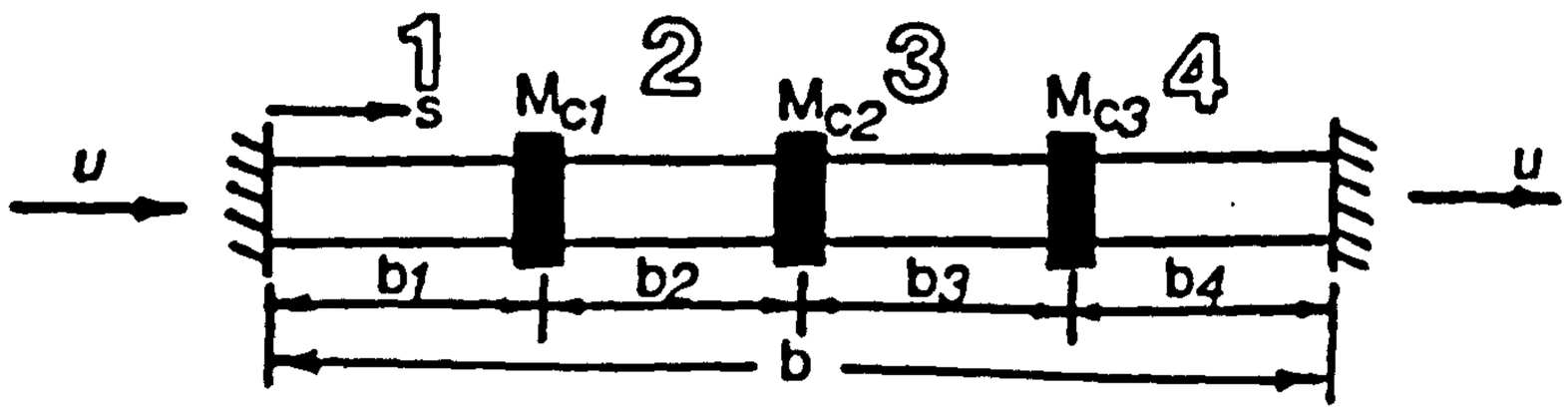

Figure 3.25 STRAIGHT TUBE WITH THREE ADDED MASSES

The boundary conditions at fixed ends and at mass points are as follows

at $s = 0$ and $s = \sum_{j \le i}^{4} b_j$

$$v_1^* = \partial v_1^*/\partial s = v_4^* = \partial v_4^*/\partial s = 0 \qquad (3.24)$$

and at $s = b_1$

$$\left.\begin{aligned} & v_1^* = v_2^* \;,\; \partial v_1^*/\partial s = \partial v_2^*/\partial s \;,\; \partial^2 v_1^*/\partial s^2 = \partial^2 v_2^*/\partial s^2 \\ & \frac{\partial^3 v_1^*}{\partial s^3} + \frac{M_{c1}}{EI}\frac{\partial^2 v_1^*}{\partial t^2} = \frac{\partial^3 v_2^*}{\partial s^3} \end{aligned}\right\} \qquad (3.25)$$

Equation 3.25 can be applied similarly at other mass points.

Now, let non-dimensional quatities $\bar{v}^*$, $\bar{s}$,..... be related to actual quantities v^*, s, ... as follows

$$\bar{v}^* = v^*/b \;,\; \bar{s} = s/b \;,\; \bar{u} = U\, b\, (M_f/EI)^{1/4} \;,\; \bar{t} = t\left[\frac{M_t+M_f}{EI}\right]^{-1/4} b^{-2},$$

$$\beta = \frac{M_f}{M_t+M_f} \;,\; \bar{\omega} = \omega\left[\frac{M_t+M_f}{EI}\right]^{1/4} b^2 \quad \text{and} \quad \gamma_i = \frac{M_{ci}}{(M_t+M_f)b}$$

where i = 1, 2 or 3 .

Using the same method as in section 2.3.4 (for straight tube only), sixteen relations between sixteen constants (A_{ij}) can be found from equations (3.24) and (3.25). These relations are listed in appendix E.

The numerical method of section(2.3.5) is used here as a means of calculating non-dimensional frequency, using the new boundary condition [16x16] determinant for the straight tube with three concentrated masses.

Figure 3.26 indicates the effect of a single mass at the middle of the straight tube for $u=\beta=0$ and $L_1=L_2=0.5$. The reduction in fundamental

frequency with increasing γ is clearly seen.

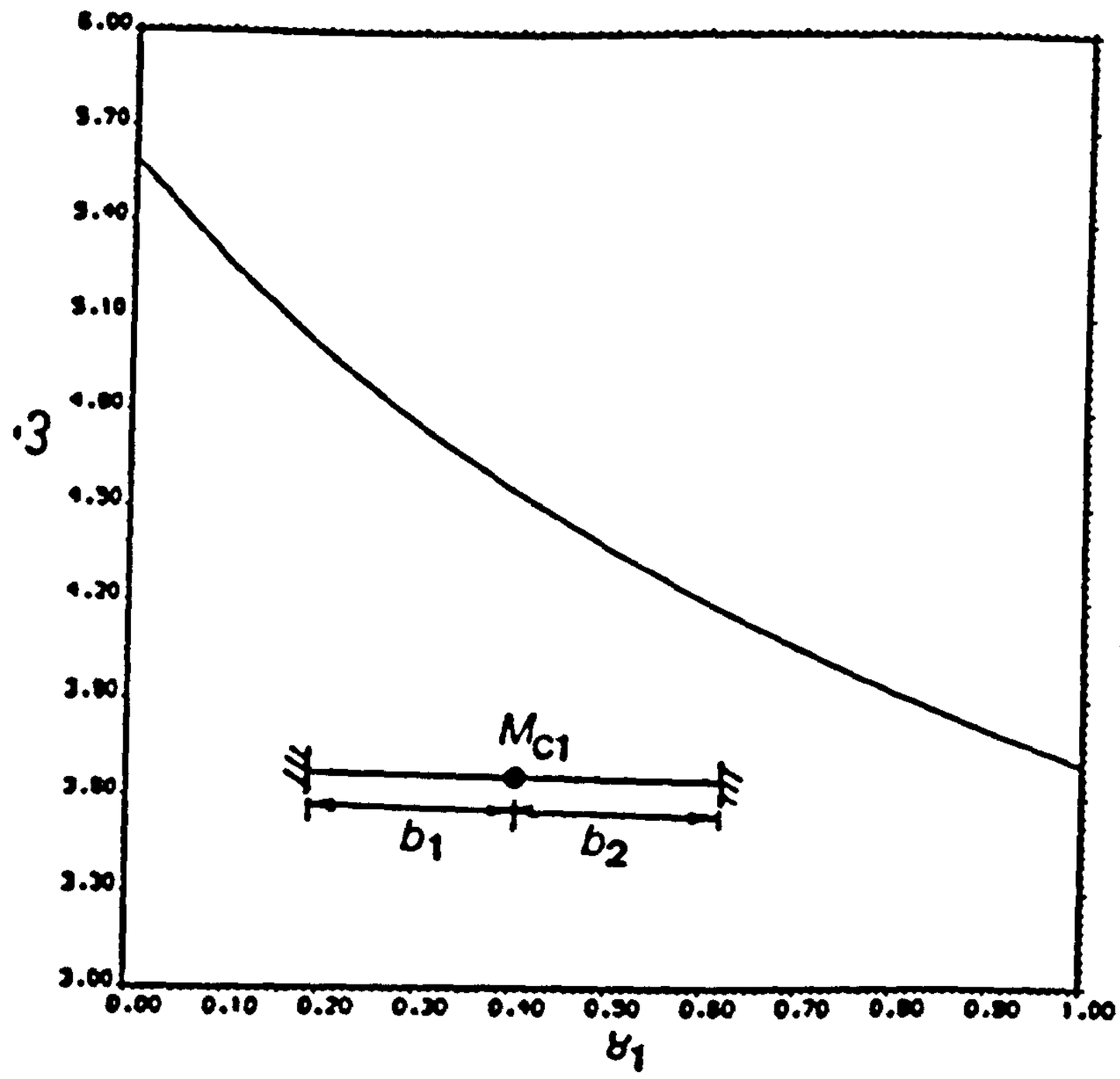

Figure 3.26 THE EFFECT OF ADDED MASS ON TUBE FUNDAMENTAL FREQUENCY

3.4 THE EFFECT OF NEW BOUNDARY CONDITIONS ON PHASE DIFFERENCE $\Delta\Phi$

In Figures 3.27, 3.28 and 3.29 the phase difference $\Delta\Phi$ is plotted as a percentage against $\bar{K}_1$, $\bar{K}_2$ and $\bar{K}_3$ respectively, for example

$$\%\left[\frac{\Delta\Phi}{\Omega}\right]_{\bar{K}_1} = \frac{\left[\frac{\Delta\Phi}{\Omega}\right]_{\bar{K}_1\neq 0} - \left[\frac{\Delta\Phi}{\Omega}\right]_{\bar{K}_1=0}}{\left[\frac{\Delta\Phi}{\Omega}\right]_{\bar{K}_1=0}} \times 100$$

for U-tube configuration incorporating four intermediate supports ($\Delta\Phi$

is calculated at $\bar{s}=\sum_{i=1}^{4} L_i$ and $\bar{s}=\sum_{i=1}^{5} L_i$) for $L_1=L_2=L_3=1$ and $L_4=\pi$ and $\beta=0.3$.

In Figure 3.30 $\%(\Delta\phi/\bar{U})$ is plotted against γ_1 for straight tube with a single added mass ($\Delta\phi$ is calculated at $\bar{s}=L_1/2$ and $\bar{s}=L_1+L_2/2$) for $L_1=L_2=0.5$ and $\beta=0.3$.

Figure 3.27 indicates a rapid increase in $\%(\Delta\phi/\bar{U})$ with increasing $\bar{K}_1$ reaching its peak value at $\bar{K}_1$ approximately 200. Further increase in $\bar{K}_1$ results in steady decline, though beyoned $K_1=700$ $\%(\Delta\phi/\bar{U})$ becomes constant with increasing $\bar{K}_1$.

The effect of $\bar{K}_2$ on phase difference is shown in Figure 3.28 displaying an increase in $\%(\Delta\phi/\bar{U})$ with increasing $\bar{K}_2$.

Figure 3.29 illustrates the effect of $\bar{K}_3$ on phase difference showing considerable decrease in $\%(\Delta\phi/\bar{U})$ with increasing $\bar{K}_3$ (applying equation (3.7) with typical values of $E=208$ GN/m^2, $G=80$ GN/m^2, $I=9\times10^{-8}$ m^4, $J=18\times10^{-8}$ m^4 and $a_1=15$ cm gives: $\bar{K}_1=1.8\times10^{-7}$ K_1, $\bar{K}_2=8\times10^{-6}$ K_2 and $\bar{K}_3=1\times10^{-5}$ K_3).

Finally, Figure 3.30 shows the effect of single added mass at the middle of a straight tube indicating decrease in $\%(\Delta\phi/\bar{U})$ with increasing γ_1.

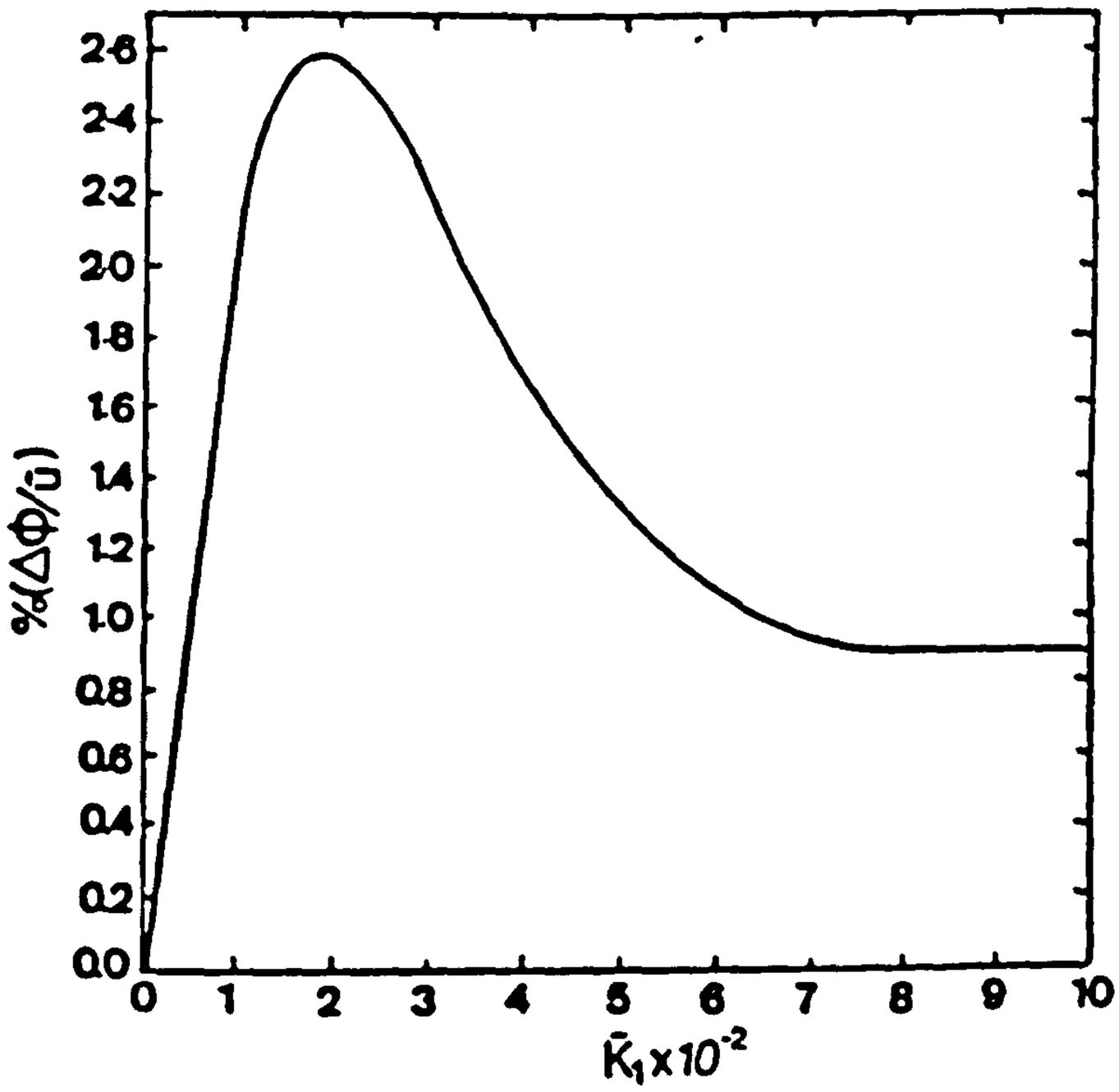

Figure 3.27 PERCENTAGE INCREASE IN PHASE DIFFERENCE VERSUS $\tilde{K}_1$

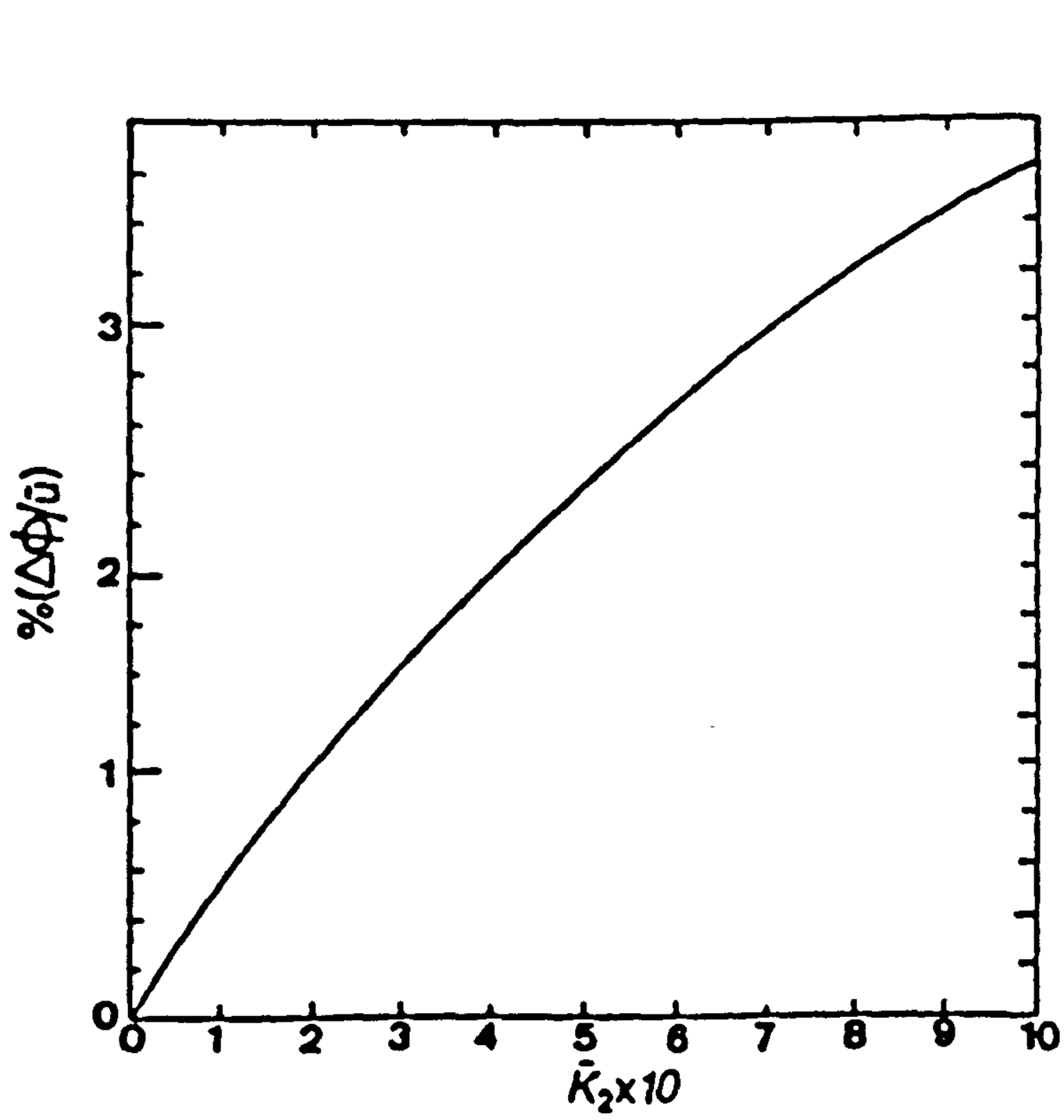

Figure 3.28 PERCENTAGE INCREASE IN PHASE DIFFERENCE VERSUS $\tilde{K}_2$

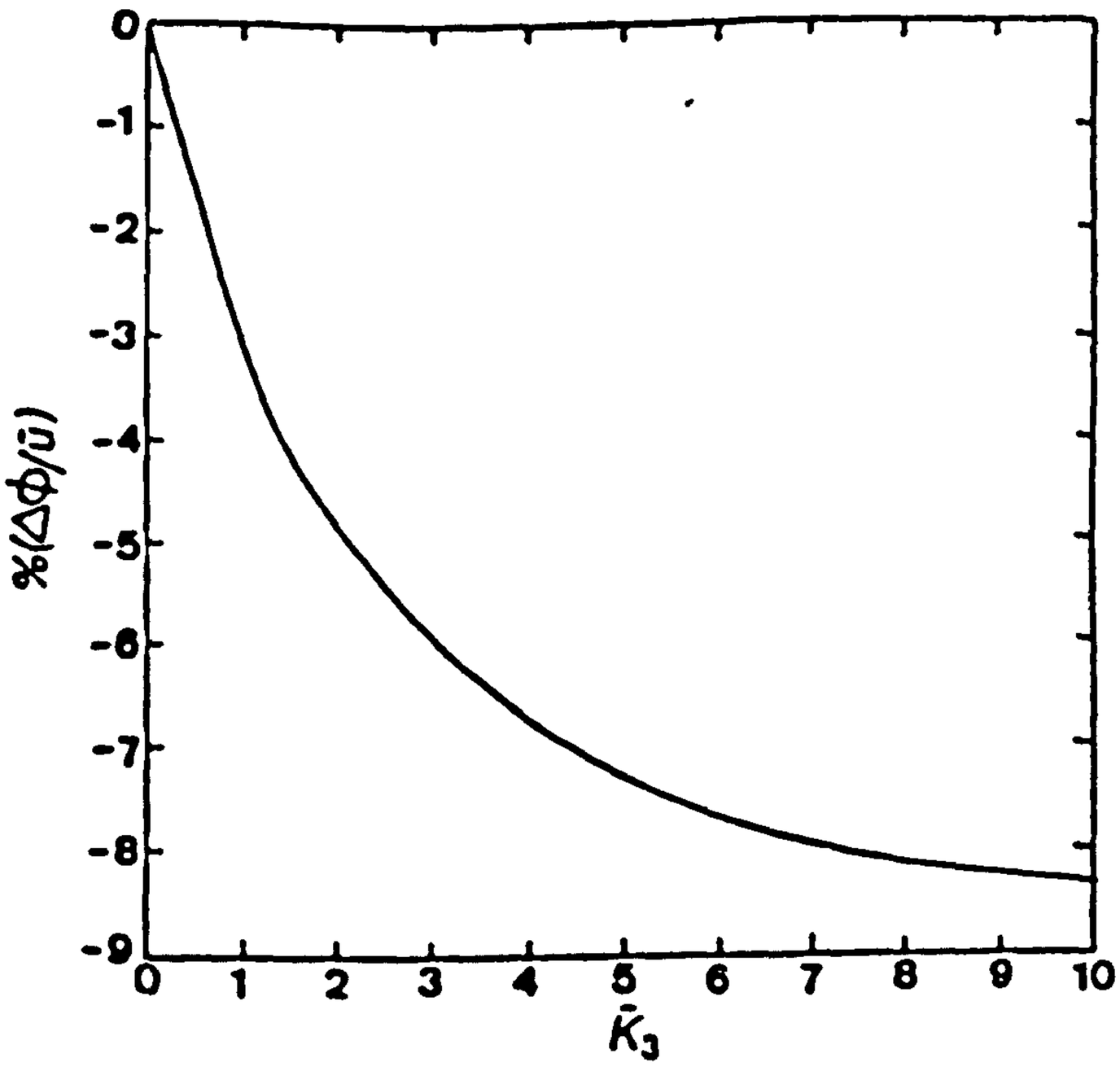

Figure 3.29 PERCENTAGE DECREASE IN PHASE DIFFERENCE VERSUS $\tilde{K}_3$

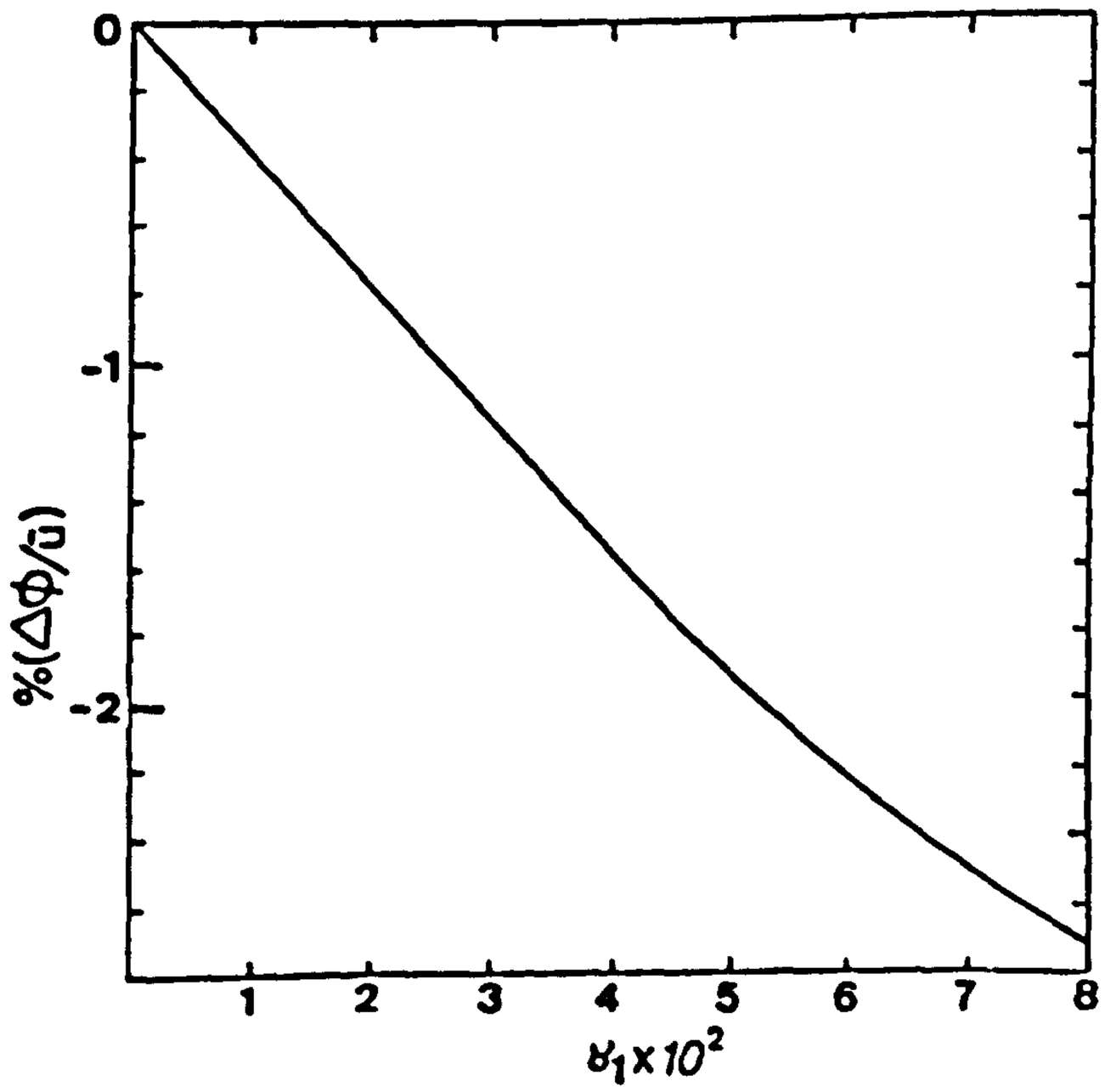

Figure 3.30 PERCENTAGE DECREASE IN PHASE DIFFERENCE VERSUS α_1

CHAPTER FOUR

PREDICTION OF THE OPTIMUM POSITIONS OF MEASURING POINTS

CHAPTER FOUR

PREDICTION OF THE OPTIMUM POSITIONS OF MEASURING POINTS

In this chapter a method is suggested for predicting the optimum positions of the electromagnetic (or optical) detectors for phase difference measurement.

4.1 BACKGROUND

4.1.1 Phase Difference Measurement

As previously mentioned in section 1.4, the Coriolis effect is exceedingley small in relation to the main tube vibration. Thus, very small phase differences are obtained between the output signals of the electromagnetic (or optical) detectors.

Mahmud [74] presented a number of phase difference measurement techniques for different wave form shapes, including waves distorted by higher harmonics.

Generally, the phase difference measurement between two waves is preformed by

(i) locating the zero crossings of the two waves,

(ii) measuring the time interval between each zero crossing, using high frequency clock pulse,

(iii) taking an average of many measurements to improve accuracy and resolution [75] (see Figure 4.1) and finally

(iv) multiply by $2\pi f$.

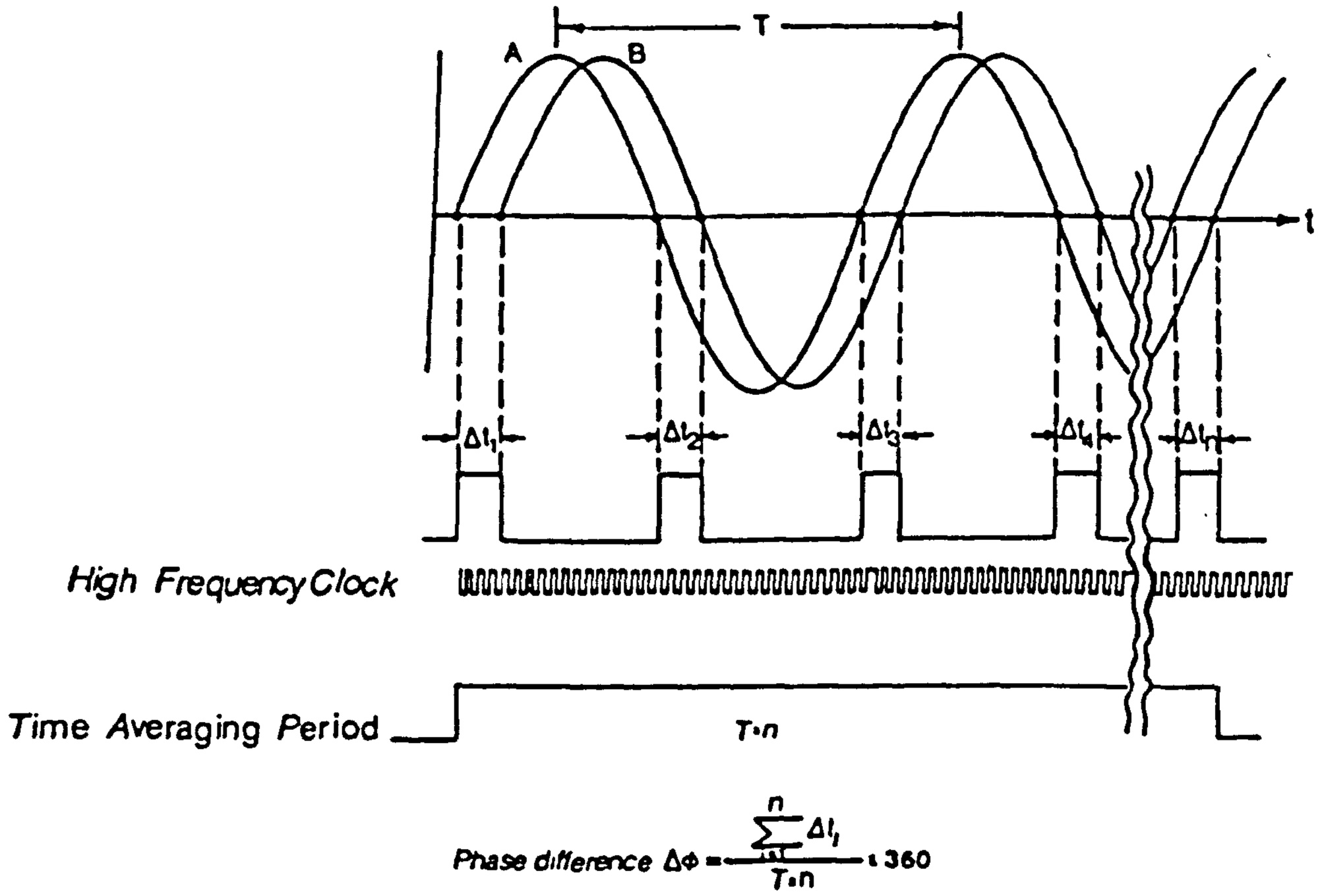

Figure 4.1 PHASE DIFFERENCE MEASUREMENT

4.1.2 Zero Crossing

The most essential aspect of phase difference measurement is to accurately locate the zero crossings of the wave forms. The error arising from mislocating the zero crossings is summarized by Wagdy et al [76]. The accuracy can be improved by increasing the sampling frequency, number of A/D quantitization levels and the amplitude of the analogue signals.

When finding the zero crossings it is usual to have a hysteresis band (or tolerance in level) for establishing noise immunity (see Figure 4.2). However, there is trane off in that increasing the hysteresis band width gives better noise immunity but similtaneously, a less accurate zero location (wider uncertainty band).

Moreover, it is possible to decrease the uncertainty band width (for the same noise level) by having a higher signal amplitude (higher slew rate) as shown in Figure 4.2.

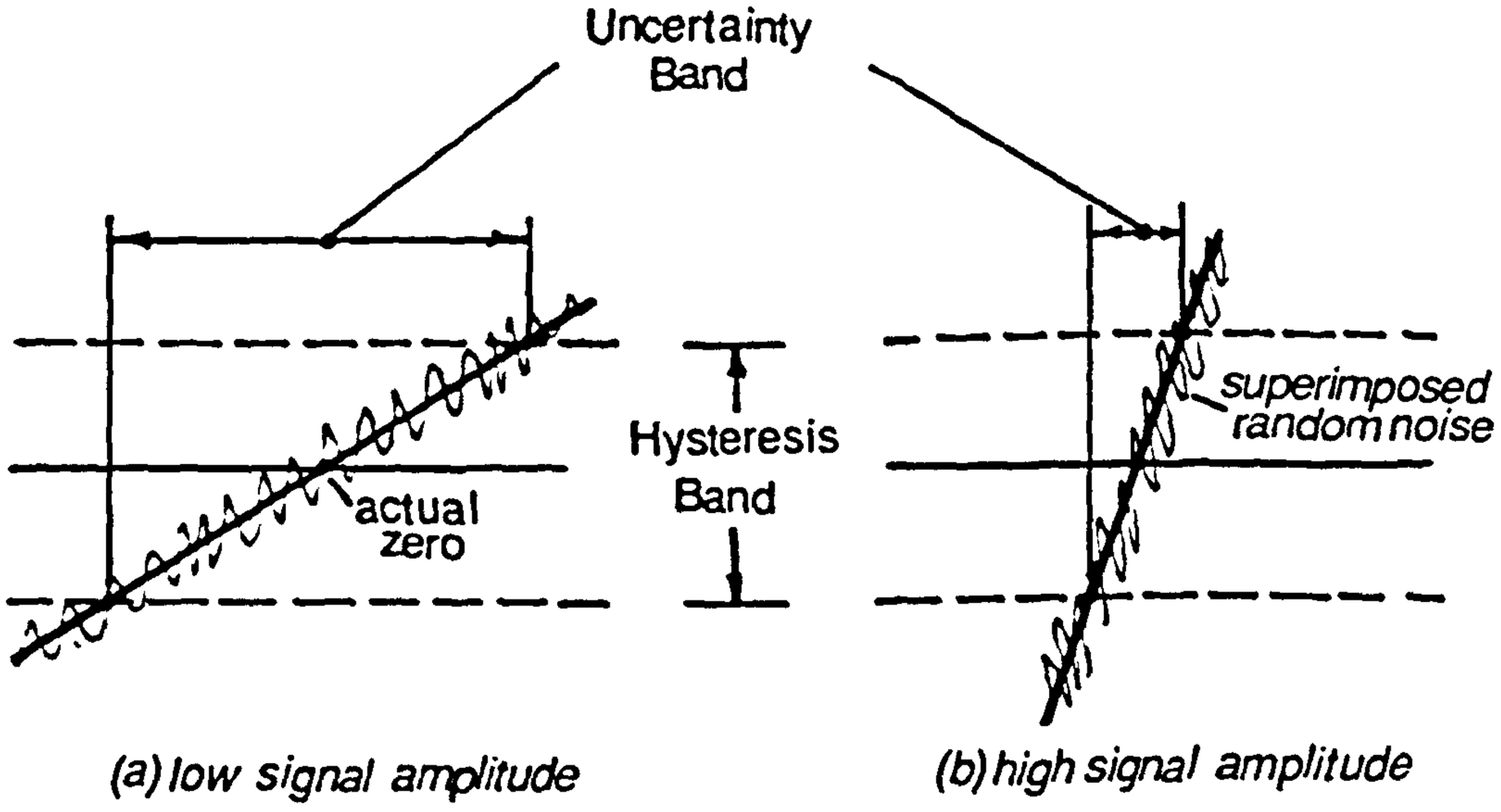

Figure 4.2 ZERO CROSSING AND HYSTERESIS BAND

4.2 OPTIMUM DETECTOR POSITIONS IN RELATION TO SIGNAL-TO-NOISE RATIO

Assume that the signal to be measured has an amplitude A and phase Φ and a random noise with amplitude N superimposed on it, as shown in Figure 4.3.

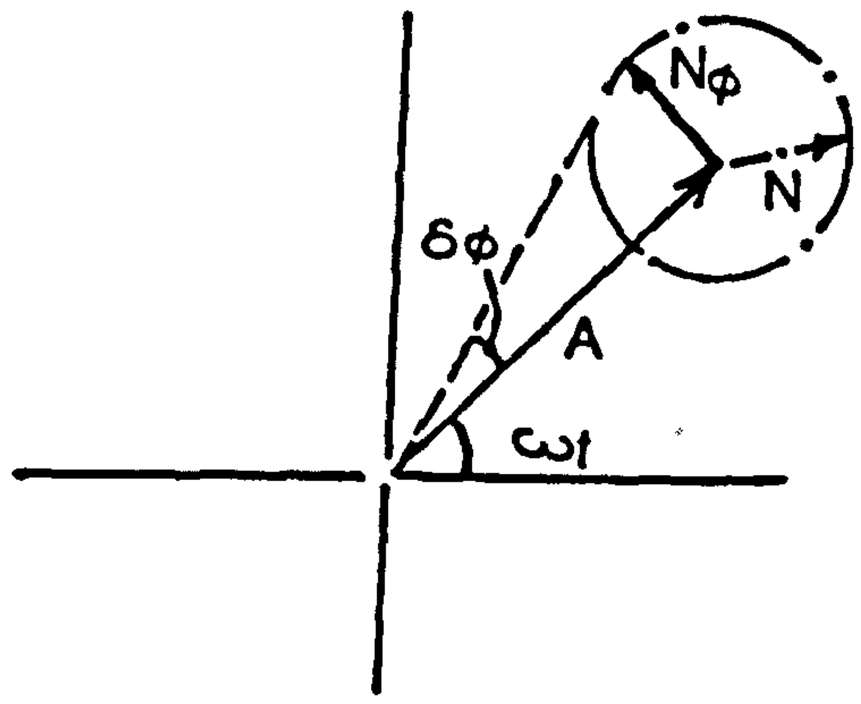

Figure 4.3 SUPERIMPOSED RANDOM NOISE

Taking the component of the noise (N_o) which contributes to the phase Φ we have

$$\delta\Phi = \frac{N_o}{A} \qquad (4.1)$$

Dividing both sides of (4.1) by Φ gives the fractional error due to the random noise component N_o

$$\frac{\delta\Phi}{\Phi} = \frac{N_o}{A\,\Phi} \qquad (4.2)$$

Now, to minimize the error $\delta\Phi/\Phi$ for constant noise level, $A\,\Phi$ must be maximized. Therefore, the optimum positions of the detectors is established when $A\,\Phi$ is a maximum.

4.3 RESULTS

The numerical method presented in section 2.3.5 is used here as a means of calculating the multiplication parameter $A\,\Delta\phi$ for three different geometries (straight, U and S-tube). $A\,\Delta\phi$ is then plotted against the non-dimensional distance (D/b for straight-tube and D/a_1 for U-tube and S-tube) in order to predict the optimum position (the amplitude of tube vibration is taken as constant while the distance between sensors is varied and sensors are assumed to have zero mass). This is illustrated in Figures 4.4, 4.5 and 4.6 for $\beta=0.3, L_1=1$ (for straight tube), $L_1=L_3=4.43$ and $L_2=\pi$ (for U-tube) and $L_1=L_3=L_5=1$, $L_2=L_4=3$ (for S-tube).

From Figures 4.4, 4.5 and 4.6, the non-dimensional optimum distance between measuring points are 0.44, 3 and 4.56 for straight-tube, U-tube and S-tube respectively. The optimum distances vary with non-dimensional velocity Ω due to nonlinear effects at high velocities (section 2.3.6). Note that the amplitude of tube vibration for different Ω values are not the same. This affects the location of optimum sensor distance.

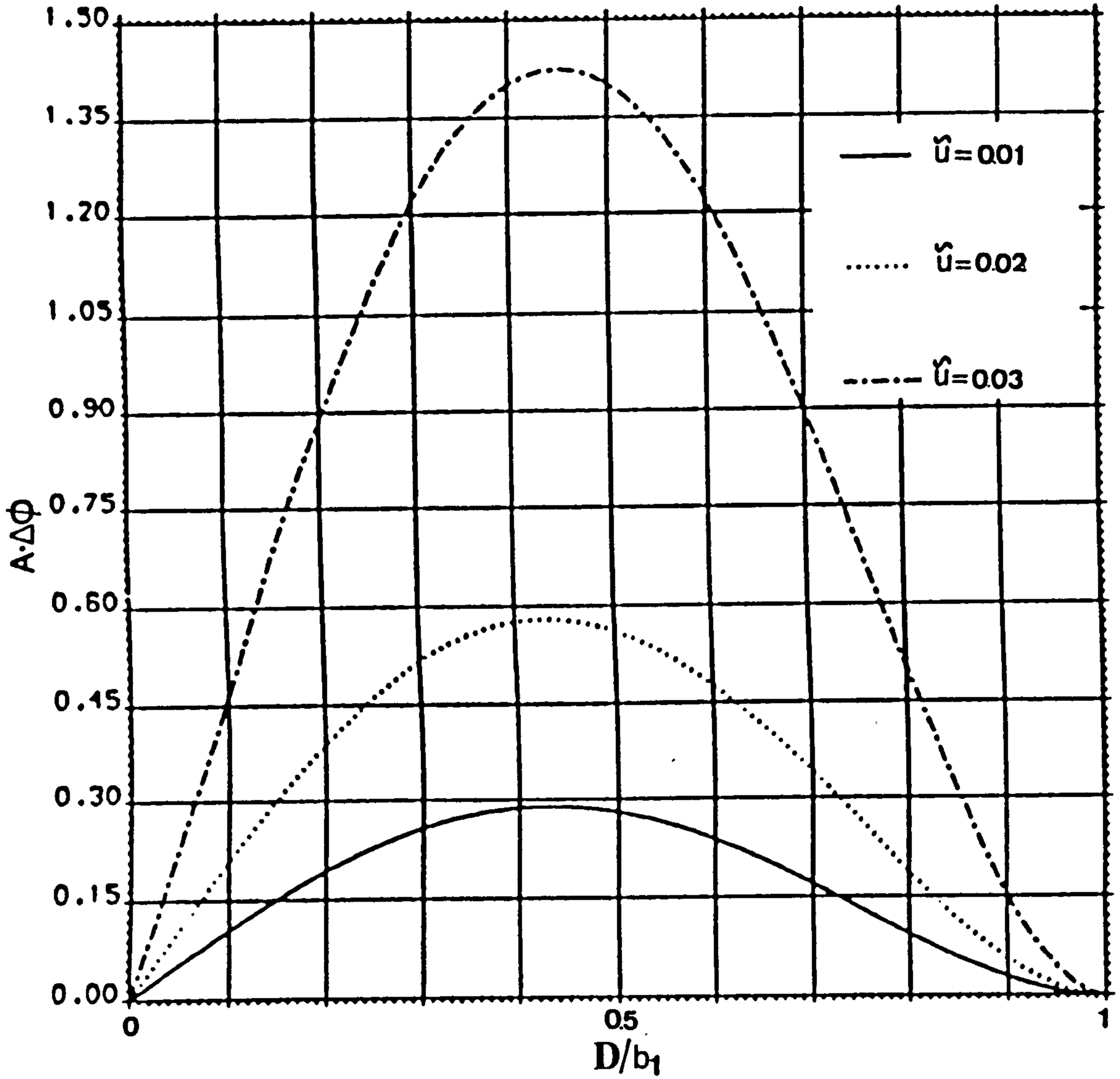

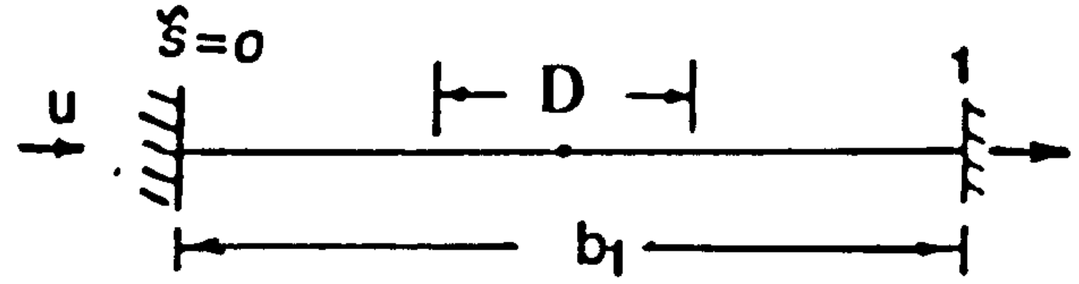

Figure 4.4 THE OPTIMUM MEASURING DISTANCE FOR STRAIGHT TUBE CONFIGURATION

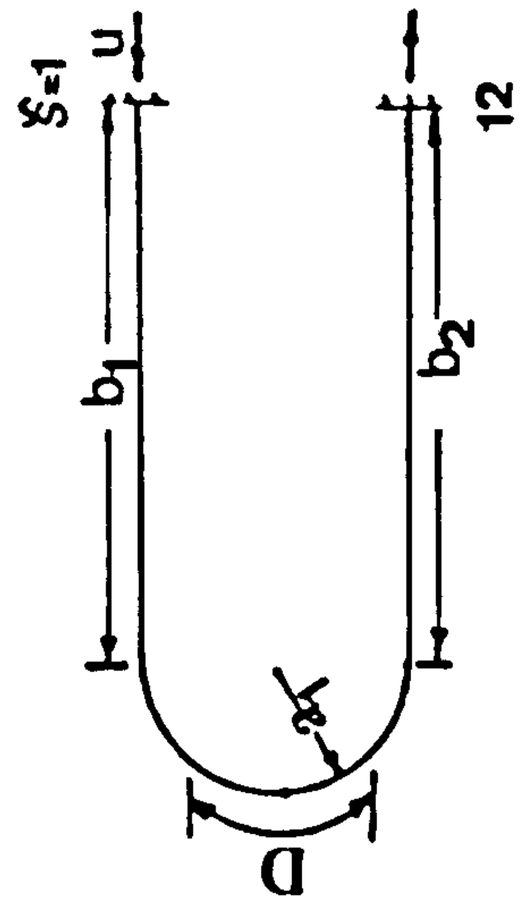

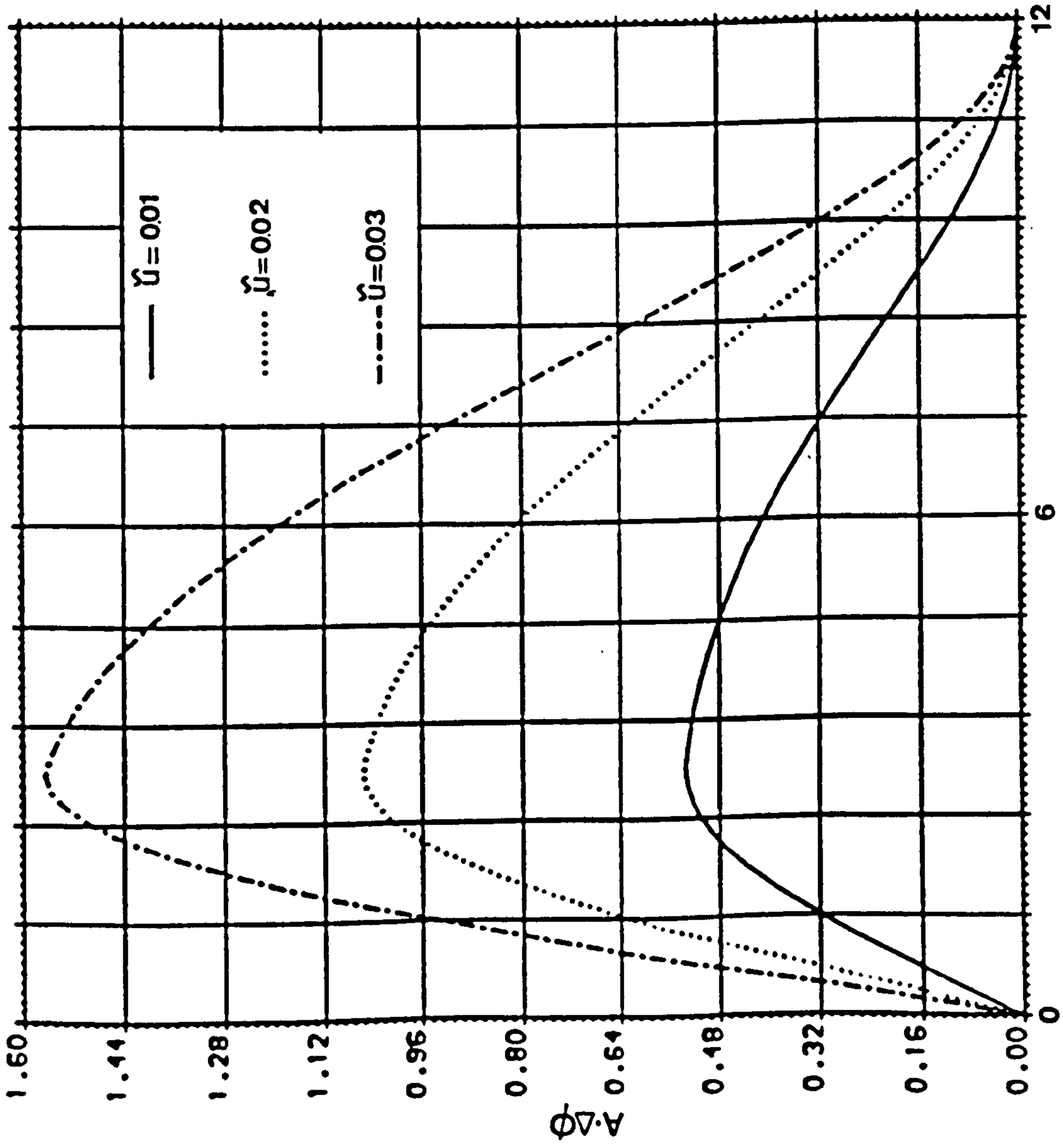

Figure 4.5 THE OPTIMUM MEASURING DISTANCE FOR U TUBE CONFIGURATION

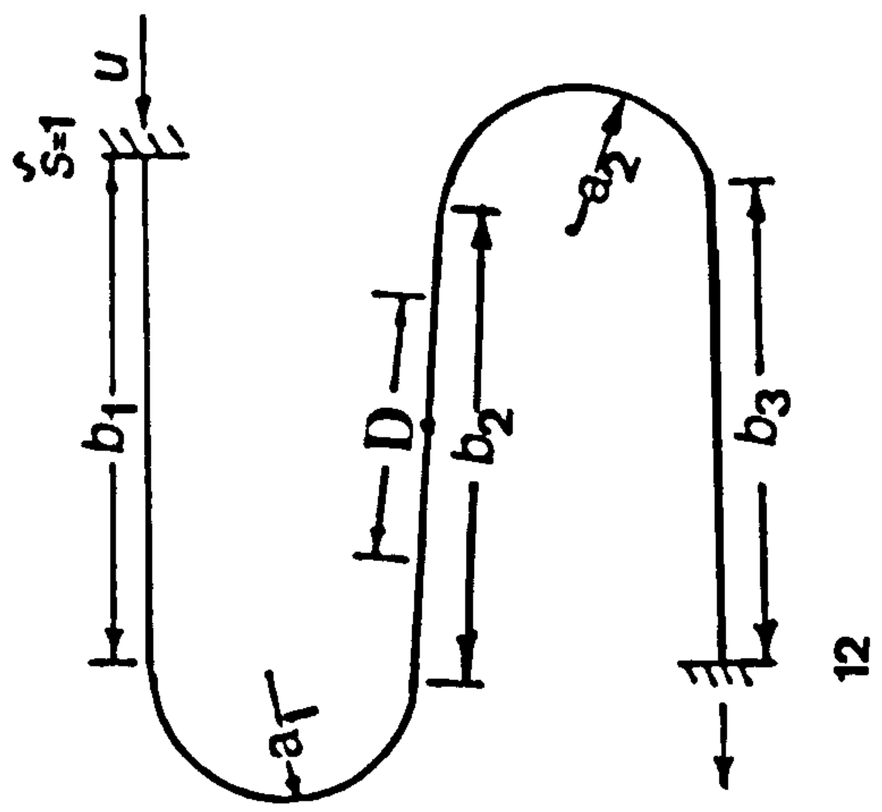

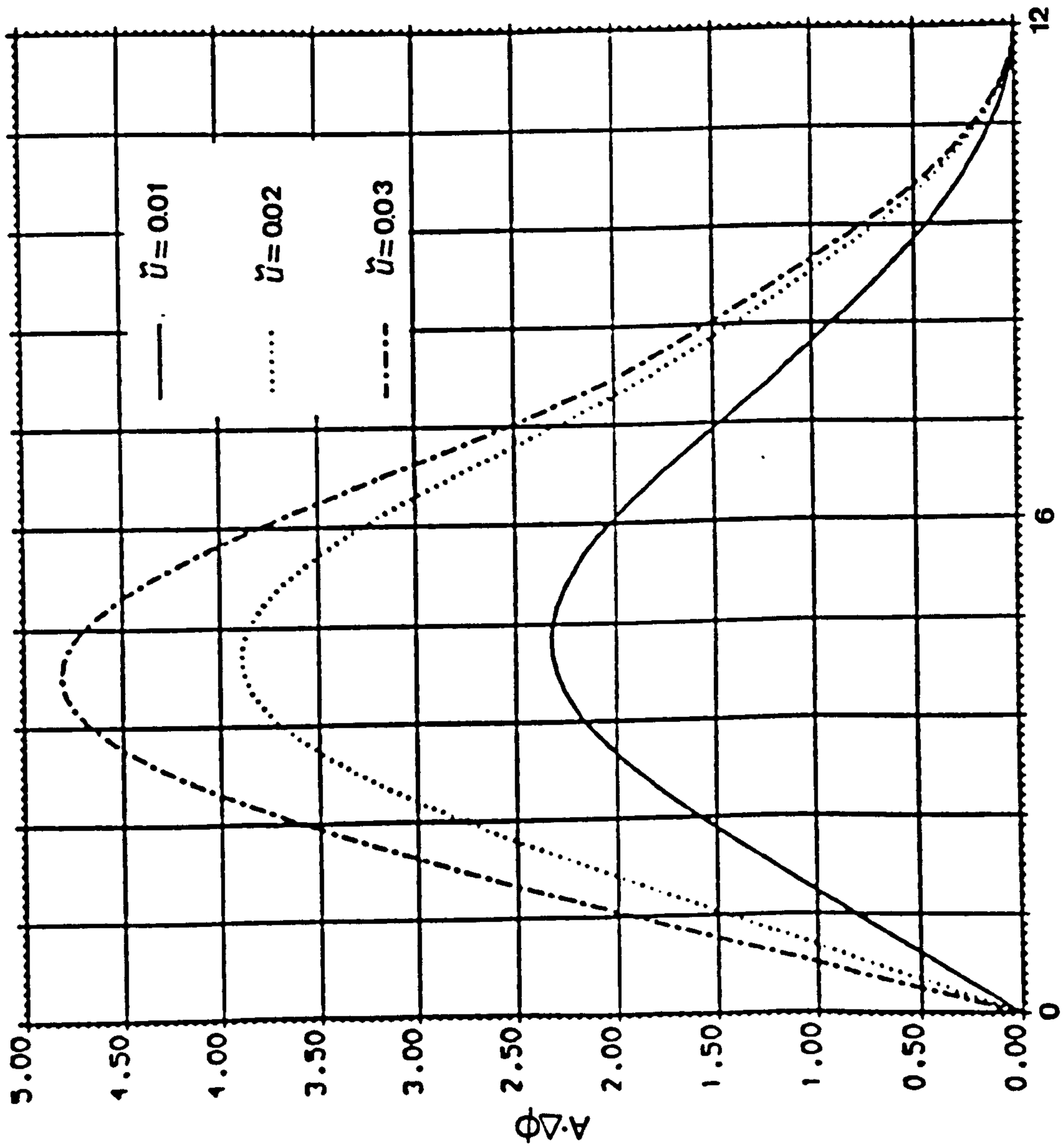

Figure 4.6 THE OPTIMUM MEASURING DISTANCE FOR S TUBE CONFIGURATION

CHAPTER FIVE

SINGLE-PHASE FLOW EXPERIMENTS

CHAPTER FIVE

SINGLE-PHASE FLOW EXPERIMENTS

The purpose of the experimental study reported in this chapter is to check the validity of the theoretical model presented in previous chapters. Experiments were conducted on two flowmeters (i) a commercial 3-inch Micro Motion (U-shape) Coriolis mass flowmeter and (ii) an experimental 1-inch straight tube flowmeter.

5.1 COMMERCIAL CORIOLIS FLOWMETER

Measurements were taken of time delays and frequencies of vibration of the commercial U-shape, 3-inch tube (model D-300) Micro Motion Coriolis mass flowmeter (Figure 5.1).

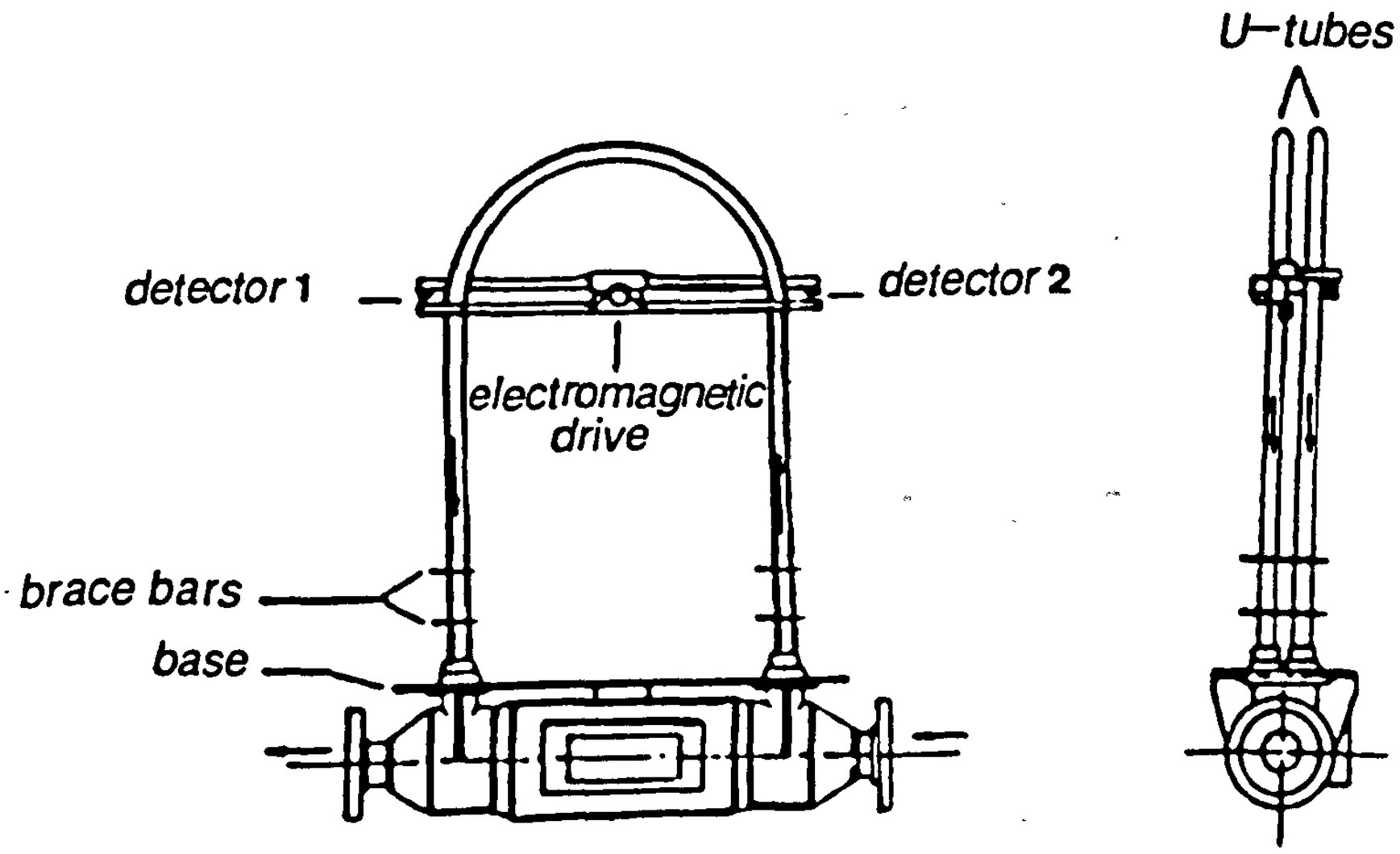

Figure 5.1 D-300 MICRO MOTION CORIOLIS MASS FLOWMETER

Signals from the electromagnetic pick-ups were processed directly (indepedently of meter electronics). A block diagram of the flowmeter driving electronics and the processing electronics used here is given in Figure 5.2. Waveforms at points in the block diagram are shown in Figure 5.3.

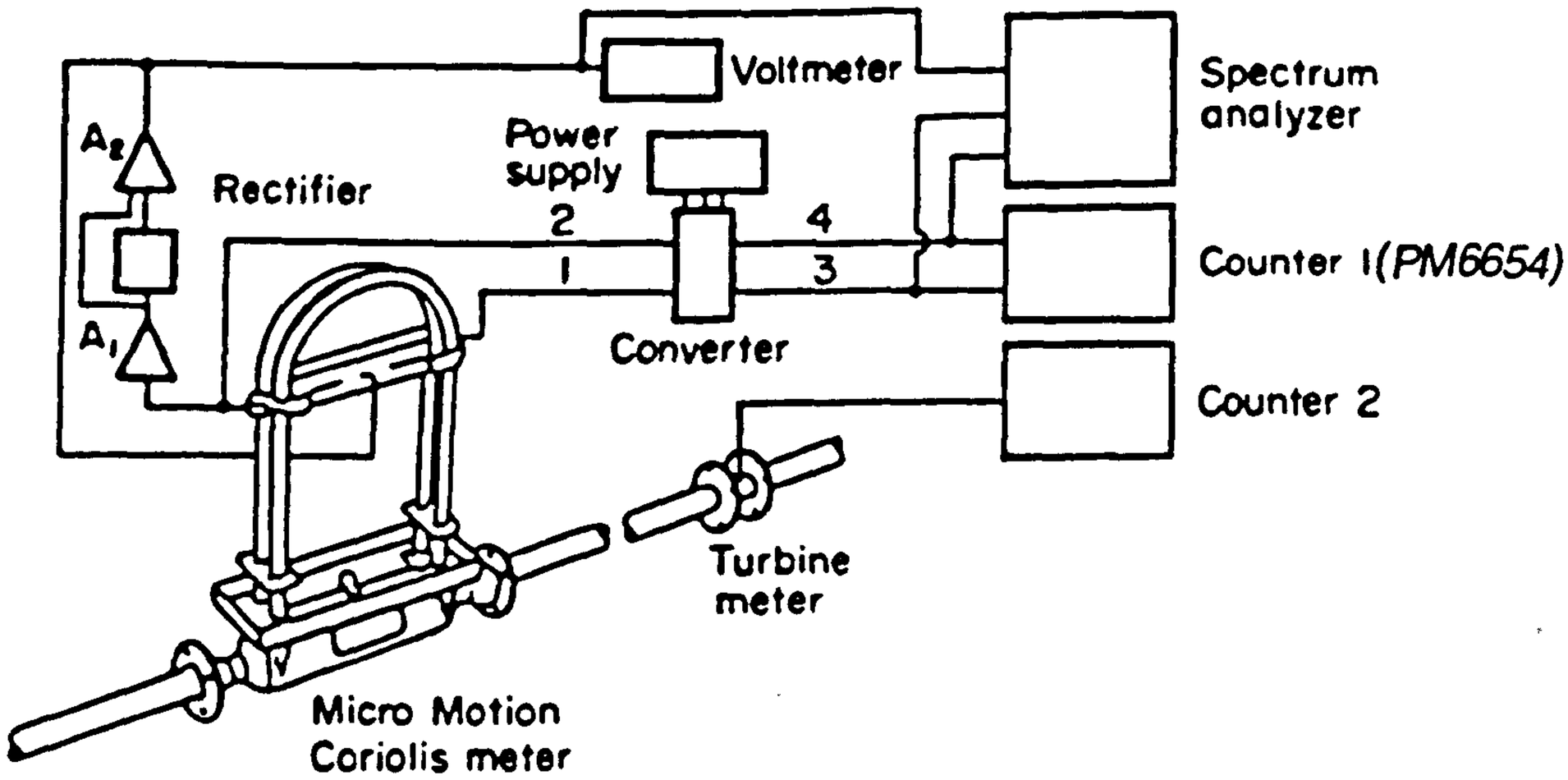

Figure 5.2 BLOCK DIAGRAM OF THE FLOWMETER ELECTRONICS AND READOUT INSTRUMENTATION

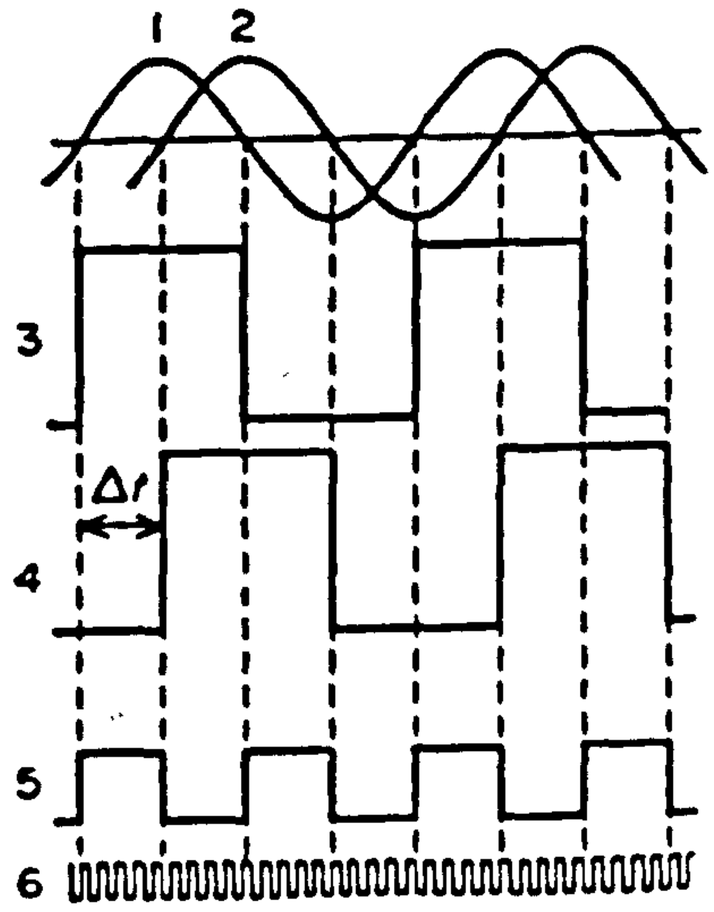

Figure 5.3 WAVE FORMS AT POINTS IN FIGURE 5.2 (points 5 and 6 are internal to counter 1)

Note that to reduce the effect of external vibration it is common practice in industrial Coriolis mass flowmeters to employ two parallel tubes (as shown in Figure 5.1) and to drive them in opposite directions by means of an electromagnetic drive situated between the tubes and not externally mounted. Similarly the relative displacement of the tubes is measured by means of electromagnetic detectors positioned between the tubes at two points. Fluid flows in the same direction in the two tubes.

Experiments were carried out (i) with the empty meter, (ii) with meter in a water flow rig and (iii) with meter in a kerosene flow rig.

5.1.1 Flow Rigs

The water rig is schematically illustrated in Figure 5.4. There are two pumps. The smallest is used for flow rates up to 4 m/s (in 4-inch pipe) and the largest for flow rates up to 10 m/s. The Coriolis meter is positioned in 3-inch horizontal test section with the plane of its U-tube either vertical or horizontal.

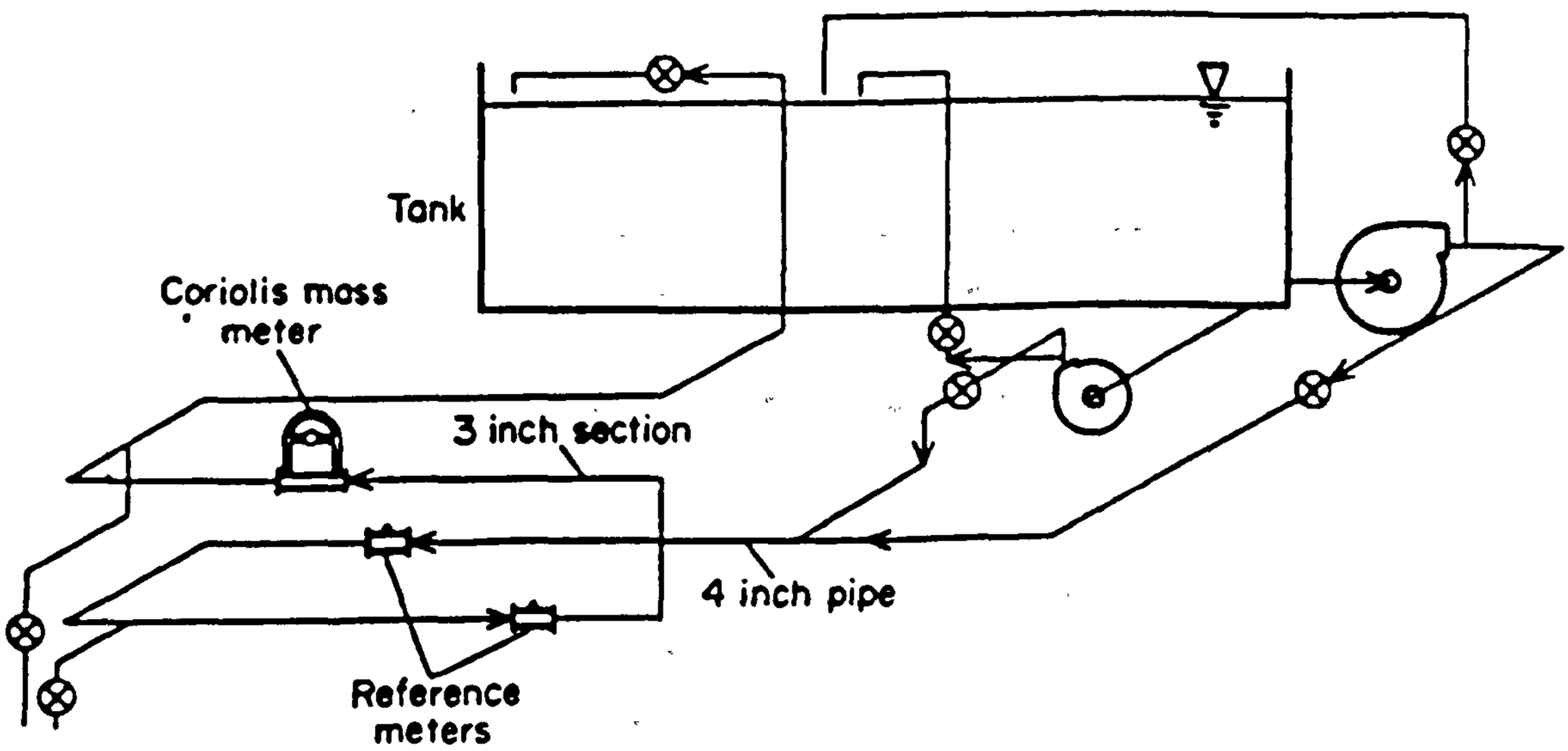

Figure 5.4 WATER FLOW RIG.

Two 4-inch turbine flowmeters (a KENT PTW and a FISHER CONTROL series 7104) were used as reference meters. The accuracy of the reference meters in situ is estimated to be within ∓0.26% and ∓0.24% respectively (the calibration curves of the reference flowmeters are shown in Figure 5.5). The reference meters were calibrated on the BCS approved facilities at CEGB Hams Hall. The accuracy ranges stated apply to the traceable uncertainties given for these facilities plus the added uncertainties of the line fits to calibration curves. These accuracies are typical of good turbine flowmeters.

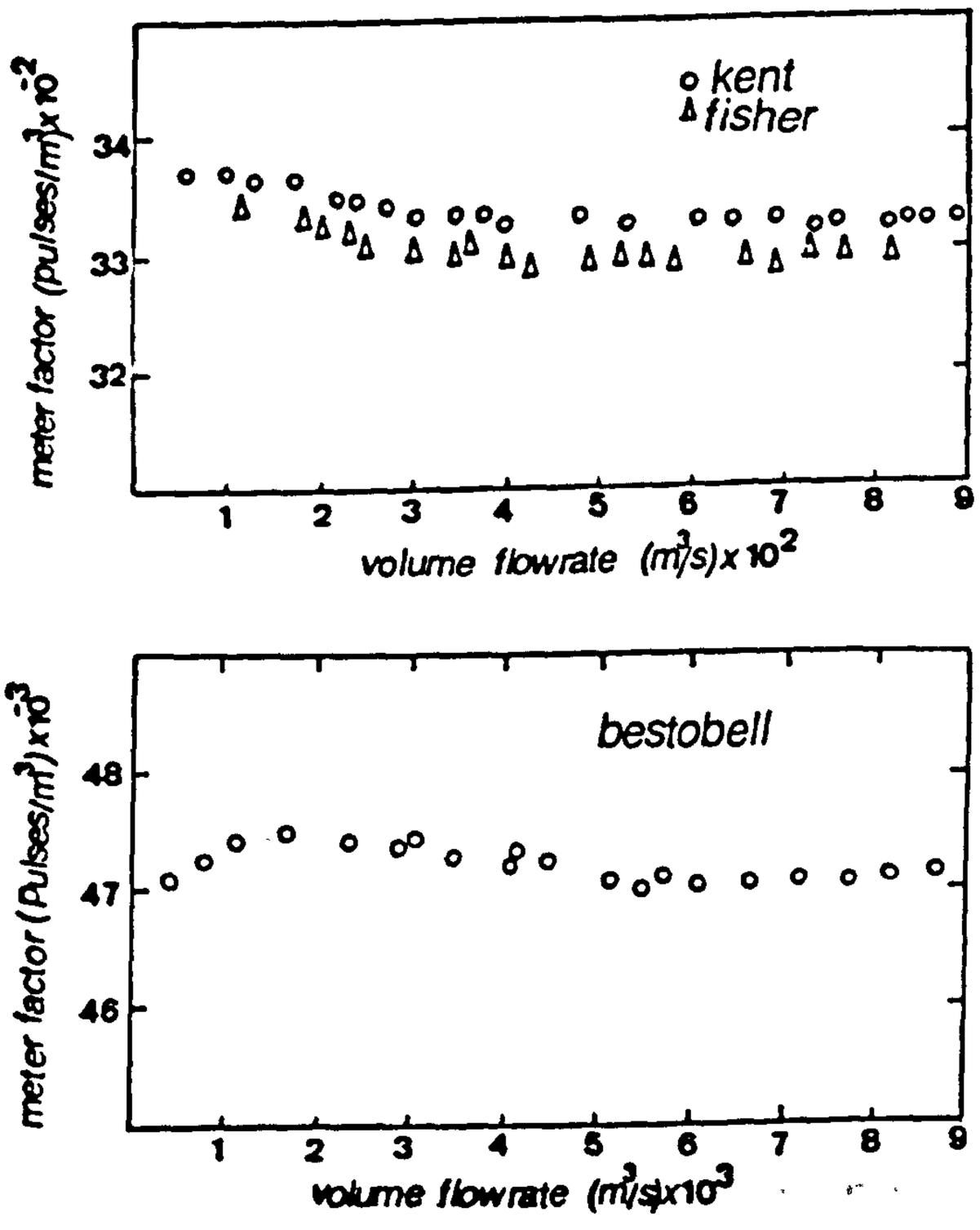

Figure 5.5 CALIBRATION CURVES OF REFERENCE FLOWMETERS

The kerosene rig (Figure 5.6) operates up to a maximum flow rate of 9 m/s (in a 2-inch pipe) the reference meter being a 2-inch turbine flowmeter (BESTOBELL type M6/2000/1325) with an estimated in situ accuracy ∓0.37% (its calibration is shown in Figure 5.5). The Coriolis meter is situated in the 3-inch vertical test section.

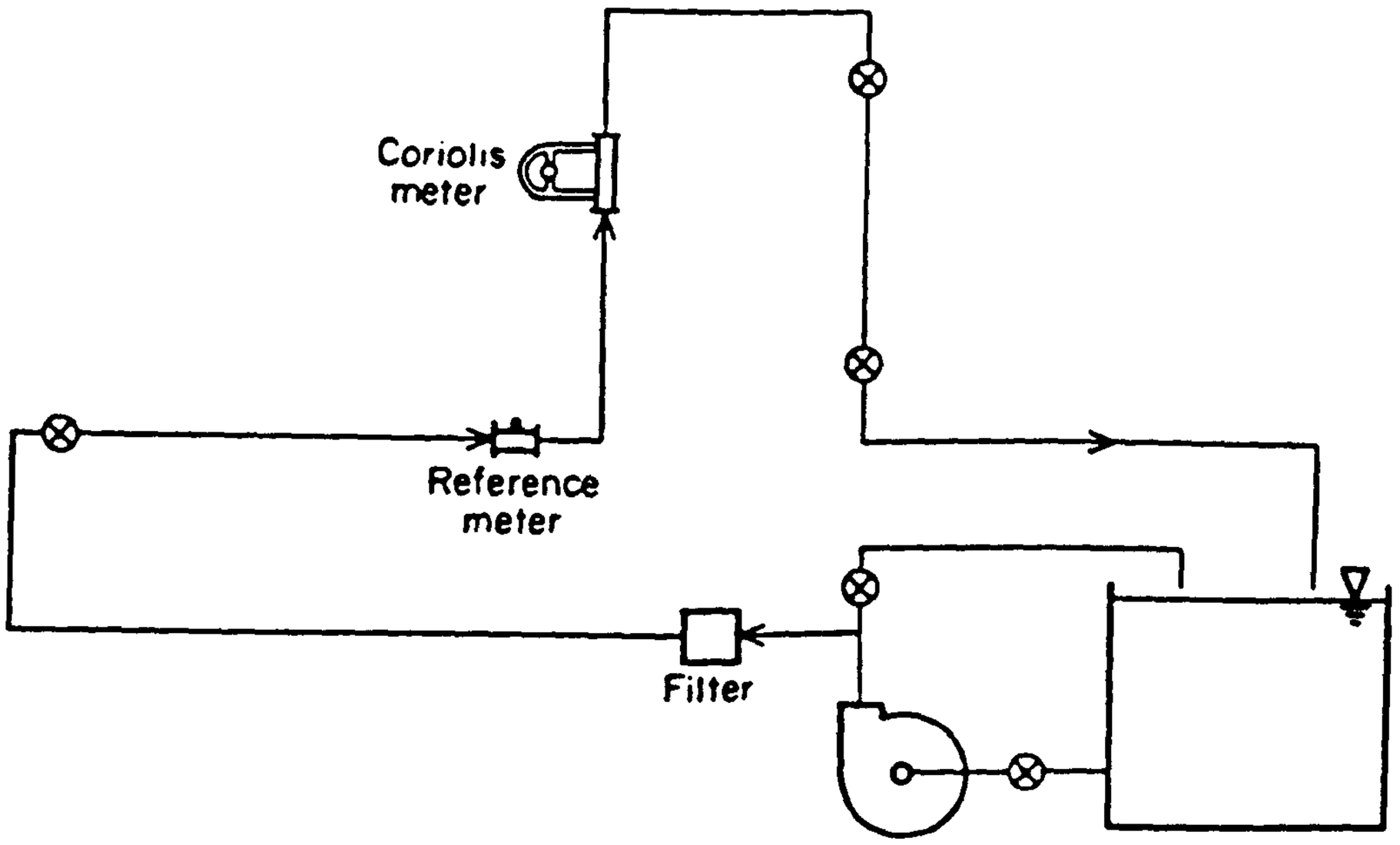

Figure 5.6 KEROSENE FLOW RIG.

5.1.2 *Electronic Processing*

In Figure 5.2 the driving electronics (as supplied with meter) is on the left. Here amplifier A1 amplifies the sine wave voltage from one of the electromagnetic detectors and sends its output to a power amplifier A2 which powers the electromagnetic drive. The output level of A2 is controlled by the rectified output of A1, causing the tube oscillation amplitude to be maintained at a fixed level. This level is such that the output voltage amplitude of the detecting coils is 0.1V.

On the right in Figure 5.2 is the processing electronics to which the waveforms in Figure 5.3 refer. Sinewave voltage 1 and 2 representing the velocities at two points of the tubes are converted into square waves 3 and 4, the rising and falling edges of which coincide with zero crossing points of the sinewave signals. A programmable timer/counter type PM6654 [75] with high frequency oscillator (waveform 6) measures the interval Δt between the rising edges of 3 and 4 and

also the (identical) frequencies of signals 3 and 4. In a frequncy measuring mode the range of the counter is 0.1 Hz to 120 MHz with resolution 1 or 2 LSD (least-square digit). In a time delay measuring mode the range is 8 ns-100 s, with a systematic error of ∓2 ns and resolution of 1 LSD. Average readings for Δt can be obtained by adjusting the time averaging period (section 4.1.1) in the PM6654 counter. An ONO SOKKI FFT analyser is also used for frequency measurement of received and driving voltages. A voltmeter is used to measure the driving voltage.

5.1.3 Measurements

Values of time difference Δt and frequency f were recorded (time averaging period = 5 seconds) at various flow rates. The corresponding phase difference $\Delta\phi$ between tube displacements or tube velocities at the positions of the sensing coils is, of course, related to Δt through the simple equation

$$2\pi f \Delta t = \Delta\phi \qquad (5.1)$$

The time difference Δt is plotted against the mean fluid velocity for two different fluid densities as shown in Figure 5.7. The scatter of points in the kerosene case is almost certainly related to the tendency of kerosene in the rig to release disolved gases or to entrain air. Improvement in rig design should overcome this problem.

Zero drift in the time difference Δt was taken into consideration by subtracting the mean of readings taken under zero flow conditions at the beginning and at the end of each test. The variation of zero flow readings were small during one test.

During experiments the voltage output of the power amplifier A2 was monitored. This was found not to change with flow rate, verifying that the vibration is conservative over one complete oscillation cycle (ie.,the Coriolis force does not cause a net damping or amplifying effect)

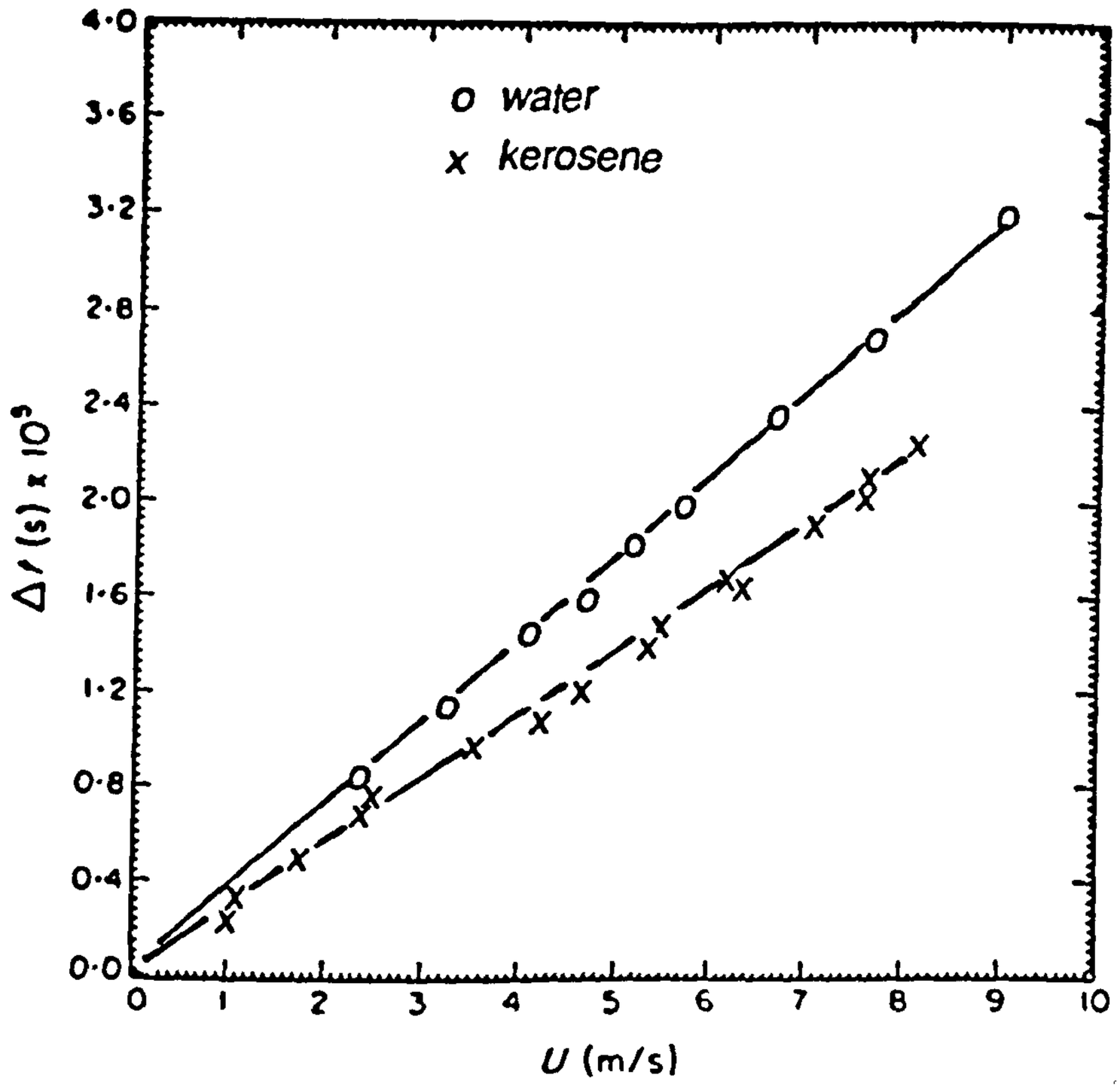

Figure 5.7 TIME DELAY VERSUS MEAN VELOCITY.

5.2 EXPERIMENTAL FLOWMETER

This section describes the mechanical construction and electronic circuitry of the single straight tube experimental flowmeter. In order to verify the theoretical model (chapters 2,3 and 4) and study the behaviour of the meter, a number of experiments were conducted and an account of these is given.

5.2.1 General Description

Figure 5.8 shows the construction of the flowmeter. It consists of a straight stainless steel tube 28 mm O.D and 141 cm length whose ends are welded to the supports in order to obtain good node points.

First, the flowmeters thin tube (t=0.65 mm) is welded to a 5 mm thickness short tube and then the assembly is welded to supports and bolted to the base as shown in Figure 5.8.

A straight tube geometry was chosen for the simplicity of its mechanical design and for the fact that flow control in two phase flow applications is facilitated (chapter 5).

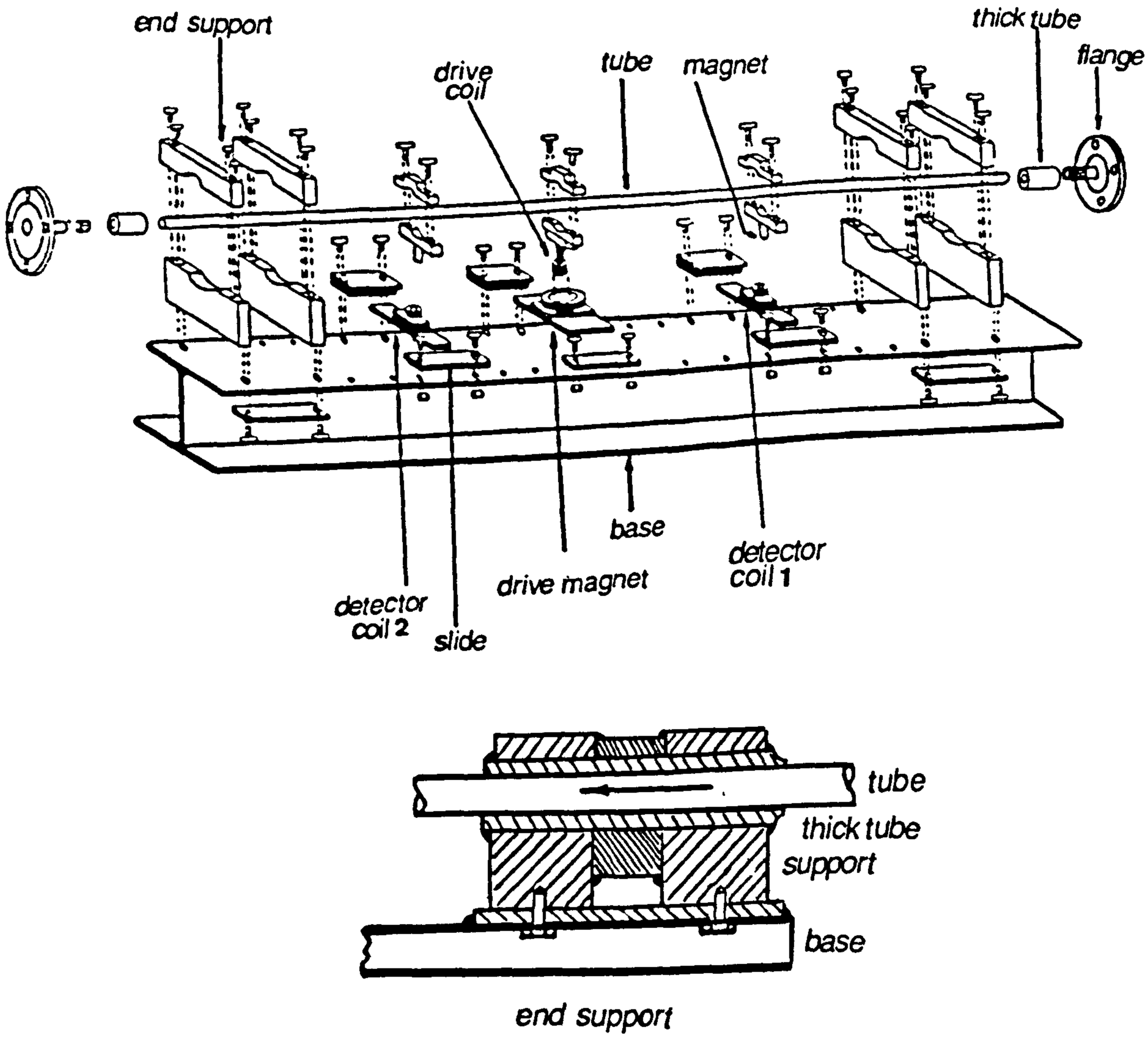

Figure 5.8 THE CONSTRUCTION OF THE EXPERIMENTAL FLOWMETER.

The overall flowmeter is shown in Figure 5.9 and complete with the electromagnetic drive and detectors. The electromagnetic drive consists of a 6000 turn, 16Ω coil attached to the clamp at the middle of the tube and placed inside a disc-shaped permanent magnet (1 mm air

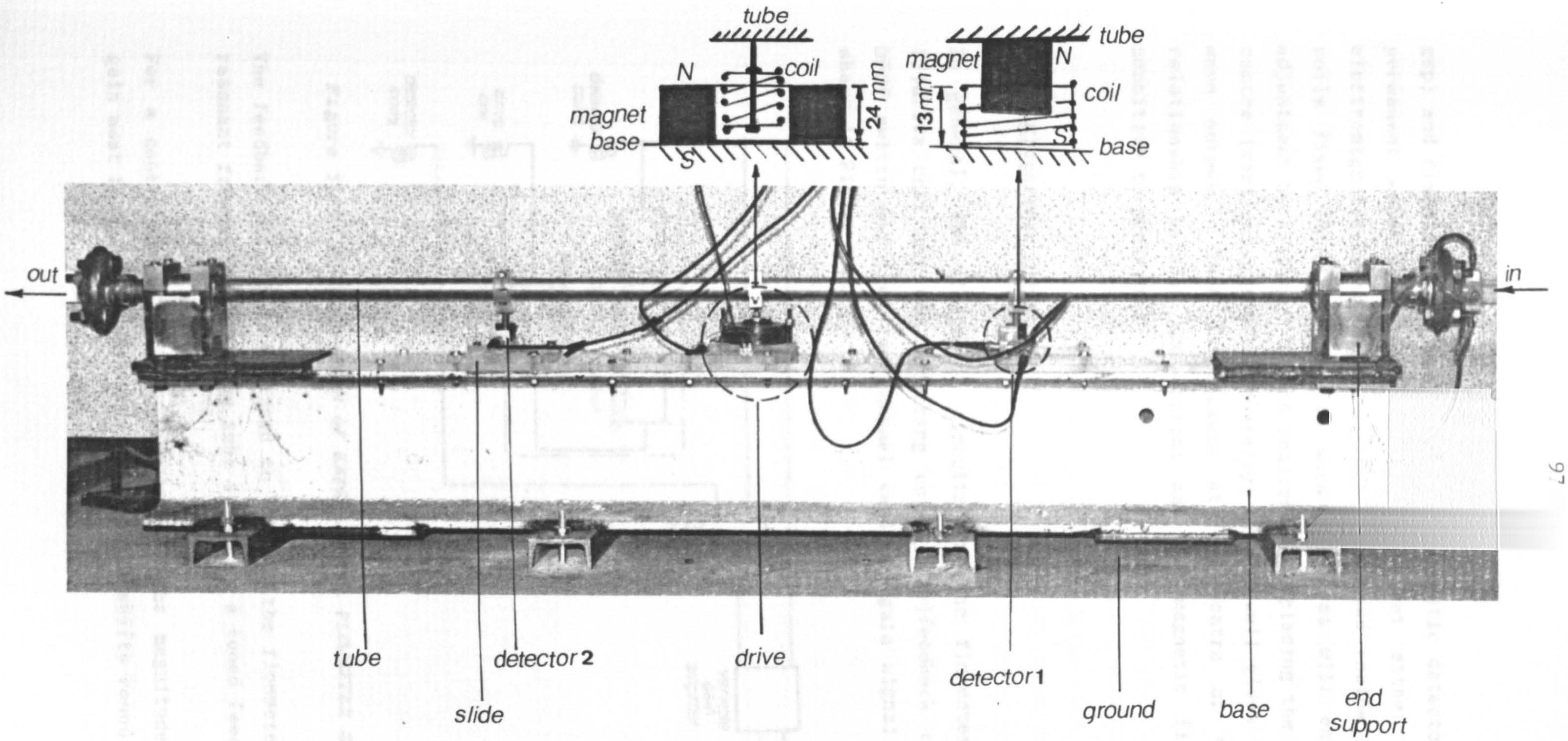

Figure 5·9 1" STRAIGHT TUBE EXPERIMENTAL FLOWMETER

gap) and fixed to the base. The electromagnetic detectors consist of permanent magnets clamped onto the tube at either side of the electromagnetic drive. The magnets are placed inside 2000 turn, 9Ω coils fixed onto the base in such a way as will enable position adjustment by sliding. It was realised that placing the magnet at the centre (vertically and horizontally) of the coil gives the best sine wave output. This is because at the centre of the coil the relationship between the current and the magnetic field is least sensitive to position.

5.2.2 Electronic Circuitry

In general, the electronic circuitry of the flowmeter consists of (i)drive coil and two detecting coils, (ii)feedback circuit, (iii) DPDT switch and (iv) two channel variable gain signal amplifier as shown in Figure 5.10.

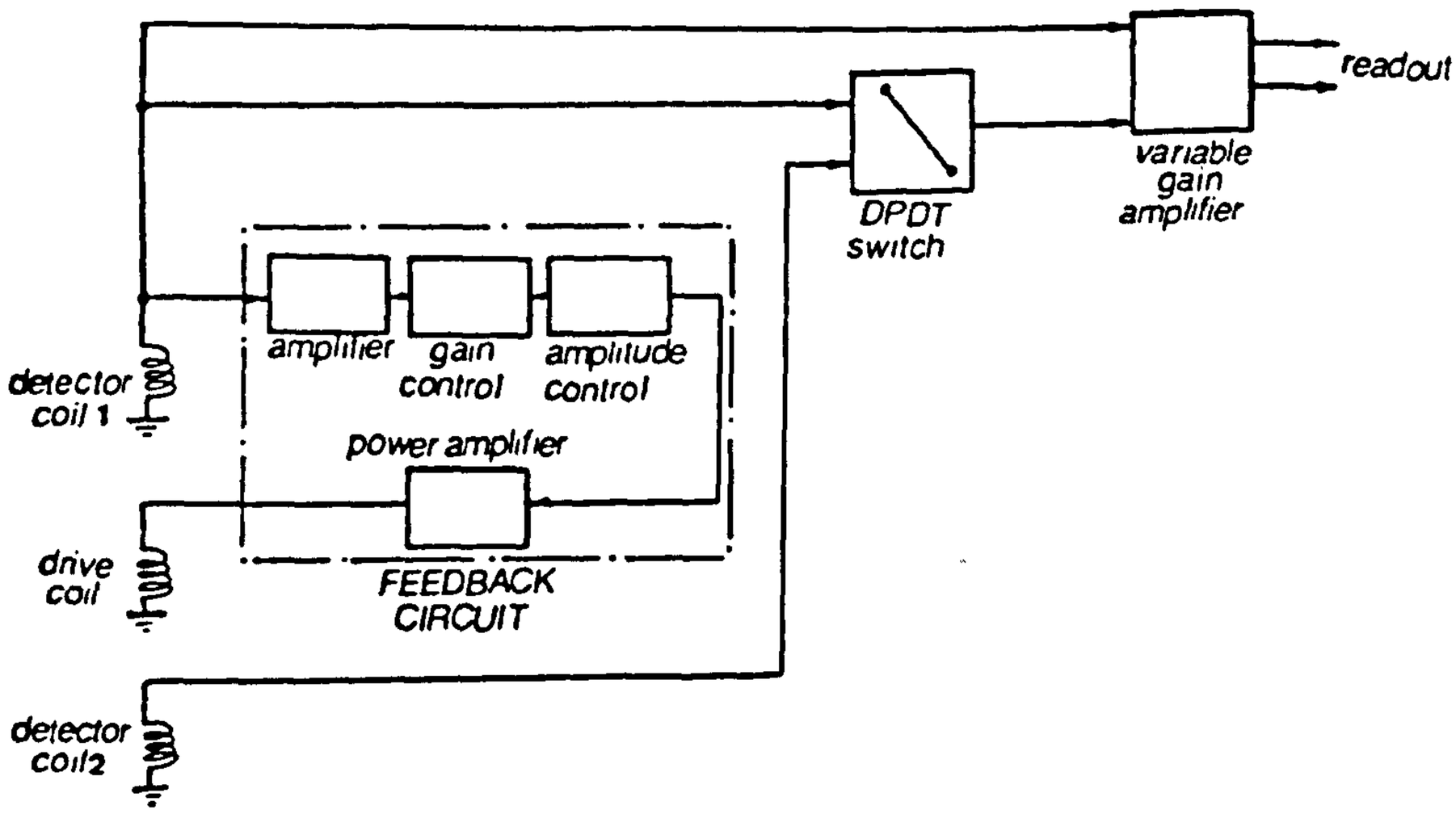

Figure 5.10 BLOCK DIAGRAM OF EXPERIMENTAL FLOWMETER ELECTRONICS.

The feedback circuit is designed to vibrate the flowmeter tube at its resonant frequency, using the tube itself as a tuned feedback element.

For a continuous sinusoidal oscillation, the magnitude of the loop gain must be exactly unity whilst the phase shifts round the loop must

be zero [77]. If the loop gain is slightly more than 1 then continuous amplification of the signal occurs, until it is clipped by the power rails giving a square wave. However, if the loop gain is slightly less than 1 then continuous signal attenuation occurs until it becomes zero. In order to achieve the zero phase shift requirement, the phase shift of the output signal from the feedback circuit must be opposite in sign to the output signal from detector 1.

Details of the feedback circuit including the gain and amplitude control means are given in Figure 5.11. To compensate for losses in the system the signal from detector 1 is amplified with a voltage gain of approximately 50 by IC1. VR1 is used in conjuction with IC2 to set the loop gain to slightly more than 1. The clipping level (amplitude limitation level) is set by VR2 together with ICs 3, 4 and 5. IC5 prevents the output from rising above the clipping level whilst IC4 prevents it from falling below the negative clipping level. IC3 is a voltage amplifier with a gain of -1 which converts the positive clipping level to a negative one. The output from this is then fed to the drive coil via a power amplifier. However, the clipping method used here does introduce a small yet acceptable distortion.

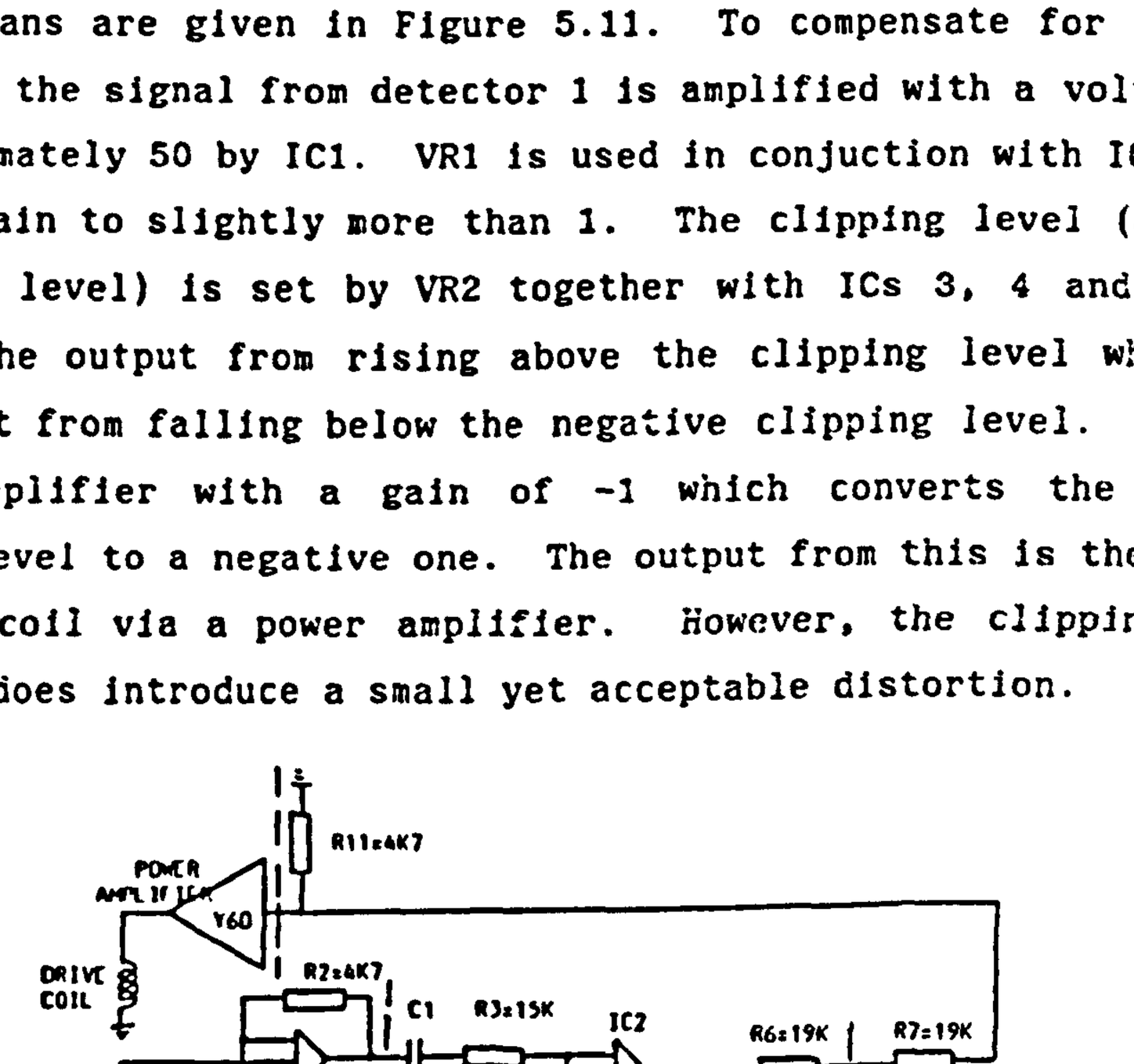

Figure 5.11 ELECTRONIC CIRCUITRY OF THE EXPERIMENTAL FLOWMETER.

The DPDT (double pole double throw) switch was used to compensate for differences in phase shifts in the signal amplifiers. The compensation (for time delay measurements) was made at zero flow by switching one signal (from detector 1) into both sides of the two channel variable gain signal amplifier. The time delay measured in this condition was used to obtain the curve in Figure 5.19 (see section 5.2.5).

5.2.3 Flow Loop and Flow Instrumentation

As the flowmeter performance was affected by external vibration it was necessary to select optimum installation. Therefore two piping arrangements were constructed which are illustrated schematically in Figure 5.12.

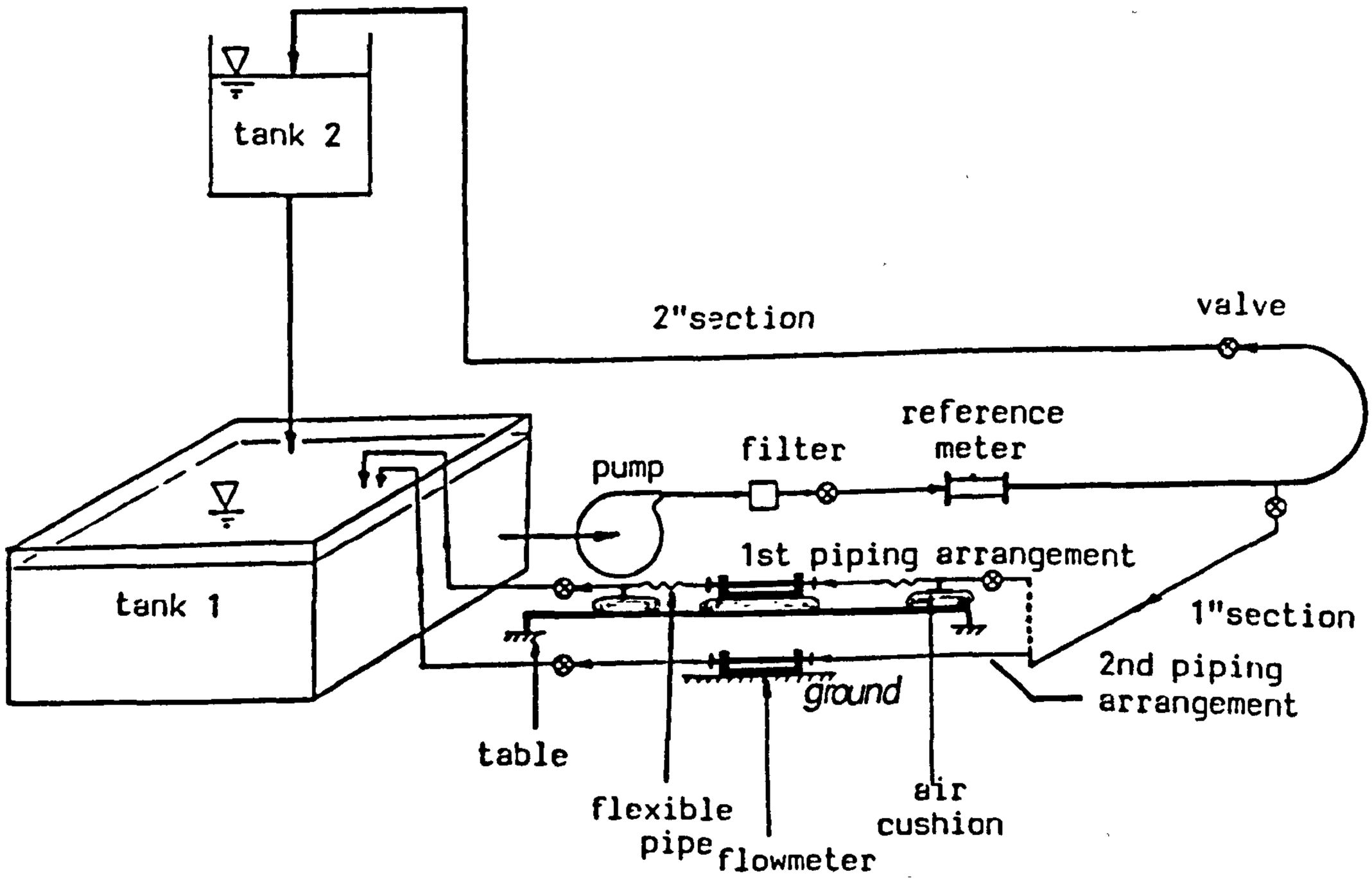

Figure 5.12 FLOW LOOP.

The test section of the first piping arrangement was placed on an air cushion and seperated from the remaining pipe work by flexible tubing. In the second arrangement the test section was fixed rigidly to the (concrete) ground.
The rig operates up to a maximum water flow rate of 6 m/s (in 1-inch pipe). Flow was controlled by valves using a by-pass loop.

A 2-inch turbine flowmeter (KDG 25458/83) was used as a reference. The accuracy of the reference flowmeter in situ is estimated to be within ∓0.4% (Figure 5.13 shows the calibration line, the reference meter was calibrated on the BCS approved facilities at CEGB Hams Hall).

Figure 5.14 shows a photograph of the flow loop in the second piping arrangement.

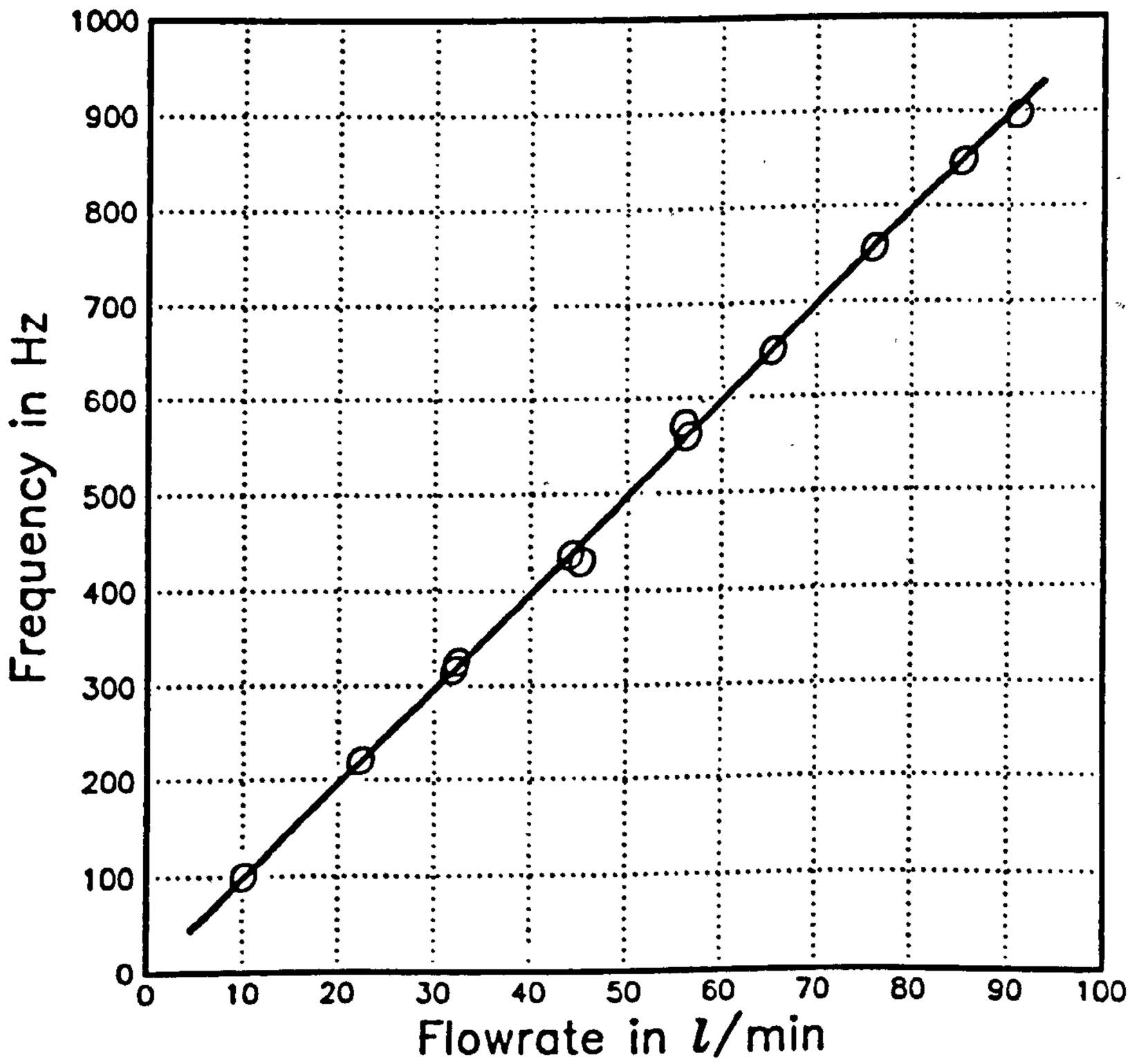

Figure 5.13 CALIBRATION LINE OF THE REFERENCE FLOWMETER.

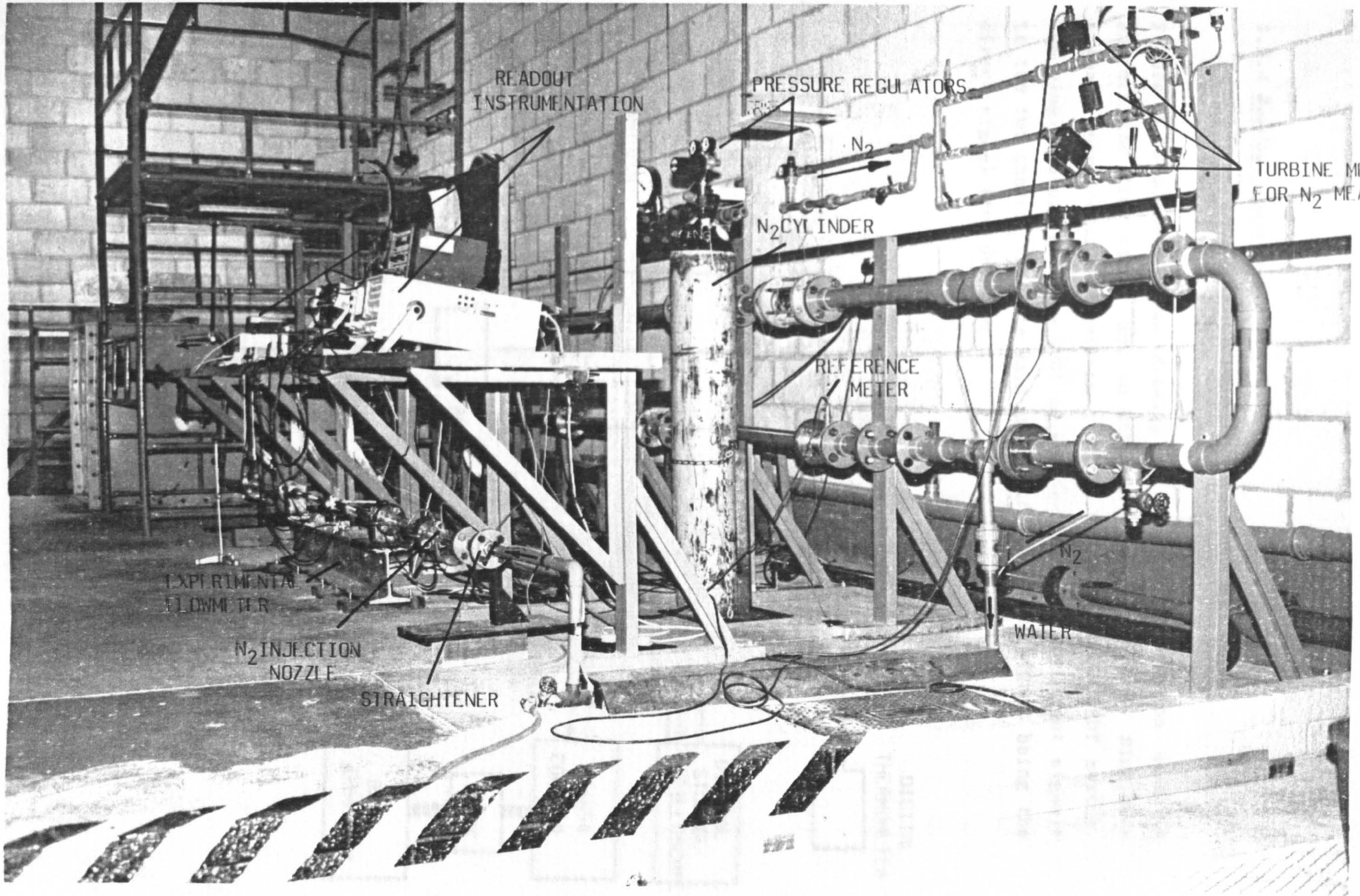

Figure 5.14 FLOW LOOP IN SECOND PIPING ARRANGEMENT

5.2.4 Readout Instrumentation

Figure 5.15 shows a line drawing of the instrumentation used to extract the flow signal and to measure other variables. Sine-wave signals obtained from detectors 1 and 2 were fed to a DPDT switch. The single output from the DPDT switch forms one of the input signals to the two channel variable gain amplifier, the other signal being the direct signal from detector 1.

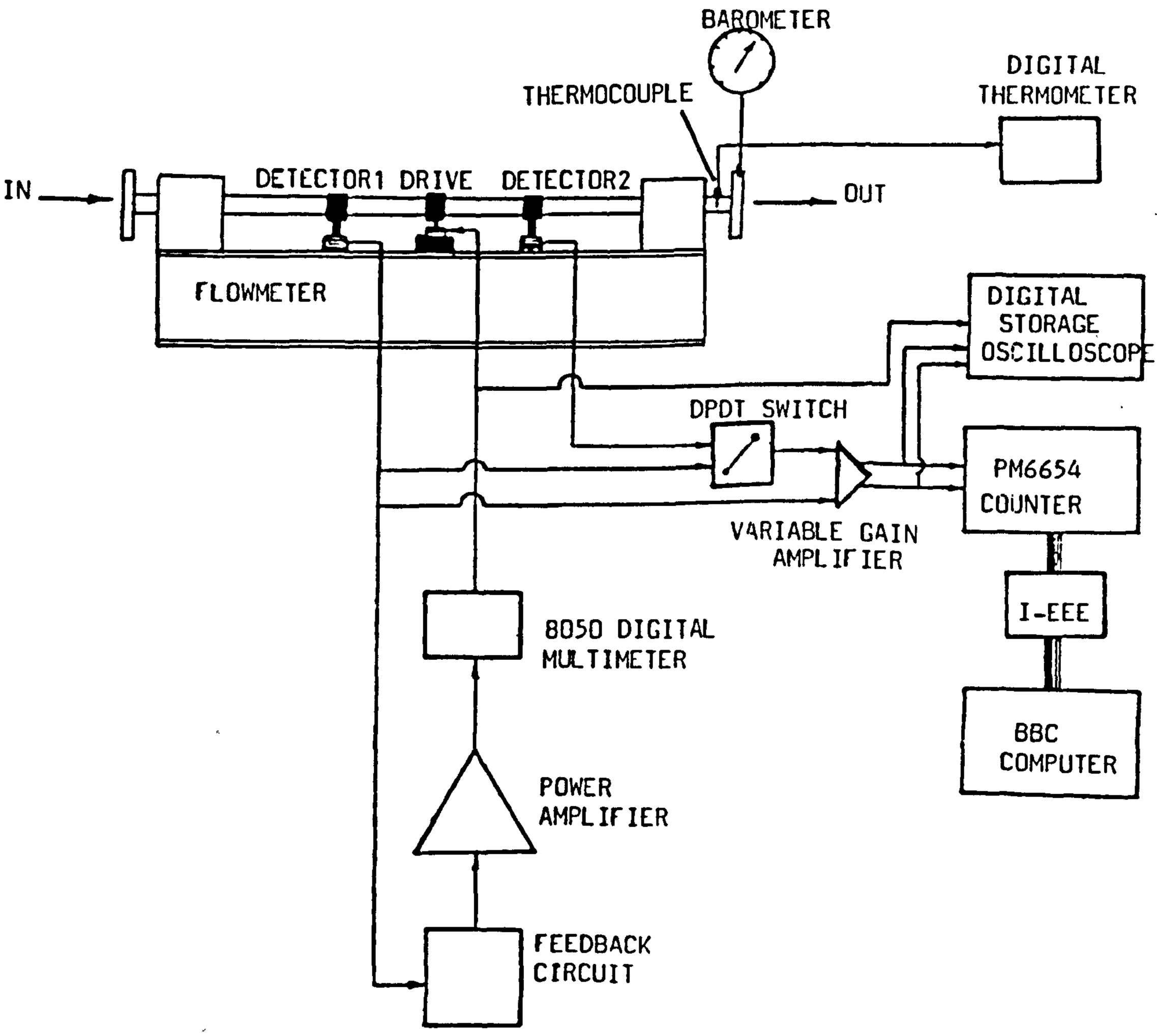

Figure 5.15 READOUT INSTRUMENTATION.

In order to measure the time delay Δt and frequency f (see section 5.2.2) a programmable timer/counter type PM6654 was used directly on the amplified sine-waves. The values of Δt and f were then transferred to a BBC Master microcomputer via IEEE-488 interface so that the averages over many measurements could be taken.
The amplitude of the detector voltage was recorded using a Gould Digital Storage Oscilloscope 4050 whilst the drive current was monitored by a Fluke 8050 Digital Multimeter.

Water temperature was measured using a sealed thermocouple inserted into the inlet of the flowmeter with digital readings being obtained by a Newport Digital Thermometer. Finally, the inlet pressure was monitored by a standard barometer. Figure 5.16 shows a photograph of the instrumentation described above.

5.2.5 Zero Flow Test

It was necessary to obtain continuous zero readings because undesirable zero shifts were observed during the experiments. The zero flow condition was obtained by closing the up-stream and down-stream valves and ensuring no entrained air in the test section. In this condition the effects of water temperature and external vibration on base line stability were assessed.

5.2.5.1 Temperature Effect

At zero flow time delay Δt, frequency f and water temperature were measured simultaneously. Water temperatures above ambient temperature were obtained by running the water for a certain length of time, closing the up-stream and down-stream valves and then allowing cooling back to ambient temperature.

Figure 5.17 shows the considerable zero shifts in terms of Δt (Δt and

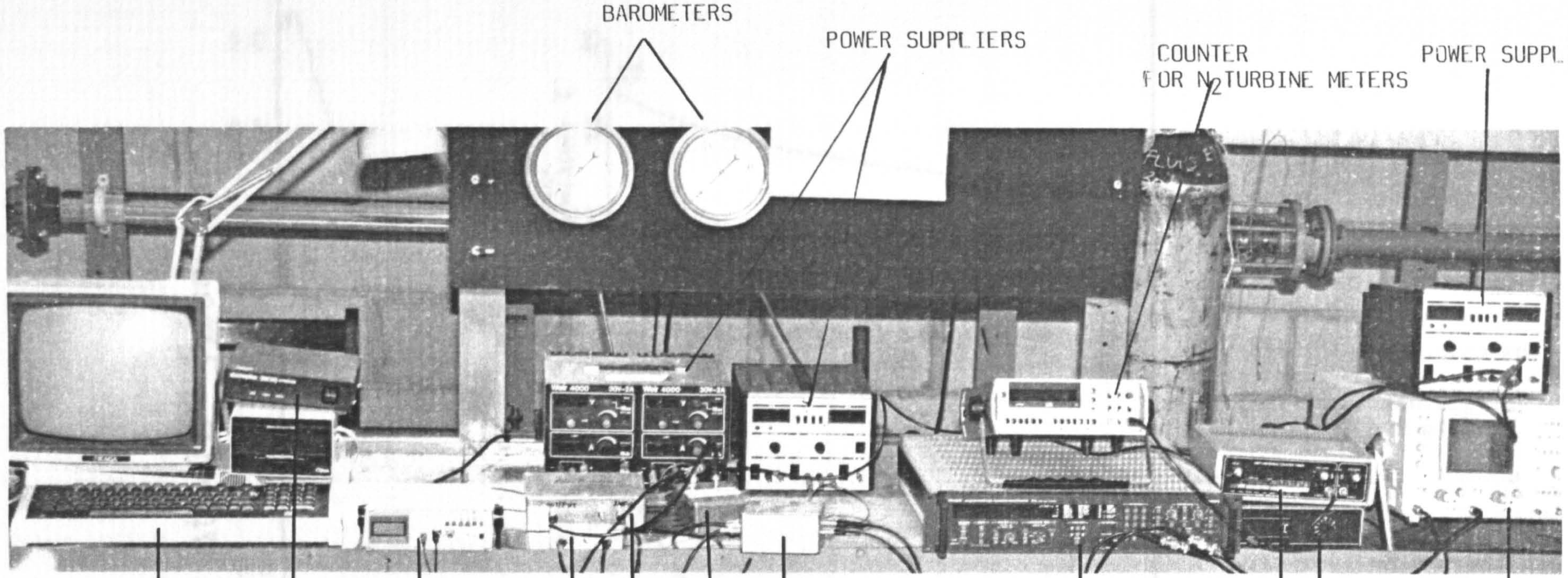

Figure 5.16 FLOWMETER ELECTRONICS AND READOUT INSTRUMENTATION.

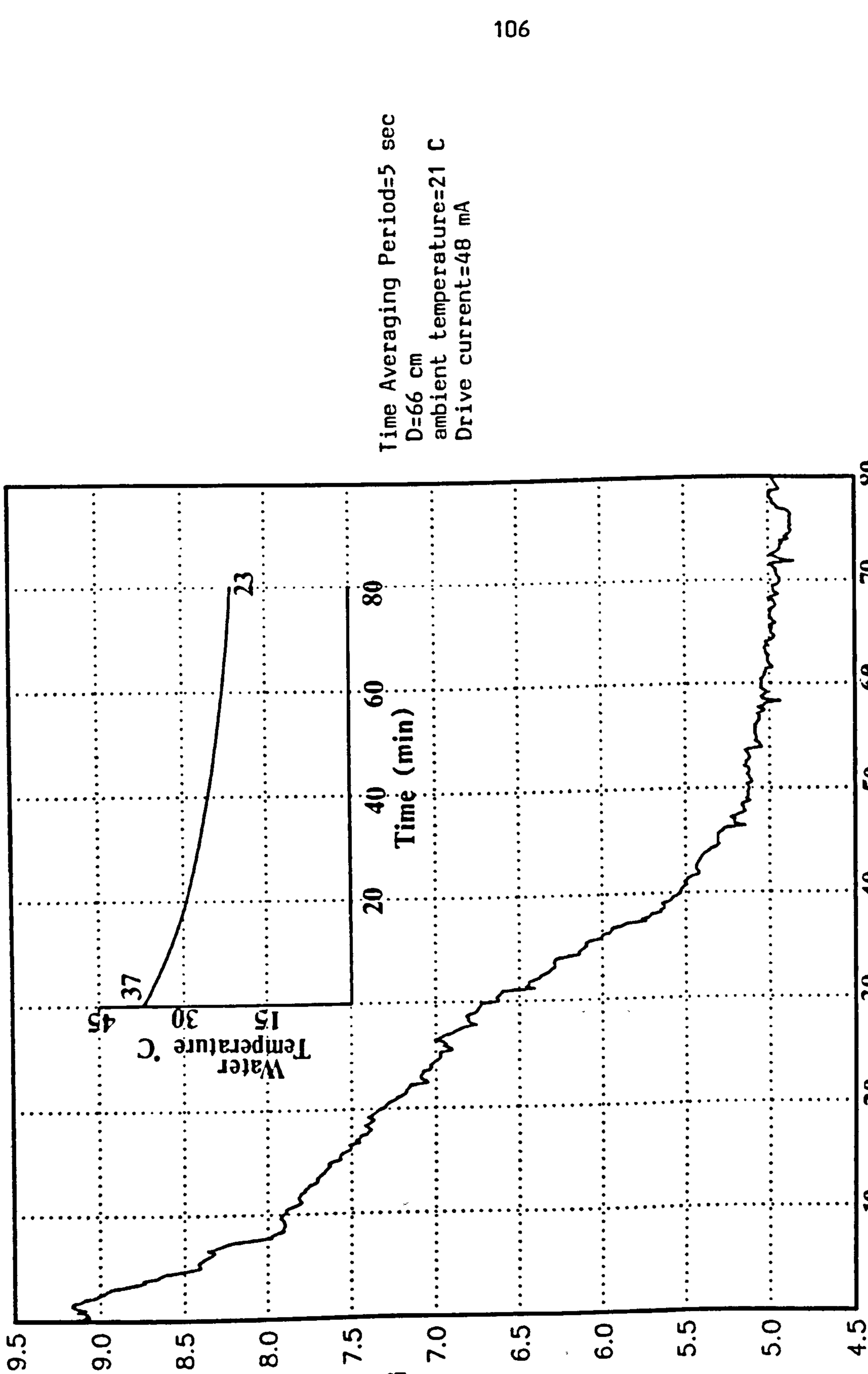

Figure 5.17 EFFECT OF WATER TEMPERATURE ON BASE LINE STABILITY.

f were recorded every 5 seconds) when water temperature (and consequently tube temperature) was initially increased to 16°C above ambient temperature (in Figure 5.17 10 μsec time delay corresponds to 1 m/s flow velocity).

Note that the base line becomes more stable at temperatures near ambient temperature (effectively the temperature of the flowmeter base). This is due to the fact that the base line stability is affected by thermal equilibrium of the tube/supports/base system. The difference in the temperature of the tube, supports and/or base produces differential thermal expansion resulting in change in the end conditions and consequently in the differential damping characteristic of the tube.

In general, increase in the tube temperature decreases the frequency due to a decrease in the modulus of elasticity [78]. Figure 5.18 shows the effect of water temperature on tube frequency. Observation of the frequency suggests a greater decrease than could be accounted for by the modulus of elasticity (eg. 5 °C increase in temperature leads to 0.05 Hz decrease in frequency). This is almost certainly due to the change in the tube end conditions.

Finally, the time delay between the two variable gain signal amplifiers was plotted against tube frequency (Figure 5.19) to show the presence of an electronic zero drift which is superimposed on the mechanical zero drift (in Figure 5.17 the electronic zero drift is included).

5.2.5.2 External Vibration Effect

It is a manufacturer recommendation [38] that Coriolis flowmeters be installed as far away as possible from likely sources of vibration (ie.,pumps, compressors, motors, walkways etc.). This section investigates the effect of the water pump vibration on zero flow readings.

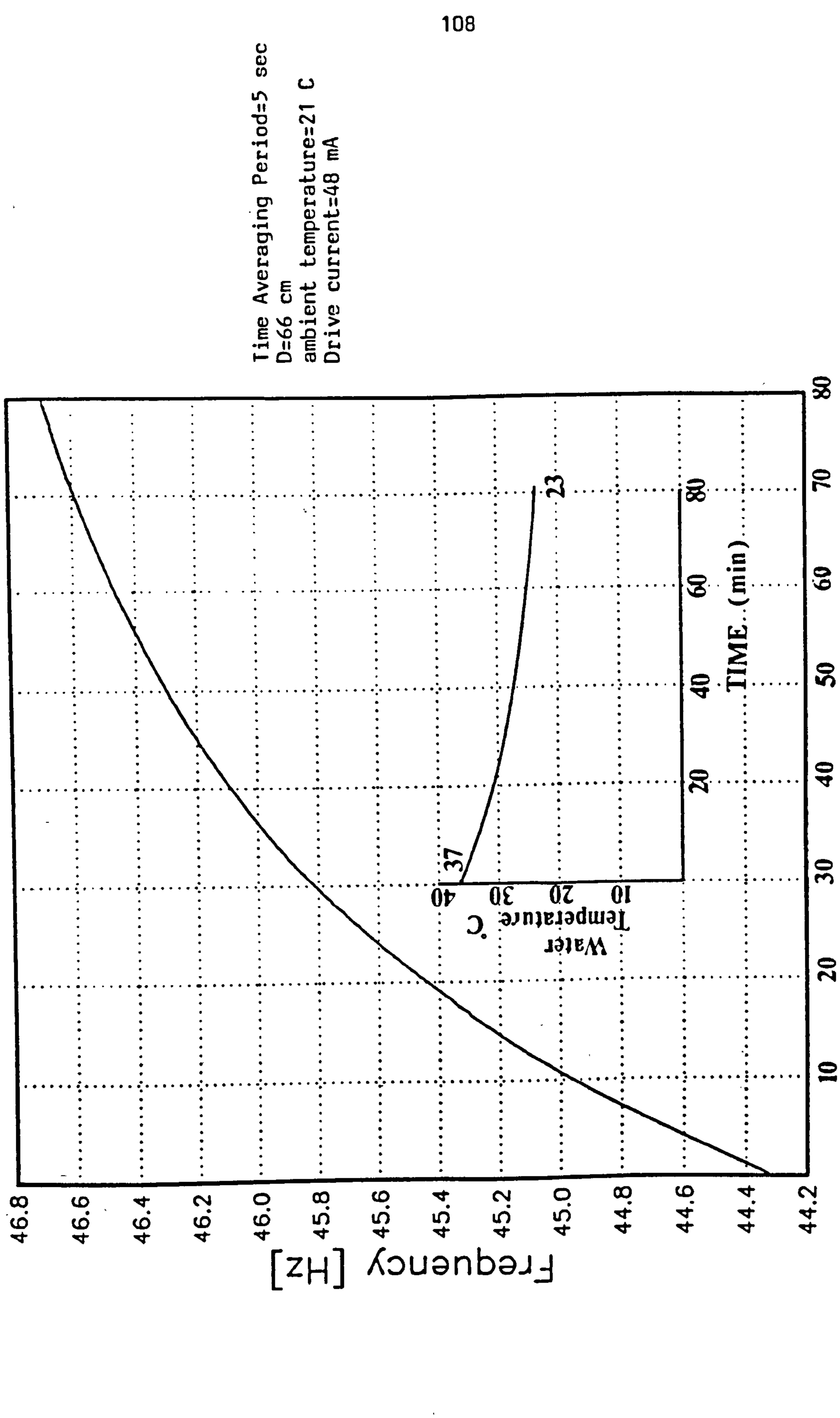

Figure 5.18 EFFECT OF WATER TEMPERATURE ON TUBE FREQUENCY.

The water pump provides external vibrations which can be either hydraulically and/or mechanically transmitted to the flowmeter. Depending on the amplitude and frequency of the external vibration this could interfere with the flowmeter tube vibration resulting in distorted signals from the detectors.

Figure 5.20 shows the effect of the water pump, operating at 2850 rpm, on zero flow reading (for first piping arrangement). It seems impossible to completely prevent the external vibration from reaching the flowmeter. However, the time averaging period was smaller by 1/2 for the first piping arrangement in comparison with second arrangement (15 sec for first arrangement and 30 sec for second arrangement). Thus, it seems that the external vibration is less influential in the first arrangement.

5.2.6 Flow Test

Due to the possibility of undesirable zero shifts (section 5.2.5) the flow test was conducted under certain conditions. These were (i) constant and equal water and ambient temperatures (ii) sufficient averaging of time delay measurement.

Figure 5.21 illustrates flowmeter calibration results and tube frequencies for different distances (D) between detection points. The zero reading was recorded and subtracted from each flow reading in order to remove any zero drift and thus improve the repeatability of the fowmeter. Figure 5.22a and 5.22b show the effect of zero drift on repeatability. In Figure 5.22a the zero readings were taken for each flow readings while in Figure 5.22b one zero reading was taken for each set of tests. The averaging time period was 30 seconds, but this was increased for D=90 cm and D=40 cm to 50 seconds due to reduction in signal amplitude (for D=90 cm) and reduction in time delay (for D=40cm).

The optimum measuring distance was located (see section 4.3) by

recording the detector signal amplitude and time delay for each measuring distance D. Figure 5.23 shows the multiplication parameter $A \cdot \Delta t$ plotted against measuring distance for two flow rates.

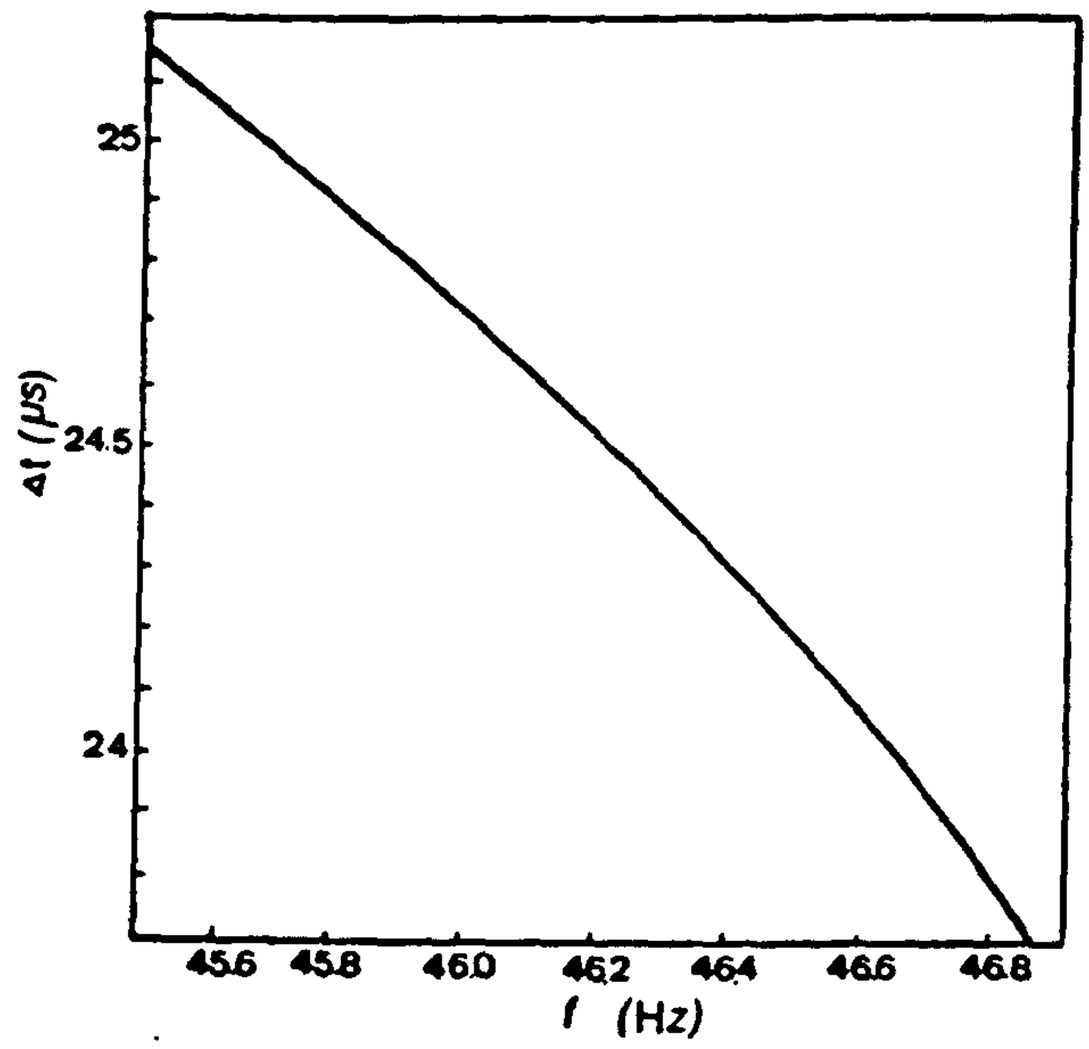

Figure 5.19 TIME DELAY BETWEEN THE TWO VARIABLE GAIN SIGNAL AMPLIFIERS VERSUS TUBE FREQUENCY.

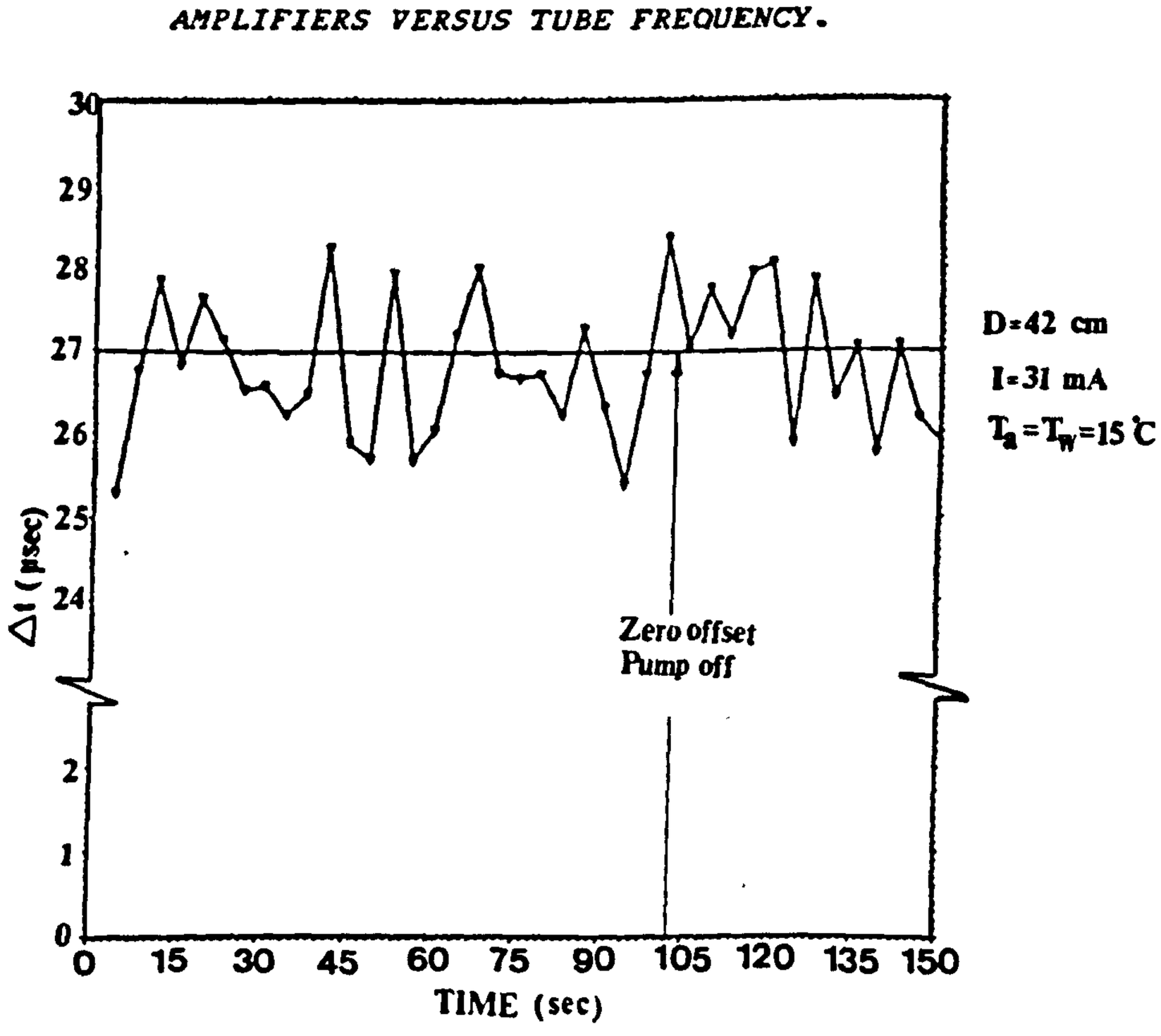

Figure 5.20 EXTERNAL VIBRATION EFFECT ON BASE LINE STABILITY.

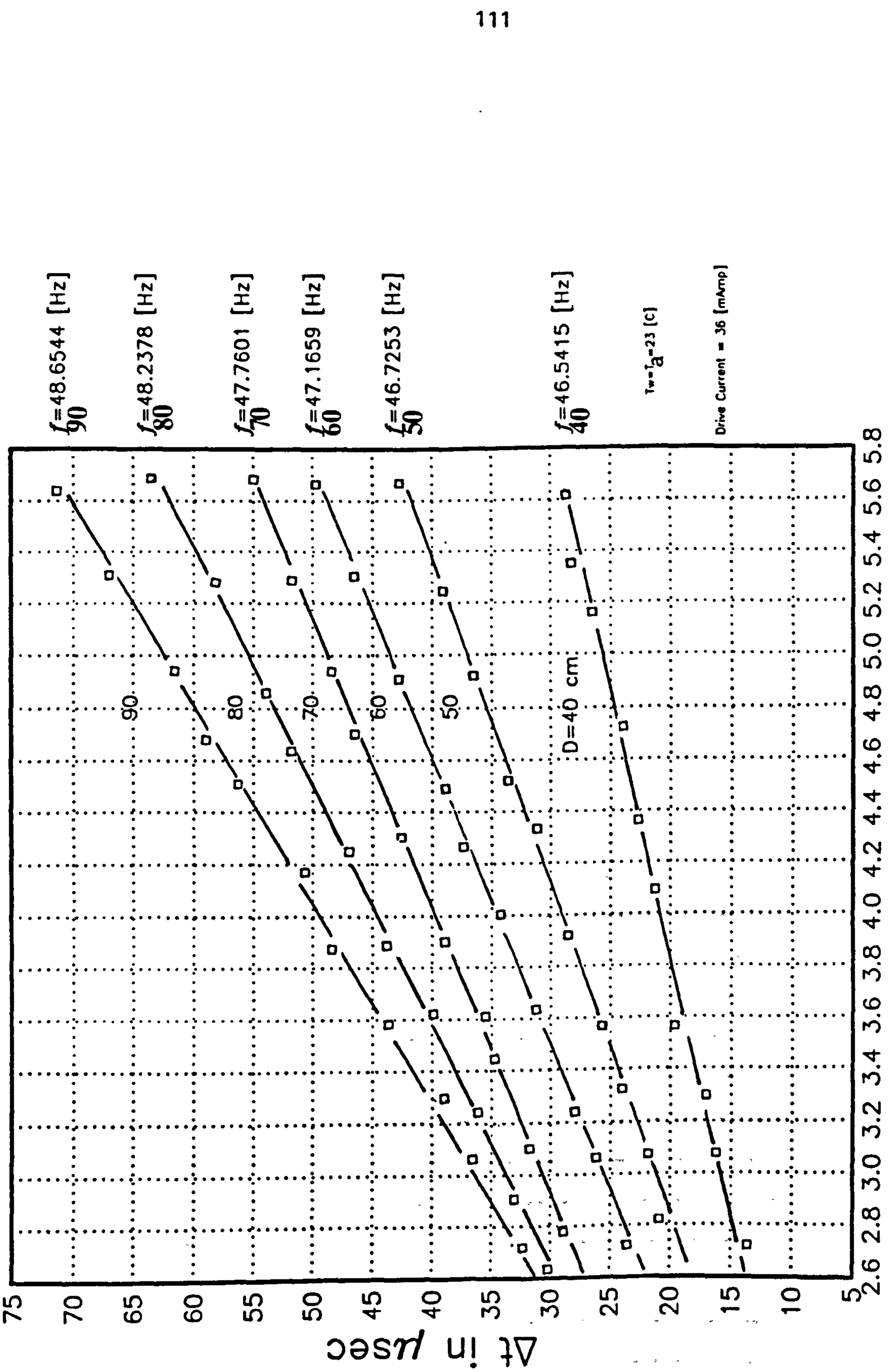

Figure 5.21 FLOWMETER CALIBRATION LINES FOR DIFFERENT SENSOR POSITION.

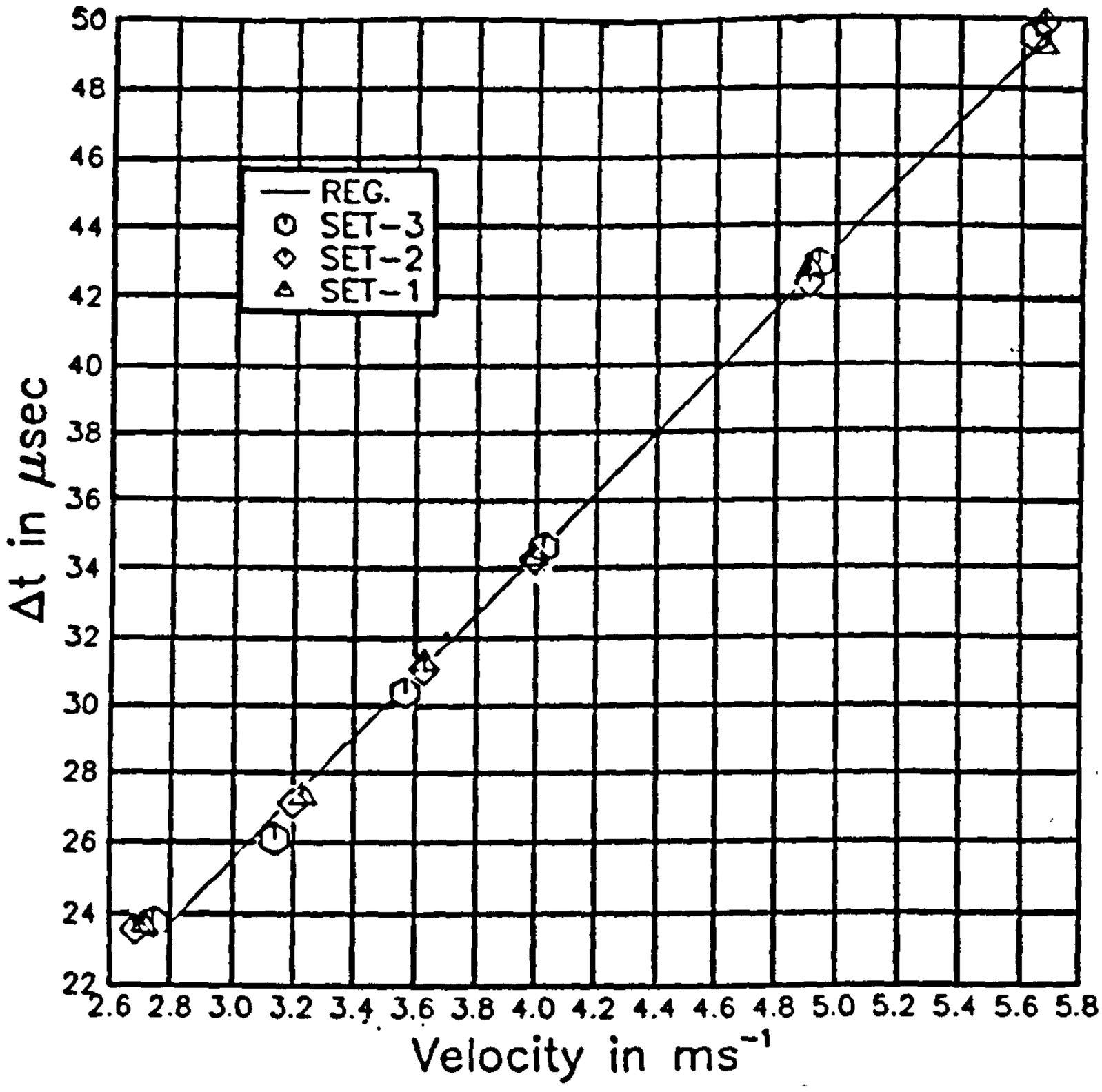

D=60 cm

$T_a=T_w$=23 C

Drive current=36 mA

T.A.P= 30 sec

(a) zero readings for each flow reading.

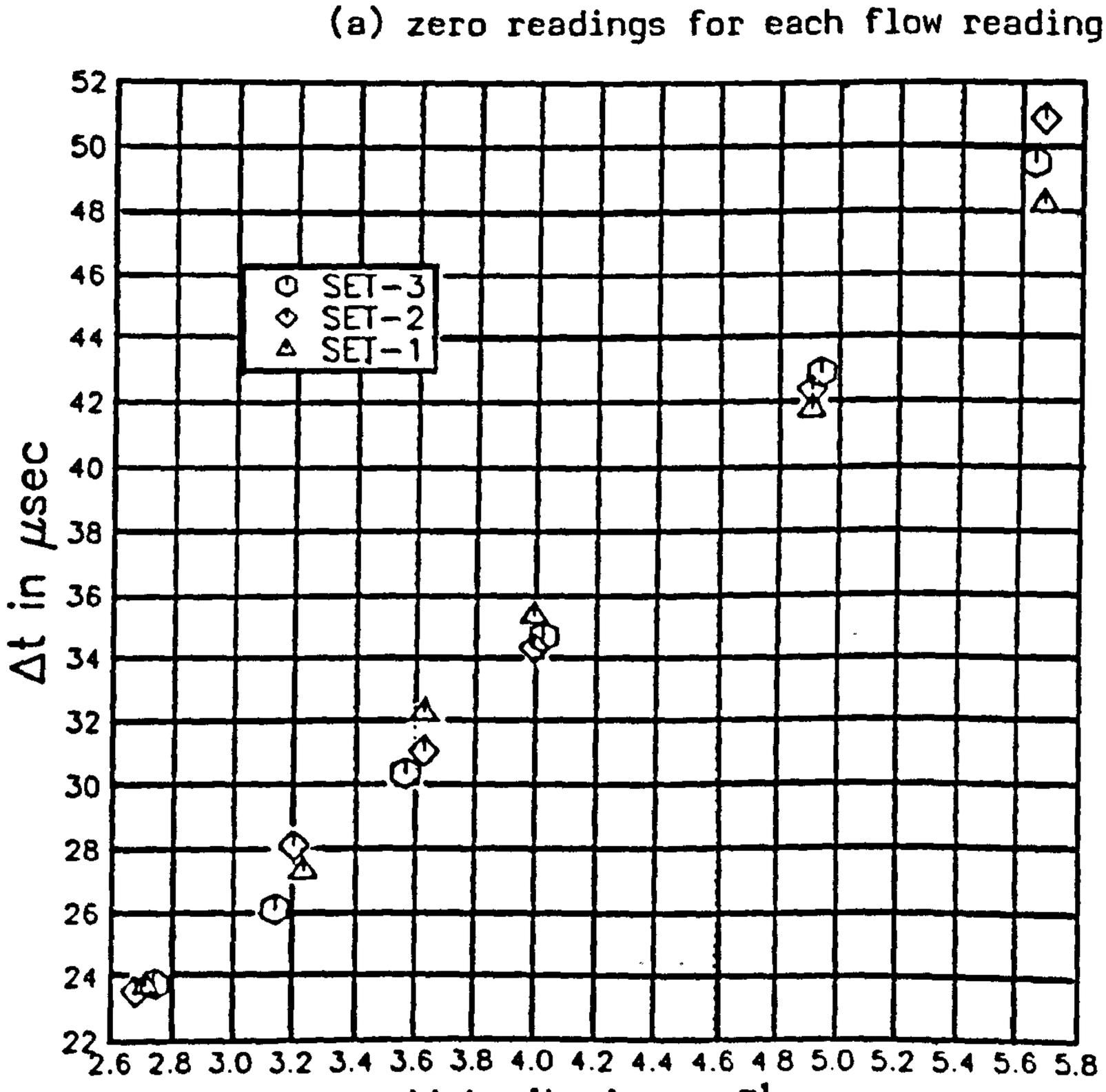

(b) one zero reading for each set of readings.

Figure 5.22 ZERO SHIFT EFFECT ON REPEATABILITY

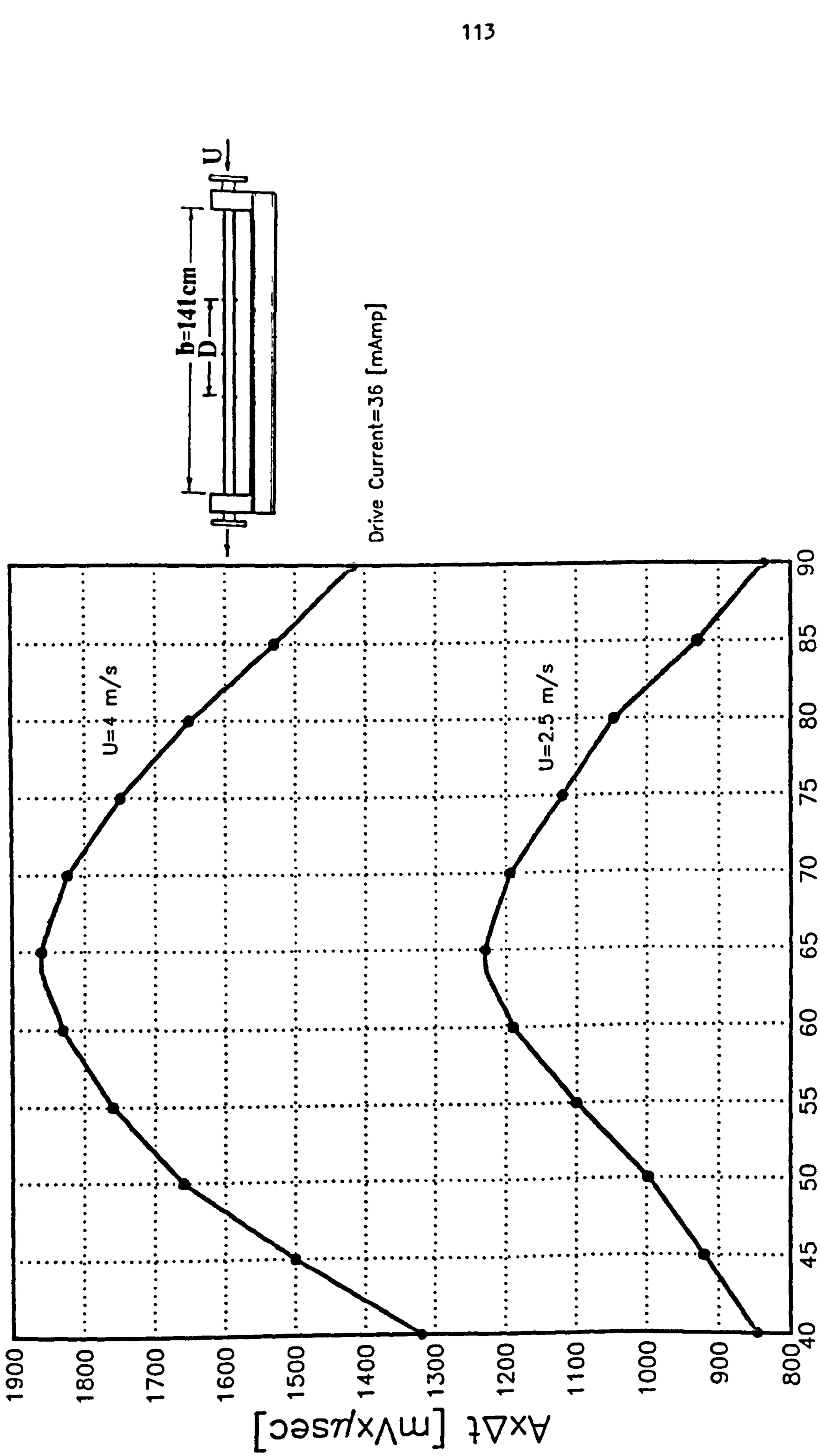

Figure 5.23 EXPERIMENTAL GRAPH FOR LOCATING OPTIMUM SENSOR POSITIONS.

CHAPTER SIX

THE EFFECT OF TWO-PHASE (LIQUID-GAS) FLOW

CHAPTER SIX

THE EFFECT OF TWO-PHASE (LIQUID-GAS) FLOW

6.1 INTRODUCTION

Two-phase (liquid-gas) flows occur in a variety of engineering apparatus and processes (ie. absorbers, evaporators; cavitation, aeration ... etc). They are frequently found in the chemical, petroleum and related industries [79].

In order to optimize the processes and minimize the cost (eg. avoid expensive and bulky separation equipment in the oil industry) the need for accurate mass flow measurement of the two-phase flow becomes increasingly important.

In general, mass flow rate of two-phase mixtures is determined indirectly by two measurements (i) void fraction measurement (normally by means of gamma-ray or X-ray absorption [80]) and (ii) a flow measurement (using for example differential pressure devices, ultrasonic meters, turbine meters, drag screens, tracer techniques ...etc). Hewitt [81] has summarized this method, highlighting its shortcomings and giving recommendations for its improvement. Hewitt has also indicated the future possibilty of using true (direct) mass flow meters for measuring two-phase flows.

It can be seen from the published literture such as those by Wyatt [82] electromagnetic flowmeter), Kinghorn and McHugh [83] (turbine flowmeter) and Grumski and Bajura [33] (Coriolis flowmeter) that considerable error is produced in applying conventional flowmeters (which were designed to measure single-phase flow) to two-phase (liquid-gas) mixtures. This is due to the interaction between the liquid and gas phases and the fluctuations of the flow and fluid properties.

In this chapter a method is given for predicting the effect of a dilute suspension of small bubbles or particles in the liquid on a Coriolis flowmeter. An attempt is also made to determine experimentally the feasibility of using the Coriolis flowmeter for measuring the total mass flow of bubbly (water-nitrogen) flows. First however a general review of the topic is given.

6.2 *PERFORMANCE OF THE U-TUBE CORIOLIS MASS FLOWMETER IN MEASURING TWO-PHASE (LIQUID-GAS) MIXTURES*

Liquid/gas two-phase flow effects have been investigated experimentally by others (for example [33]). When a gaseous phase is present in small quantities (small bubbles) the Coriolis mass flowmeter usually reads too low, that is, it somewhat underestimates the total mass flowrate of the mixture. As the void fraction of the gas is increased this negative error slowly increase until a point is reached when the flowmeter suddenly gives very large errors or fails to function properly at all. This is illustrated in Figure 6.1 taken from [33]. Here the two lines give the measured error versus the void fraction in two types of flowmeter employing U-tubes (manufactured by Micro Motion Inc.) mounted in a horizontal plane. The liquid is ethylene glycol and the gas is air and the glycol flowrate is 90.2 Kg/min.

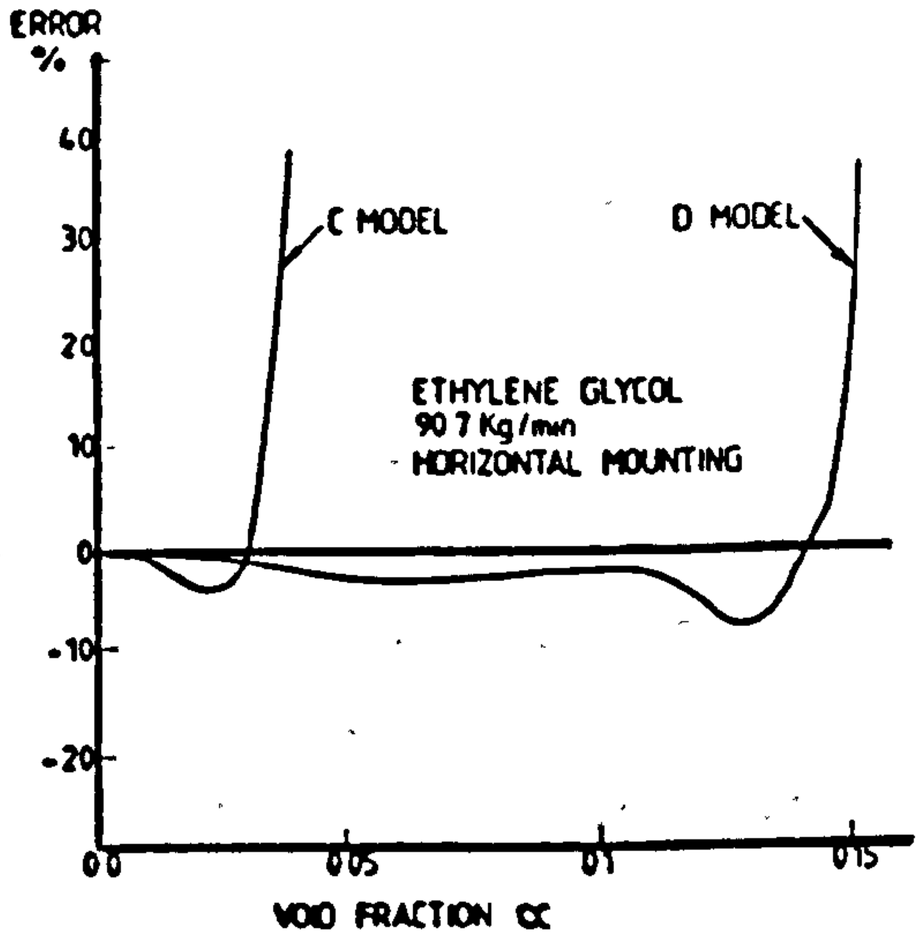

Figure 6.1 ERRORS DUE TO TWO-PHASE FLOW (from Grumski and Bajura [33])

The sudden appearance of large errors or break down at a critical void fraction is almost certainly related to a change in flow regime. Figure 6.2 illustrates the way flow regime in a U-tube can change as void fraction is increased [84]. The formation of large bubbles or of gas filled sections of the tube will of course greatly affect the vibration of the tube.

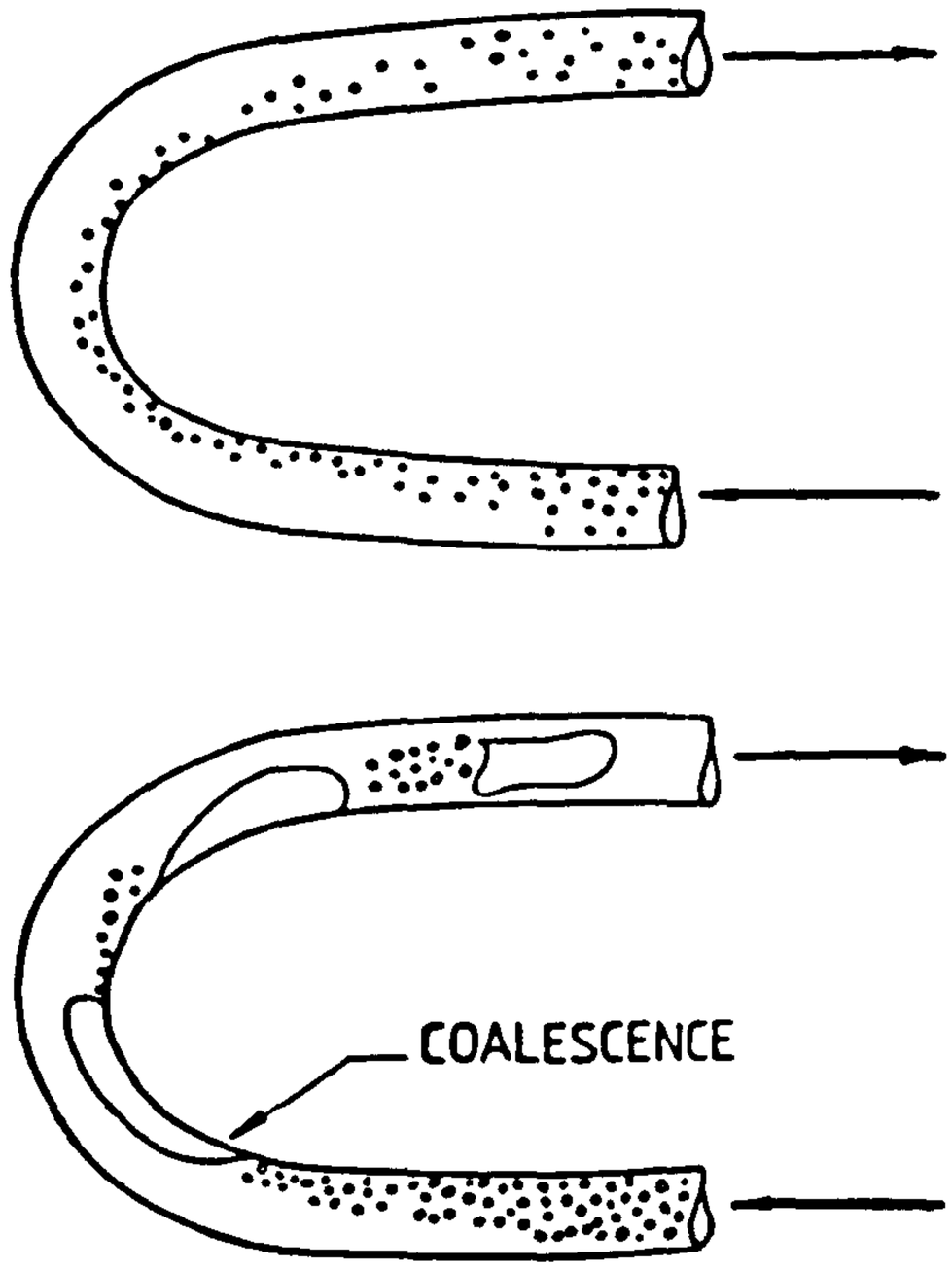

Figure 6.2 TWO-PHASE (WATER-AIR) FLOW IN 180° BEND.

The stability of the vibration of the tube can be affected differently by the two-phase mixtures according to the flow regimes. For instance, one can relate the effect of slug flow to the instability of a gun tube during multiple firing [85]. Due to the periodic changes in mass and therefore in the momentum of the system, slug flow introduces a parametric instability. This can occur at frequency ratios (f_{slug}/f_{system}) of approximately 1, 2, 2/3 ... [63].
In stratified flow regime considerable damping results due to the oscillation of the free surface of the liquid and sloshing of its mass [86]. Depending on the height of the liquid, the frequency of the tube and the amplitude of vibration the system may act as a dynamic vibration obsorber [87].

6.3 *EFFECTIVE MASS CONCEPT*

The tendancy of the Coriolis flowmeter to read low at small void fractions (below the critical level of void fraction) can probably be understood in terms of the simplified concept of effective mass of bubbles in a liquid.

The concept of effective mass is illustrated in Figure 6.3. Here a small sphere of material (density ρ_b) is situated at the centre of a large spherical container of fluid (density ρ_l). When the container is accelerated at a_c m/s^2 the sphere does not accelerate at the same rate but at another rate a_b related to a_c by

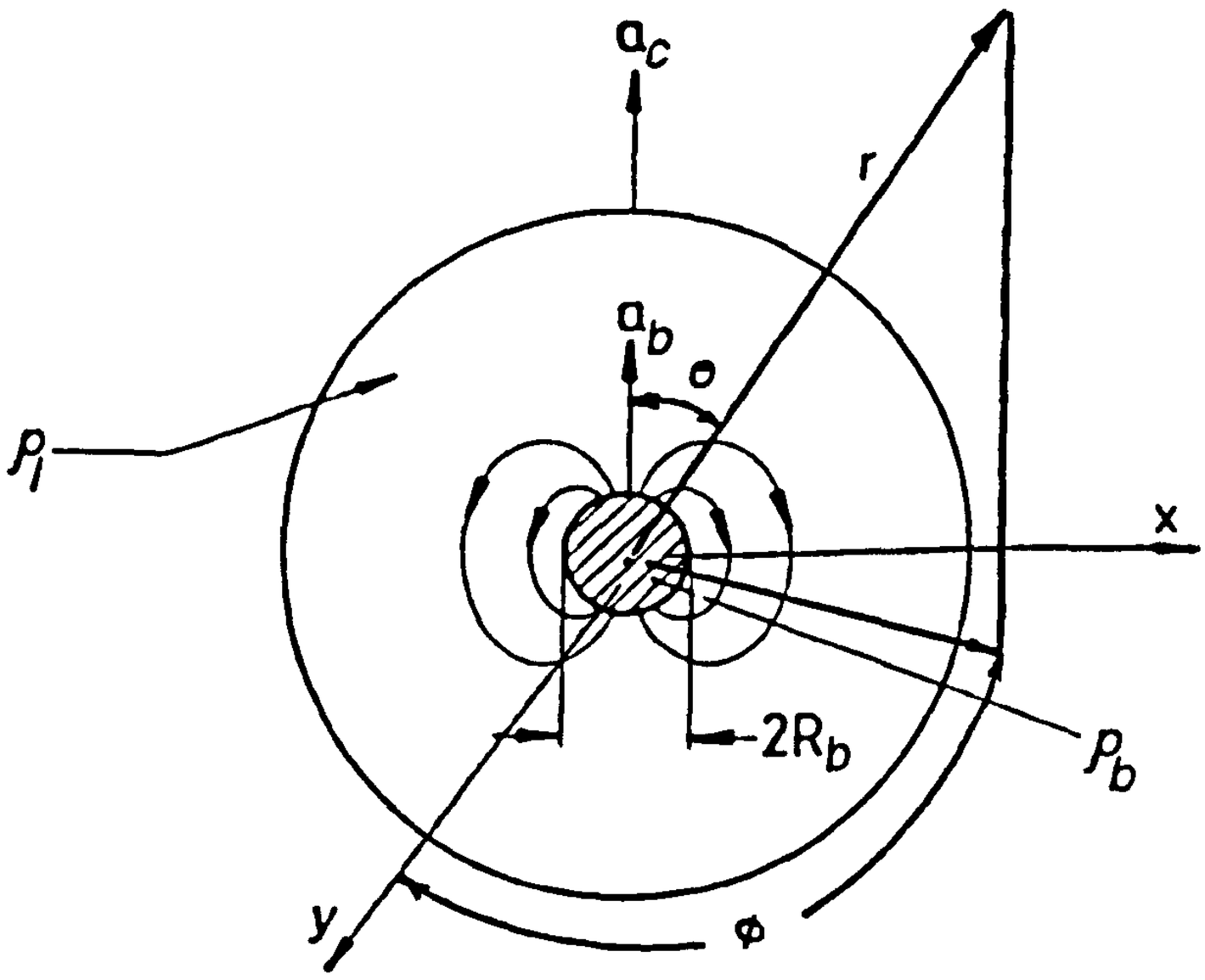

Figure 6.3 MOTION OF SMALL SPHERE IN A LIQUID FILLED CONTAINER.

$$a_b = \frac{3\,\rho_l}{\rho_l + 2\,\rho_b}\,a_c \qquad (6.1)$$

(see for example p36 of [88]). Only when $\rho_l = \rho_b$ are a_c and a_b the same, otherwise there is relative motion of the sphere in the container and a flow of fluid around the sphere. This causes the

inertia of the whole system to be lower than would be reckoned from the total mass. Equation (6.1) holds true under certain assumptions. The flow around the sphere must be small amplitude potential flow, there should be no pulsation or changing in shape of the sphere and finally, the sphere should be sufficiently far away from any surface so that interaction with the surface may be neglected.

Under the above assumptions and taking the sphere to be a fluid different from the surrounding fluid, the flow equations for both fluids can be written as follows. The pressures are

$$P_l = \rho_l \, (\partial \Phi_l / \partial t) \qquad (6.2)$$

and

$$P_b = \rho_b \, (\partial \Phi_b / \partial t) \qquad (6.3)$$

where the velocity potential Φ satisfies Laplace's equation

$$\nabla^2 \Phi = 0 \qquad (6.4)$$

and velocity at any point is

$$\underline{V} = - \nabla \Phi \qquad (6.5)$$

Let P_l and P_b be spherical harmonic functions as follows

$$P_l = (ar + br^{-2}) \cos\theta \qquad (6.6)$$

$$P_b = cr \cos\theta \qquad (6.7)$$

where a, b and c are constants and r,θ are spherical co-ordinates (Figure 6.3). The boundary conditions at $r=R_l$ and $r=R_b$ are as follows. At $r=R_l$ the radial velocity component of the fluid equals the radial velocity of the container, ie

$$(\underline{V}_l)_r = V_c \cos\theta \quad \text{or} \quad -(\partial \Phi / \partial r)_{r=R_l} = V_c \cos\theta \qquad (6.8)$$

so $- \{\partial(\partial\Phi/\partial t)/\partial r\}_{r=R} = \partial V_c/\partial t \cos\theta$ (6.9)

from equation (6.2)

$$(\partial P_1/\partial r)_{r=R_1} = \rho_1\{\partial(\partial\Phi/\partial t)/\partial r\}_{r=R_1} = -\rho_1(\partial V_c/\partial t)\cos\theta \quad (6.10)$$

differentianting equation (6.6) with respect to r and equating the result with equation (6.10) gives

$$a - 2b\, R_1^{-3} = -\rho_1 (\partial V_c/\partial t) \quad (6.11)$$

At $r=R_b$ the pressure and the radial velocity components are continuous. Thus

$$(P_1)_{r=R_b} = (P_b)_{r=R_b} \quad (6.12)$$

gives

$$aR_b + bR_b^{-2} = cR_b \quad (6.13)$$

and

$$(V_1)_r = (V_b)_r \quad (6.14)$$

gives

$$(\partial\Phi_1/\partial r)_{r=R_b} = (\partial\Phi_b/\partial r)_{r=R_b} \quad \text{and}$$

$$\{\partial(\partial\Phi_1/\partial t)/\partial r\}_{r=R_b} = \{\partial(\partial\Phi_b/\partial t)/\partial r\}_{r=R_b} \quad (6.15)$$

Substituting equations (6.2) and (6.3) in the equation (6.15) gives

$$a - 2b\, R_b^{-3} = (\rho_1/\rho_b)\, c \quad (6.16)$$

Solving the equations (6.11), (6.13) and (6.16) simultaneously and then substituting for a, b and c in the (6.6) and (6.7) gives

$$P_1 = \left(-\frac{x}{x + 2R_1^{-3}} r + \frac{1}{x + 2R_1^{-3}} r^{-2} \right) \rho_1 (\partial V_c/\partial t) \cos\theta \quad (6.17)$$

and

$$P_b = -\left(\left(\frac{x}{x + 2R_1^{-3}} + \frac{2R_b^{-3}}{x + 2R_1^{-3}}\right) r\right) \rho_b \, (\partial V_c/\partial t) \cos\theta \qquad (6.18)$$

where $$x = \left(\frac{\rho_1 + 2\rho_b}{\rho_1 - \rho_b}\right) R_b^{-3}$$

The inertia force F_I due to material within the container can be expressed as an integral of P_1 over internal surface area of the container as follows

$$F_I = -2 \int_0^{\pi} \int_0^{\pi} (P_1)_{r=R_1} R_1^2 \cos\theta \sin\theta \, d\theta d\phi \qquad (6.19)$$

where r,θ and φ are the spherical co-ordinates. Equation (6.19) gives

$$F_I = -\frac{4}{3} \pi R_1^2 \rho_1 \left(-\frac{R_1 x}{x + 2R_1^{-3}} + \frac{R_1^{-2}}{x + 2R_1^{-3}}\right) \partial V_c/\partial t \qquad (6.20)$$

On the other hand the inertia force equals the effective mass times the acceleration, therefore from (6.20) , the effective mass is

$$M_{eff} = \frac{4}{3} \pi R_1^3 \rho_1 \left(\frac{x}{x + 2R_1^{-3}}\right) - \frac{4}{3} \pi \rho_1 \left(\frac{1}{x + 2R_1^{-3}}\right) \qquad (6.21)$$

but the actual mass of the material within the container is

$$M_{act} = \frac{4}{3} \pi (R_1^3 - R_b^3) \rho_1 + \frac{4}{3} \pi R_b^3 \rho_b \qquad (6.22)$$

The difference between M_{eff} and M_{act} gives the reduction in the mass of the system due to a single small sphere, as follows

$$\Delta M = M_{eff} - M_{act} = \frac{4}{3} \pi R_b^3 \left(\rho_1 - 3\rho_1 \frac{\rho_1 - \rho_b}{\rho_1 + 2\rho_b} - \rho_b\right) \qquad (6.23)$$

where $R_l \gg R_b$. In other words, the effective mass of the sphere is reduced from $^4/_3 \pi R_b^3 \rho_b$ by the amount

$$\frac{4}{3} \pi R_b^3 \, 2 \frac{(\rho_l - \rho_b)^2}{\rho_l + 2\rho_b} \tag{6.24}$$

For a gas bubble in a liquid $\rho_b \ll \rho_l$, (6.24) becomes twice the mass of the liquid displaced by the sphere. For many small gas bubbles separated by distances large compared with their diameter the percentage reduction in mass is therefore

$$\frac{2\alpha}{1 - \alpha} \times 100\% \tag{6.25}$$

where α is the void fraction

$$\alpha = \frac{\text{VOLUME OF GAS}}{\text{VOLUME OF MIXTURE}} = N \frac{4}{3} \pi R_b^3$$

where N is number of gas bubbles per unit volume. The percentage reduction in the mass (equation (6.25)) is plotted against void fraction in Figure 6.4.

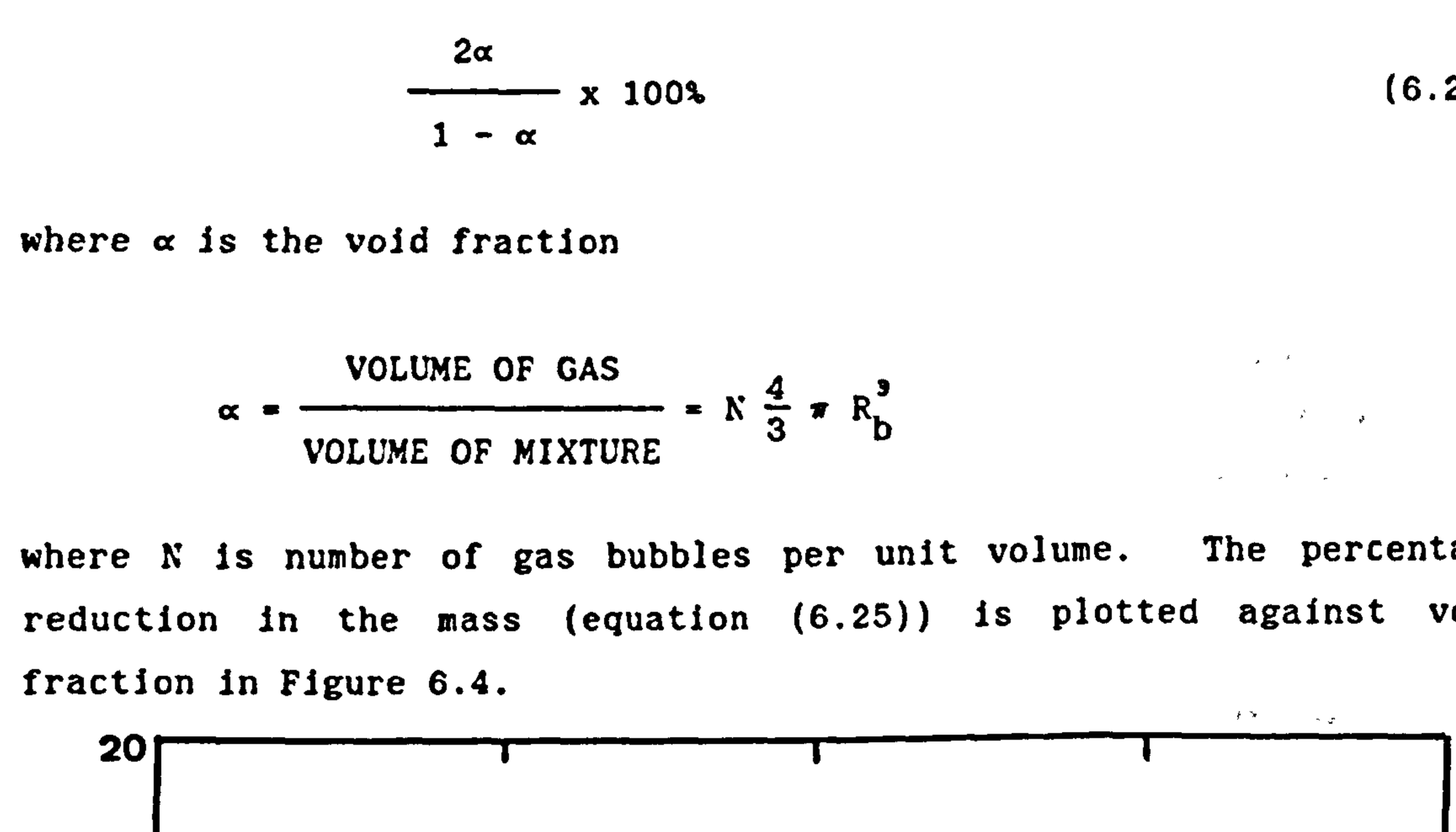

Figure 6.4 PERCENTAGE REDUCTION IN THE MASS VERSUS VOID FRACTION.

6.4 TWO-PHASE (WATER-NITROGEN) FLOW EXPERIMENTS

The major objective of the experimental study was to assess the performance of the straight-tube experimental flowmeter in measuring two-phase (liquid-gas) mixtures (the experiments were restricted to bubbly flow regimes). The other objective was to reproduce the negative error effect (Figure 6.1). Measurements were taken of time delays Δt, frequencies f and amplitudes Amp of the vibration for various water and nitrogen flowrates.

6.4.1 Flow Rig and Instrumentation

The single-phase flow rig (illustrated in section 5.2.3) was used with some modifiction (second piping arrangement was used). Nitrogen was injected to the test section at 35D from the inlet of the flowmeter as shown in Figure 6.5. A fine screen (with 0.3mm diameter holes) was used in order to produce very small nitrogen bubbles. The nitrogen injection nozzle used is illustrated in Figure 6.6.

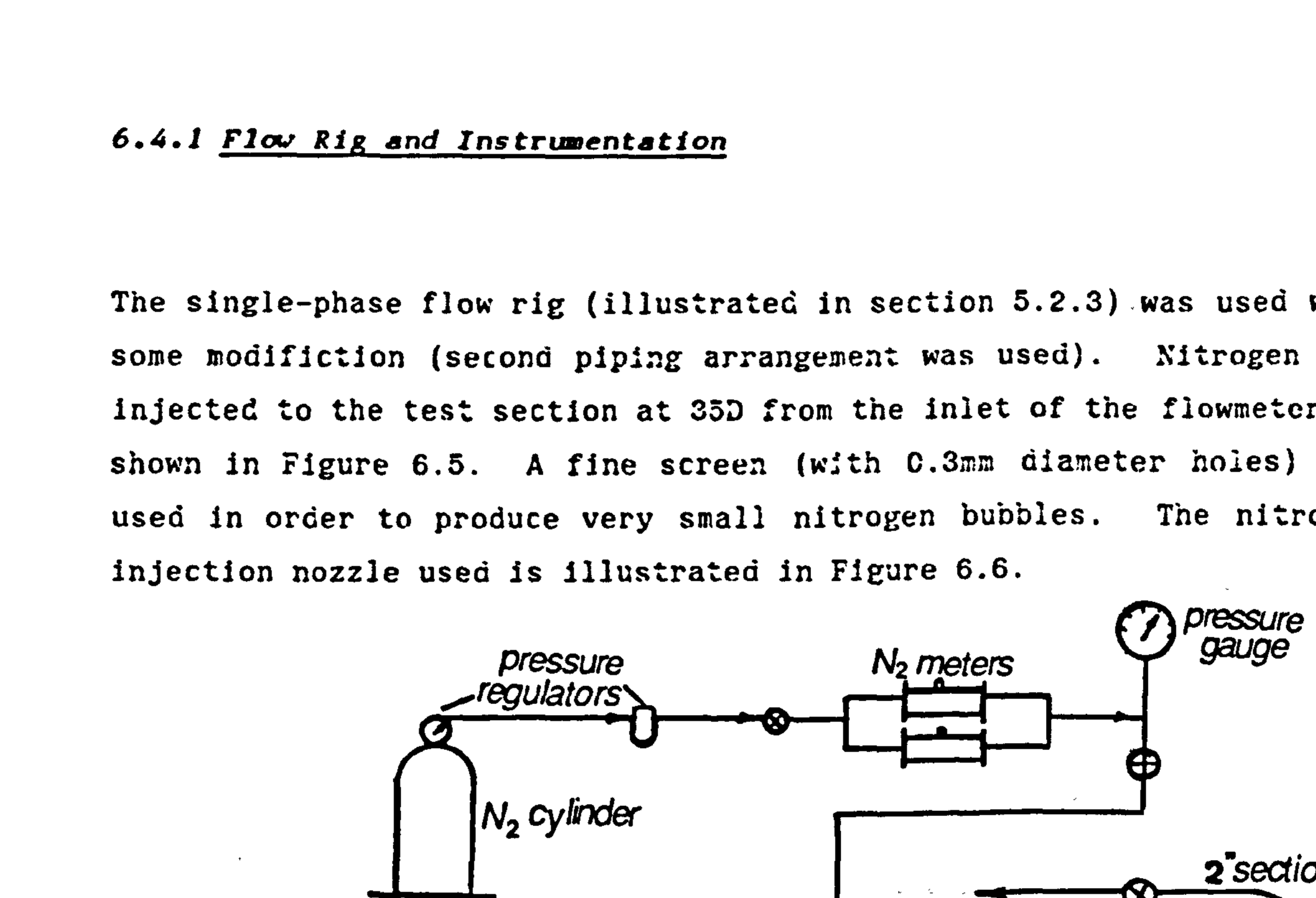

Figure 6.5 TWO-PHASE (WATER-NITROGEN) FLOW RIG.

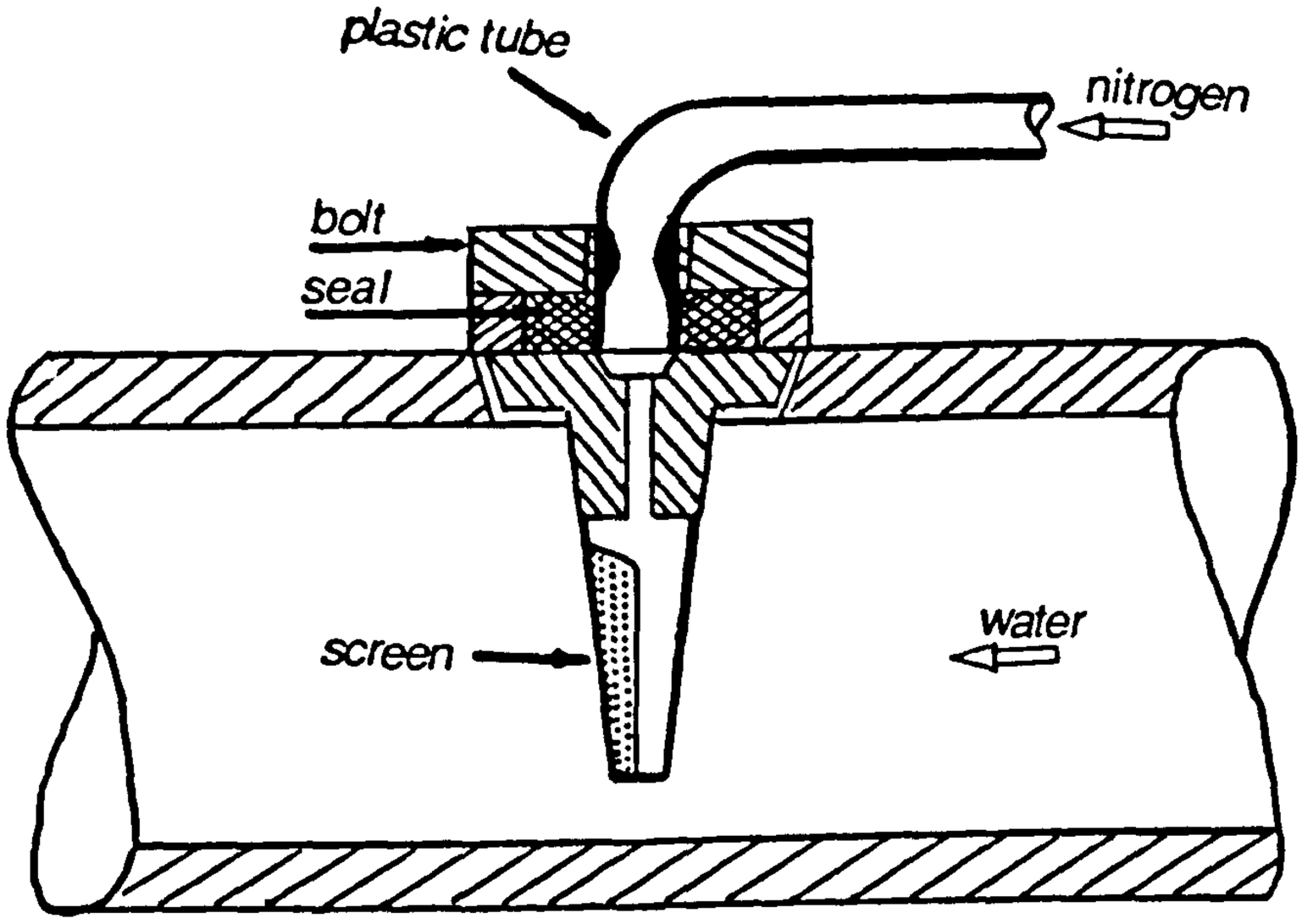

Figuire 6.6 NITROGEN INJECTION NOZZLE.

Nitrogen flowrate was controlled using two pressure regulators and an upstream valve. Two pelton wheel flowmeters (PWG7 and PWG2/EPI with different flow ranges) were used to measure nitrogen flowrates. Their calibration lines are shown in Figure 6.7 (calibration is done by Quadrian Ltd. using air as a calibration fluid, the accuracy of the meters in situ is ∓1.4% and ∓1% respectively). Nitrogen pressure and water line pressure were monitored using standard barometers, whilst the water flowrate was measured using a KDG 25458/83 turbine flowmeter.

The flow regime visualization was observed at the entrance and exit of the flowmeter using a high speed camera.

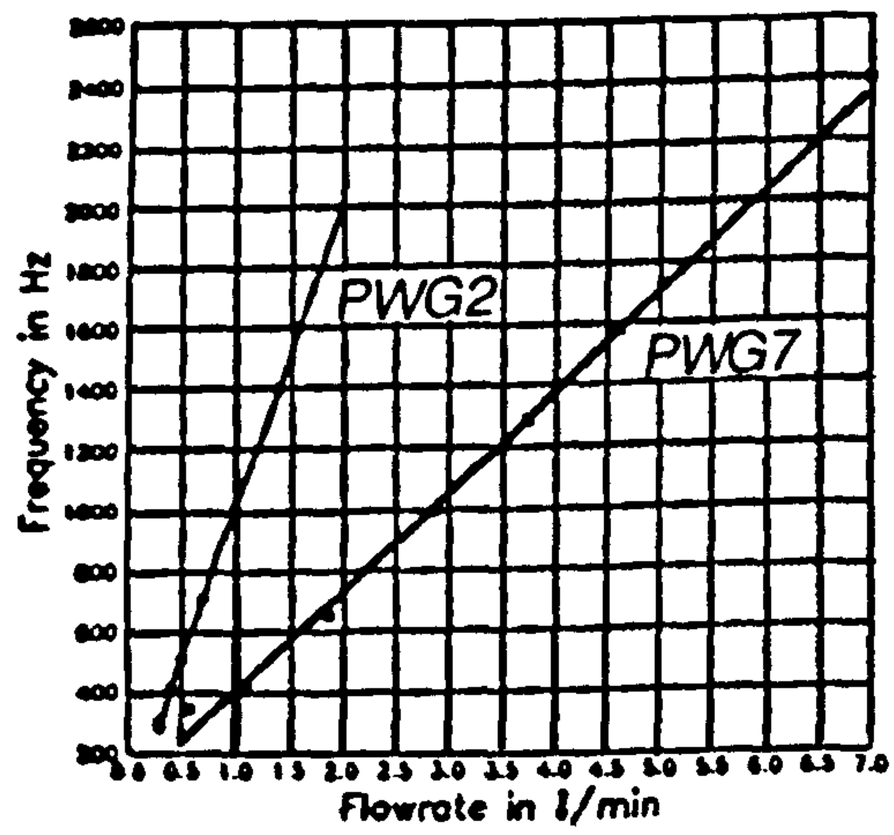

Figure 6.7 CALIBRATION LINES OF PELTON WHEEL FLOWMETERS.

6.4.2 *Calculation of the Test Variables*

To determine the volume which the nitrogen would occupy in the water line, it was assumed that the nitrogen was a perfect gas and that on entering the water line it would obey the law of adiabatic expansion.

$$PV^{\gamma} = \text{constant} \qquad (6.26)$$

where P is the absolute pressure of the gas
V is the volume of the gas
γ is the ratio of the two specific heats

The flowrate of the nitrogen in the water line was therefore calculated as follows

$$Q_L = Q_N \times (P_N/P_L)^{1/1.4} \qquad (6.27)$$

where Q_N and Q_L, P_N and P_L are flowrates and pressures of nitrogen before and after the injection respectively.

The percentage of nitrogen flowing in the water/nitrogen mixture and the percentage error in mass flowrate were then calculated respectively for each test point as follows

$$\%N_2 = \frac{Q_L}{Q_W} \times 100 \qquad (6.28)$$

and

$$\%\Sigma = \frac{\Delta t_M - \Delta t_W}{\Delta t_W} \times 100 \qquad (6.29)$$

where Δt_M and Δt_W are the time delays in measuring water/nitrogen mixture and pure water respectively at same mass flowrate. Finaily, the percentage reduction in the amplitude of vibration and percentage

increase in the frequency are as follows

$$\%Amp = \frac{Amp_M - Amp_W}{Amp_W} \times 100 \qquad (6.30)$$

$$\%f = \frac{f_M - f_W}{f_W} \times 100 \qquad (6.31)$$

where Q_W is water flowrate and the subscripts M and W denote for two-phase mixture and water respectively.

6.5 *RESULTS AND DISCUSSIONS*

In order to verify the effective mass concept (section 6.3) one aim of the experiments was to obtain homogeneous bubbly flows with small bubbles far away from their neighbours and the tube walls. This is achieved only at low percentage nitrogen and high water flowrates (eg. $\%N_2$≈1-10 and Q_W≈182 Kg/min) as can be seen in Figure 6.10.

In most cases the flow is in the bubbly regime, though at some low water flowrates there is a transition to stratified flow as the nitrogen flowrate was increased. However, the flow patterns are mostly as follows. Bubbles are dispersed homogeneously at the entrance of the flowmeter whilst they move upwards (and coalesce at certain nitrogen flowrates) due to gravity as they move along the tube. This non-uniform flow pattern probably introduces a differential damping into the system and leads to a reduction in the amplitude of the vibration. Figures 6.8, 6.9 and 6.10 illustrate the range of flow patterns at the the entrance and exit of the flowmeter for different water flowrates and percentages of nitrogen. Figure(6.11a) indicates the effect of $\%N_2$ on the detector output signals for 125.3 Kg/min water flowrate. At $\%N_2$>%60 the flow regime was stratified, introducing almost total damping to the system. The percentage reduction in the amplitude of the vibration for same water flowrate is plotted against $\%N_2$ in Figure 6.11b.

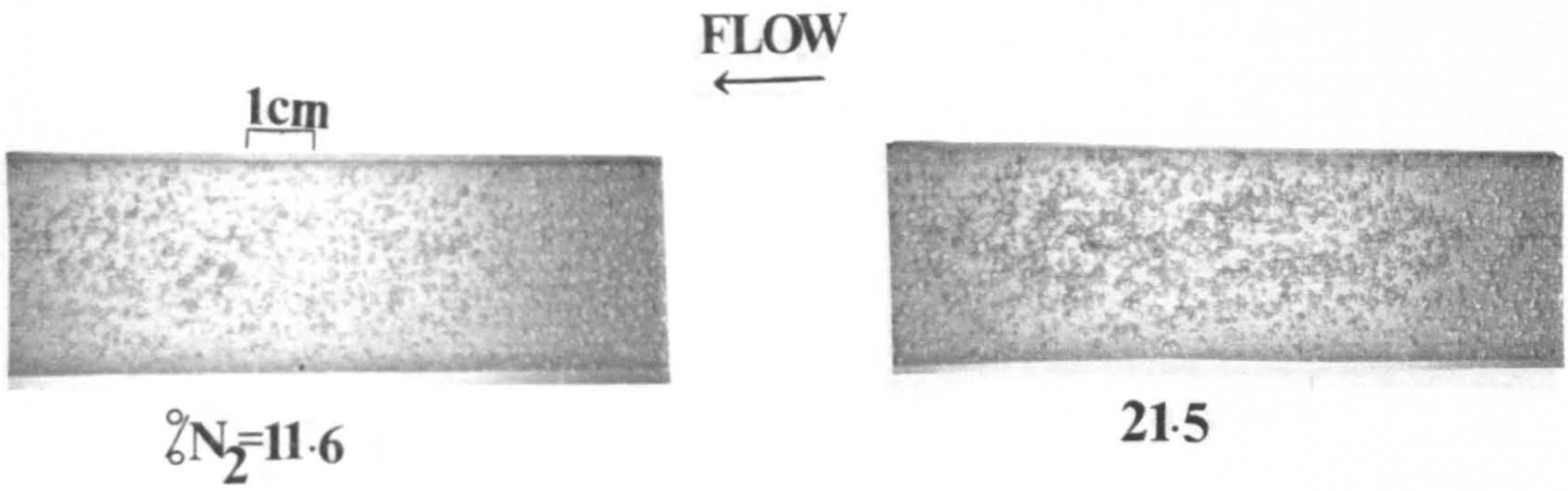

Figure 6.8 FLOW PATTERNS AT THE ENTRANCE AND EXIT OF THE FLOWMETER.

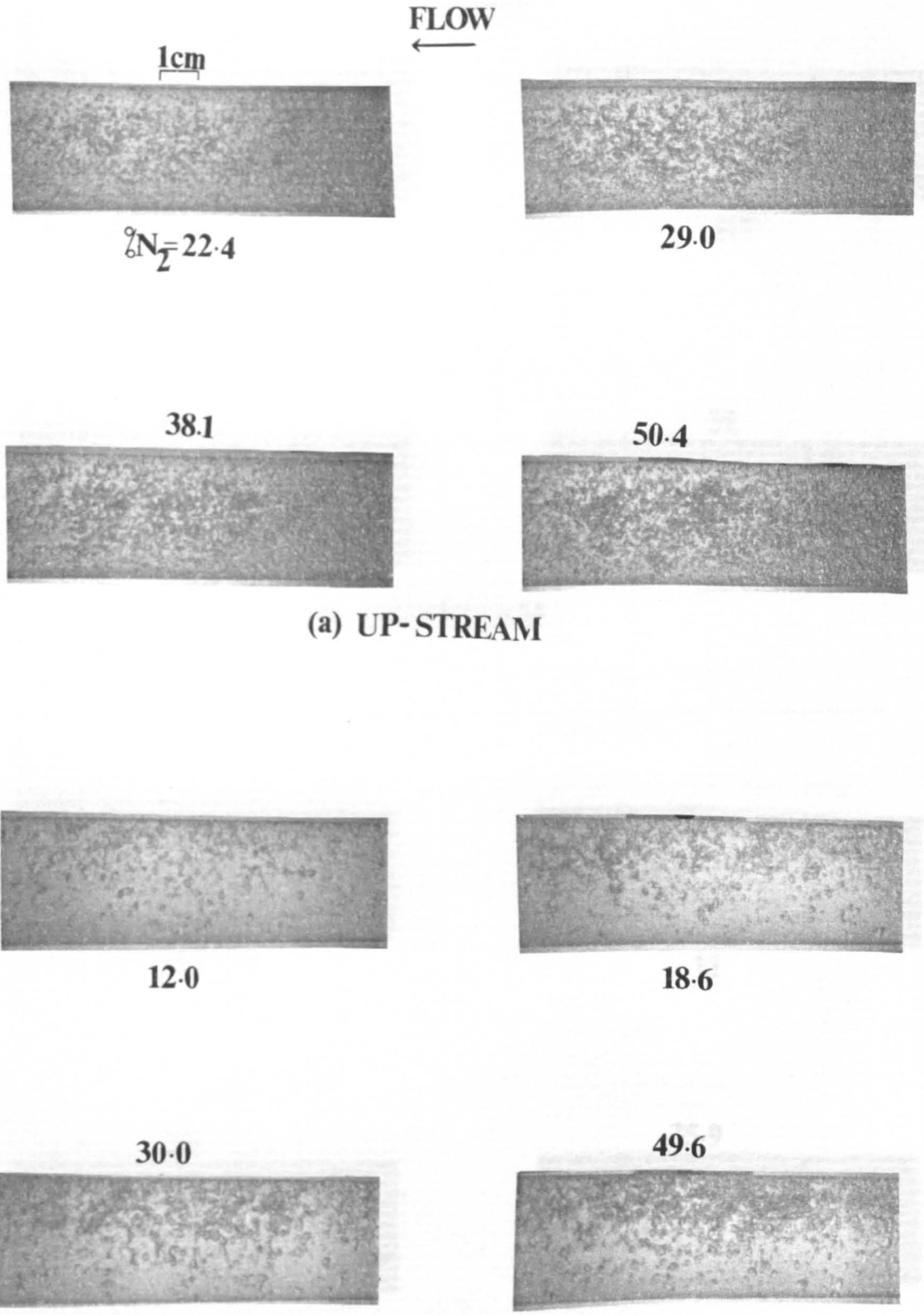

Figure 6.9 FLOW PATTERNS AT THE ENTRANCE AND EXIT OF THE FLOWMETER.

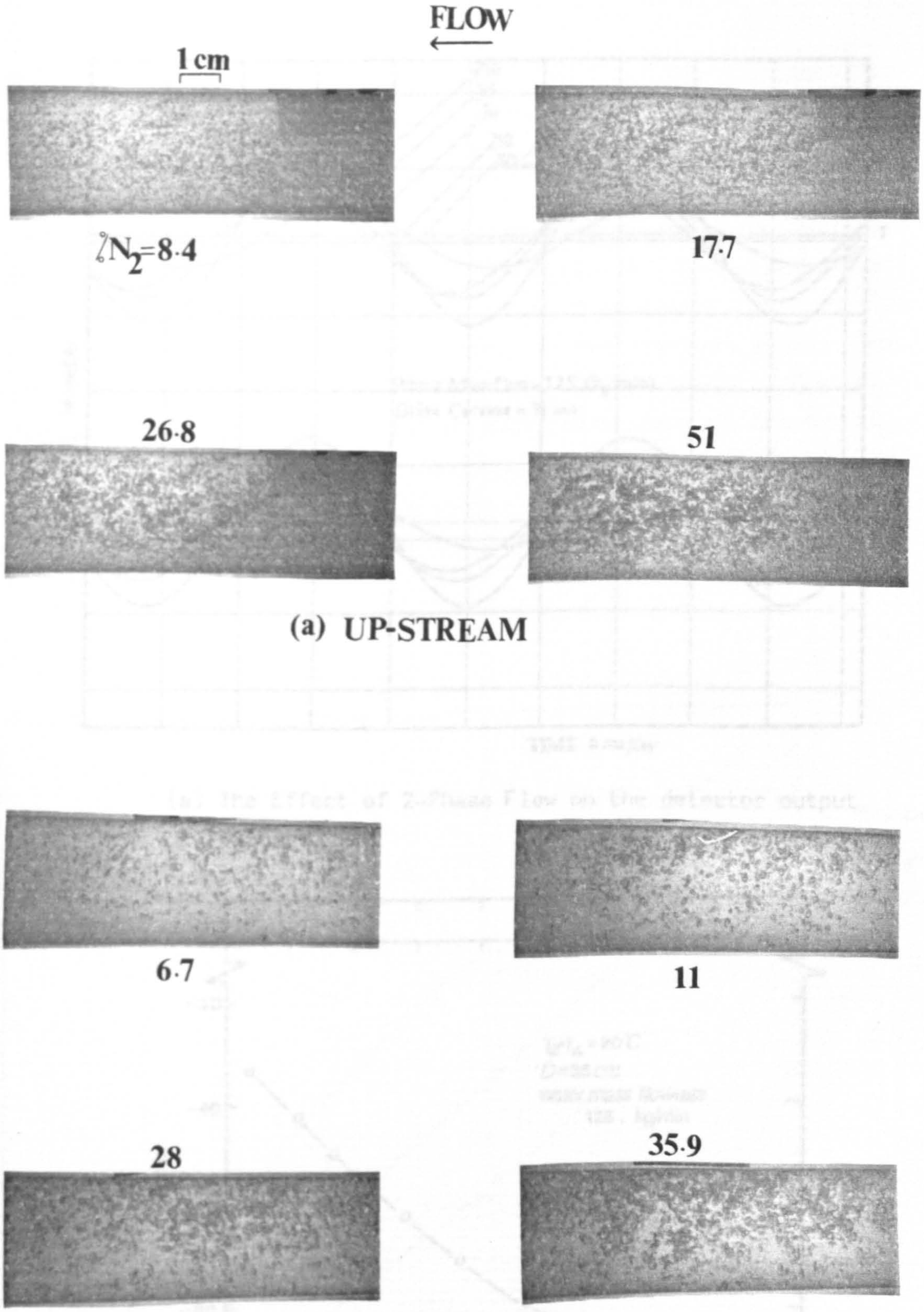

Figure 6.10 FLOW PATTERNS AT THE ENTRANCE AND EXIT OF THE FLOWMETER

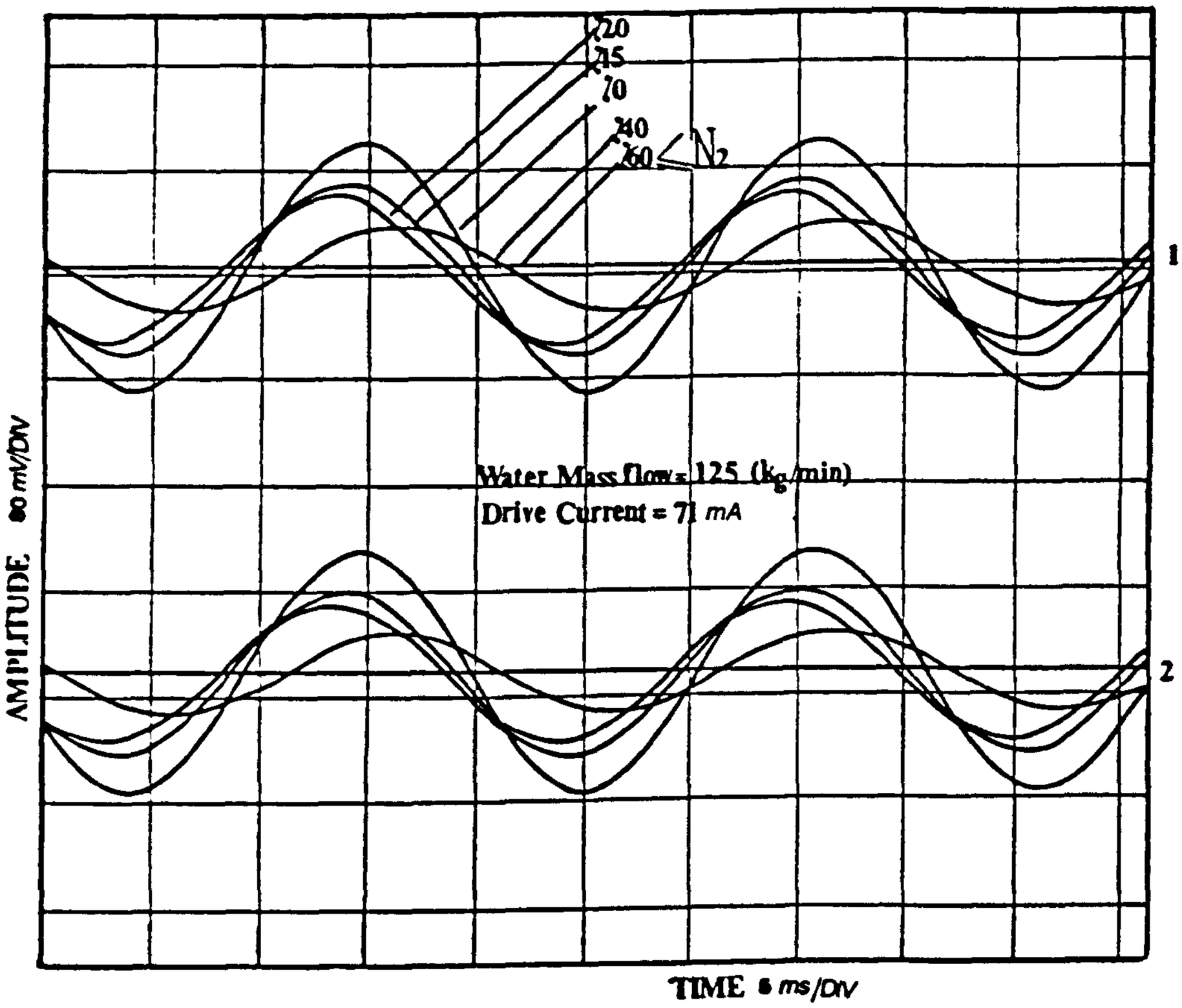

(a) The Effect of 2-Phase Flow on the detector output Signal.

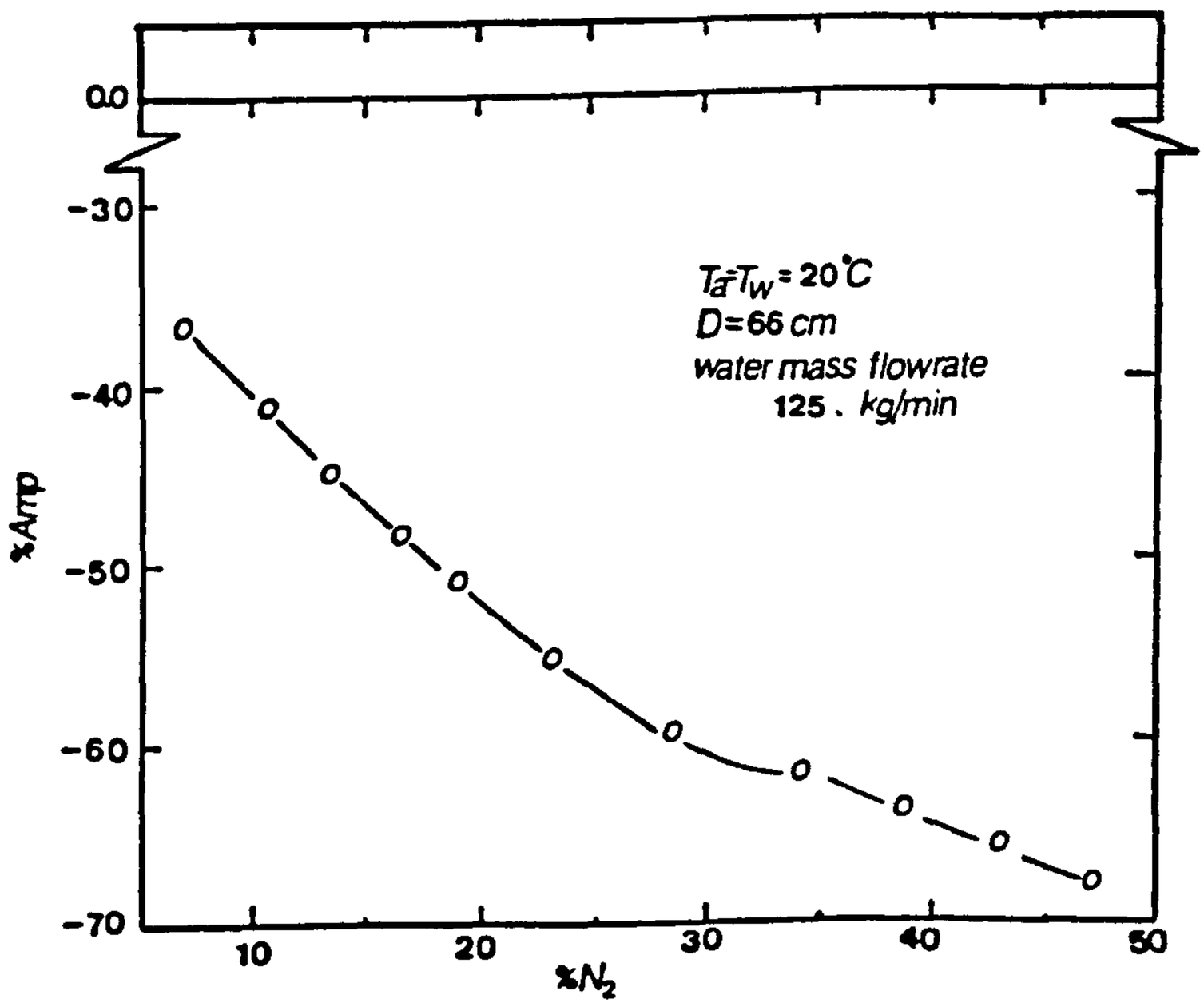

(b) Percentage Decrease in Amplitude Versus Percentage N_2 in Water.

Figure 6.11 THE EFFECT OF TWO-PHASE FLOW ON THE AMPLITUDE OF VIBRATION.

Figure 6.12 illustrates the effect of $\%N_2$ on the tube frequency for three water flowrates. Obviously, the increase in the frequency is due to the reduction in the inertia of the system.

The percentage error in the reading of the mass flowrate is shown in Figure 6.13 in terms of time delays. In Figure 6.13a the percentage error is plotted against $\%N_2$ for three water flowrates. Figure 6.13b illustrates the effect of drive current on the observed error. By increasing the drive current the percentage error decreases. This may be because vibration of tube at higher amplitudes leads to decrease in the effective mass influence (bubbles will move with liquid). However, the negative errors are probably due to a combination of the effective mass and the differential damping.

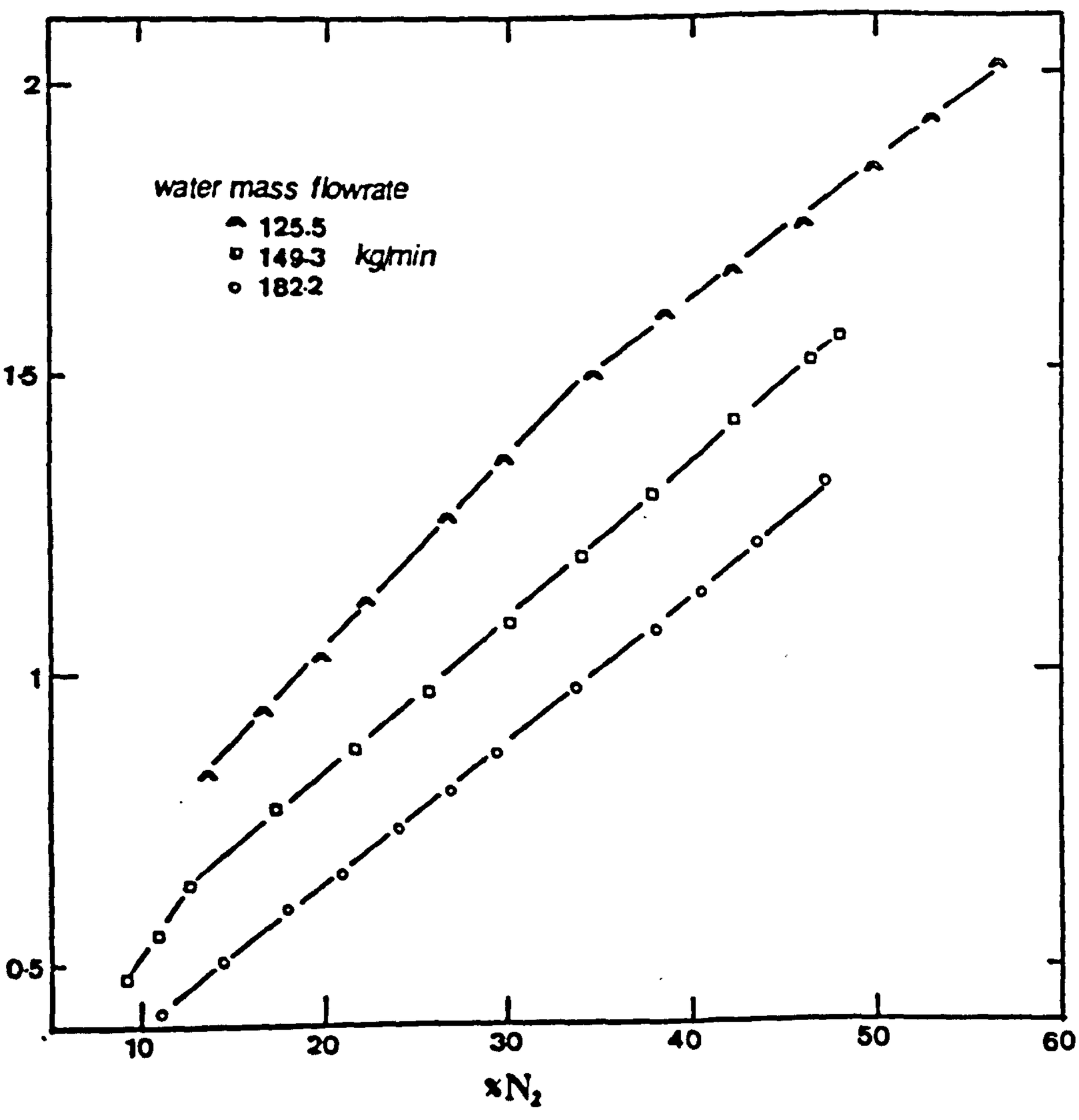

Figure 6.12 THE EFFECT OF TWO-PHASE FLOW ON TUBE FREQUENCY.

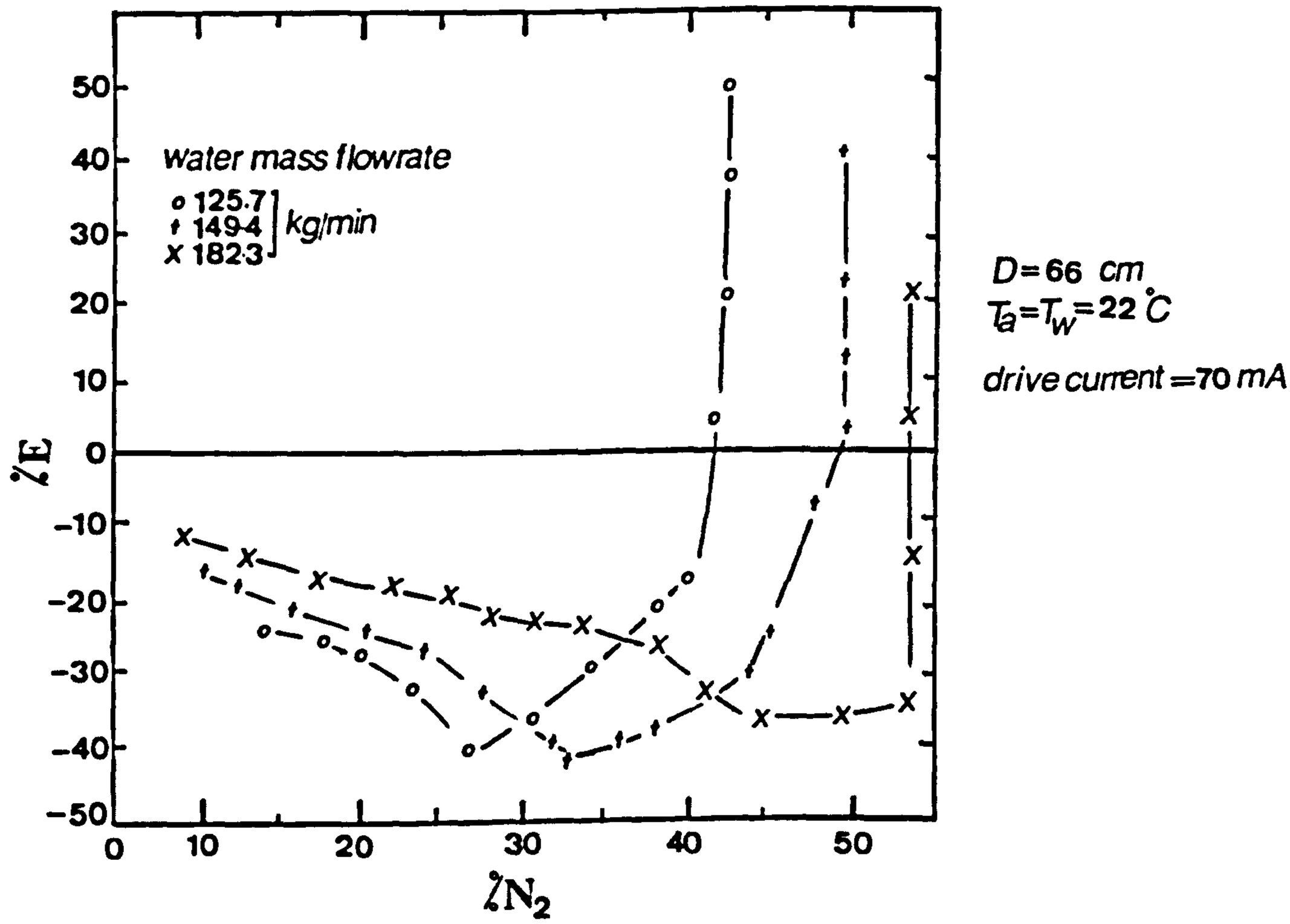

(a) Error Versus Percentage N_2 in Water for Three Water Flowrates.

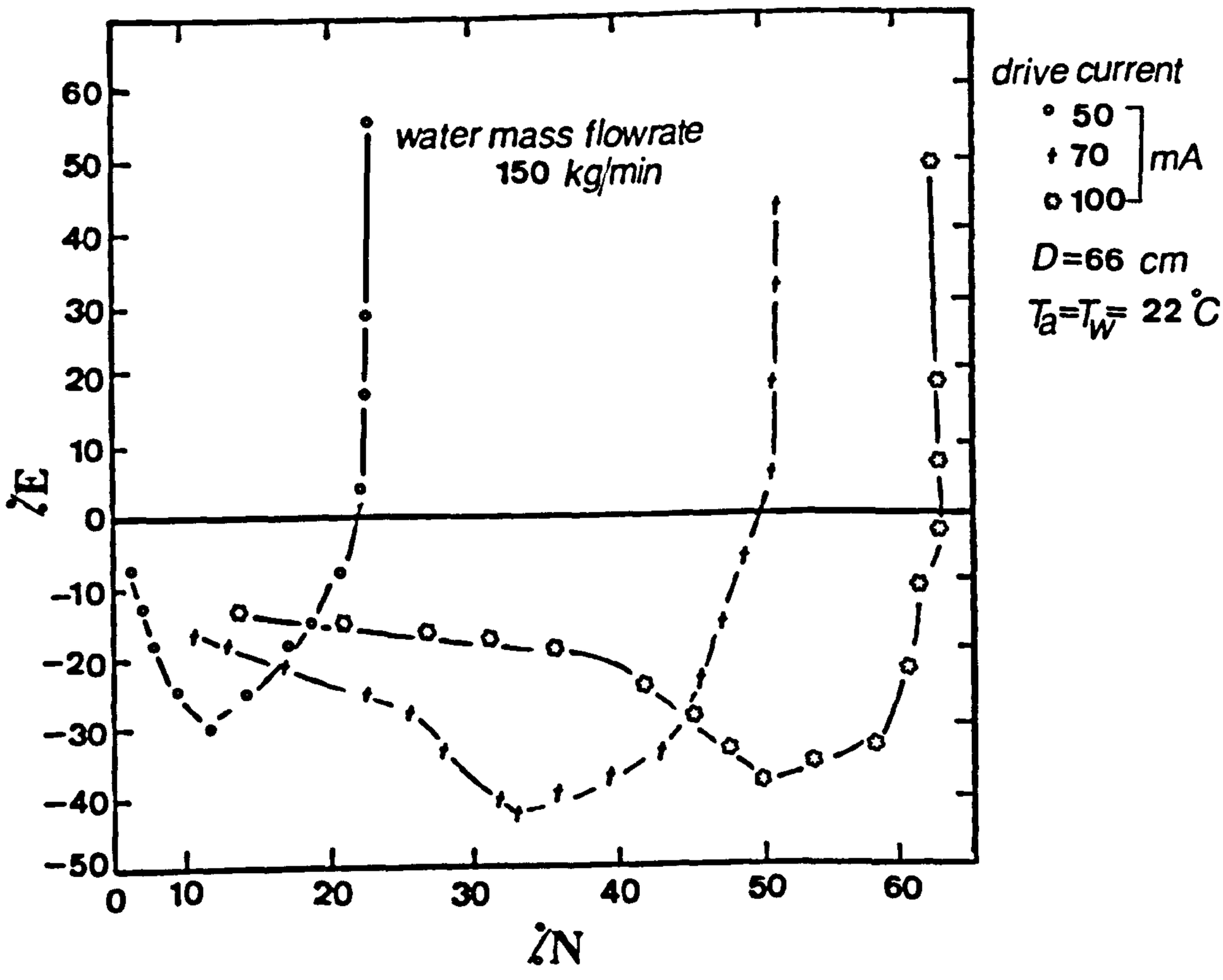

(b) Error Versus Percentage N_2 in Water for Three Drive Currents.

Figure 6.13 ERRORS DUE TO TWO-PHASE FLOW.

CHAPTER SEVEN

COMPARISON BETWEEN THEORETICAL AND EXPERIMENTAL RESULTS

CHAPTER SEVEN

COMPARISON BETWEEN THEORETICAL AND EXPERIMENTAL RESULTS

In this chapter frequency and time delay predictions for both commercial and experimental flowmeters are compared with experimental results. The predicted values of optimum measuring positions and the effect of gas bubbles are also compared with corresponding experimental data.

7.1 COMMERCIAL FLOWMETER

7.1.1 Single-Phase Flow

A commercial flowmeter of U-tube configuration incorporating four brace bars and added mass was modelled. The dimensions of one half of the (double tube) flowmeter are shown in Figure 7.1. Predictions of frequencies and time delays were calculated by the methods described in chapters 2 and 3 along with the values of the constants summarized in Table 7.1 (the dimensional parameters were converted to non-dimensional ones using equations (2.23) and (3.7). These were then entered into the computer programme "appendix C" using new boundary condition equations for U-tube configuration incorporating brace bars "appendix D" and added mass "appendix E" in order to obtain non-dimensional and then dimensional tube frequency and time delays).

Due to the complexity of the added mass construction (masses of the drive and detectors in the commercial flowmeter) an equivalent added mass, placed at the middle of the circular length of the U-tube was employed and set at M_{eq}=0.45 kg.This value was obtained by finding the quauntity of the added mass for which the mathematical model gave the

measured result for the fundamental natural frequency of the empty tube (101 Hz). This equivalent added mass was not chosen so as to obtain agreement between the experimental and theoretical data in Figure 7.2. It was based *solely* on the observed fundamental frequency of the empty tube

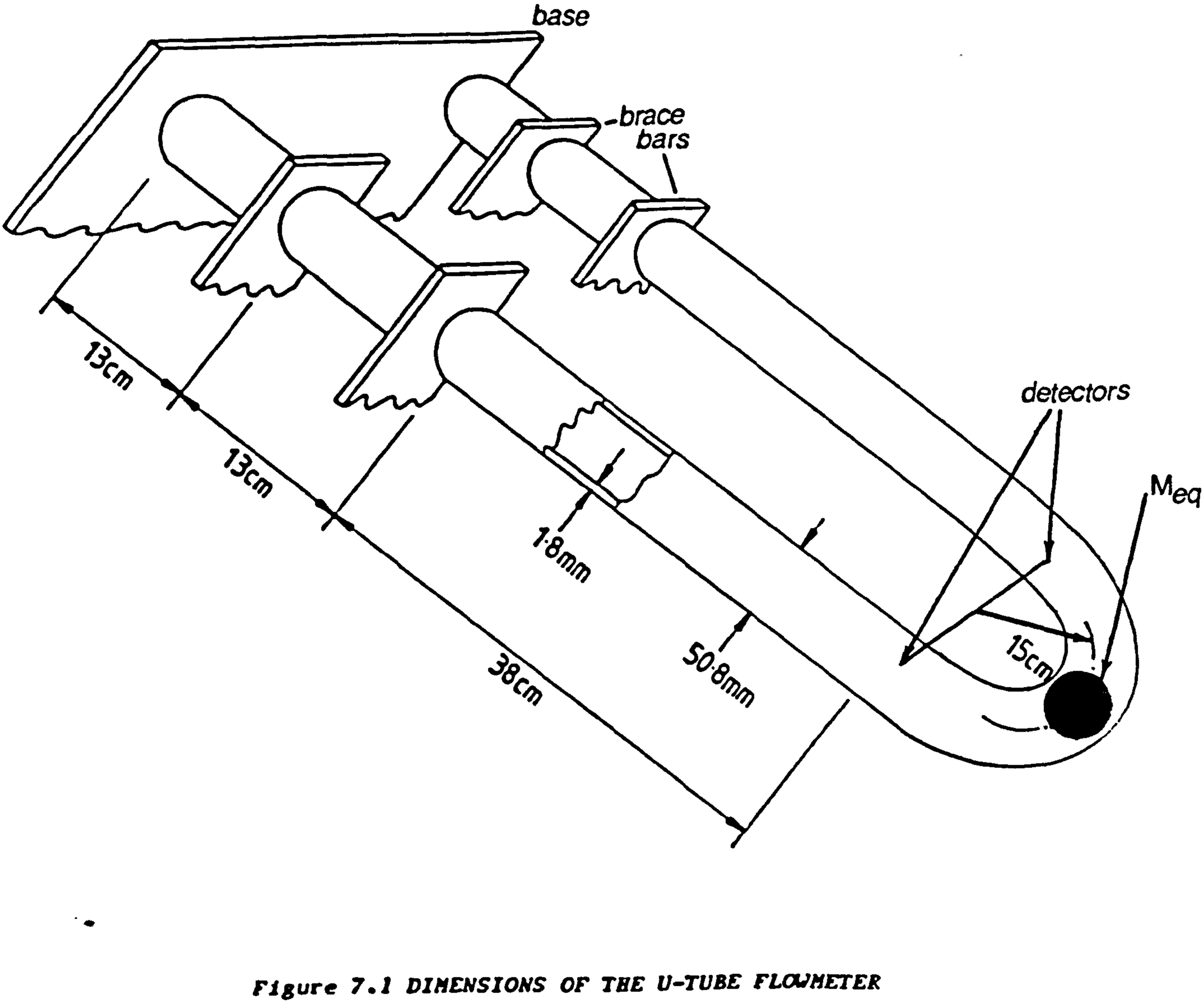

Figure 7.1 DIMENSIONS OF THE U-TUBE FLOWMETER

On this basis the comparison between experimental data and numerical results works out as shown in Figure 7.2. Note that the measured velocity is the mean velocity calculated from the measured flowrate and tube diameter.

PARAMETER		UNIT	VALUE
Fluid Velocity	(U)	m/s	0-10
Fluid Density	(ρ_f)	kg/m^3	1000(water) 780(kerosene)
Tube Density	(ρ_t)	kg/m^3	8027(316L SS)
Young's Modulus	(E_t)	GN/m^2	208
Shear Modulus	(G_t)	GN/m^2	80
O.D of Tube	(d_o)	mm	50.8
Tube Thickness	(t)	mm	1.8
Radius of circular Tube Length	(a_1)	cm	15
Straight Tube Lengths	(b_1=b_6)	cm	13
	(b_2=b_5)	cm	13
	(b_3=b_4)	cm	38
Stiffness Constants of Brace Bars*	(K_1)	GN/m	2.18
	(K_2)	KN.m	1.27
	(K_3)	KN.m	87.7
Equivalent Added Mass	(M_{eq})	kg	0.45

**The values of the stiffness constants of the brace bars, in this table, were obtained by using the numerical method described in chapter 3 and assumed equal for all braces.*

Table 7.1 THE VALUES OF THE CONSTANTS USED IN MODELLING THE COMMERCIAL MASS FLOWMETER

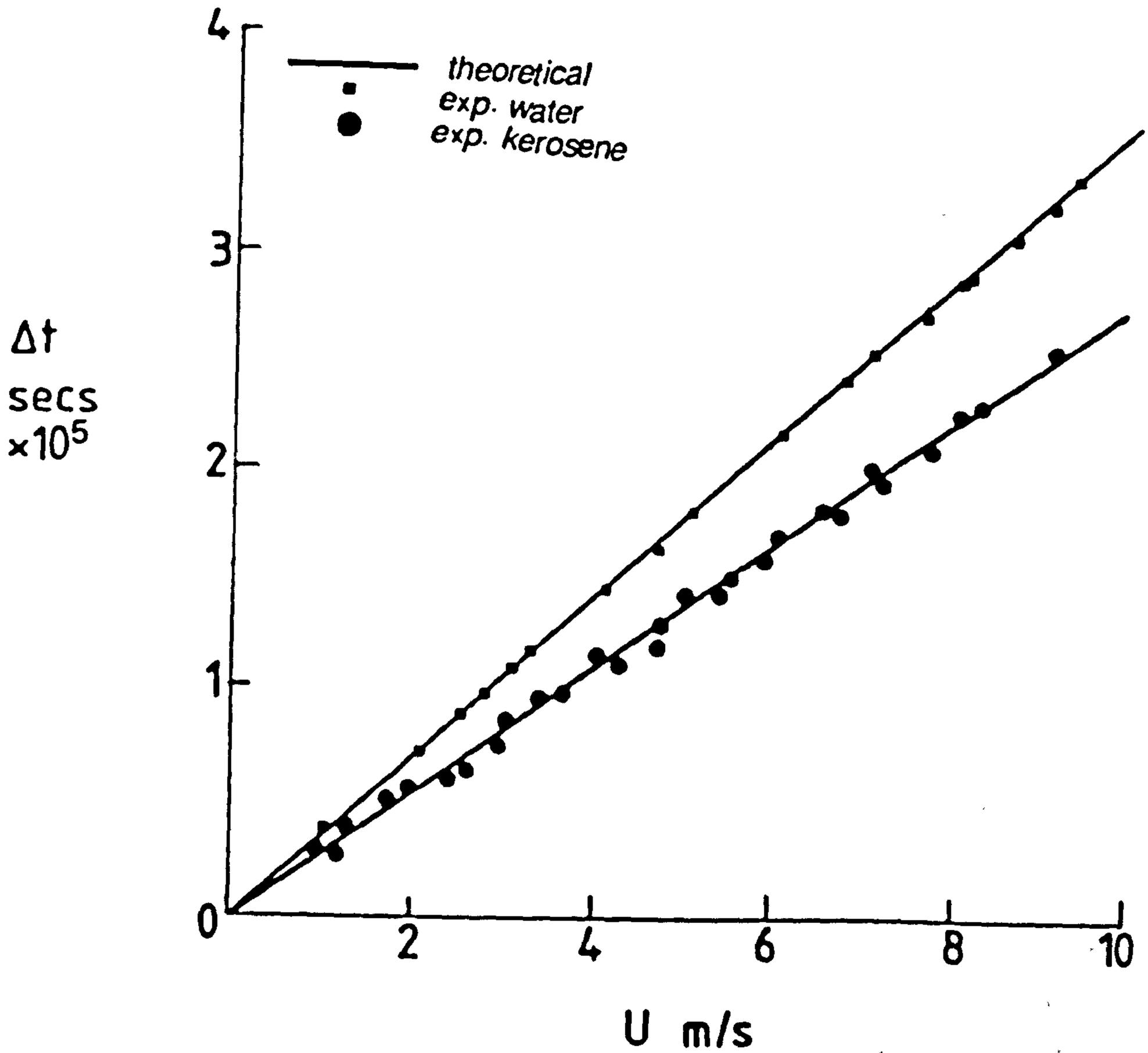

Figure 7.2 COMPARISON OF THEORETICAL AND EXPERIMENTAL CALIBRATION CHARACTERISTICS FOR THE U-TUBE FLOWMETER

At low fluid velocities the frequency variation (due to flow) is extremely small (see Figure 2.14) and as this was the region in which the experiments were performed it was not possible to confirm the effect of fluid velocity on tube frequency. The small frequency variation that were observed during the experiments was seemed to be due to fluid temperature variation affecting the Young's and shear moduli [78]. This was confirmed theoretically as shown in Table 7.2 using data on the temperature variation of the moduli.

WATER TEMPERATURE °C	OBSERVED FREQUENCY Hz	PREDICTED* FREQUENCY Hz
15	72.49	72.36
20	72.45	72.31
25	72.39	72.26

** Predicted values of tube frequency are not identical to observed ones because M_{eq} set at 0.45 Kg which gives an approximate value of empty tube frequency (eg. measured frequency is 101 Hz and predicted frequency is 100.86 Hz).*

Table 7.2 FREQUENCY VARIATION DUE TO WATER TEMPERATURE

In the time delay comparison (Figure 7.2) agreement is reasonable; the maximum difference between experimental data and theoretical prediction being 3% for water and 10% for kerosene. It is not clear why the predicted sensitivity of the meter (slope of characteristic) is slightly higher than the measured (mean) sensitivity. This may be due to errors arising from the use of simple beam theory or to the use of the equivalent added mass.

7.1.2 Bubbly Flow

It is reasonable to suppose that the percentage reduction in effective mass (formula (6.25)) applies to the observed reading of a Coriolis flowmeter when bubbles are present in it. The Coriolis flowmeter, after all, uses inertia forces to obtain its measurement.

The expected error using formula (6.25) is drawn as a dashed line in Figure 7.3 where it can be compared with actual meter measurements

(obtained by Grumski and Bajura [33]). Formula (6.25) is seen to over-estimate the error. This may be because there is considerable interaction between bubbles and/or between bubbles and the tube wall, the distances between these not being small compared with the bubble size.

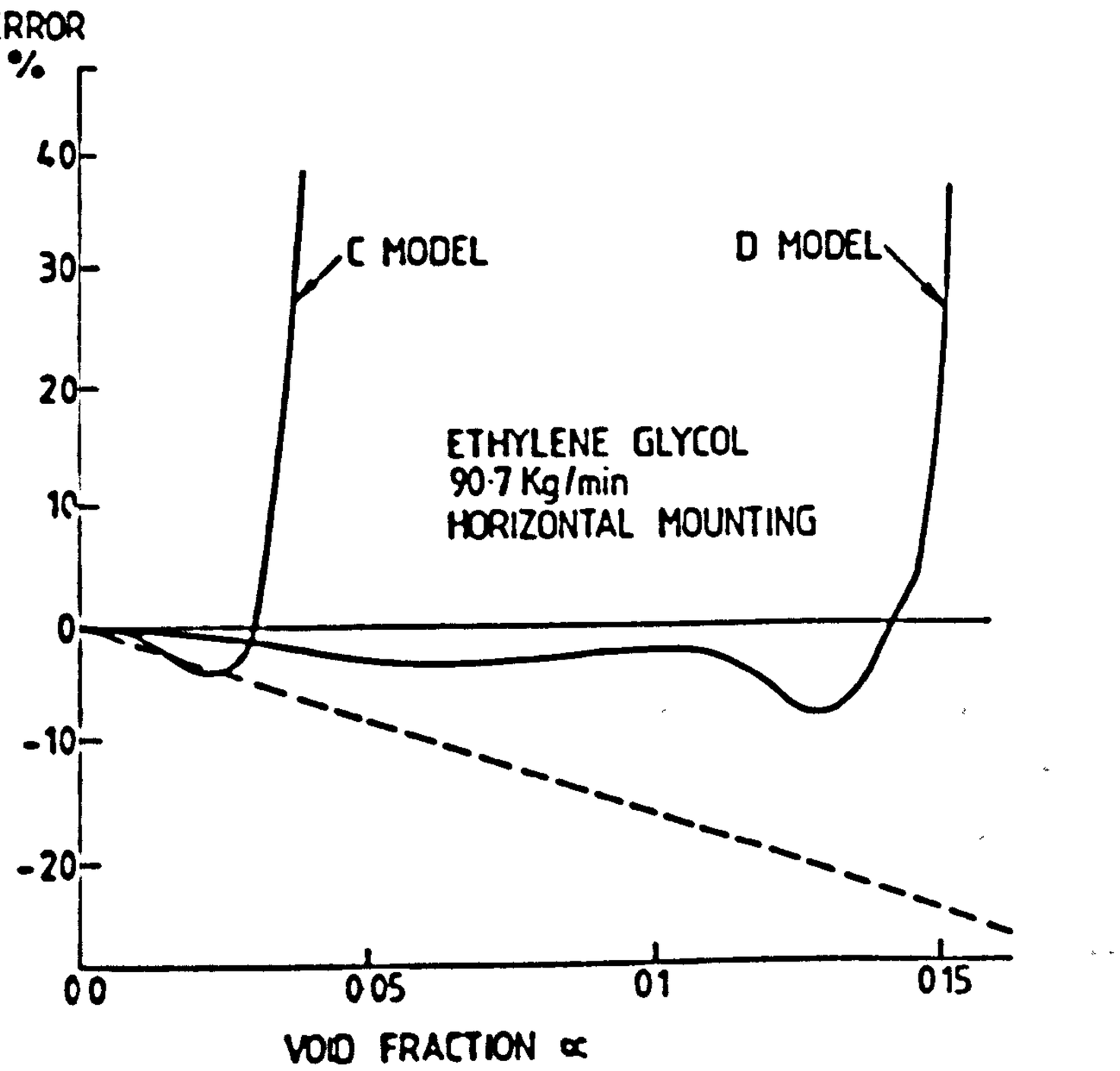

Figure 7.3 COMPARISON BETWEEN THEORY "FORMULA (6.25)" AND EXPERIMENT " BY GRUMSKI AND BAJURA [33]".

7.2 EXPERIMENTAL FLOWMETER

7.2.1 Water Flow

The experimental flowmeter was modelled using the straight tube computer programme option with three added masses.

The basic parameters entered into the programme were flow velocity, water density, water temperature, masses of the detectors and the

drive and tube characteristics. These are summarized in Table 7.3.

PARAMETER	UNIT	VALUE
Water Velocity (U)	m/s	0-6
Water Density (ρ_f)	kg/m^3	999-986
Water Temperature (T_w)	^{o}C	0-40
Tube Density (ρ_t)	kg/m^3	7918
Young's Modulus (E_t)	GN/m^2	203 at 15^{o}C
O.D of Tube (d_o)	mm	28.0
Tube Thickness (t)	mm	0.65*
Tube length (b)	cm	141
Detector Mass (M_{c1}=M_{c3})	kg	0.1
Drive Mass (M_{c2})	kg	0.2

** Tube thickness was taken as an average measurement. Error in the thickness leads to uncertainty in calculated time delay (eg. a variation of ±0.05 mm results in ±4% uncertainty in Δt calculations).*

Table 7.3 BASIC COMPUTER PROGRAMME INPUT PARAMETERS FOR THE STRAIGHT-TUBE EXPERIMENTAL FLOWMETER.

Water temperature was introduced in order to account for any effects of temperature on water density and tube moduli of elasticity.

Figure 7.4 illustrates the comparison between numerical predictions of the sensitivity and experimental data for three different distances between measuring points D=40, 60 and 90 cm. The maximum difference between experimental data and theoretical predictions is 10% for D=40cm, 4% for D=60cm and 8% for D=90cm.

The prediction of the optimum measuring distance for the straight-tube configuration (Figure 4.4) is consistent with experimental data (Figure 5.23). Here, the non-dimensional predicted distance ($\tilde{D}$=D/b) is 0.44 whilst the experimental distance is 0.46 (D=65 cm).

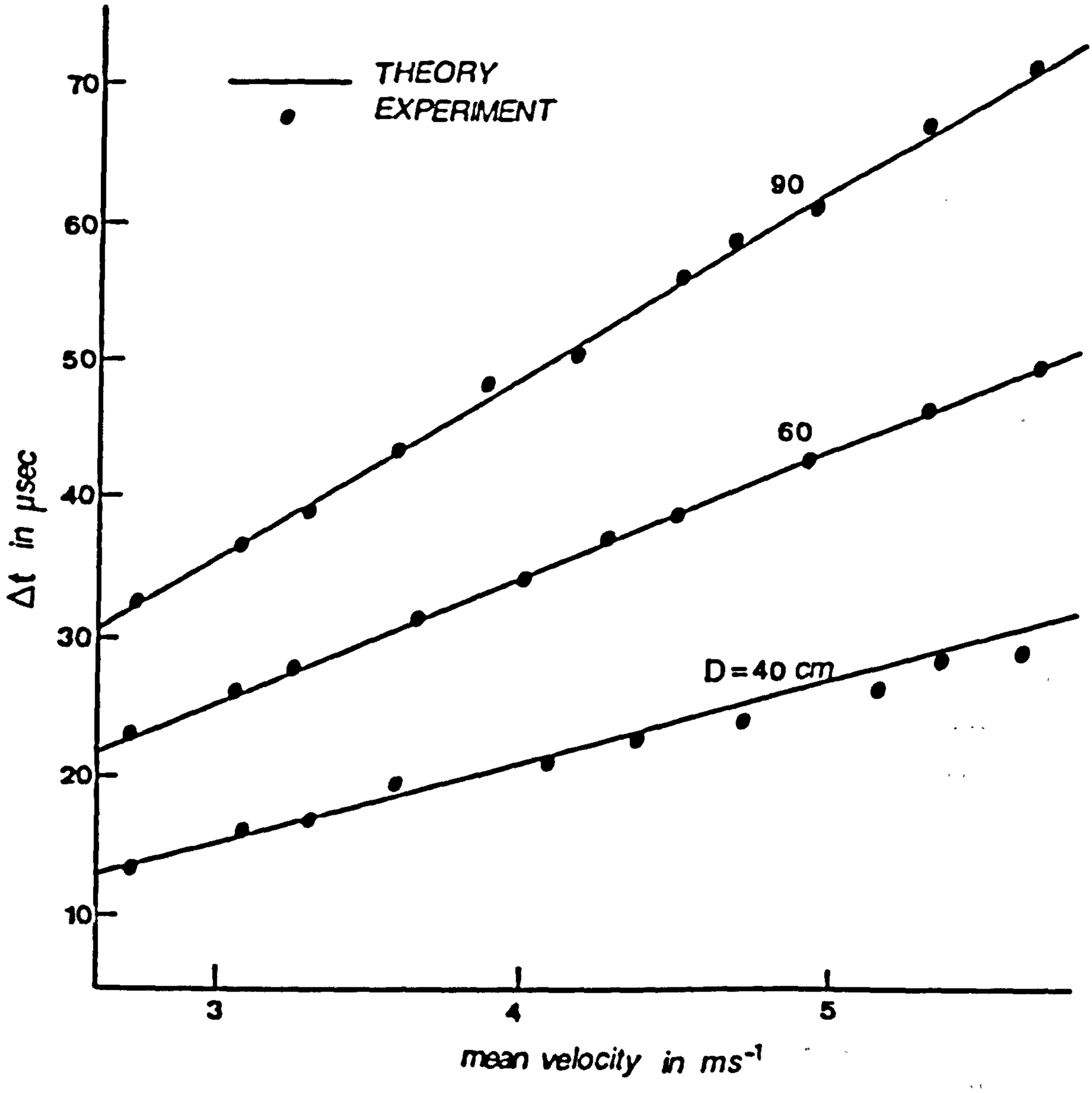

Figure 7.4 COMPARISON OF THEORETICAL AND EXPERIMENTAL CALIBRATION CHARACTERISTICS FOR THE STRAIGHT TUBE EXPERIMENTAL FLOWMETER.

Note that the maximum difference between experimental data and theoretical predictions of the sensitivity (Figure 7.4) is large for D=40 and 90 cm compared with the sensitivity for D=60 cm. This is because at D=60 cm the signal-to-noise ratio is larger than for D=40 and 90 cm (see section 5.2.6). This confirms the optimum position concept discussesd in chapter 4.

7.2.2 Water-Nitrogen Flow

The change in flowmeter sensitivity noted in section 6.4 caused when nitrogen was introduced into water flow in the straight tube experimental flowmeter are here compared with the theoretical explanation of this effect based on effective mass considerations.

Figure 7.5 covers the negative experimental error range; showing the experimental results and the prediction based on effective mass (formula (6.25) with $\%\alpha=[Q_n/(Q_n+Q_w)]\times100$). Formula 6.25 shows good agreement with experimental data at low void fractions (8%-16%) at the 182.3 kg/min water flowrate. In this condition the flow regime was homogeneous along the tube as shown in Figure 6.10. At other void fractions and water flowrates, interaction between bubbles and/or between bubbles and the tube seems to become more significant. As well as reducing the effective mass error this also introduces somewhat greater damping into the system leading to new errors in time delay measurements.

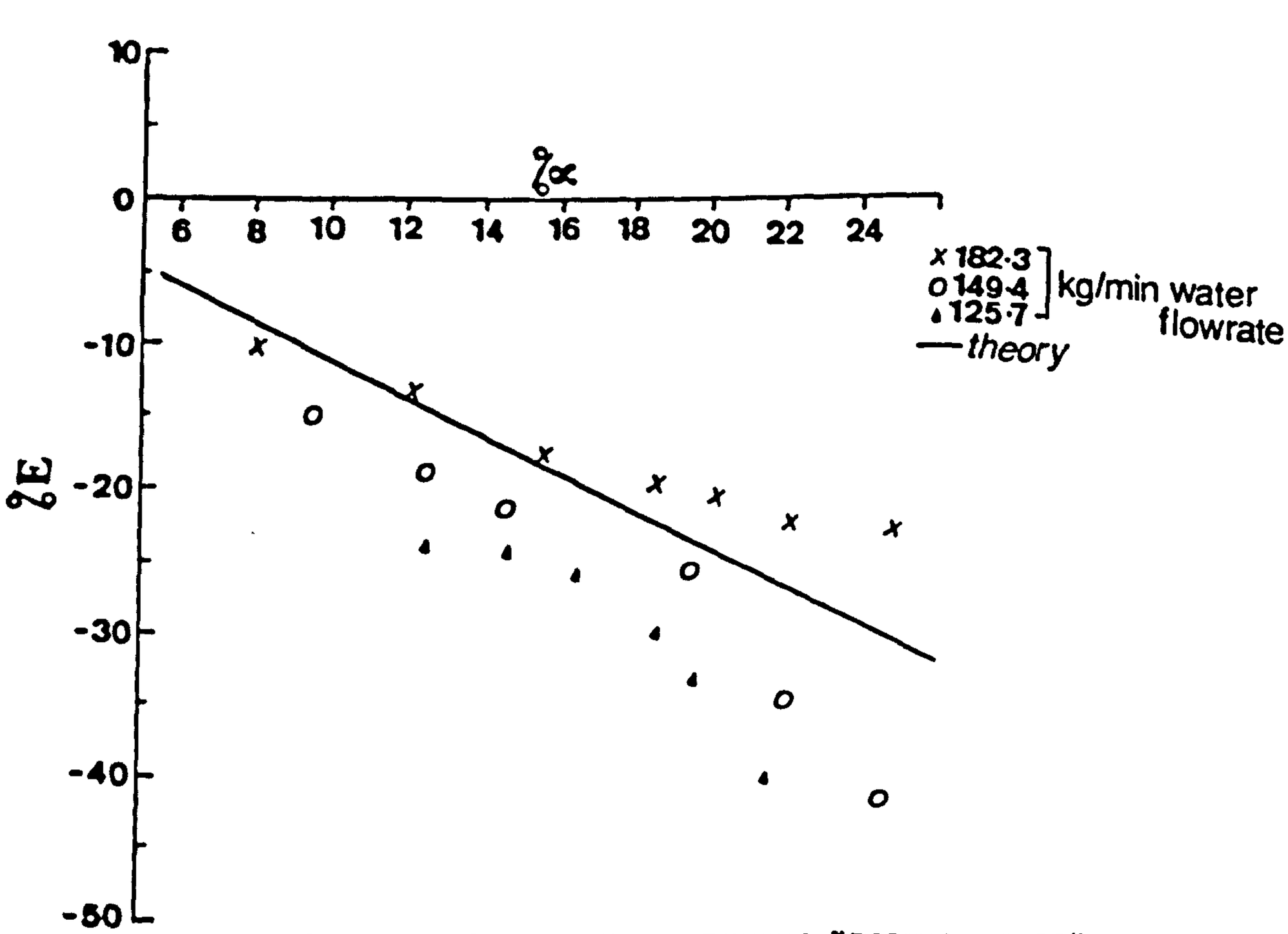

Figure 7.5 COMPARISON BETWEEN THEORY "FORMULA 6.25" AND WATER-NITROGEN EXPERIMENT FOR STRAIGHT TUBE EXPERIMENTAL FLOWMETER

CHAPTER EIGHT

CONCLUSIONS

CHAPTER EIGHT

CONCLUSIONS

The work of this thesis has been largely concerned with the modelling of Coriolis flowmeters of any tube geometry using beam theory. The most general tube geometry considered consisted of three straight and two circular lengths joined in series from which the alternative geometries could be derived. An improved model taking into account elastic boundary conditions and the effects of the masses of the electromagnetic drive and detectors was also discussed. A method for predicting the optimum detection positions was suggested in relation to signal-to-noise ratio. The effective mass concept was presented to account for the performance of Coriolis flowmeters in measuring bubbly flows at relatively low void fractions. A variety of experiments were conducted in order to demonstrate the validity of the theoretical models.

Although the work presented has developed a better understanding of the theory and the behaviour of Coriolis flowmeters it has simultaneously highlighted further complexities and problems to overcome. Hence this work is offered not as the ultimate solution but as the first steps into an area of explosive potential.

It is important to recall that a number of assumptions have been made in the theoretical model which may limit its application. For example, the flat velocity profile assumption is only valid in narrow and relatively long straight tubes at very high Reynolds numbers. Also the further assumption of the free undamped vibration of the tube is an idealization. This is connected with the fact that the drive coil exerts a concentrated force on the tube whilst the damping force is distributed along it so that total cancellation is not possible. The effective mass concept does not include the effect of liquid viscosity or the compressiblity of the mixture. The latter is likely to be the major cause of the observed damping.

The solutions presented give no indication of the effects of some other parameters such as rotatory inertia, shear deformation, axial stresses, fluid pressure and zero drift.

The theoretical model is useful in the primary stages of the design of a flowmeter enabling meter sensitivity, maximum stresses ...etc to be calculated. The ability to locate the optimum distance between measuring points is also of value. The non-dimensional optimum distances obtained theoretically were 0.44, 3 and 4.56 for straight-tube, U-tube and S-tube respectively. The theoretical optimum distance differs from that actualy used in a commercial flowmeter of straight tube configuration but agrees well for one of U-tube configuration. The non-dimensional distance for the straight tube flowmeter manufactured by ENDRESS & HAUSER Ltd. is 0.66 and for the U-tube meter manufactured by MICRO MOTION Inc. is 3.14. The difference in the straight tube case is probably due to some noise process different from that assumed here. In the commercial straight-tube flowmeter the fundamental frequency is relatively high (800-1000 Hz) and the time delays are very small (10-100 nsec).

In the experimental investigations it was found that the single straight tube configuration suffers from a considerable zero drift problem. It was observed that balancing the tube and base temperatures leads to a more stable base line. In two-phase (water-nitrogen) flow experiments an interesting differential damping effect seemed to be present as the flow pattern changed along the tube length. Thus increased damping in the first half of the tube leads to overestimation of total massflow while increased damping in the second half causes underestimation.

In order to gain greater understanding and progress, work should be carried out in the following areas; (i) study of the forced vibration of the tube including the damping, (ii) investigation of the velocity profile and fluid viscosity effects, (iii) optimization of the end conditions and/or using reciprocal drive in order to overcome zero drift problems, (iv) Study of the effects of external vibrations and optimization the installation and (v) analysis of the damping effects of two-phase (liquid/gas) mixtures.

REFERENCES

REFERENCES

1 SIEV, R. "Mass Flow Measurement" Instruments and Control Systems, vol. 33 , 1960 , PP. 966-970.

2 FLANAGAN, T.P. and COLMAN, D.E. "Mass Flowmeters" Control, vol. 7 (65), 1963, PP. 242-245.

3 ORLANDO, V.A. and JENNINGS, F.R. "The Momentum Principle Measures True Mass Rate" Transactions of American Society of Mechanical Engineers, vol. 76 (6), 1954 , PP. 961-965.

4 BRAIN, T.J.S. "Mass Flow Measurement Methods" Metron, Vol. 1 , No. 1 January 1969.

5 DOEBELIN, E.O. "Measurement Systems; Application and Design" 3rd edition 1983 , McGraw-Hill

6 CHESTER, W. "Mechanics" 1979 Allen and Unwin.

7 LI, Y.T. and LEE, S-Y. "A Fast-Response True-Mass-Rate Flowmeter" Transactions of American Society of Mechanical Engineers, July 1953, PP. 835-841.

8 PEARSON, J.M. "Flowmeter"
United States Patent
No. 2,624,198 Jan 1953.

9 ROTH, W. "Gyroscopic Mass Flowmeter"
United States Patent
No. 2,865,201 Dec 1958.

10 ROTH, W. "Mass Flowmeter"
United States Patent
No. 3,049,919 Aug 1962.

11 SIPIN, A.J. "Mass Flow Metering Means"
United States Patent
No. 3,329,019 July 1967.

12 SIPIN, A.J. "Mass Flow Metering Means"
United States Patent
No. 3,355,944 Dec 1967.

13 WILEY, W.C., GOODRICH,G.W. and ADAMS, F.L. "Oscillating Mass Flowmeter"
United States Patent
No. 3,080,750 March 1963.

14 PAVLIN, C.F., MANTOUX, G., GIRALD, A. and GROSSION, M. "Apparatus and Method for Measuring the Mass Flow of a Fluid Stream"
United States Patent
No. 3,927,565 Dec 1975.

15 COX, B.M.
and
HO, D.M.
"Mass Flowmeter With Sensor Gain Control"
United States Patent
No. 4,311,054 Jan 1982.

16 FURNESS, R.A.
"Micro Motion Mass Flowmeter- a Technical Assessment"
Union Carbide Corp.
Techical Report TEC2-8485913
January 1984.

17 CASCETTA, F.,
VALLE, S.D.,
GUIDO, A.R.
and
VIGO, P.
"A Coriolis Mass Flowmeter Based on a New Type of Elastic Suspension"
TO BE PUBLISHED IN MEASUREMENT ; 1990

18 WILSON, JR.M.P.
"A Survey of Mass Flow Meters"
Measuring Devices
May 1971, PP. 865-870.

19 THOMSON, W.T.
"Mechanical Vibration"
2nd edition 1964
Allen and Unwin.

20 KATYS, G.P.
"Continous Measurement of Unsteady Flow"
1964 Pergamon Press Ltd., London

21 PLACHE, K.O.
"Coriolis Gyroscopic Meter"
Mechanical Engineering
vol. 101 (3), 1979, PP. 36-41.

22 GAST, T.
and
FURNESS, R.A.
"Mass Flow Measurement Technology"
International Conference on Flow
measurement in the Mid-80's
Paper 10.2 ,NEL, East Kilbride,
Glasgow, June 1986.

23 TULLIS, P.
and
SMITH, J.
"Coriolis Mass Flowmeter"
NEL Fluid Mechanics Silver Jubilee
Conference Paper 6.3, East Kilbride
Glasgow, 27-29 Nov. 1979.

24 CAMPONOVO, R.E.
and
GERLICH, J.L.
"Mass Flow Measurement and Control"
Dow Chemical U.S.A , Texas Division
Technical Report 87664-492-2 1980.

25 ALTFILLISCH, M.D.,
POWERS, H.A.,
and
WHITE, R.B.
"Gyroscopic Mass Flowmeter"
United States Patent
No. 2,813,423 Nov. 1957.

26 ALTFILLISCH, M.D.,
CHERNIAK, G.S.,
POWERS, H.A
and
WHITE, R.B.
"Flow Control Devices for Flowmeters"
United States Patent
No. 2,821,084 Jan. 1958.

27 ALTFILLISCH, M.D.,
CHERNIAK, G.S.,
POWERS, H.A
and
WHITE, R.B.
"Square Gyroscopic Flowmeters"
United States Patent
No. 2,831,349 Apr. 1958.

28 DRUZHKOVA, L.M. "Damping the Free Oscillations of Constricted Pipe During the Flow of Gas-Liquid Mixtures" Gas Practice, Moscow, All-Union Scientific Research Institute of the Organization of the Management and Economics of the Petroleum and Gas Industry. Collection No. 11 , 1969. (ENGLISH TRANSLATION AVAILABLE FROM THE AUTHOR)

29 DRUZHKOVA, L.M., BULYGIN, V.G., EGOROV, V.E., NESTERENKO, V.S. and LAVROV-AVERIN, A.L. "An Oscillatory Mass Flowmeter for Gas-Liquid Flows" Soviet Journal of Instrumentation and Control Nov. 1972 , PP.22-24. (ENGLISH TRANSLATION AVAILABLE FROM CANADA INSTITUTE FOR SCIENTIFIC AND TECHNICAL INFORMATION)

30 TUCKER, H.G. and HAYES, W.F. "Operating Principle of a Vibrating Pendulum Multiphase Flowmeter for Oil Field Wellhead Fluid Discharge Monitoring" National Research Council Canada Technical Report LTR-CS-207 , Feb. 1980.

31 TUCKER, H.G. and HAYES, W.F. "Error Analysis of a Vibrating Pendulum Two-Phase Flowmeter for Oil Well Application" American Society of Mechanical Engineers Symposium on Measurements in Polyphase Flows 1982 , PP. 45-53.

32 RIVKIA, I.Y., AISIN, S.M., GARKUSHA, O.I., DONDOSHANSKY, A.L., ZELLIS, E.A., KARPOV, V.E., SOROKIN, V.K. and SHISHKIN, O.P. "Mehod and Apparatus for Measuring Mass Flow Rate of Individual Components of Two-Phase Gas-Liquid Medium" United States Patent No. 4,096,745 Jun 1978.

33 GRUMSKI, J.T. and BAJURA, R.A. "Performance of a Coriolis-Type Mass Flowmeter in the Measuring of Two-Phase (Air-Liquid) Mixtures" American society of Mechanical Engineers Winter Annual Meeting, New Orleans, U.S.A Vol.17 , 9-14 Dec 1984 , PP. 75-83.

34 BAUCUM, W.B. "Evaluation of a Coriolis Mass Flowmeter for Pulverized Coal Flows" Topical Report TR-7-7-8-79, The Energy Conversion Division, University of Tennessee, Space Institute Tullahoma, Tennessee , Dec. 1979.

35. MATHUR, M.P. and KLINZING, G.E. "Flow Measurement in Pneumatic Transport of Pulverized Coal" Power Technology vol. 40 1984, PP. 309-321.

36 KLEIZEN, H.H. and VAN BRAKEL, J. "On Line Measurement Techinques in Coal-Handling Systems" REVIEW PAPER Power Technology vol. 40 1984, PP. 133-128.

37 DOMNICK. J., DURST, F., RASZILLIER, H. and ZEISEL, H.
"A Method to Measure Mass and Volume Flow Rates of Two-Phase Flows"
International Journal of Multiphase Flow,
vol. 13 (5) , 1987 , PP. 685-698.

38 WAGNE, J.J.
"Effects of Sensor Design and Application Characteristics on Coriolis Mass Meter Performance: an Overview"
2nd International Conference on Flow Measurement , Paper C1
Held in London, Organised by BHRA
11-13 May 1988.

39 HEMP, J.
"Flowmeters and Reciprocity"
Quarterly Journal of Mathematics and Applied Mechanics,
vol 41 (4) 1988, PP.503-520.

40 HEMP, J. and SULTAN, G.
"On the Theory and Performance of Coriolis Mass Flowmeters"
International Conference on Mass Flow Measurement; Direct and Indirect,
Coriolis Metering I, London 21-22 Feb. 1989
Organised by IBC Technical Services Ltd.

41 KEITA, N.M.
"The Zero Drift Effects in Coriolis Mass Flowmeters"
International Conference on Mass Flow Measurement; Direct and Indirect,
Coriolis Metering I, London 21-22 Feb. 1989
Organised by IBC Technical Services Ltd.

42 KARKAR, F.

"The Performance of a Coriolis Meter When Used to Measure Density" International Conference on Mass Flow Measurement; Direct and Indirect, Coriolis Metering I, London 21-22 Feb. 1989 Organised by IBC Technical Services Ltd.

43 BIRKER, B.

"Theory, Design and Performance of the Straight Tube Mass Flowmeter" International Conference on Mass Flow Measurement; Direct and Indirect, Coriolis Metering II, London 21-22 Feb. 1989 Organised by IBC Technical Services Ltd.

44 KIEHL, W.
and
GÄRHNER, U.

"Two Coriolis Meters in One Line" International Conference on Mass Flow Measurement; Direct and Indirect, Coriolis Metering II, London 21-22 Feb. 1989 Organised by IBC Technical Services Ltd.

45 FRANKVOORT, W.
and
NEDERLOF, A-J.

"Results of the Evaluation of the Performance of Mass Flowmeters Using a Prover Loop" International Conference on Mass Flow Measurement; Direct and Indirect, Coriolis Metering II, London 21-22 Feb. 1989 Organised by IBC Technical Services Ltd.

46 WEAVER, D.S.

"An Introduction to Flow Induced Vibration" Short Course Notes, Department Of Fluid Engineering and Instrumentation, Cranfield Institute of Technology, 12-15 May 1986.

47 BLEVINS, R.D. "Flow-Induced Vibration"
1977, Van Nostrand Reinhold, Canada

48 ASHLEY, H.
and
HAVILAND, G. "Bending Vibrations of a Pipe Line Containing Flowing Fluid"
Journal of Applied Mechanics
vol. 72 , 1950 , PP. 229-232.

49 HOUSNER, G.W. "Bending Vibrations of a Pipe Line Containing Flowing Fluid"
Journal of Applied Mechanics
vol. 74 , 1952 , PP. 205-208.

50 LONG, JR.R.E. "Experimental ana Theoretical Study of Transverse Vibration of a tube Containing Flowing Fluid"
Journal of Applied Mechanics
vol. 77 , 1955 , PP. 65-68.

51 BENJAMIN, T.B. "Dynamics of System of Articulated Pipes Conveying Fluid"
Proceedings of the Royal Society,
London, vol. 261 , 1961 , PP. 457-499.

52 GREGORY, R.W.
and
PAIDOUSSIS, M.P. "Unstable Oscillation of Tubular Cantilevers Conveying Fluid"
Proceedings of the Royal Society , London
vol. 293 , 1966 , PP. 521-542.

53 STEIN, R.A.
and
TOBRINER, M.W.
"Vibration of Pipes Containing Flowing Fluid"
Transactions of the American Society of Mechanical Engineers, Journal of Applied Mechanics,
vol. 37 , 1970 , PP. 906-916.

54 HILL, J.L.
and
SWANSON, C.P.
"Effect of Lumped Masses on the Stability of Fluid Conveying Tubes"
Transactions of the American Society of Mechanical Engineers, Journal of Applied Mechanics,
vol. 37 , 1970 , PP. 494-496.

55 UNNY, T.E.,
MARTIN, E.L.
and
DUBEY, R.N.
"Hydroelastic Instability of Uniformly Curved Pipe Fluid System"
Transactions of the American Society of Mechanical Engineers, Journal of Applied Mechanics,
vol. 37 , 1970 , PP. 817-822.

56 CHEN, S.S.
"Vibration and Stability of a Uniformly Curved Tube Conveying Fluid"
The Journal of the Acoustical Society of America,
vol. 51 , 1972 , PP. 223-232.

57 CHEN, S.S.
"Out-of-Plane Vibration and Stability of Curved tubes Conveying Fluid"
Transactions of the American Society of Mechanical Engineers, Journal of Applied Mechanics,
vol. 40 , 1973 , PP. 362-368.

58 HILL, J.L.
and
DAVIS, C.G.
"The Effect of Initial Forces on the Hydroelastic Vibration and Stability of Planar Curved Tubes"
Transactions of the American Society of Mechanical Engineers, Journal of Applied Mechanics,
vol. 41 , 1974 , PP. 355-359.

59 DOLL, R.W.
and
MOTE, JR.C.D.
"On the Dynamic Analysis of Curved and Twisted Cylinders Transporting Fluids"
Transactions of the American Society of Mechanical Engineers, Journal of Pressure Vessel Technology,
vol. 98 , 1976 , PP. 143-150.

60 KOHLI, A.K.
and
NAKRA, B.C.
"Vibration Analysis of Straight and Curved Tubes Conveying Fluid by Means of Straight Beam Finite Elements"
Journal of Sound and Vibration
vol. 93 (2) , 1984 , PP. 307-311
(LETTERS TO THE EDITOR)

61 CHEN, W.H.
and
FAN, C.N.
"Stability Analysis With Lamped Mass and Friction Effects in Elastically Supported Pipes Conveying Fluids"
Journal of Sound and Vibration
vol. 119 (3) , 1987 , PP.429-442.

62 HARA, F.
"A Theory on the Two-Phase Flow Induced Vibrations in Piping Systems"
Paper F 5/1, 2nd International Conference on Structure Mechanics in Reactor Technology,
Berlin 1973.

63 HIRAMATSU, T., KOMURA, Y. and YANO, S. "Analysis of Two-Phase Flow Induced Vibrations in Piping Systems" In Flow-Induced Vibration of Circular Cylindrical Structures, Presented at Pressure Vessel and Piping Conference Orlando , U.S.A ,1982 , PP. 139-149.

64 LOVE, A.E.H. "The Mathematical Theory of Elasticity" 1944, NewYork : Dover.

65 OJALVO, I.U. "Coupled Twist-Bending Vibrations of Incomplete Elastic Rings" International Journal of Mechanical Sciences, vol. 4 , 1962 , PP. 53-72.

66 ROARK, R.J. "Formulas for Stress and Strain" 4th edition , 1965 McGraw-Hill.

67 NUMERICAL ALGORITHMS GROUP User's Guide to NAG Library Subroutines in Fortran, NAGFLIB Mark 12, July 1987.

68 BANNISTER, R.H. Msc Course Notes, School of Mechanical Engineering, Cranfield Institute of technology , 1986.

69 I-DEAS GEOMOD "Integrated Design Engineering Analysis Software" , GEOMOD Solid Modelling and Design, User's Guide SDRC, Ohio,USA, 1988

70 I-DEAS
SUPERTAB
"Integrated Design Engineering Analysis Software", SUPERTAB Engineering Analysis Pre and Post-Processing, Use's Guide SDRC, Ohio,USA, 1988.

71 PAFEC
"Programme for Automatic Finite Element Calculations"
User's Guide , Nottingham,UK, 1978.

72 HETÉNYI, M.
"Beams on Elastic Foundation; Theory and Applications in the Fields of Civil and Mechanical Engineering"
Scientific Series , vol. 15, 1946
University of Michigan.

73 BICKLEY, W.G.
and
TALBOT, A.
"An Introduction to the Theory of Vibration Systems"
1961 , Oxford.

74 MAHMUD, S.M.
"Error Analysis of Digital Phase Measurement of Distorted Waves"
IEEE Transactions of Instrumentation and Measurement
vol. 38 (1) Feb. 1989 , PP. 6-9.

75 PM6652..54
COUNTERS
Operating Manual of the Programmable Timer/Counter
PYE Unicam Ltd., U.K.

76 WAGDY, M.F.
and
LUCAS, M.S.P.
"Errors in Sampling Data Phase Measurement"
IEEE Transactions of Instrumentation and Measurement
vol. IM-34 (4) Dec. 1985 , PP. 507-509.

77 HOROWITZ, P.
and
HILL, W.
"The Art of Electronics"
1980
Cambridge University Press.

78 KAYE, G.W.C.
and
LABY, T.H.
"Tables of Physical and Chemical constants"
15th edition , 1986
Longman Inc. NewYork.

79 SOO, S.L.
"Fluid Dynamics of Multiphase Systems"
1967 , Blaisdell.

80 MIROPOLSKY, Z.L.
and
SHNEYEROVA, R.I
"Application of X-rays, Excited by β-Sources to Studying Hydrodynamics of Two-Phase Media"
Journal of Heat and Mass Transfer
vol. 5 , 1962 , PP. 723-728.

81 HEWITT, G.F.
"Measurement of Two-Phase Flow Parameters"
1978
Academic Press.

82 WYATT, D.G.
"Electromagnetic Flowmeter Sensitivity With Two-Phase Flow"
International Journal of Multiphase Flow
vol. 12 (6) , 1986 , PP. 1009-1017.

83 KINGHORN, F.C.
and
McHUGH, A.

"The Performance of Turbine Meters in Two-Component Gas/Liquid Flow"
Proceedings of 2nd symposium on FLOW: Its Measurement and Control in Science and Industry
Paper 542 ,vol.2 , 1981 , PP.471-492,
Instrumentation Society of America.

84 GEORGE, K.K.

"Two-Phase Flow in 180° Return Bends"
High Speed Cine Film
U.K Atomic Energy Authority,
Research Group Momorandum, 1971.

85 IBRAHIM, R.A.

"Parametric Random Vibration"
1985
Research Studies Press.

86 BAUER, H.F.

"Oscillation of Imiscible Liquids in a Rectangular Container: A New Damper for Excited Structures"
Journal of Sound and Vibration
vol. 93 (1) , 1984 , PP. 117-133.

87 WALSHAW, A.C.

"Mechanical Vibrations With Applications"
1984
Halsted Press.

88 LANDAU, L.D.
and
LIFSHITZ, E.M.

"Fluid Mechanics-Course of Theoretical Physics"
2nd edition , vol.6 , 1987
Pergamon Press.

APPENDICES

APPENDIX "A"

CALCULATION OF THE COEFFICIENT OF EQUATION (1.14)

The basic relation between mass flowrate ($\dot{m}$) and time difference (Δt) is developed for U-tube configuration in chapter one (equation (1.14)). The coeficient of equation (1.14) consists of a geometrical constant, stiffness constant and frequency ratio. Assume that the tube is driven at its fundamental frequency, equation (1.14) becomes

$$\dot{m} = \frac{c\ K\ (1-(\omega_n/\omega_{nt})^2)}{2\ \ell\ d^2}\ \Delta t \qquad (A\text{-}1)$$

where c, ℓ and d are geometrical constants, K is stiffness constant and ω_n and ω_{nt} are fundamental and 2nd mode frequencies. The stiffness constant is a combined torsional and bending stiffnesses (see Figure A.1)

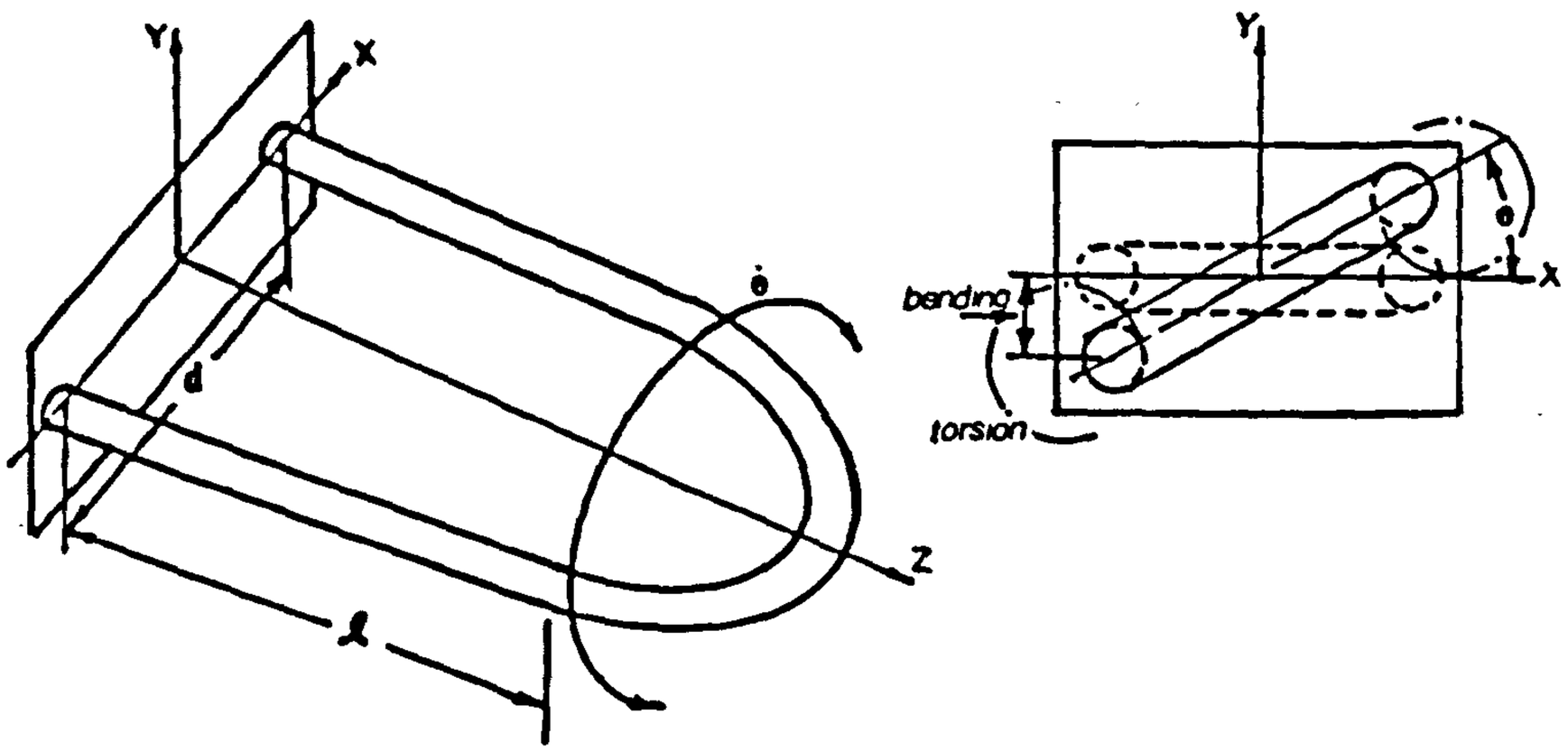

Figure A.1 THE COMBINED TORSIONAL AND BENDING VIBRATION OF A U-TUBE.

Assume that the twist is linear in the straight and circular lengths of the tube and applying the simple torsion and bending theories gives

$$K = \frac{GJ}{(\ell+(d/2))} + \frac{3EI_x(d/2)^2}{(\ell+(d/2))^3} \qquad (A-2)$$

where E is Young's modulus,
G is shear modulus,
I_x is 2nd moment of area and
J is polar moment of area.

Now, assume that the U-tube is a cantilever beam fixed at one end with total length of $\ell+(d/2)$, the fundamental frequency, therefore, is

$$\omega_n = \frac{c_1^2}{(\ell+(d/2))^2}\left[\frac{EI_x}{(\rho_f+\rho_t)}\right]^{1/2} \qquad (A-3)$$

where $c_1 = 1.8883$ for a cantilever. For undamped torsional vibration, the differential equation is

$$I_z\ddot{\theta} + K\theta = 0 \qquad (A-4)$$

where I_z is the moment of inertia of the U-tube around z-axis,
K is the combined torsional and bending stiffness constant and
θ is the twist angle of the U-tube (see Figure A.1)

from equation (A-4) the 2nd natural mode frequency (torsional frequency) is

$$\omega_{nt} = \left[\frac{K}{I_z}\right]^{1/2} \qquad (A-5)$$

where $I_z = \frac{\pi^2}{2}(d/2)^3\,(\rho_t(r_o^2-r_i^2) + \rho_f\, r_i^2)$ (A-6)

where r_o and r_i are radius of tube cross-section.

APPENDIX "B"

BOUNDARY CONDITION EQUATIONS FOR GENERAL TUBE GEOMETRY

The boundary conditions (2.20) and (2.21) result in thirty relations between thirty constants A_{ij}, B_{ij} and B_{oj}. These are summarized as follows

$$\sum_{j=1}^{4} A_{j1} = 0 \qquad \text{(B-1)}$$

$$\sum_{j=1}^{4} \alpha_j A_{j1} = 0 \qquad \text{(B-2)}$$

$$B_{o1} = 0 \qquad \text{(B-3)}$$

$$\sum_{j=1}^{4} A_{j1} e^{\alpha_j L_1} + (1+K)^{-1} \sum_{j=1}^{6} A_{j2} (K-\lambda^{-2}) e^{\lambda_j L_1} = 0 \qquad \text{(B-4)}$$

$$\sum_{j=1}^{4} \alpha_j A_{j1} e^{\alpha_j L_1} + (1+K)^{-1} \sum_{j=1}^{6} A_{j2} \lambda_j (K-\lambda^{-2}) e^{\lambda_j L_1} = 0 \qquad \text{(B-5)}$$

$$(B_{11} L_1 + B_{o1}) - \sum_{j=1}^{6} A_{j2} e^{\lambda_j L_1} = 0 \qquad \text{(B-6)}$$

$$\sum_{j=1}^{4} \alpha_j^2 A_{j1} e^{\alpha_j L_1} + \sum_{j=1}^{6} A_{j2} e^{\lambda_j L_1} + (1+K)^{-1} \sum_{j=1}^{6} A_{j2} \lambda_j^2 (K-\lambda_j^{-2}) e^{\lambda_j L_1} = 0 \qquad \text{(B-7)}$$

$$\sum_{i=1}^{4} \alpha_i^3 A_{i1} e^{\alpha_i L_1} + K(1+K)^{-1} \sum_{i=1}^{6} A_{i2} \lambda_i(\lambda_i^2+\lambda_i^{-2}+2) e^{\lambda_i L_1} = 0 \qquad \text{(B-8)}$$

$$B_{11} - \sum_{i=1}^{6} A_{i2} \lambda_i e^{\lambda_i L_1} + (1+K)^{-1} \sum_{i=1}^{6} A_{i2} \lambda_i(K-\lambda_i^{-2}) e^{\lambda_i L_1} = 0 \qquad \text{(B-9)}$$

$$\sum_{i=1}^{4} A_{i1} e^{\alpha_i(L_1+L_2)} + (1+K)^{-1} \sum_{i=1}^{6} A_{i2} (K-\lambda^{-2}) e^{\lambda_i(L_1+L_2)} = 0 \qquad \text{(B-10)}$$

$$\sum_{i=1}^{4} \alpha_i A_{i1} e^{\alpha_i(L_1+L_2)} + (1+K)^{-1} \sum_{i=1}^{6} A_{i2} \lambda_i(K-\lambda^{-2}) e^{\lambda_i(L_1+L_2)} = 0 \qquad \text{(B-11)}$$

$$(B_{11} \sum_{i=1}^{2} L_i + B_{01}) - \sum_{i=1}^{6} A_{i2} e^{\lambda_i(L_1+L_2)} = 0 \qquad \text{(B-12)}$$

$$\sum_{i=1}^{4} \alpha_i^2 A_{i1} e^{\alpha_i(L_1+L_2)} + \sum_{i=1}^{6} A_{i2} e^{\lambda_i(L_1+L_2)} +$$

$$(1+K)^{-1} \sum_{i=1}^{6} A_{i2} \lambda_i^2(K-\lambda_i^{-2}) e^{\lambda_i(L_1+L_2)} = 0 \qquad \text{(B-13)}$$

$$\sum_{i=1}^{4} \alpha_i^3 A_{i1} e^{\alpha_i(L_1+L_2)} + K(1+K)^{-1} \sum_{i=1}^{6} A_{i2} \lambda_i(\lambda_i^2+\lambda_i^{-2}+2) e^{\lambda_i(L_1+L_2)} = 0 \qquad \text{(B-14)}$$

$$B_{11} - \sum_{i=1}^{6} A_{i2} \lambda_i e^{\lambda_i(L_1+L_2)} + (1+K)^{-1} \sum_{i=1}^{6} A_{i2} \lambda_i(K-\lambda_i^{-2}) e^{\lambda_i(L_1+L_2)} = 0 \qquad \text{(B-15)}$$

$$\sum_{i=1}^{4} A_{i1} e^{\alpha_i(L_1+L_2+L_3)} + (1+K)^{-1} \sum_{i=1}^{6} A_{i4} (K-\lambda^{-2}) e^{\lambda_i(L_1+L_2+L_3)} = 0 \qquad \text{(B-16)}$$

$$\sum_{i=1}^{4} \alpha_i \, A_{i3} \, e^{\alpha_i(L_1+L_2+L_3)} + (1+K)^{-1} \sum_{i=1}^{6} A_{i4} \, \lambda_i(K-\lambda^{-2}) e^{\lambda_i(L_1+L_2+L_3)} = 0 \quad \text{(B-17)}$$

$$(B_{13} \sum_{i=1}^{3} L_i + B_{03}) - \sum_{i=1}^{6} A_{i4} \, e^{\lambda_i(L_1+L_2+L_3)} = 0 \quad \text{(B-18)}$$

$$\sum_{i=1}^{4} \alpha_i^2 \, A_{i3} \, e^{\alpha_i(L_1+L_2+L_3)} + \sum_{i=1}^{6} A_{i4} \, e^{\lambda_i(L_1+L_2+L_3)} +$$

$$(1+K)^{-1} \sum_{i=1}^{6} A_{i4} \, \lambda_i^2(K-\lambda_i^{-2}) \, e^{\lambda_i(L_1+L_2+L_3)} = 0 \quad \text{(B-19)}$$

$$\sum_{i=1}^{4} \alpha_i^3 \, A_{i3} \, e^{\alpha_i(L_1+L_2+L_3)} + K(1+K)^{-1} \sum_{i=1}^{6} A_{i4} \, \lambda_i(\lambda_i^2+\lambda_i^{-2}+2) e^{\lambda_i(L_1+L_2+L_3)} = 0 \quad \text{(B-20)}$$

$$B_{13} - \sum_{i=1}^{6} A_{i4} \, \lambda_i \, e^{\lambda_i(L_1+L_2+L_3)} + (1+K)^{-1} \sum_{i=1}^{6} A_{i4} \, \lambda_i(K-\lambda_i^{-2}) e^{\lambda_i(L_1+L_2+L_3)} = 0 \quad \text{(B-21)}$$

$$\sum_{i=1}^{4} A_{i5} \, e^{\alpha_i(L_1+L_2+L_3+L_4)} + (1+K)^{-1} \sum_{i=1}^{6} A_{i4} \, (K-\lambda^{-2}) e^{\lambda_i(L_1+L_2+L_3+L_4)} = 0 \quad \text{(B-22)}$$

$$\sum_{i=1}^{4} \alpha_i \, A_{i5} \, e^{\alpha_i(L_1+L_2+L_3+L_4)} + (1+K)^{-1} \sum_{i=1}^{6} A_{i4} \, \lambda_i(K-\lambda^{-2}) e^{\lambda_i(L_1+L_2+L_3+L_4)} = 0 \quad \text{(B-23)}$$

$$(B_{15} \sum_{i=1}^{4} L_i + B_{05}) - \sum_{i=1}^{6} A_{i4} \, e^{\lambda_i(L_1+L_2+L_3+L_4)} = 0 \quad \text{(B-24)}$$

$$\sum_{i=1}^{4} \alpha_i^2 \, A_{i5} \, e^{\alpha_i(L_1+L_2+L_3+L_4)} + \sum_{i=1}^{6} A_{i4} \, e^{\lambda_i(L_1+L_2+L_3+L_4)} +$$

$$(1+K)^{-1} \sum_{i=1}^{6} A_{i4} \, \lambda_i^2(K-\lambda_i^{-2}) e^{\lambda_i(L_1+L_2+L_3+L_4)} = 0 \quad \text{(B-25)}$$

$$\sum_{i=1}^{4} \alpha_i^3 \, A_{i1} e^{\alpha_i (L_1+L_2+L_3+L_4)} + K(1+K)^{-1} \sum_{i=1}^{6} A_{i2} \, \lambda_i (\lambda_i^2 + \lambda_i^{-2} + 2) e^{\lambda_i (L_1+L_2+L_3+L_4)} \geq 0 \qquad \text{(B-26)}$$

$$B_{1s} - \sum_{i=1}^{6} A_{i4} \, \lambda_i \, e^{\lambda_i (L_1+L_2+L_3+L_4)} + (1+K)^{-1} \sum_{i=1}^{6} A_{i4} \, \lambda_i (K - \lambda_i^{-2}) e^{\lambda_i (L_1+L_2+L_3+L_4)} \geq 0 \qquad \text{(B-27)}$$

$$\sum_{i=1}^{4} A_{i5} \, e^{\alpha_i (L_1+L_2+L_3+L_4+L_5)} = 0 \qquad \text{(B-28)}$$

$$\sum_{i=1}^{4} \alpha_i \, A_{i5} \, e^{\alpha_i (L_1+L_2+L_3+L_4+L_5)} = 0 \qquad \text{(B-29)}$$

$$B_{1s} \sum_{i=1}^{5} L_i + B_{0s} = 0 \qquad \text{(B-30)}$$

APPENDIX C

PROGRAMME FOR GENERAL TUBE GEOMETRY

The programme calculates tube natural frequencies(ω), phase difference($\Delta\Phi$),mode shapes and optimum measuring distanc(D) for general tube geometry (S-shape).

VARIABLES USED IN THE PROGRAMME

BB= mass ratio
FV= non-dimensional fluid velocity
W = non-dimensional angular frequency
K= GJ/EI
PR= poisson's ratio
Q = roots of complex polynomial (2.33)
U = roots of complex polynomial (2.29)
P(1)and P(2)= measuring distances
R1,2,..= b1/a1,b2/a2,..
MODVS1,2..= displacement mode shapes
MODPHS1,2..= twist mode shapes
MAmp = amplitude of vibration at the measuring points
DP1P2= phase difference between two measuring points
APHI= multiplication parameter

LISTING OF THE PROGRAMME

```
PROGRAM GENERAL

INTEGER NCALL,IFAIL,IZERO,N1,IR1,IA1,IB1,ID1

REAL*8 E1,E2,Wmin,Wmax,W,FW,TOL,Wminold,R1,R2,R3,R4,R5,K,PR,
       BB,FV,BBmin,BBmax,BBinc,Vmin,Vmax,Vinc,Rang1,Rang2,
       DRang,P(2),DER1,DEI1,RINT(3000),S1,S2,S3,S4,S5,GG,MIDP,
       MODVS1,MODVS2,MODVS3,MODVS4,MODVS5,MODPHS1,MODPHS2,MAmp,
       MODPHS3,MODPHS4,MODPHS5,BVS1,BVS2,BVS3,BVS4,BVS5,BPHS1,
       BPHS2,BPHS3,BPHS4,BPHS5,BP(2),DBP1P2,Amp,CONST,APHI,
       MODSIG

COMPLEX*16 U(6),Q(4),C1(29,29),B1(29,1),FC11(6),FC12(6),
           FC13(6),FC21(6),FC22(6),FC23(6),CC,CC1,VS1,VS2,VS3,
           VS4,VS5,PHS1,PHS2,PHS3,PHS4,PHS5,FB1,FB2,FB3,SIG,CCM


COMMON/A1/U,Q
COMMON/A2/R1,R2,R3,R4,R5,K,BB,FV

EXTERNAL FUNCT

CALL DATA (R1,R2,R3,R4,R5,PR,BBmin,BBmax,BBinc,Vmin,Vmax,Vinc,
           Rang1,Rang2,DRang,CONST,MIDP)


K=1.0/(1.0+PR)

-----------ITERATION FOR MASS RATIO-------------

DO BB=BBmin,BBmax,BBinc

----ITERATION FOR NON-DIMENSIONAL FLUID VELOCITY---
```

```
DO FV=Vmin,Vmax,Vinc

IK=1

----------ITERATION FOR MEASURING DISTANCE----------

DO aa=0.01,MIDP-0.01,0.01

P(1)=MIDP-aa
P(2)=MIDP+aa

II=0
IZERO=0
Wmin=Rang1
Wmax=Rang2

----------ITERATION FOR TUBE NATURAL FREQUENCY--------

DO WHILE(IZERO.LT.2)

TOL=1.0D-04

-------------------- MINIMIZING SOLVER-----------------

E1=0.0
E2=0.0
NCALL=1000
IFAIL=1
Wminold=Wmin

CALL E04ABF (FUNCT,E1,E2,Wmin,Wmax,NCALL,W,FW,IFAIL)

---- E04ABF searches for minimum values of the --------
-----------------modulus of |Y|----------------------

IF (FW.LT.TOL) THEN
WRITE(1,*)IZERO,FV,BB,W,FW
IZERO=IZERO+1
ELSE IF (DABS(Wmin-Wminold).LT.1.0D-02)THEN
GO TO 999
END IF
Wmin=Wmin+DRang
Wmax=Wmax+DRang


------------ SET THE ELEMENTS OF REDUCED MATRIX -------


DO I=1,29
DO J=1,29
C1(I,J)=(0.0,0.0)
END DO
END DO

DO J=1,4
C1(1,J)=(1.0,0.0)
C1(2,J)=Q(J)
C1(3,J)=EXP(Q(J)*R1)
C1(4,J)=Q(J)*C1(3,J)
C1(5,J)=Q(J)*C1(4,J)
C1(6,J)=Q(J)*C1(5,J)
END DO

DO J=5,8
C1(7,J)=EXP(Q(J-4)*(R1+R2))
```

```
C1(8,J)=Q(J-4)*C1(7,J)
C1(9,J)=Q(J-4)*C1(8,J)
C1(10,J)=Q(J-4)*C1(9,J)
C1(11,J)=EXP(Q(J-4)*(R1+R2+R3))
C1(12,J)=Q(J-4)*C1(11,J)
C1(13,J)=Q(J-4)*C1(12,J)
C1(14,J)=Q(J-4)*C1(13,J)
END DO

GG=1.0/(1.0+K)
DO J=25,29
FC11(J-24)=GG*(K-(1.0/U(J-24)**2.0))
FC12(J-24)=EXP(U(J-24)*R1)
FC13(J-24)=EXP(U(J-24)*(R1+R2))
C1(3,J)=FC11(J-24)*FC12(J-24)
C1(4,J)=U(J-24)*C1(3,J)
C1(5,J)=FC12(J-24)+(U(J-24)*C1(4,J))
C1(6,J)=GG*K*U(J-24)*FC12(J-24)*((1.0/U(J-24)**2.0)+U(J-24)
        **2.0+2.0)
C1(7,J)=FC11(J-24)*FC13(J-24)
C1(8,J)=U(J-24)*C1(7,J)
C1(9,J)=FC13(J-24)+(U(J-24)*C1(8,J))
C1(10,J)=GG*K*U(J-24)*FC13(J-24)*((1.0/U(J-24)**2.0)+U(J-24)
         **2.0+2.0)
C1(22,J)=-FC12(J-24)
C1(23,J)=U(J-24)*(FC11(J-24)-1.0)*FC12(J-24)
C1(24,J)=-FC13(J-24)
C1(25,J)=U(J-24)*(FC11(J-24)-1.0)*FC13(J-24)
END DO

DO J=9,14
FC21(J-8)=GG*(K-(1.0/U(J-8)**2.0))
FC22(J-8)=EXP(U(J-8)*(R1+R2+R3))
FC23(J-8)=EXP(U(J-8)*(R1+R2+R3+R4))
C1(11,J)=FC21(J-8)*FC22(J-8)
C1(12,J)=U(J-8)*C1(11,J)
C1(13,J)=FC22(J-8)+(U(J-8)*C1(12,J))
C1(14,J)=GG*K*U(J-8)*FC22(J-8)*((1.0/U(J-8)**2.0)+U(J-8)**2.0+2.0)
C1(15,J)=FC21(J-8)*FC23(J-8)
C1(16,J)=U(J-8)*C1(15,J)
C1(17,J)=FC23(J-8)+(U(J-8)*C1(16,J))
C1(18,J)=GG*K*U(J-8)*FC23(J-8)*((1.0/U(J-8)**2.0)+U(J-8)**2.0+2.0)
C1(26,J)=-FC22(J-8)
C1(27,J)=U(J-8)*(FC21(J-8)-1.0)*FC22(J-8)
C1(29,J)=U(J-8)*(FC21(J-8)-1.0)*FC23(J-8)
END DO

DO J=15,18
C1(15,J)=EXP(Q(J-14)*(R1+R2+R3+R4))
C1(16,J)=Q(J-14)*C1(15,J)
C1(17,J)=Q(J-14)*C1(16,J)
C1(18,J)=Q(J-14)*C1(17,J)
C1(19,J)=EXP(Q(J-14)*(R1+R2+R3+R4+R5))
C1(20,J)=Q(J-14)*C1(19,J)
END DO

C1(21,20)=(1.0,0.0)
C1(22,19)=R1
C1(22,20)=(1.0,0.0)
C1(23,19)=(1.0,0.0)
C1(24,21)=R1+R2
C1(24,22)=(1.0,0.0)
C1(25,21)=(1.0,0.0)
C1(26,21)=R1+R2+R3
C1(26,22)=(1.0,0.0)
C1(27,21)=(1.0,0.0)
```

```
C1(28,23)=R1+R2+R3+R4+R5
C1(28,24)=(1.0,0.0)
C1(29,23)=(1.0,0.0)

---------- SET THE ELEMENTS OF R.H.S OF MATRIX----------

DO I=1,29
B1(I,1)=(0.0,0.0)
END DO
FB1=GG*((1.0/U(6)**2.0)-K)
FB2=EXP(U(6)*R1)
FB3=EXP(U(6)*(R1+R2))
B1(3,1)=FB1*FB2
B1(4,1)=U(6)*B1(3,1)
B1(5,1)=U(6)*B1(4,1)-FB2
B1(6,1)=-GG*K*U(6)*FB2*((1.0/U(6)**2.0)+U(6)**2.0+2.0)
B1(7,1)=FB1*FB3
B1(8,1)=U(6)*B1(7,1)
B1(9,1)=U(6)*B1(8,1)-FB3
B1(10,1)=-GG*K*U(6)*FB3*((1.0/U(6)**2.0)+U(6)**2.0+2.0)
B1(22,1)=FB2
B1(23,1)=U(6)*(1.0+FB1)*FB2
B1(24,1)=FB3
B1(25,1)=U(6)*(1.0+FB1)*FB3

---------- SOLVE 29 SIMELTINOUS EQUATIONS ---------------

N1=29
IR1=1
IA1=29
IB1=29
IFAIL=0

------ F03AHF & F04AKF are simeltinous equations solvers----

CALL F03AHF (N1,C1,IA1,DER1,DEI1,ID1,RINT,IFAIL)
CALL F04AKF (N1,IR1,C1,IA1,RINT,B1,IB1)

---------- CALCULATE MODE SHAPES, PHASE DIFFERENCE ----------
--------------- AND MULTIPLICATION PARAMETER---------------
II=1
IJ=0
DO S1=0.01,R1,0.01
VS1=(0.0,0.0)
CC=(0.0,0.0)
IJ=IJ+1
DO I=1,4
CC=B1(I,1)*EXP(Q(I)*S1)
VS1=VS1+CC
END DO
PHS1=B1(19,1)*S1+B1(20,1)
BVS1=DATAN2(DIMAG(VS1),DREAL(VS1))
BPHS1=DATAN2(DIMAG(PHS1),DREAL(PHS1))
MODVS1=(A02ABF(DREAL(VS1),DIMAG(VS1)))*DCOS(BVS1)
MODPHS1=(A02ABF(DREAL(PHS1),DIMAG(PHS1)))*DCOS(BVS1)
Amp=MODVS1
IF (DABS(S1-P(II)).LT.0.0001) THEN
BP(II)=BVS1
MAmp=Amp
II=II+1
END IF
WRITE(2,*)IJ,S1,MODVS1,MODPHS1
END DO

DO S2=R1,R1+R2,0.01
VS2=(0.0,0.0)
```

```
PHS2=(0.0,0.0)
CC=(0.0,0.0)
CC1=(0.0,0.0)
IJ=IJ+1
DO I=1,5
CC=GG*B1(I+24,1)*((1.0/U(I)**2.0)-K)*EXP(U(I)*S2)
CC1=B1(I+24,1)*EXP(U(I)*S2)
VS2=VS2+CC
PHS2=PHS2+CC1
END DO
VS2=VS2+GG*1.0*((1.0/U(6)**2.0)-K)*EXP(U(6)*S2)
PHS2=PHS2+1.0*EXP(U(6)*S2)
BVS2=DATAN2(DIMAG(VS2),DREAL(VS2))
BPHS2=DATAN2(DIMAG(PHS2),DREAL(PHS2))
MODVS2=(A02ABF(DREAL(VS2),DIMAG(VS2)))*DCOS(BVS2)
MODPHS2=(A02ABF(DREAL(PHS2),DIMAG(PHS2)))*DCOS(BPHS2)
Amp=MODVS2
IF (DABS(S2-P(II)).LT.0.0001) THEN
BP(II)=BVS2
MAmp=Amp
II=II+1
END IF
WRITE(2,*)IJ,S2,MODVS2,MODPHS2
END DO

DO S3=R1+R2,R1+R2+R3,0.01
VS3=(0.0,0.0)
CC=(0.0,0.0)
IJ=IJ+1
DO I=1,4
CC=B1(I+4,1)*EXP(Q(I)*S3)
VS3=VS3+CC
END DO
PHS3=B1(21,1)*S3+B1(22,1)
BVS3=DATAN2(DIMAG(VS3),DREAL(VS3))
BPHS3=DATAN2(DIMAG(PHS3),DREAL(PHS3))
MODVS3=(A02ABF(DREAL(VS3),DIMAG(VS3)))*DCOS(BVS3)
MODPHS3=(A02ABF(DREAL(PHS3),DIMAG(PHS3)))*DCOS(BPHS3)
Amp=MODVS3
IF (DABS(S3-P(II)).LT.0.0001) THEN
BP(II)=BVS3
MAmp=Amp
II=II+1
END IF
WRITE(2,*)IJ,S3,MODVS3,MODPHS3
END DO

DO S4=R1+R2+R3,R1+R2+R3+R4,0.01
VS4=(0.0,0.0)
PHS4=(0.0,0.0)
CC=(0.0,0.0)
CC1=(0.0,0.0)
IJ=IJ+1
DO I=1,6
CC=GG*B1(I+8,1)*((1.0/U(I)**2.0)-K)*EXP(U(I)*S4)
CC1=B1(I+8,1)*EXP(U(I)*S4)
VS4=VS4+CC
PHS4=PHS4+CC1
END DO
BVS4=DATAN2(DIMAG(VS4),DREAL(VS4))
BPHS4=DATAN2(DIMAG(PHS4),DREAL(PHS4))
MODVS4=(A02ABF(DREAL(VS4),DIMAG(VS4)))*DCOS(BVS4)
MODPHS4=(A02ABF(DREAL(PHS4),DIMAG(PHS4)))*DCOS(BPHS4)
Amp=MODVS4
IF (DABS(S4-P(II)).LT.0.0001) THEN
BP(II)=BVS4
```

```
MAmp=Amp
II=II+1
END IF
WRITE(2,*)IJ,S4,MODVS4,MODPHS4
END DO

DO S5=R1+R2+R3+R4,R1+R2+R3+R4+R5-0.01,0.01
VS5=(0.0,0.0)
CC=(0.0,0.0)
IJ=IJ+1
DO I=1,4
CC=B1(I+14,1)*EXP(Q(I)*S5)
VS5=VS5+CC
END DO
PHS5=B1(23,1)*S5+B1(24,1)
BVS5=DATAN2(DIMAG(VS5),DREAL(VS5))
BPHS5=DATAN2(DIMAG(PHS5),DREAL(PHS5))
MODVS5=(A02ABF(DREAL(VS5),DIMAG(VS5)))*DCOS(BVS5)
MODPHS5=(A02ABF(DREAL(PHS5),DIMAG(PHS5)))*DCOS(BPHS5)
Amp=MODVS5
IF (DABS(S5-P(II)).LT.0.0001) THEN
BP(II)=BVS5
MAmp=Amp
II=II+1
END IF
WRITE(2,*)IJ,S5,MODVS5,MODPHS5
END DO
IK=IK+1
DBP1P2=BP(2)-BP(1)
APHI=MAmp*DBP1P2
DMID=P(2)-P(1)
WRITE(3,*)IK,FV,DBP1P2
WRITE(4,*)IK,DMID,APHI
WRITE(7,*)IK,DMID,DBP1P2
END DO
END DO
999    CONTINUE
END DO
END DO
STOP
END
```

---- SUBROUTINE FOR MINIMIZING NAG ROUTINE (E04ABF)----------
------ INCLUDING THE COMPLEX BOUNDARY CONDITION DETERMINANT--------
-------------SOLVER AND COMPLEX POLYNOMIAL SOLVERS-----------------

---

```
SUBROUTINE FUNCT (W,FW)

INTEGER IA,IN,IFAIL,N1,N2,M

REAL*8 W,FW,TOL,ARE(7),ACO(7),REX(7),IMX(7),
       BRE(5),BCO(5),REY(5),IMY(5),DETR,DETI,
       WKSPCE(3000),R1,R2,R3,R4,R5,K,BB,FV,GG

COMPLEX*16 C(30,30),F11(6),F12(6),F13(6),F21(6),F22(6),F23(6),
           U(6),Q(4)

COMMON/A1/U,Q
COMMON/A2/R1,R2,R3,R4,R5,K,BB,FV
```

```
----- SET THE ELEMENTS OF COMPLEX POLYNOMIAL 2.29 ---------

DO I=1,7
ARE(I)=0.0
ACO(I)=0.0
END DO

ARE(1)=1.0
ARE(3)=2.0+FV**2.0
ARE(5)=1.0-W**2.0-(FV**2.0/K)
ARE(7)=W**2.0/K
ACO(4)=2.0*BB**0.5*FV*W
ACO(6)=-(2.0*BB**0.5*FV*W)/K

N1=7
TOL=X02AAF(0.1)
IFAIL=0

---------- SOLVE COMPLEX POLYNOMIAL 2.29 ------------

CALL C02ADF (ARE,ACO,N1,REX,IMX,TOL,IFAIL)

DO I=1,6
U(I)=CMPLX(REX(I),IMX(I))
END DO

 ------- SET THE ELEMENTS OF COMPLEX POLYNOMIAL 2.33 -----

DO I=1,5
BRE(I)=0.0
BCO(I)=0.0
END DO
BRE(1)=1.0
BRE(3)= FV**2.0
BRE(5)=-W**2.0
BCO(4)=2.0*FV*W*BB**0.5

M=5
TOL=X02AAF(0.1)
IFAIL=0

---------- SOLVE COMPLEX POLYNOMIAL 2.33 ----------------

CALL C02ADF (BRE,BCO,M,REY,IMY,TOL,IFAIL)

DO I=1,4
Q(I)=CMPLX(REY(I),IMY(I))
END DO

 -------SET COMPLEX BOUNDARY CONDITION DETERMINANT [30*30]------

DO I=1,30
DO J=1,30
C(I,J)=(0.0,0.0)
END DO
END DO

DO J=1,4
C(1,J)=(1.0,0.0)
C(2,J)=Q(J)
C(3,J)=EXP(Q(J)*R1)
C(4,J)=Q(J)*C(3,J)
C(5,J)=Q(J)*C(4,J)
C(6,J)=Q(J)*C(5,J)
END DO
```

```
DO J=5,8
C(7,J)=EXP(Q(J-4)*(R1+R2))
C(8,J)=Q(J-4)*C(7,J)
C(9,J)=Q(J-4)*C(8,J)
C(10,J)=Q(J-4)*C(9,J)
C(11,J)=EXP(Q(J-4)*(R1+R2+R3))
C(12,J)=Q(J-4)*C(11,J)
C(13,J)=Q(J-4)*C(12,J)
C(14,J)=Q(J-4)*C(13,J)
END DO

GG=1.0/(1.0+K)
DO J=25,30
F11(J-24)=GG*(K-(1.0/U(J-24)**2.0))
F12(J-24)=EXP(U(J-24)*R1)
F13(J-24)=EXP(U(J-24)*(R1+R2))
C(3,J)=F11(J-24)*F12(J-24)
C(4,J)=U(J-24)*C(3,J)
C(5,J)=F12(J-24)+(U(J-24)*C(4,J))
C(6,J)=GG*K*U(J-24)*F12(J-24)*((1.0/U(J-24)**2.0)+U(J-24)
      **2.0+2.0)
C(7,J)=F11(J-24)*F13(J-24)
C(8,J)=U(J-24)*C(7,J)
C(9,J)=F13(J-24)+(U(J-24)*C(8,J))
C(10,J)=GG*K*U(J-24)*F13(J-24)*((1.0/U(J-24)**2.0)+U(J-24)
       **2.0+2.0)
C(22,J)=-F12(J-24)
C(23,J)=U(J-24)*(F11(J-24)-1.0)*F12(J-24)
C(24,J)=-F13(J-24)
C(25,J)=U(J-24)*(F11(J-24)-1.0)*F13(J-24)
END DO

DO J=9,14
F21(J-8)=GG*(K-(1.0/U(J-8)**2.0))
F22(J-8)=EXP(U(J-8)*(R1+R2+R3))
F23(J-8)=EXP(U(J-8)*(R1+R2+R3+R4))
C(11,J)=F21(J-8)*F22(J-8)
C(12,J)=U(J-8)*C(11,J)
C(13,J)=F22(J-8)+(U(J-8)*C(12,J))
C(14,J)=GG*K*U(J-8)*F22(J-8)*((1.0/U(J-8)**2.0)+U(J-8)**2.0+2.0)
C(15,J)=F21(J-8)*F23(J-8)
C(16,J)=U(J-8)*C(15,J)
C(17,J)=F23(J-8)+(U(J-8)*C(16,J))
C(18,J)=GG*K*U(J-8)*F23(J-8)*((1.0/U(J-8)**2.0)+U(J-8)**2.0+2.0)
C(26,J)=-F22(J-8)
C(27,J)=U(J-8)*(F21(J-8)-1.0)*F22(J-8)
C(29,J)=U(J-8)*(F21(J-8)-1.0)*F23(J-8)
C(30,J)=-F23(J-8)
END DO

DO J=15,18
C(15,J)=EXP(Q(J-14)*(R1+R2+R3+R4))
C(16,J)=Q(J-14)*C(15,J)
C(17,J)=Q(J-14)*C(16,J)
C(18,J)=Q(J-14)*C(17,J)
C(19,J)=EXP(Q(J-14)*(R1+R2+R3+R4+R5))
C(20,J)=Q(J-14)*C(19,J)
END DO

C(21,20)=(1.0,0.0)
C(22,19)=R1
C(22,20)=(1.0,0.0)
C(23,19)=(1.0,0.0)
C(24,21)=R1+R2
C(24,22)=(1.0,0.0)
C(25,21)=(1.0,0.0)
```

```
C(26,21)=R1+R2+R3
C(26,22)=(1.0,0.0)
C(27,21)=(1.0,0.0)
C(28,23)=R1+R2+R3+R4+R5
C(28,24)=(1.0,0.0)
C(29,23)=(1.0,0.0)
C(30,23)=R1+R2+R3+R4
C(30,24)=(1.0,0.0)

-------------- SOLVE THE COMPLEX DETERMINANT------------

IA=30
IN=30
IFAIL=1
CALL F03ADF (C,IA,IN,DETR,DETI,WKSPCE,IFAIL)
FW=A02ABF(DETR,DETI)
RETURN
END


------------------------------------------------------------
-------------------- INPUT DATA ROUTINE --------------------
------------------------------------------------------------

SUBROUTINE DATA (R1,R2,R3,R4,R5,PR,BBmin,BBmax,BBinc,
                 Vmin,Vmax,Vinc,Rang1,Rang2,DRang,CONST,MIDP)
REAL*8 R1,R2,R3,R4,R5,PR,BBmin,BBmax,BBinc,Vmin,Vmax,Vinc,
       Rang1,Rang2,DRang,CONST,MIDP

PRINT*,' ENTER Radius To Length Ratios '
READ*, R1,R2,R3,R4,R5
PRINT*, ' ENTER Tube POISSION Ratio '
READ*, PR
PRINT*,' ENTER Min,Max & Increment For Mass Ratio '
READ*, BBmin,BBmax,BBinc
PRINT*,' ENTER Min,Max & Increment For Fluid Velocity '
READ*, Vmin,Vmax,Vinc
PRINT*,' ENTER Lower,Upper & Increment For Searching '
READ*, Rang1,Rang2,DRang
PRINT*,' ENTER Mid-Distance'
READ*,MIDP
RETURN
END
------------------------------------------------------------
NOTE: EQUATIONS (2.23) CAN BE USED TO OBTAIN DIMENSIONAL PARAMETERS
      (eg. for comparison purposes in chapter 7).
```

APPENDIX "D"

BOUNDARY CONDITION EQUATIONS FOR U-TUBE CONFIGURATION INCORPORATING INTERMEDIATE SUPPORTS

Fourty two relations between fourty two constants A_{ij},B_{ij} and B_{oj} can be found from the boundary conditions (3.3), (3.4), (3.5) and (3.6), these relations are

$$\sum_{i=1}^{4} A_{i1} = 0 \qquad \text{(D-1)}$$

$$\sum_{i=1}^{4} \alpha_i A_{i1} = 0 \qquad \text{(D-2)}$$

$$B_{o1} = 0 \qquad \text{(D-3)}$$

$$\sum_{i=1}^{4} A_{i1} e^{\alpha_i L_1} - \sum_{i=1}^{4} A_{i2} e^{\alpha_i L_1} = 0 \qquad \text{(D-4)}$$

$$\sum_{i=1}^{4} \alpha_i A_{i1} e^{\alpha_i L_1} - \sum_{i=1}^{4} \alpha_i A_{i2} e^{\alpha_i L_1} = 0 \qquad \text{(D-5)}$$

$$B_{11}L_1 + B_{o1} - B_{12}L_1 - B_{o2} = 0 \qquad \text{(D-6)}$$

$$\sum_{i=1}^{4} \alpha_i^3 A_{i1} e^{\alpha_i L_1} - \bar{K}_1 \sum_{i=1}^{4} A_{i1} e^{\alpha_i L_1} - \sum_{i=1}^{4} \alpha_i^3 A_{i2} e^{\alpha_i L_1} = 0 \qquad \text{(D-7)}$$

$$\sum_{i=1}^{4} \alpha_i^2 A_{i1} e^{\alpha_i L_1} + \bar{K}_2 \sum_{i=1}^{4} \alpha_i A_{i1} e^{\alpha_i L_1} - \sum_{i=1}^{4} \alpha_i^2 A_{i2} e^{\alpha_i L_1} = 0 \qquad \text{(D-8)}$$

$$B_{11} - K_3(B_{11}L_1 + B_{01}) - B_{12} = 0 \qquad \text{(D-9)}$$

$$\sum_{i=1}^{4} A_{i2} e^{\alpha_i (L_1+L_2)} \sum_{i=1}^{4} A_{i3} e^{\alpha_i (L_1+L_2)} = 0 \qquad \text{(D-10)}$$

$$\sum_{i=1}^{4} \alpha_i A_{i2} e^{\alpha_i (L_1+L_2)} \sum_{i=1}^{4} \alpha_i A_{i3} e^{\alpha_i (L_1+L_2)} = 0 \qquad \text{(D-11)}$$

$$B_{12} \sum_{i=1}^{2} L_1 + B_{02} - B_{13} \sum_{i=1}^{2} L_1 - B_{03} = 0 \qquad \text{(D-12)}$$

$$\sum_{i=1}^{4} \alpha_i^3 A_{i2} e^{\alpha_i (L_1+L_2)} \bar{K}_1 \sum_{i=1}^{4} A_{i2} e^{\alpha_i (L_1+L_2)} - \sum_{i=1}^{4} \alpha_i^3 A_{i3} e^{\alpha_i (L_1+L_2)} = 0 \qquad \text{(D-13)}$$

$$\sum_{i=1}^{4} \alpha_i^2 A_{i2} e^{\alpha_i (L_1+L_2)} + \bar{K}_2 \sum_{i=1}^{4} \alpha_i A_{i2} e^{\alpha_i (L_1+L_2)} - \sum_{i=1}^{4} \alpha_i^2 A_{i3} e^{\alpha_i (L_1+L_2)} = 0 \qquad \text{(D-14)}$$

$$B_{12} - \bar{K}_3(B_{12} \sum_{i=1}^{4} L_1 + B_{02}) - B_{13} = 0 \qquad \text{(D-15)}$$

$$\sum_{i=1}^{4} A_{i3} e^{\alpha_i (L_1+L_2+L_3)} + (1+K)^{-1} \sum_{i=3}^{6} A_{i4} (K-\lambda^{-2}) e^{\lambda_i (L_1+L_2+L_3)} = 0 \qquad \text{(D-16)}$$

$$\sum_{i=1}^{4} \alpha_i A_{i3} e^{\alpha_i (L_1+L_2+L_3)} + (1+K)^{-1} \sum_{i=1}^{6} A_{i4} \lambda_i (K-\lambda^{-2}) e^{\lambda_i (L_1+L_2+L_3)} = 0 \qquad \text{(D-17)}$$

$$(B_{13}\sum_{i=1}^{3}L_i + B_{03}) - \sum_{i=1}^{6} A_{i4}\, e^{\lambda_i(L_1+L_2+L_3)} = 0 \qquad \text{(D-18)}$$

$$\sum_{i=1}^{4}\alpha_i^2 A_{i3}e^{\alpha_i(L_1+L_2+L_3)} + \left[\sum_{i=1}^{6}A_{i4} + (1+K)^{-1}\sum_{i=1}^{6}A_{i4}\lambda_i^2(K-\lambda_i^{-2})\right]e^{\lambda_i(L_1+L_2+L_3)} \geq 0 \qquad \text{(D-19)}$$

$$\sum_{i=1}^{4}\alpha_i^3 A_{i3}e^{\alpha_i(L_1+L_2+L_3)} + K(1+K)^{-1}\sum_{i=1}^{6}A_{i4}\lambda_i(\lambda_i^2+\lambda_i^{-2}+2)e^{\lambda_i(L_1+L_2+L_3)} \geq 0 \qquad \text{(D-20)}$$

$$B_{13} - \left[\sum_{i=1}^{6}A_{i4}\,\lambda_i + (1+K)^{-1}\sum_{i=1}^{6}A_{i4}\,\lambda_i(K-\lambda_i^{-2})\right]e^{\lambda_i(L_1+L_2+L_3)} \geq 0 \qquad \text{(D-21)}$$

$$\sum_{i=1}^{4}A_{i5}e^{\alpha_i(L_1+L_2+L_3+L_4)} + (1+K)^{-1}\sum_{i=1}^{6}A_{i4}(K-\lambda^{-2})e^{\lambda_i(L_1+L_2+L_3+L_4)} \geq 0 \qquad \text{(D-22)}$$

$$\sum_{i=1}^{4}\alpha_i A_{i5}e^{\alpha_i(L_1+L_2+L_3+L_4)} + (1+K)^{-1}\sum_{i=1}^{6}A_{i4}\lambda_i(K-\lambda^{-2})e^{\lambda_i(L_1+L_2+L_3+L_4)} = 0 \qquad \text{(D-23)}$$

$$(B_{13}\sum_{i=1}^{4}L_i + B_{03}) - \sum_{i=1}^{6} A_{i4}\, e^{\lambda_i(L_1+L_2+L_3+L_4)} = 0 \qquad \text{(D-24)}$$

$$\sum_{i=1}^{4}\alpha_i^2 A_{i3}e^{\alpha_i(L_1+L_2+L_3+L_4)} + \left[\sum_{i=1}^{6}A_{i4} + (1+K)^{-1}\sum_{i=1}^{6}A_{i4}\lambda_i^2(K-\lambda_i^{-2})\right]e^{\lambda_i(L_1+L_2+L_3+L_4)} \geq 0 \qquad \text{(D-25)}$$

$$\sum_{i=1}^{4}\alpha_i^3 A_{i3}e^{\alpha_i(L_1+L_2+L_3+L_4)} + K(1+K)^{-1}\sum_{i=1}^{6}A_{i4}\lambda_i(\lambda_i^2+\lambda_i^{-2}+2)e^{\lambda_i(L_1+L_2+L_3+L_4)} \geq 0 \qquad \text{(D-26)}$$

$$B_{13} - \left[\sum_{i=1}^{6}A_{i4}\,\lambda_i + (1+K)^{-1}\sum_{i=1}^{6}A_{i4}\,\lambda_i(K-\lambda_i^{-2})\right]e^{\lambda_i(L_1+L_2+L_3+L_4)} \geq 0 \qquad \text{(D-27)}$$

$$\left[\sum_{j=1}^{4} A_{js} - \sum_{j=1}^{4} A_{j6}\right] e^{\alpha_j(L_1+L_2+L_3+L_4+L_5)} = 0 \qquad \text{(D-28)}$$

$$\left[\sum_{j=1}^{4} \alpha_j A_{js} - \sum_{j=1}^{4} \alpha_j A_{j6}\right] e^{\alpha_j(L_1+L_2+L_3+L_4+L_5)} = 0 \qquad \text{(D-29)}$$

$$B_{1s}\sum_{j=1}^{2} L_j + B_{0s} - B_{16}\sum_{j=1}^{2} L_j - B_{06} = 0 \qquad \text{(D-30)}$$

$$\left[\sum_{j=1}^{4} \alpha_j^3 A_{js} - \bar{K}_1 \sum_{j=1}^{4} A_{js} - \sum_{j=1}^{4} \alpha_j^3 A_{j6}\right] e^{\alpha_j(L_1+L_2+L_3+L_4+L_5)} = 0 \qquad \text{(D-31)}$$

$$\left[\sum_{j=1}^{4} \alpha_j^2 A_{js} + \bar{K}_2 \sum_{j=1}^{4} \alpha_j A_{js} - \sum_{j=1}^{4} \alpha_j^2 A_{j6}\right] e^{\alpha_j(L_1+L_2+L_3+L_4+L_5)} = 0 \qquad \text{(D-32)}$$

$$B_{1s} - \bar{K}_3\left(B_{1s}\sum_{j=1}^{3} L_j + B_{0s}\right) - B_{16} = 0 \qquad \text{(D-33)}$$

$$\left[\sum_{j=1}^{4} A_{j6} - \sum_{j=1}^{4} A_{j7}\right] e^{\alpha_j(L_1+L_2+L_3+L_4+L_5+L_6)} \geq 0 \qquad \text{(D-34)}$$

$$\left[\sum_{j=1}^{4} \alpha_j A_{j6} - \sum_{j=1}^{4} \alpha_j A_{j7}\right] e^{\alpha_j(L_1+L_2+L_3+L_4+L_5+L_6)} \geq 0 \qquad \text{(D-35)}$$

$$B_{16}\sum_{j=1}^{6} L_j + B_{08} - B_{17}\sum_{j=1}^{6} L_j - B_{07} = 0 \qquad \text{(D-36)}$$

$$\left[\sum_{j=1}^{4} \alpha_j^3 A_{j6} - \bar{K}_1 \sum_{j=1}^{4} A_{j6} - \sum_{j=1}^{4} \alpha_j^3 A_{j7}\right] e^{\alpha_j(L_1+L_2+L_3+L_4+L_5+L_6)} \geq 0 \qquad \text{(D-37)}$$

$$\left[\sum_{i=1}^{4}\alpha_i^2 A_{i6} + \bar{K}_2\sum_{i=1}^{4}\alpha_i A_{i6} - \sum_{i=1}^{4}\alpha_i^2 A_{i7}\right] e^{\alpha_i(L_1+L_2+L_3+L_4+L_5+L_6)} = 0 \qquad \text{(D-38)}$$

$$B_{i6} - \bar{K}_3\left(B_{i6}\sum_{i=1}^{6} L_i + B_{06}\right) - B_{i7} = 0 \qquad \text{(D-39)}$$

$$\sum_{i=1}^{4} A_{i7}\, e^{\alpha_i(L_1+L_2+L_3+L_4+L_6+L_7)} = 0 \qquad \text{(D-40)}$$

$$\sum_{i=1}^{4} \alpha_i\, A_{i7}\, e^{\alpha_i(L_1+L_2+L_3+L_4+L_6+L_7)} = 0 \qquad \text{(D-41)}$$

$$B_{i7}\sum_{i=1}^{7} L_i + B_{07} = 0 \qquad \text{(D-42)}$$

APPENDIX "E"

BOUNDARY CONDITION EQUATIONS FOR STRAIGHT TUBE CONFIGURATION INCORPORATING ADDED MASSES

Sixteen relations between sixteen constants A_{ij} can be found from boundary condition equations (3.24) and (3.25), these relations are

$$\sum_{j=1}^{4} A_{j1} = 0 \qquad (E-1)$$

$$\sum_{j=1}^{4} \alpha_j A_{j1} = 0 \qquad (E-2)$$

$$\left[\sum_{j=1}^{4} A_{j1} - \sum_{j=1}^{4} A_{j2}\right] e^{\alpha_j L_1} = 0 \qquad (E-3)$$

$$\left[\sum_{j=1}^{4} \alpha_j A_{j1} - \sum_{j=1}^{4} \alpha_j A_{j2}\right] e^{\alpha_j L_1} = 0 \qquad (E-4)$$

$$\left[\sum_{j=1}^{4} \alpha_j^2 A_{j1} - \sum_{j=1}^{4} \alpha_j^2 A_{j2}\right] e^{\alpha_j L_1} = 0 \qquad (E-5)$$

$$\left[\sum_{j=1}^{4} \alpha_j^3 A_{j1} + \gamma_1 \bar{\omega}^2 \sum_{j=1}^{4} A_{j1} - \sum_{j=1}^{4} \alpha_j A_{j2}\right] e^{\alpha_j L_1} = 0 \qquad (E-6)$$

$$\left[\sum_{j=1}^{4} A_{j2} - \sum_{j=1}^{4} A_{j3}\right] e^{\alpha_j (L_1+L_2)} = 0 \qquad (E-7)$$

$$\left[\sum_{i=1}^{4} \alpha_i A_{i2} - \sum_{i=1}^{4} \alpha_i A_{i3}\right] e^{\alpha_i(L_1+L_2)} = 0 \qquad \text{(E-8)}$$

$$\left[\sum_{i=1}^{4} \alpha_i^2 A_{i2} - \sum_{i=1}^{4} \alpha_i^2 A_{i3}\right] e^{\alpha_i(L_1+L_2)} = 0 \qquad \text{(E-9)}$$

$$\left[\sum_{i=1}^{4} \alpha_i^3 A_{i2} + \gamma_2 \bar{\omega}^2 \sum_{i=1}^{4} A_{i2} - \sum_{i=1}^{4} \alpha_i A_{i3}\right] e^{\alpha_i(L_1+L_2)} = 0 \qquad \text{(E-10)}$$

$$\left[\sum_{i=1}^{4} A_{i3} - \sum_{i=1}^{4} A_{i4}\right] e^{\alpha_i(L_1+L_2+L_3)} = 0 \qquad \text{(E-11)}$$

$$\left[\sum_{i=1}^{4} \alpha_i A_{i3} - \sum_{i=1}^{4} \alpha_i A_{i4}\right] e^{\alpha_i(L_1+L_2+L_3)} = 0 \qquad \text{(E-12)}$$

$$\left[\sum_{i=1}^{4} \alpha_i^2 A_{i3} - \sum_{i=1}^{4} \alpha_i^2 A_{i4}\right] e^{\alpha_i(L_1+L_2+L_3)} = 0 \qquad \text{(E-13)}$$

$$\left[\sum_{i=1}^{4} \alpha_i^3 A_{i3} + \gamma_3 \bar{\omega}^2 \sum_{i=1}^{4} A_{i3} - \sum_{i=1}^{4} \alpha_i A_{i4}\right] e^{\alpha_i(L_1+L_2+L_3)} = 0 \qquad \text{(E-14)}$$

$$\sum_{i=1}^{4} A_{i4} e^{\alpha_i(L_1+L_2+L_3+L_4)} = 0 \qquad \text{(E-15)}$$

$$\sum_{i=1}^{4} \alpha_i A_{i4} e^{\alpha_i(L_1+L_2+L_3+L_4)} = 0 \qquad \text{(E-16)}$$

PUBLICATIONS

(1)

G.SULTAN AND J.HEMP "MODELLING OF THE CORIOLIS MASS FLOWMETER" JOURNAL OF SOUND AND VIBRATION VOL.132 (3), 1989, PP. 473-489.

(2)

J.HEMP AND G.SULTAN "ON THE THEORY AND PERFORMANCE OF CORIOLIS MASS FLOWMETERS" INTERNATIONAL CONFERENCE ON MASS FLOW MEASUREMENT; DIRECT AND INDIRECT, CORIOLIS METERING I, LONDON 21-22 FEB. 1989.